NORTH-WEST UNIVERSITY
YUNIBESITI YA BOKONE-BOPHIRIMA
NOORDWES-UNIVERSITEIT

Inhibition of monoamine oxidase by 8-[(phenylethyl)sulfanyl]caffeine analogues

Samantha Mostert

B.Pharm

Dissertation submitted in partial fulfilment of the requirements for the degree *Magister Scientiae* in Pharmaceutical Chemistry at the North-West University, Potchefstroom Campus.

Supervisor: Prof. J.P. Petzer

Co-supervisor: Prof. J.J. Bergh

2012

Potchefstroom

Acknowledgements

During the course of this study, much required advice and aid were necessary for completion of this study. I would like to take this opportunity to thank the following people and express my utmost gratitude for all that they have done:

- Prof. J.P. Petzer for his guidance, knowledge and invaluable inputs.
- Dr. A. Petzer for her unwavering willingness to help and assist whenever possible.
- Prof J.J. Bergh for his readily assistance.
- My parents, Amanda and Mossie Mostert, for their unconditional love and support, the sacrifices you have made, especially financial. Thank you for allowing me the opportunity to pursue my dreams and goals in life and for walking my life's journey with me.

I would also like to thank the following institutions for their assistance during the study:

- Northwest University for the financial support and granting me the opportunity to study at their institution.
- André Joubert at the SASOL Centre for Chemistry, for the numerous NMR spectra.
- The National Research Foundation of South Africa for their financial support.

"What do you mean, 'If I can'?" Jesus asked.

"Anything is possible if a person believes." - Mark 9:23

TABLE OF CONTENTS

LIST OF ABBREVIATIONS..... i

LIST OF FIGURES..... iv

ABSTRACT..... 1

UITREKSEL..... 4

CHAPTER 1: Introduction..... 8

1.1. Introduction and overview..... 8
1.2. Rationale..... 9
1.3. Objectives of this study..... 12

CHAPTER 2: Literature study..... 14

2.1. Parkinson's disease..... 14

2.1.1 General background..... 14
2.1.2. Neurochemical and neuropathological features..... 14
2.1.3. Pathogenesis..... 15
2.1.4. Symptomatic treatment..... 18

2.2. Monoamine oxidase..... 21

2.2.1. General background..... 21
2.2.2. The therapeutic role of MAO-A..... 22
2.2.3. The therapeutic role of MAO-B..... 24
2.2.4. Inhibitors of MAO..... 26
2.2.5. The three dimensional structure of MAO..... 30
2.2.6. Mechanistic proposals for MAO catalysis..... 34

2.3. Copper containing amine oxidase..... 38

2.4. *In vitro* measurements of MAO activity..... 42

2.5. Enzyme kinetics..... 44

2.6. Conclusion..... 48

CHAPTER 3: Synthesis…… 49

3.1. Introduction…… 49
3.2. Materials and instrumentation…… 53
3.3. Synthesis of 8-[(2-phenylethyl)sulfanyl]caffeine analogues…… 54
3.4. Synthesis of the appropriate mercaptans…… 55
3.5. Method for the synthesis of the 8-[(2-phenylethyl)sulfinyl]caffeine analogues…… 57
3.6. Synthesis of chlorine gas. …… 59
3.7. Synthesis of 8-chlorocaffeine…… 60
3.8. Results. …… 60
3.9. Interpretation of the mass spectra…… 71
3.10. Interpretation of the HPLC analysis…… 71
3.11. Conclusion…… 72

CHAPTER 4: Enzymology…… 73

4.1 Introduction…… 73
4.2 Chemicals and instrumentation…… 73
4.3 Determining the IC_{50} values…… 73
4.3.1. Method…… 75
4.3.2. Results…… 76
4.4 Time dependent studies…… 82
4.4.1. Method…… 82
4.4.2. Results…… 84
4.5 Lineweaver-Burk plots…… 85
4.5.1. Method…… 85
4.5.2. Results…… 87
4.6 Hansch-type structure-activity relationship studies…… 91
4.6.1 Results…… 93
4.7 Molecular docking studies…… 99
4.7.1 Method…… 99
4.7.2. Results…… 101
4.8 Conclusion…… 105

CHAPTER 5: Summary…… 106

BIBLIOGRAPHY…… 112

Appendix..…… 126

Section 1: ^{1}H and ^{13}C NMR spectra…… 128

Section 2: HPLC traces…… 139

Section 3: Mass spectra..... 144

Acknowledgements..... 147

LIST OF ABBREVIATIONS AND ACRONYMS

A	
ADH	Aldehyde dehydrogenase
C	
CNS	Central nervous system
COMT	Catechol-o-methyltransferase
CSC	8-(3-Chlorostyryl)caffeine
Cys	Cysteine
D	
DA	Dopamine
DOPAC	Dihydroxyphenylacetic acid
E	
E	Enzyme
ES	Enzyme-substrate
F	
FAD	Flavin adenine dinucleotide
G	
Gly	Glycine
GPO	Glutathione peroxidase
GSH	Glutathione
H	
HCl	Hydrochloric acid
5-HIAA	5-Hydroxyindole acetic acid
5-HT	Serotonin
I	
IC_{50}	Inhibitor concentration at 50% inhibition
Ile	Isoleucine

K

K_d	Dissociation constant
K_i	Inhibitor constant
K_m	Michaelis constant

L

Lys	Lysine

M

MAO	Monoamine oxidase
MPP^+	1-Methyl-4-phenylpyridinium
MPTP	1-methyl-4-phenyl-1,2,3,6-tetrahydropyridine

N

NA	Noradrenaline
NMDA	N-methyl-D-aspartate

P

PD	Parkinson's disease

Q

QSAR	Quantitive structure-activity relationship

R

ROS	Reactive oxygen species

S

S	Substrate
SAR	Structure-activity relationship
SD	Standard deviation
SSAO	Semicarbazide-sensitive amine oxidase
SET	Single electron transfer
SNpc	Substantia nigra pars compacta

T

TPQ	2,4,5-Trihydroxyphenylalanine quinone
Tyr	Tyrosine

U

UCH-L1	Ubiquitin C-terminal hydrolase L1
UPS	Ubiquitin-proteosome system

V

v_i	Initial velocity
V_{max}	Maximum velocity

LIST OF FIGURES

Figure 2.1 A schematic representation of environmental and genetic factors leading to neurodegeneration..... 16
Figure 2.2 The Fenton reaction..... 17
Figure 2.3 Structures of drugs frequently used in the symptomatic treatment of PD..... 19
Figure 2.4 Structures of drugs with potential use in PD..... 20
Figure 2.5 Structures of irreversible MAO-A inhibitors and hydrazine..... 22
Figure 2.6 Structure of the reversible MAO-A inhibitor, moclobemide..... 23
Figure 2.7 Reaction pathway of the degradation of dopamine to dopanal and DOPAC..... 24
Figure 2.8 Oxidative deamination pathway of amines by MAO..... 25
Figure 2.9 The mechanism of neurotoxicity of H_2O_2 induced by the Fenton reaction..... 26
Figure 2.10 Examples of reversible MAO-B inhibitors..... 27
Figure 2.11 Structures of selective reversible MAO-A inhibitors..... 28
Figure 2.12 Structures of the irreversible MAO-A inhibitor, clorgyline (left) and the non-selective reversible inhibitor, isocarbaxazide..... 29
Figure 2.13 Structures of irreversible MAO-B inhibitors..... 29
Figure 2.14 The structure of covalent FAD in MAO..... 30
Figure 2.15 Ribbon diagram displaying the structures of human MAO-A, human MAO-B and rat MAO-A..... 31
Figure 2.16 The structure of the active site cavity of MAO-B with isatin and 1,4-diphenyl-2-butene bound..... 32
Figure 2.17 An illustration of conserved amino acids present in human MAO-A and MAO-B..... 33
Figure 2.18 The mechanism of MAO catalysis..... 35
Figure 2.19 The SET mechanism..... 36
Figure 2.20 The polar nucleophilic mechanism..... 37
Figure 2.21 A ribbon diagram of the copper containg amine oxidase homodimer found in the *E.coli* species..... 39
Figure 2.22 A representation of the active site of E.coli copper amine oxidase..... 40
Figure 2.23 The catalytic cycle of amine oxidation through TPQ..... 41
Figure 2.24 The oxidative deamination of kynuramine to yield 4-hydroxyquinoline by MAO-A or MAO-B..... 43
Figure 2.25 An illustration of a Lineweaver-Burk plot..... 45

Figure 2.26 A Lineweaver-Burk plot of competitive inhibition with the y-intercept equal to $1/V_{max}$ and x- intercepts equal to $-1/K_m$ and $-1/K_m$', for no inhibitor and inhibitor, respectively..... 46
Figure 2.27 A Lineweaver-Burk plot of noncompetitive inhibition with the y-intercepts equal to $-1/V'_{max}$ and $1/V_{max}$, for inhibitor and no inhibitor, respectively..... 46
Figure 2.28 Determination of K_i values for competitive inhibition (left) and non-competitive inhibition (right) according to Dixon's method..... 47
Figure 3.1 A general reaction scheme to illustrate the synthesis of 8-sulfanylcaffeine analogues from 8-chlorocaffeine and a mercaptan..... 51
Figure 3.2 The general synthetic route for the preparation of mercaptans from an appropriately substituted phenylethylbromide..... 51
Figure 3.3 A general reaction scheme to illustrate the synthesis of 8-sulfinylcaffeine analogues from 8-sulfanylcaffeine analogues..... 52
Figure 3.4 The synthesis of 8-chlorocaffeine from the reaction between caffeine and chlorine gas..... 52
Figure 3.5 Illustration of experimental setup for the synthesis of the 8-[(2-phenylethyl) sulfanyl]caffeine analogues **1a**–**g**..... 54
Figure 3.6 Reaction scheme for the synthesis of 8-[(2-phenylethyl)sulfanyl]caffeine analogues **1a**–**g**..... 55
Figure 3.7 Reaction scheme for the synthesis of the required mercaptans **3a**–**g**..... 55
Figure 3.8 Illustration of the experimental setup for synthesis of the required mercaptans **3a**–**g**..... 57
Figure 3.9 Illustration of the experimental setup for synthesis of the 8-[(2-phenylethyl) sulfinyl]caffeine analogues **2a**–**b**..... 58
Figure 3.10 The synthetic route for the synthesis of 8-[(2-phenylethyl)sulfinyl]caffeine analogues..... 58
Figure 3.11 The chemical reaction for the synthesis of chlorine gas..... 59
Figure 3.12 An illustration of the apparatus setup for the synthesis of 8-chlorocaffeine..... 59
Figure 3.13 Reaction scheme for the synthesis of 8-chlorocaffeine..... 60
Figure 4.1 Diagrammatic representation of the method for determining IC_{50} values for the inhibition of MAO-A and MAO-B..... 74
Figure 4.2 An example of the calibration curves routinely constructed in this study..... 75

Figure 4.3 A sigmoidal graph used to determine the IC_{50} value of 8-{[2-(4-bromophenyl) ethyl]sulfanyl}caffeine towards MAO-B..... 78
Figure 4.4 A sigmoidal graph used to determine the IC_{50} value of 8-{[2-(4-chlorophenyl) ethyl]sulfanyl}caffeine towards MAO-A..... 78
Figure 4.5 Diagrammatic representation of the method followed for the time-dependent studies..... 83
Figure 4.6 A histogram depicting the rate of kynuramine oxidation by MAO-A after pre-incubation of the enzyme with inhibitor **1b** for various periods of time (0 - 60 min)..... 84
Figure 4.7 A histogram depicting the rate of kynuramine oxidation by MAO-B after pre-incubation of the enzyme with inhibitor **1b** for various periods of time (0 - 60 min)..... 85
Figure 4.8 Diagrammatic representation of the method used for the construction of Line-weaver-Burk plots..... 86
Figure 4.9 Lineweaver-Burk plots for the oxidation of kynuramine by MAO-B in the absence and presence of various concentrations of 8-{2-4-chlorophenyl) ethyl]sulfanyl} caffeine..... 87
Figure 4.10 Graph of the slopes of the Lineweaver-Burk plots versus the concentration of inhibitor **1b**..... 88
Figure 4.11 Experimental determination of the K_m value from the Lineweaver-Burk plot constructed in the absence of inhibitor..... 89
Figure 4.12 Experimental determination of the K_m value for MAO-A..... 89
Figure 4.13 Graph depicting the correlation between the inhibition potencies ($LogIC_{50}$ values) of MAO-B by C-4 substituted 8-[(2-phenylethyl)sulfanyl]caffeine analogues and the Swain-Lupton constant (*F*)..... 96
Figure 4.14 Graph depicting the correlation between the inhibition potencies ($LogIC_{50}$ values) for MAO-B by C-4 substituted 8-[(2-phenylethyl)sulfanyl]caffeine analogues with the Swain-Lupton constant (F) and the Van der Waals volume (V_w)..... 98
Figure 4.15 An illustration of 8-{[2-(phenyl)ethyl]sulfanyl}caffeine (**1a**) docked within the active site of MAO-B..... 101
Figure 4.16 An illustration of 8-{[2-(4-chlorophenyl)ethyl]sulfanyl}caffeine (**1c**) docked within the active site of MAO-B..... 102
Figure 4.17 An illustration of 8-{[2-(4-bromophenyl)ethyl]sulfinyl}caffeine (**2c**) docked

within the active site of MAO-B..... 103

Figure 4.18 An illustration of the co-crystallized ligand, harmine in the MAO-A active site (left) and, 8-{[2-(4-chlorophenyl)ethyl]sulfanyl}caffeine (**1c**, right) docked into the active site of MAO-A..... 104

ABSTRACT

Keywords: Monoamine oxidase; Sulfanylcaffeine; Sulfinylcaffeine; Reversible inhibition; Selective inhibition; Structure-activity relationship; Molecular docking.

Parkinson's disease (PD) is classified as a neurodegenerative disease in which patients have reduced amounts of dopamine (DA) in the substantia nigra pars compacta (SNpc) of the brain. The main pathology of PD is the progressive death of nigrostriatal dopaminergic neurons. One strategy for the symptomatic treatment of PD is to conserve dopamine in the brain by inhibiting the enzymes responsible for its degradation. Monoamine oxidase (MAO) B is the main enzyme responsible for the degradation of DA. Inhibition of this enzyme, in the brain may conserve the depleted dopamine in the PD brain and provide symptomatic relief to the patients. In addition MAO-B inhibitors may enhance the levels of dopamine that is derived from administered levodopa, the metabolic precursor of dopamine.

While MAO-B inhibitors have been employed for the treatment of PD for several years, the most commonly used drugs are irreversible inhibitors of the enzyme. The most commonly used irreversible MAO-B inhibitor, (R)-deprenyl (selegiline) is particularly associated with neurotoxic adverse effects such as cardiovascular and psychiatric effects. Apart from the above effects, irreversible inhibitors have additional disadvantages following repeated drug administration. These include the loss of selectivity at higher doses and an effect that persists for weeks after the drug treatment had been terminated. In contrast, with reversible inhibitors loss of selectivity is reduced because the action of duration is shorter. Also the MAO-B inhibitory effects of the drugs are terminated once drug treatment has been stopped and the drug has been cleared from the tissues. Considering the disadvantages of irreversible inhibitors, the need for the development of safe novel reversible inhibitors is of utmost importance.

Recent studies have discovered reversible inhibitors such as 8-benzyloxycaffeine and 8-sulfanylcaffeine analogues. These compounds have been shown to be potent inhibitors of MAO-B. These compounds consist of a caffeine ring linked to a side chain at the C-8 position of the caffeine ring either with an oxygen or a thio linker. Caffeine by itself is a weak inhibitor of MAO but substitution on the C-8 position greatly improves its inhibition potencies, as was shown by the potent 8-sulfanylcaffeine inhibitor, 8-[(2-phenylethyl)sulfanyl]caffeine, with an IC_{50} value of 0.223 μM for MAO-B. In this study we expanded on this result obtained with 8-[(2-phenylethyl)sulfanyl]caffeine by substitution on the C-4 position of the phenyl ring with a variety

of halogen and alkyl substituents. Also, to explore structure-activity relationships (SAR) of MAO-B inhibition, selected 8-[(2-phenylethyl)sulfinyl]caffeine analogues were synthesized.

The structures of 8-[(2-phenylethyl)sulfanyl]caffeine (**A**) and 8-[(2-phenylethyl)sulfinyl]caffeine (**B**) are shown below.

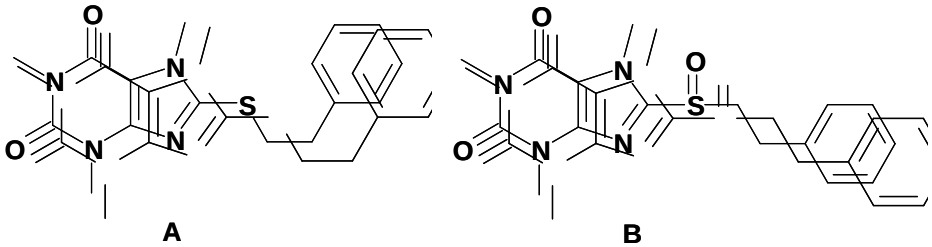

A **B**

The C-4 substituted 8-[(2-phenylethyl)sulfanyl]caffeine analogues were synthesized by reacting 8-chlorocaffeine with the appropriate substituted mercaptan in a basic medium. The 8-[(2-phenylethyl)sulfinyl]caffeine analogues were synthesized by reacting the selected 8-[(2-phenylethyl)sulfanyl]caffeine analogues with hydrogen peroxide in the presence of glacial acetic acid and acetic acid anhydride. The compounds were purified through recrystallization with either ethanol or ethylacetate as solvents. The structures of the compounds were verified by NMR and MS analyses, and the purities were estimated by HPLC analysis.

The inhibition potencies of the respective compounds towards recombinant human MAO-A and MAO-B were determined and expressed as IC_{50} values. The compounds showed significant potency towards MAO-B and to a lesser extent MAO-A. This is of value since the main isoenzyme targeted for the treatment of PD is MAO-B. The most potent MAO-B inhibitors were 8-{[2-(4-bromophenyl)ethyl]sulfanyl}caffeine and 8-{[2-(4-(trifluoromethyl)phenyl)ethyl]sulfanyl} caffeine with IC_{50} values of 0.019 µM each. These inhibitors are more potent than the lead compound, 8-[(2-phenylethyl)sulfanyl]caffeine (IC_{50} = 0.223 µM). With respect to the results, it can be concluded that substitution on the phenyl ring with halogens and halogen containing substituents greatly enhances the MAO-B inhibition potency of the lead compound. The 8-[(2-phenylethyl)sulfinyl]caffeine analogues, however, were weak inhibitors of both MAO isoforms.

In addition, the reversibility and mode of inhibition were examined for a representative compound. 8-{[2-(4-Chlorophenyl)ethyl]sulfanyl}caffeine (IC_{50} = 0.020 µM) was selected as representative inhibitor. The results showed no time-dependent inhibition of the catalytic oxidation rates of MAO-A and MAO-B by this compound. Therefore, it can be concluded that the compound binds reversibly to both the MAO-A and MAO-B enzymes. Lineweaver-Burk plots

were constructed to determine the mode of MAO-B inhibition of 8-{[2-(4-chlorophenyl)ethyl] sulfanyl}caffeine. The results showed that the plots intersect at the y-axis and is thus indicative of competitive inhibition. It can be concluded that 8-{[2-(4-chlorophenyl)ethyl]sulfanyl}caffeine is a competitive and reversible inhibitor of MAO-B.

A Hansch-type QSAR study showed that the inhibition potencies of MAO-B correlated with an electronic descriptor, the Swain-Lupton constant (*F*), of the substituents on C-4 of the phenyl ring. This indicates that for 8-[(2-phenylethyl)sulfanyl]caffeine analogues, C-4 substituents, which are electron withdrawing, would lead to an enhancement of the MAO-B inhibition potency. The more electron withdrawing the C-4 substituent, the more potent the inhibition would be towards MAO-B. The study also suggested that an increase of the Van der Waals volume (V_w) of the C-4 substituent may possibly also enhance the inhibition potencies of the 8-[(2-phenylethyl)sulfanyl]caffeine analogues. It can therefore be concluded that electron withdrawing and bulky C-4 substituents are favourable for MAO-B inhibition.

Docking studies revealed that the 8-[(2-phenylethyl)sulfanyl]caffeine analogues traverse both the entrance and substrate cavities of MAO-B. The caffeine ring binds within the substrate cavity while the phenylethyl side-chain protrudes into the entrance cavity. Various interactions are present which is considered crucial for the inhibitory effect that the 8-[(2-phenylethyl)sulfanyl]caffeine analogues have on MAO-B.

This study recommends that the substitution on the C-4 position of the phenyl ring of 8-[(2-phenylethyl)sulfanyl]caffeine with more electron withdrawing functional groups should be undertaken. This most likely would lead to compounds with highly potent MAO-B inhibitory properties.

To conclude, the 8-[(2-phenylethyl)sulfanyl]caffeine analogues are potent, selective, reversible and competitive inhibitors of human MAO-B and are therefore promising drug candidates and lead compounds for the future symptomatic treatment of PD.

UITTREKSEL

Sleutelwoorde: Monoamineoksidase; Sulfanielkafeïen; Sulfinielkafeïen; Omkeerbare inhibeerders; Selektiewe inhibisie; Struktuur-aktiwiteitverwantskap; Rekenaarmodellering-studies.

Parkinson se siekte (PS) word geklassifiseer as 'n neurodegeneratiewe siekte wat gekarakteriseer word deur verlaagde konsentrasies van dopamien in die substantia nigra pars compacta van die brein. Hierdie toestand word veroorsaak deur die afsterwe van die nigrostriatale dopaminergiese neurone in die brein. 'n Strategie om simptomatiese verligting aan PS pasiente te bied, is die voorkoming van dopamienafbraak in die brein, deur die ensieme te inhibeer wat verantwoordelik is vir die metabolisme van dopamien. Die belangrikste ensiem wat verantwoordelik is vir die metabolisme van dopamien in die brein, is monoamienoksidase (MAO), veral die MAO-B isoform. Inhibisie van dié ensiem, kan moontlik die konsentrasie van dopamien in die brein verhoog en sodoende simptomatiese verligting aan pasiënte bring. Boonop mag MAO-B-inhibeerders ook die konsentrasie van dopamien verhoog na behandeling met levodopa, die metaboliese voorloper van dopamien.

MAO-B-inhibeerders word algemeen gebruik vir die behandeling van PS. Die MAO-B-inhibeerders wat tans in gebruik is, is onomkeerbare inhibeerders van die ensiem. Die bekenste onomkeerbare inhibeerder is (R)-depreniel (Seligilien), 'n geneesmiddel wat met neurotoksiese effekte, soos kardiovaskulêre en psigiatriese newe-effekte, geassosieer word. Onomkeerbare inhibeerders veroorsaak verdere bykomende newe-effekte met herhaalde geneesmiddel-toediening wat 'n verlies van selektiwiteit met hoër dosisse en 'n inhibeerende effek wat etlike weke voortduur nadat geneesmiddel behandeling gestaak is, insluit. In teenstelling hiermee, is omkeerbare inhibeerders meer selektief omdat die duur van werking kort is en die inhiberende effek op MAO-B staak sodra geneesmiddelbehandeling beëindig word. Met inagneming van die bogenoemde, bestaan daar 'n behoefte aan die ontwikkeling van nuwe omkeerbare inhibeerders van MAO-B.

Onlangse studies het 8-bensieloksiekafeïen- en 8-tiokafeïen-analoë ontdek as nuwe inhibeerders van MAO. Hierdie verbindings tree op as potente inhibeerders van MAO-B en word gekarakteriseer deur 'n kafeïenring met 'n syketting op die C-8 posisie van die kafeïenring. Die syketting is aan die kafeïenring gekoppel deur 'n suurstof- of 'n tioeterskakel. Alhoewel kafeïen 'n swak inhibeerder van MAO is, kan die inhibisiepotensie aansienlik verbeter word deur substitusie op die C-8 posisie. 'n Potente inhibeerder, 8 -[(2-fenieletiel)sulfaniel]kafeïen, met 'n

IC_{50} waarde van 0.223 µM vir die inhibisie van MAO-B, is'n voorbeeld hiervan. Met hierdie studie word daar beoog om die MAO-B-inhiberende eienskappe van 8-[(2-fenieletiel)sulfaniel]kafeïen verder te verbeter deur die C-4 posisie op die fenielring te substitueer met 'n verskeidenheid halogene en alkielsubstituente. Om struktuur-aktiwiteitverwantskappe (SAV) van MAO-B-inhibisie verder te ontleed, sal geselekteerde 8-[(2-fenieletiel)sulfiniel]kafeïen-analoë ook gesintetiseer word.

Die strukture van die 8-[(2-fenieletiel)sulfaniel]kafeïen-analoë (**A**) en 8-[(2-fenieletiel) sulfiniel]kafeïen-analoë (**B**) wat in hierdie studie ondersoek is, word hieronder aangetoon.

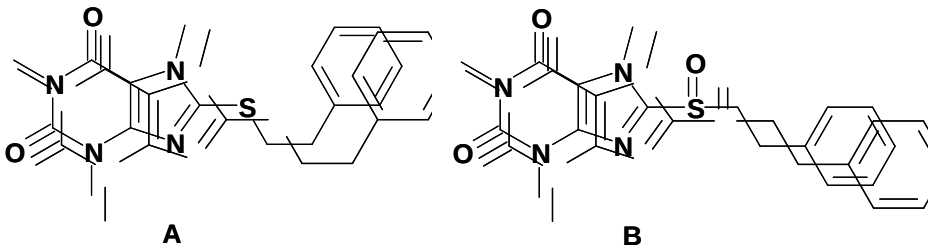

Sewe C-4 gesubstitueerde 8-[(2-fenieletiel)sulfaniel]kafeïen-analoë is gesintetiseer deur 8-chlorokafeïen met 'n toepaslike gesubstitueerde merkaptan in 'n basiese omgewing te laat reageer. Twee 8-[(2-fenieletiel)sulfiniel]kafeïen-analoë is gesintetiseer deur die toepaslike 8-[(2-fenieletiel)sulfaniel]kafeïen-analoog met waterstofperoksied, in die teenwoordigheid van ysasynsuur en asynsuuranhidried te laat reageer. Om die teikenverbinding te suiwer, is dit gerekristalliseer vanuit etanol of etielasetaat. Die chemiese strukture van die teikenverbindings is deur KMR en massaspektroskopie (MS) bevestig, en hul suiwerhede is deur hoëdruk-vloeistofchromatografie (HDVC) analise bepaal.

Inhibisiestudies is op die teikenverbindings uitgevoer en hul inhibisieaktiwiteite is teenoor rekombinante menslike MAO-A en MAO-B bepaal en uitgedruk as IC_{50}-waardes. Die teikenverbindings toon betekenisvolle inhibisieaktiwiteit vir MAO-B, maar toon baie minder aktiwiteit teenoor MAO-A. Hierdie bevinding is van waarde, aangesien die MAO-B-ensiem die teikenensiem in die behandeling van PS is. Die beste MAO-B-inhibeerders wat in die studie ontdek is, is 8-{[2-(4-bromofeniel)etiel]sulfaniel}kafeïen en 8-{[2-(4-(trifluorometiel)feniel)etiel] sulfaniel}kafeïen, beide met IC_{50} waardes van 0.019 µM. Hierdie verbindings is meer potent as die leidraadverbinding, 8-[(2-fenieletiel)sulfaniel]kafeïen (IC_{50} = 0.223 µM). Op grond van die resultate kan tot die gevolgtrekking gekom word dat substitusie op die C-4-posisie van die fenielring, met halogene en alkielsubstituente tot betekenisvolle verhogings in die leidraad-

verbinding se MAO-B-aktiwiteit lei. In teenstelling hiermee, het hierdie studie gevind dat die 8-[(2-fenieletiel)sulfiniel]kafeïen analoë swak inhibeerders van beide MAO isoforme is.

8-{[2-(4-Chlorofeniel)etiel]sulfaniel}kafeïen (IC_{50} = 0.020 µM) is gekies as 'n verteenwoordigende verbinding om die tydsafhanklikheid en meganisme van inhibisie te ondersoek. Die resultate toon dat hierdie verbinding geen tydsafhanklike inhibisie van die katalitiese aktiwiteit van MAO-A of MAO-B veroorsaak nie. Hierdie bevinding dui daarop dat 8-{[2-(4-chlorofeniel)etiel]sulfaniel}kafeïen omkeerbaar aan MAO-A en -B bind. Lineweaver-Burk grafieke is ook gekonstrueer om die meganisme van inhibisie van 8-{[2-(4-chlorofeniel)etiel] sulfaniel}kafeïen te ondersoek. Die resultate toon dat die grafieke op een punt op die y-as sny, 'n eienskap wat op daarop dui dat 8-{[2-(4-chlorofeniel)etiel]sulfaniel}kafeïen 'n kompeterende inhibeerder van MAO-B is. Hierdie studie lei tot die gevolgtrekking dat 8-{[2-(4-chlorofeniel)etiel]sulfaniel}kafeïen 'n omkeerbare en kompeterende inhibeerder van MAO-B is.

'n Hansch-tipe struktuur-aktiwiteitverwantskap-studie het aangetoon dat die MAO-B-inhibisie-aktiwiteit goeie korrelasie toon met 'n elektroniese parameter van die C -4 substituente op die fenielring, die Swain-Lupton konstante *(F*). Hierdie resultaat wys daarop dat C-4 substituente, wat elektron-ontrekkende funksionele groepe bevat, die MAO-B-inhibisiepotensie van 8-[(2-fenieletiel)sulfaniel]kafeïen sal verhoog. Substituente wat elektron-ontrekkend is sal lei tot meer potente MAO-B-inhibisie. Die studie vind verder dat indien die Van der Waals volume (V_w) van die C-4 substituente vergroot word, kan dit lei tot 'n verdere verhoging van die MAO -B inhibisie-aktiwiteit van die 8-[(2-fenieletiel)sulfaniel]kafeïen. Daar kan dus tot die gevolgtrekking gekom word dat elektron-ontrekkende C-4 substituente en substituente wat steries groot is, die MAO-B-inhibisieaktiwiteit van 8-[(2-fenieletiel)sulfaniel]kafeïen sal verbeter.

Rekenaarmodelleringstudies toon dat die sulfanielkafeïen-analoë beide die ingangsholte en die substraatholte van die MAO-B okkupeer. Die kafeïenring bind in die substraatholte terwyl die fenieletielsyketting die ingangsholte beset. Verskeie interaksies is teenwoordig tussen die inhibeerders en die aktiewe setel van MAO-B wat belangrik is vir die potente inhibisie aktiwiteite van die sulfanielkafeïen analoë.

Die huidige studie stel voor dat substitusie op die C-4-posisie van die fenielring met meer elektron-ontrekkende funksionele groepe voortgesit moet word. Dit sal waarskynlik tot verbindings lei wat meer potente inhibisie van MAO-B sal veroorsaak.

Uit hierdie studie kan afgelei word dat die 8-[(2-fenieletiel)sulfaniel]kafeïen analoë potente, selektiewe, omkeerbaare en kompeterende inhibeerders van menslike MAO-B is en dus kan hierdie verbindings as moontlike geneesmiddelkandidate dien vir die simptomatiese behandeling van PS.

Chapter 1

Introduction

1.1 Introduction and overview

Parkinson's disease (PD) is defined as a progressive neurodegenerative disorder that affects a patient's muscle control, movement and balance. PD is thought to affect 1% of people over the age of 65. Studies carried out in 2005 suggest that there are 4.1 million PD patients over the age of 50. By 2030 this value is estimated to reach values as high as 8.7 million, since worldwide life expectancy is on the increase (Dorsey *et al*., 2007). The main pathology of PD is progressive deterioration of the dopaminergic neurons in the substantia nigra pars compacta (SNpc). This leads to depletion of dopamine along the nigrostriatal pathway (Fernandez & Chen, 2007). If PD is untreated, severe disability can be expected within 10 years or less of PD onset. This is due to the rapid deterioration of the motor functions. These observations emphasize the need to develop therapies to slow down the underlying progressive neurodegenerative processes of PD (Löhle & Reichmann, 2010).

The monoamine oxidase (MAO) A and B enzymes contain flavin adenine dinucleotide (FAD) cofactors, which catalyze the oxidation of endogenous and xenobiotic amines, present in the brain and peripheral tissue. MAO-A and MAO-B are encoded by different genes and have unique substrate and inhibitor specificities. Both enzymes use dopamine as substrate (Shih *et al*., 1999). MAO-B appears to be the main enzyme responsible for the metabolism of dopamine in the basal ganglia and inhibitors of MAO-B may therefore conserve the depleted dopamine in the PD brain (Youdim & Weinstock, 2004). Inhibitors of MAO, especially those with specificity and selectivity for MAO-B, prolong the activity of endogenous and exogenous derived dopamine. This enhancement of dopamine's function, make MAO inhibitors an attractive option for the treatment of PD patients, either as monotherapy in early PD or as adjuvant therapy with levodopa in PD patients who experience motor complications (Fernandez & Chen, 2007). Studies with levodopa have shown that treatment with levodopa alone leads to levodopa induced dyskinesias in about 50% of patients treated. Moreover, levodopa treatment also causes a 'wearing-off' effect (Rascol *et al*., 2002).

Inhibition of the MAO-A enzyme in the brain is useful in the treatment of depressive illness. In the striatum, the activity of MAO-A is much lower than the activity of MAO-B, but interestingly, studies have found that both MAO-A and MAO-B play a role in the dopamine catabolism in the primate brain (Fowler *et al*., 1980). The major disadvantage of MAO-A inhibitors is that peripheral inhibition of MAO-A leads to an acute syndrome, called the 'cheese reaction', which is characterized by hypertension, tachycardia, palpitations, nausea and headaches. This occurs when the inhibitor is ingested along with tyramine. Thus nonselective irreversible MAO inhibitors are contraindicated with tyramine containing foods (Chen & Swope, 2005).

As a person ages, the activity and density of MAO-B increases in most brain regions (Fowler *et a*l., 1997). Since the oxidative metabolism of dopamine by MAO-B produces toxic byproducts such as hydrogen peroxide (H_2O_2) and dopaldehyde, which may contribute towards neurodegeneration, aged persons are at higher risk. MAO-B inhibitors may reduce the formation of H_2O_2 and thus protect against its toxic effects (Youdim & Bakhle, 2006).

There are only a few MAO-inhibitors approved by the Food and Drug Administration for the treatment of PD and two examples are (R)-deprenyl (selegiline) and rasagiline. (R)-Deprenyl and rasagiline are selective irreversible MAO-B inhibitors. Reversible inhibitors present a number of advantages and may be superior to irreversible inhibitors. Disadvantages of irreversible inhibitors include loss of selectivity with repeated drug administration and an enzyme recovery that is dependent on the rate of enzyme synthesis after drug withdrawal. For reversible inhibition the rate of enzyme recovery is immediate after the inhibitor is eliminated from the tissue and the loss of selectivity is reduced because the action of duration is shorter (Tipton *et al*., 2004). Based on the important role that reversible MAO-B inhibitors play in PD, the design and development of new reversible inhibitors are of importance. The goal of this research project is to design new reversible inhibitors of MAO which may potentially be used in the symptomatic treatment of PD and may possibly possess neuroprotective properties.

1.2 Rationale

Caffeine has previously been used as a scaffold for the design of reversible MAO inhibitors. Caffeine itself is a very weak MAO-B inhibitor (K_i = 3.6 mM). However, literature has reported that substitution on C8 of the caffeine ring greatly increases the MAO-B inhibition activity (Petzer *et al*., 2003). A recent study has shown that a series of sulfanylcaffeines are potent reversible inhibitors of MAO-B and to a lesser extent reversible inhibitors of MAO-A. These structures of the sulfanylcaffeines and their MAO-A and MAO-B inhibition activities are listed in

table 1.1. As shown in the table, the best inhibitor is compound **2**, 8-[(4-bromobenzyl)sulfanyl]caffeine, with an IC_{50} value of 0.16 µM and 2.61 µM for MAO-B and MAO-A, respectively (Booysen *et al*., 2011). Another potent MAO-B inhibitor and promising drug candidate is compound **7**, 8-[(2-phenylethyl)sulfanyl]caffeine (Table 1.1) with an IC_{50} value of 0.223 µM. This compound will serve as lead for the current study and its structure will be modified in an attempt to discover new potent MAO-B inhibitors.

Table 1.1. The structures of C8 substituted sulfanylcaffeine analogues and their IC_{50} values for the inhibition of human MAO-A and –B (Booysen *et al*., 2011).

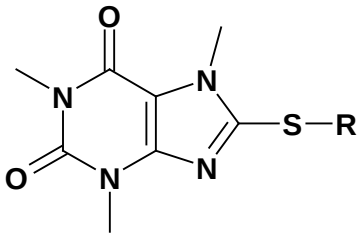

	Compound -R	IC_{50} µM MAO-A	IC_{50} µM MAO-B		Compound -R	IC_{50} µM MAO-A	IC_{50} µM MAO-B
1	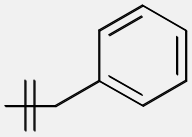	8.22	1.86	**7**	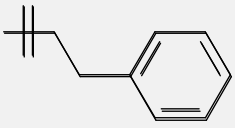	20.54	0.22
2	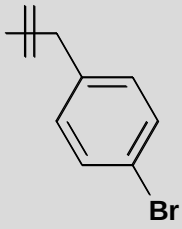	2.61	0.16	**8**	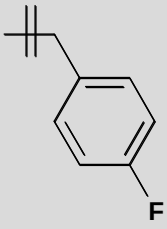	4.79	0.34
3	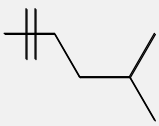	15.16	2.62	**9**	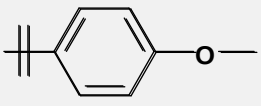	n/a	n/a
4	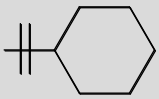	24.43	13.10	**10**	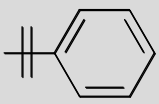	215.29	33.21

5	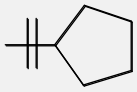	9.40	20.86	**11**	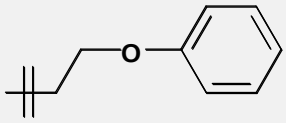	15.49	0.33
6	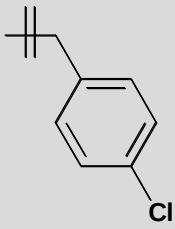	2.76	0.19	**12**	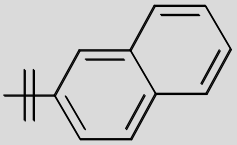	3.60	3.59

The current study will attempt to expand on this result by synthesizing a homologous series of 8-[(2-phenylethyl)sulfanyl]caffeine analogues of which the C8 phenyl rings contain a variety of halogen and alkyl substituents. These compounds will then be evaluated as inhibitors of human MAO-A and MAO-B. The compounds that will be synthesized are illustrated in table 1.2. The substituents selected were halogens (Cl, Br, F), as well as alkyl substituents, the methyl, methoxy and trifluoromethyl groups. The selection of these substituents is based on their physiochemical properties. These properties of the substituents are sufficiently diverse to allow for a Hansch-type quantitive structure-activity relationship (QSAR) study. QSAR studies will allow us to quantify the effect that the different substituents on the phenyl ring of the 8-[(2-phenylethyl)sulfanyl]caffeine analogues have on MAO-B inhibition activity. For example, the Cl, Br, F and CF_3 substituents are electron-withdrawing while CH_3 and OCH_3 substituents are electron-releasing/donating. Br and OCH_3 are relative large substituents whereas Br, CF_3 and CH_3 are considered sterically bulky. CF_3 and OCH_3 both are considered large but with a low degree of lipophilicity.

The current study will also attempt to convert selected 8-[(2-phenylethyl)sulfanyl]caffeine analogues to the corresponding 8-[(2-phenylethyl)sulfinyl]caffeines. The rationale behind this is to explore the effect that oxidation of the sulphur will have on the inhibition potencies towards MAO. The oxidation state of the sulfur of the 8-[(2-phenylethyl)sulfanyl]caffeine analogues (**1a**–**g**) is -2, while the oxidation state of the sulfur in 8-[(2-phenylethyl)sulfinyl]caffeine analogues (**2a**–**b**) is 0. These compounds will also undergo evaluation as inhibitors of MAO-A and MAO-B and their structures are illustrated in table 1.2.

Table 1.2. The structures of the 8-[(2-phenylethyl)sulfanyl]caffeine analogues and the 8-[(2-phenylethyl)sulfinyl]caffeine analogues that will be synthesized and investigated in this study.

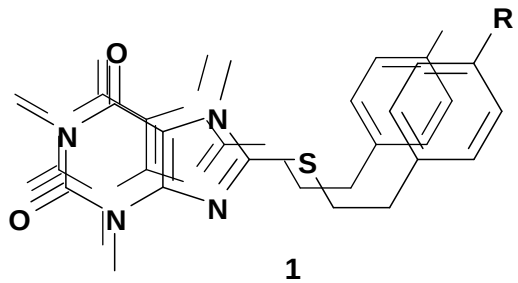

1

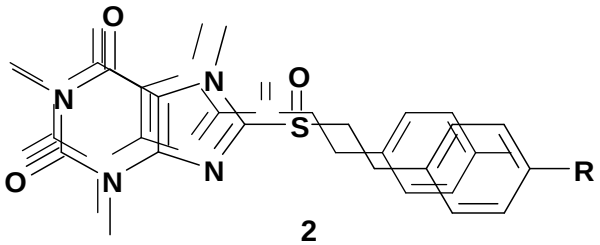

2

	R
1a	H
1b	Cl
1c	Br
1d	F
1e	CF_3
1f	CH_3
1g	OCH_3
2a	Br
2b	F

1.3 Objectives of this study

- Seven 8-[(2-phenylethyl)sulfanyl]caffeine analogues will be synthesized using chlorocaffeine and the appropriate substituted phenylethylmercaptan as starting materials. Most of the required mercaptans are not commercially available and will be prepared from the corresponding phenylethylbromide and thiourea.

- Two 8-[(2-phenylethyl)sulfinyl]caffeine analogues will be synthesized. This will be done by reacting the selected 8-[(2-phenylethyl)sulfanyl]caffeine analogues with hydrogen peroxide in the presence of glacial acetic acid and acetic acid anhydride.

- The 8-[(2-phenylethyl)sulfanyl]caffeine and the 8-[(2-phenylethyl)sulfinyl]caffeine analogues will be evaluated as inhibitors of human MAO-A and MAO-B. The recombinant human MAO enzymes are commercially available and the inhibition potencies will be expressed as IC_{50} values. A fluorometric assay will be used to measure the enzyme activities. For these assays, kynuramine will be used as substrate.

- The most potent inhibitor among the 8-[(2-phenylethyl)sulfanyl]caffeine analogues will undergo time-dependent studies to determine the reversibility of inhibition of MAO-A and MAO-B.

- A set of Lineweaver-Burk plots will be generated for a selected inhibitor to determine whether the selected inhibitor's mode of inhibition is competitive.

- A Hansch-type QSAR study will be carried out to quantify the effect that the different substituents on the phenyl ring of the 8-[(2-phenylethyl)sulfanyl]caffeine analogues have on the inhibition activity of MAO-B.

- Finally, the structures of 8-[(2-phenylethyl)sulfanyl]caffeine and the 8-[(2-phenylethyl)sulfinyl]caffeine analogues will be docked into the active sites of MAO-A and MAO-B in order to determine the possible binding orientations.

Chapter 2

Literature study

2.1 Parkinson's disease

2.1.1 General background

In 1817, Parkinson's disease (PD) was first described by a neurologist James Parkinson, in which he referred to the disease as 'Shaking Palsy' or 'paralysis agitans' (Parkinson, 2002). In 1912, Lewy bodies was first described by Friedrich Heinrich and today these inclusion bodies are seen as a pathological hallmark in idiopathic PD (Lewy, 1912). Arvid Carlsson discovered dopamine (DA) in the mammalian brain in the 1950s and reported that 80% of DA is situated in the basal ganglia. It was with this discovery that he first made the link between DA and PD (Carlsson, 1959). The dopaminergic pathway was then found to consist mainly of substantia nigra pars compacta (SNpc) neurons and this led to the discovery of:

- The loss of SNpc neurons lead to striatal DA deficiency and this causes the major symptoms of PD
- Replacement of striatal DA relieves most of these symptoms and it is possible to elevate DA levels through administration of levodopa. (Dauer & Przedborski, 2003)

Levodopa revolutionized the treatment of PD but studies have shown that long term use leads to dyskinesias which, together with the disease's impaired movement, greatly influence the patients' quality of life. The current research objective is to focus on the prevention of dopaminergic neuron degeneration but regardless of this, most treatment strategies are still symptomatic (Dauer & Przedborski, 2003).

2.1.2 Neurochemical and neuropathological features

Two major pathological hallmarks for PD are the presence of inclusion bodies (Lewy bodies and Lewy neurites) and the loss of dopaminergic nigrostriatal neurons (Dauer & Przedborski, 2003). Lewy Bodies and neurites are composed of various aggregated proteins such as α-synuclein, parkin, ubiquitin and neurofilaments and are prevalent in all affected brain areas (Forno, 1996). Neurodegeneration extends beyond dopaminergic neurons and can be divided into six consecutive stages: It starts in the gastric autonomic plexus of Meissner and olfactory nerve

endings then spreads towards the medulla oblongata and olfactory bulb, affecting the midbrain regions especially the SNpc. Degeneration then proceeds to the mesocortex where it extends towards the sensory and prefrontal neocortex and then includes the first sensory association neocortical and premotor areas (Lees *et al*., 2009).

Some neurological changes are independent of the presence of inclusion bodies filled with abnormal α-synuclein. This indicates that there are different mechanisms that congregate in the degenerative process. An example of these neurological changes is the impaired dopaminergic, noradrenergic, cholinergic and serotoninergic innervations as a result of the involvement of the cerebral cortex, which appear at the early stages of the disease. This explains why some patients develop depression long before motor symptoms become apparent (Dauer & Przedborski, 2003).

2.1.3 Pathogenesis

PD is the second most common neurodegenerative disorder of which Alzheimer's disease is first. The prevalence is 1-2/1000 and the incidence increases above 50 years of age (Korrell & Tanner, 2005). Most of these cases are sporadic and are termed idiopathic PD. However, studies have shown, in familial PD, that first degree relatives have a 2-3 times higher relative risk of developing PD (Gasser, 1998). This risk is connected to the mutation of six genes namely; Parkin, PINK1, DJ1, ATP13A2, α-synuclein, LRRK2 (Choonara *et al.*, 2009).

Demographic risk factors are also present and they include age, sex, race and geographical locations. Pre-exposure to viral encephalitis lethargic poses as a risk factor (Conley & Kirchner, 1999). Surprisingly studies also show that tobacco smokers are less likely to develop PD as opposed to lifelong non-smokers (Hernán *et al.*, 2001).

Epidemiological studies support the notion that both environmental and genetic factors contribute towards the development of PD (Bartels & Leenders, 2009). This leads to two hypotheses (Figure 2.1):

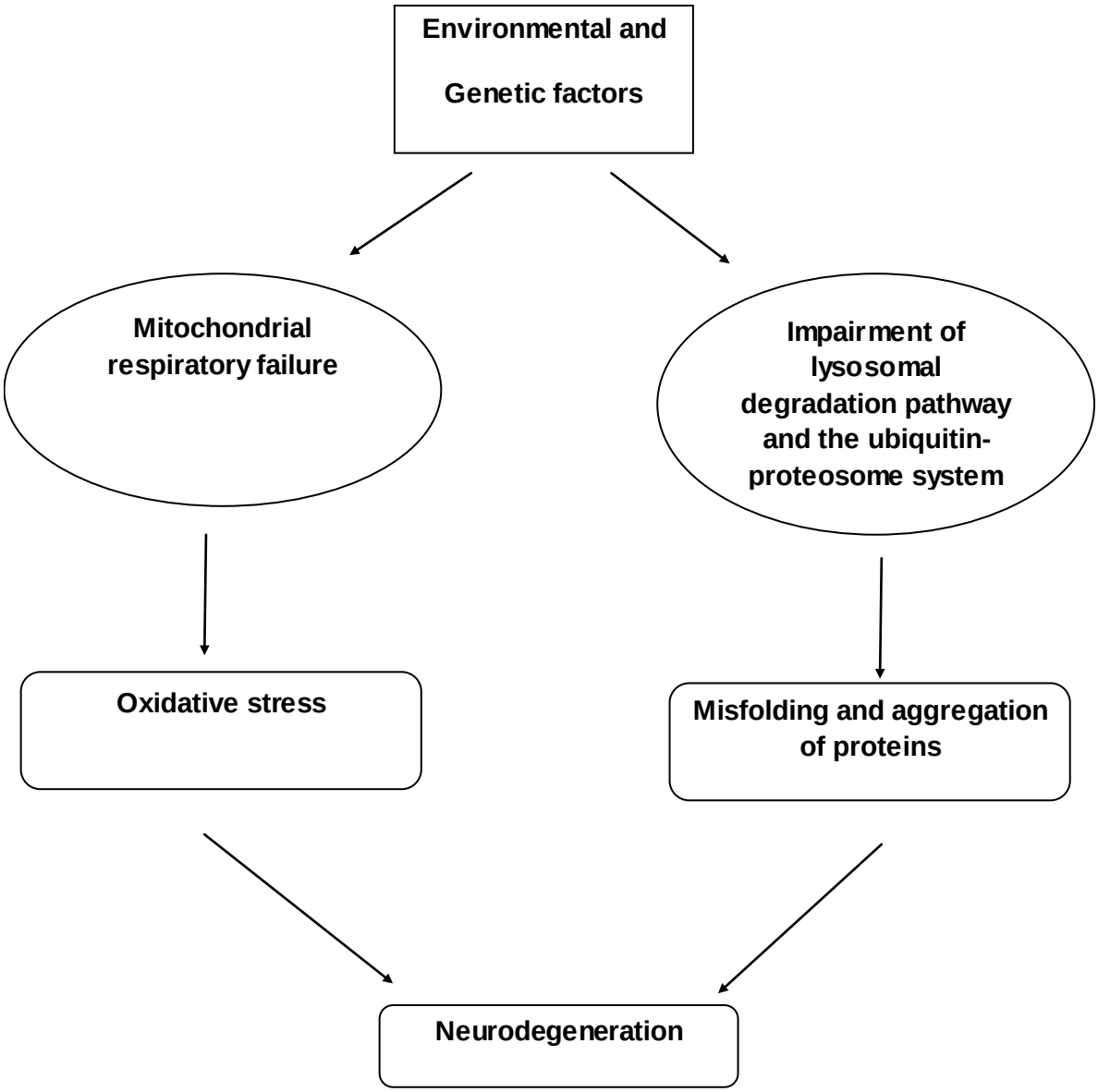

Figure 2.1 A schematic representation of environmental and genetic factors leading to neurodegeneration.

- Firstly, both these factors may induce mitochondrial respiratory failure and oxidative stress within the nigral neurons, which result in cell death (Jenner *et al.*, 1992). Oxidative stress occurs when there is an excessive amount of reactive free radicals present, usually a result of either the overproduction of reactive oxygen species or the failure of cell buffering mechanisms. These excess reactive species react with cellular macromolecules and impair their normal function (Yacoubian & Standaert, 2009). Molecular oxygen is consumed by mitochondrial respiration and produces normal byproducts such as hydrogen peroxide and

superoxide radicals that may be transformed into powerful oxidants. DA metabolism also leads to the formation of hydrogen peroxide that may induce oxidative stress (Hastings *et al.*, 1996). Mitochondrial dysfunction may also lead to an increase in the production of ROS. ROS such as hydrogen peroxide, may form toxic hydroxyl radicals, which in turn, react with nitric oxide to form peroxynitrite. Both cause cellular damage when they react with nucleic acids, proteins and lipids (Dauer & Przedborski, 2003).

Post-mortem studies on the brains of PD patients, showed a 35% increase in iron (Dexter *et al*., 1987). Interestingly the sites of neuronal death are also the sites at which iron accumulates (Zecca *et al*., 2004). Hydrogen peroxide reacts spontaneously with the ferrous iron present in the SNpc and gives rise to the formation of toxic free radicals especially the highly active hydroxyl radical (Figure 2.2) (Double *et al.*, 2002).

Figure 2.2 The Fenton reaction. Ferrous iron acts as a catalyst for oxidative reactions and catalyzes the formation of the highly reactive hydroxyl radicals and free iron (Fe^{3+}), from hydrogen peroxide (H_2O_2).

An increase of modified proteins and alterations in the antioxidant protective systems has been identified in the SNpc of PD patients. These modified proteins include UCH-L1 (Choi *et al.*, 2004) and nitrated α-synuclein (Giasson *et al.*, 2000), and the altered antioxidant protective system includes reduced levels of the antioxidant glutathione (GSH) (Sian *et al.*, 1994). Several strategies that have been proposed to limit oxidative stress include the development of monoamine oxidase inhibitors ((R)-deprenyl), enhancers of mitochondrial electron transport (Coenzyme Q10), antioxidants (Vitamin E) and molecules to promote endogenous buffering mechanisms (selenium) (Yacoubian & Standaert, 2009).

- Secondly, both these factors may decrease the activity of the ubiquitin-proteosome system (UPS) which leads to the misfolding and aggregation of proteins. This results in toxicity towards the neuron because these abnormal aggregates may have toxic properties (McNaught *et al.*, 2003). The primary protein involved is α-synuclein which is the main component of Lewy bodies and Lewy neurites in sporadic PD (Irizarry *et al*., 1998). Self aggregation is also proposed through point mutations (Conway *et al.*, 2000), overexpression (Masliah *et al.*, 2000) and oxidative damage to α-synuclein (Souza *et al.*,

2000). It is unclear which molecular form of α-synuclein is toxic as well as the mechanism of how neuronal injury occurs but it is being hypothesized that oligomers from α-synuclein exert toxic effects on cell membranes or proteosomal function, gene transcription or regulation, cell signalling pathways and cell death cascades. Modified α-synuclein may also cause changes in DA storage and release and α-synuclein may facilitate the activation of inflammatory mechanisms (Cookson & Van der Brug, 2008).

The impairment of two protein degradation systems in PD has been identified. They involve the impairment of the lysosomal degradation pathway and the ubiquitin-proteosome system (Betarbet *et al.*, 2005). The lysosomal degradation pathway is responsible for the degradation of oligomeric intermediates of α-synuclein (El-Agnaf *et al.*, 2003). Ubiquitin-proteosome is responsible for the labelling of the proteins with ubiquitin and for the facilitation of the degradation through proteosomes. Impairment of the protein degradation systems in PD involves mutations in the Parkin gene (Lücking *et al.*, 2000) that targets the protein for degradation, and the UCH-L1 gene (Leroy *et al.*, 1998) that acts as a recycling enzyme in neurons. The dysfunction of these proteins promotes protein aggregation. Strategies proposed to prevent protein aggregation or improve clearance of misfolded proteins include inhibitors of α-synuclein aggregation, enhancers of parkin or UCH-L1 function and molecules to promote lysosomal or proteosomal degradation pathways. These strategies are still being extensively studied (Yacoubain & Standaert, 2009).

2.1.4 Symptomatic treatment

PD is an incurable disease which is clinically characterized by bradykinesia, rigidity, resting tremor and postural instability. Treatment is invaluable in the improvement of the quality of life and functional capacity. Studies have shown that untreated PD patients have more rapid deterioration in motor function and that this leads to severe disability within less than 10 years. This highlights the need for neuroprotective therapies that may slow the disease progression and the development of disability (Löhle & Reichmann, 2010). Most of the drugs available are only applicable to the treatment of the psychiatric and motor symptoms of this disorder.

Levodopa still remains the most effective drug for the symptomatic treatment of PD. Levodopa is however associated with the development of dyskinesia and the ‘wearing off’ phenomenon. The occurrence of dyskinesias worsens with disease progression and with increased levodopa

dosages (Fernandez & Chen, 2007). Levodopa is a metabolic precursor of DA and can be transported across the blood-brain barrier into the central nervous system (CNS) with the aromatic amino acid transporter. Dopa decarboxylase converts levodopa to DA in the CNS and here-in lies its therapeutic effectiveness. However, levodopa is to a large extent metabolized in the intestinal mucosa and peripheral tissue before reaching the CNS. The enzyme responsible is catechol-o-methyltransferase (COMT) (Clarke, 2004). In conjunction with levodopa, COMT inhibitors (tolcapone) and MAO inhibitors ((R)-deprenyl) could help to delay the early 'wearing off' effect and together with a DA agonist (pramipexole), it may decrease motor complications such as dyskinesia (Rascol *et al*., 2002).

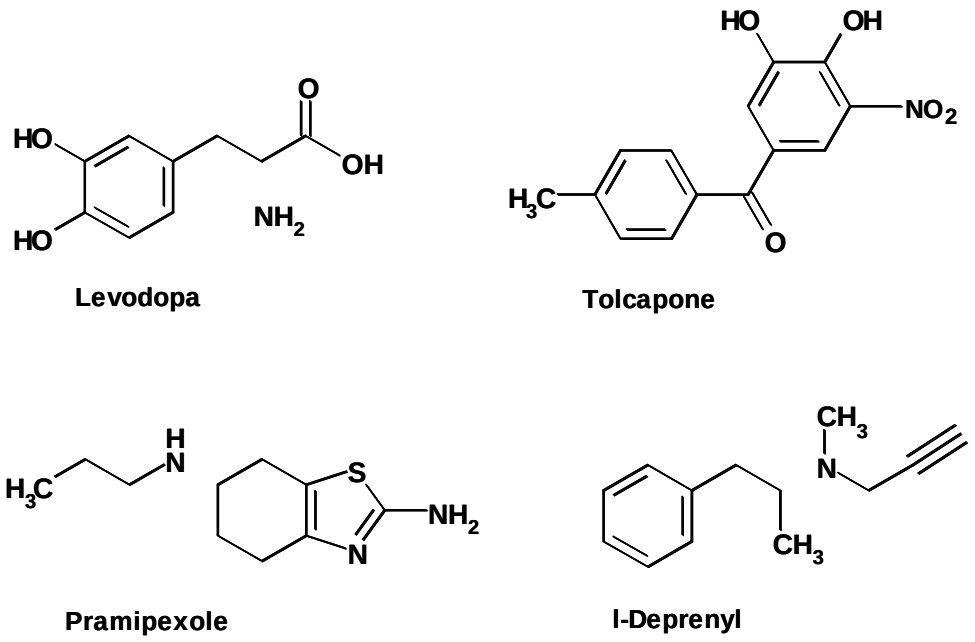

Figure 2.3 Structures of drugs frequently used in symptomatic treatment of PD.

Another drug of interest is amantadine, which is also registered as an antiviral agent for the treatment and prophylaxis of influenza A. Amantadine possesses mild anti-parkinsonian properties and can be used as initial treatment (Lees *et al*., 2009). Amantadine is a N-methyl-D-aspartate (NMDA) glutamate receptor antagonist and appears to also have anticholinergic properties that can alter DA release in the striatum. The exact mechanism of action of amantadine in PD is still unclear (Hallett & Standaert, 2004).

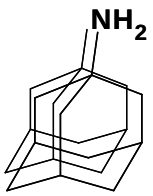

Amantadine

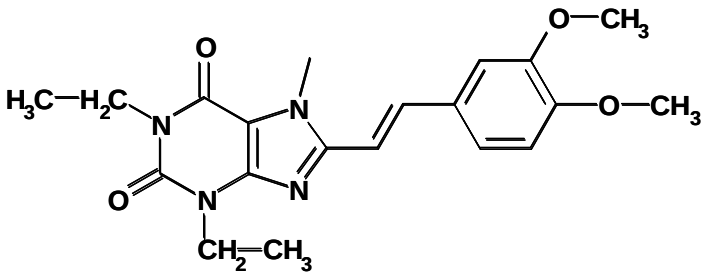

Istradefylline (KW-6002)

Figure 2.4 Structures of drugs with potential use in PD.

Adenosine A_{2A} antagonists have also been shown to be useful in the symptomatic treatment of PD. Antagonism of the A_{2A} receptor in the striatopallidal neurons reduces postsynaptic DA depletion and consequentially reduces the motor complications of PD (Schwarzschild *et al*., 2006). Studies carried out with istradefylline (KW-6002), a xanthine-based A_{2A} antagonist, showed that, when administered with a reduced dose of levodopa, the same level of symptomatic relief is experienced compared to that of an optimal levodopa dose. Istradefylline also reduces levodopa associated dyskinesias. However, when administered with an optimal levodopa dose, istradefylline only exhibit improved symptoms under some circumstances (Bara-Jimenez *et al*., 2003).

2.2 Monoamine oxidase

2.2.1 General background

In 1928, monoamine oxidase (MAO) was first discovered by Mary Hare-Bernheim who named it tyramine oxidase, because it catalyzed the oxidative deamination of tyramine. Hugh Blaschko later found that tyramine oxidase is the same enzyme responsible for the metabolism of primary, secondary and tertiary amines but not that of diamines. It was found that the enzyme is localized on the outer mitochondrial membrane of the rat liver mitochondria and Albert Zeller in 1938 subsequently renamed tyramine oxidase to mitochondrial monoamine oxidase (Schnaitman *et al*., 1967). Around this time, MAO was purified from bovine liver (Gomes *et al*., 1969) and bovine brain (Harada *et al*., 1971). During this preparation of purified MAO, the flavin adenine dinucleotide (FAD) cofactor was discovered and found to be covalently bound as 8-α-cysteinyl-FAD (Walker *et al*., 1971). Purified recombinant MAO enzymes are now produced with a *Pichia pastoris* yeast system (Edmondson *et al*., 2009).

In 1968, JP Johnston discovered that the inhibitor, clorgyline, can be used to distinguish between two isoforms of MAO, i.e. MAO-A and MAO-B. Low concentrations of clorgyline inhibits MAO-A and its preferential substrates are serotonin and noradrenaline. Low concentrations of ((R-deprenyl inhibits MAO-B and its preferential substrates are benzylamine and 2-phenylethylamine (Knoll, 1978). The substrates, dopamine, tyramine and tryptamine are oxidized by both MAOs (Glover *et al*., 1977).

The two isoenzymes of MAO (MAO-A and MAO-B) are present in most mammalian tissues (Tipton *et al*., 2004). They share an amino acid sequence identity of 70% and are encoded by separate genes (Bach *et al*., 1988). MAO-B is found predominantly in the basal ganglia of the brain (Saura *et al*., 1990). Its biological function is to participate in the degradation of DA to yield 3,4-dihydroxyphenylacetic acid and homovanillic acid and to deaminate β-phenylethylamine, an endogenous amine that stimulates DA release and inhibits neuronal DA uptake (Fernandez & Chen, 2007). MAO-A is mainly found in the intestinal tract (Grimsby *et al*., 1990). Its biological function is to deactivate circulatory catecholamines and dietary vasopressors, such as tyramine, that can act as false neurotransmitters. MAO-A also helps with the breakdown of neurotransmitters in the brain (Youdim *et al*., 1988). However, inhibition of MAO-A leads to two very serious side-effects the ‘cheese reaction’ and serotonin syndrome (discussed later).

Regulation of the concentrations of the neurotransmitters in the brain plays a role in movement, emotion and cognition and is thus thought to be associated with depression and neurodegenerative disorders such as PD (Nagatsu, 2004). MAO-B became of considerable importance when it was found to oxidize 1-methyl-4-phenyl-1,2,3,6-tetrahydropyridine (MPTP) to the active neurotoxin 1-methyl-4-phenylpyridinium (MPP^+) (Markey *et al*., 1984).

2.2.2 The therapeutic role of MAO-A

MAO inhibitors have been used in the treatment of depression because selective MAO-A inhibition in the CNS leads to elevated brain levels of DA, NA and 5-HT (Pletscher, 1991). Iproniazid was the first irreversible nonselective MAO inhibitor successfully used in depression, but it caused serious liver toxicity because of the hydrazine structure. Development of nonhydrazine MAO inhibitors resolved the liver toxicity issue but presented another serious side-effect, the 'cheese reaction' (Youdim *et al*., 1988).

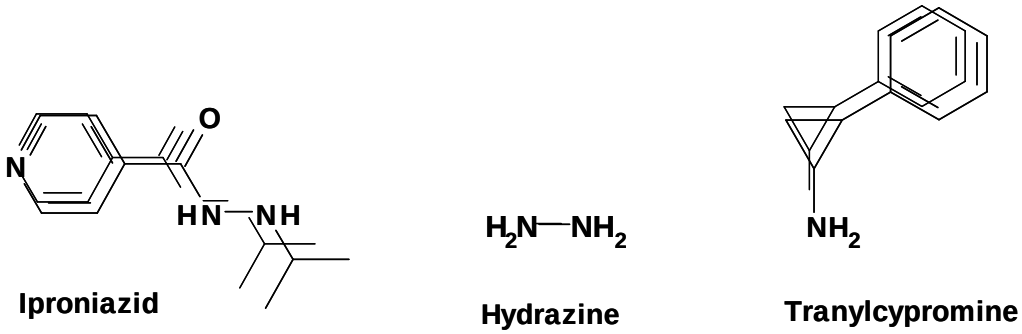

Figure 2.5 Structures of irreversible MAO-A inhibitors and hydrazine.

The 'cheese reaction' is induced by tyramine and other dietary amines, usually present in foods such as cheese, beer and wine. Under normal physiological conditions, this dietary amine is metabolized by MAO-A in the intestine and is thus prevented from entering the systemic circulation. Upon the administration of a MAO inhibitor, this protective system is deactivated and tyramine and other dietary amines are free to enter the systemic circulation. Here they release significant amounts of NA from peripheral adrenergic neurons and the consequence is severe hypertensive crises which can be fatal (Finberg *et al*., 1981).

Reversible MAO-A inhibitors, such as moclobemide, do not provoke the 'cheese reaction' because tyramine and other dietary amines in the intestine can overcome this inhibition and thus be normally metabolized (Haefely *et al*., 1992).

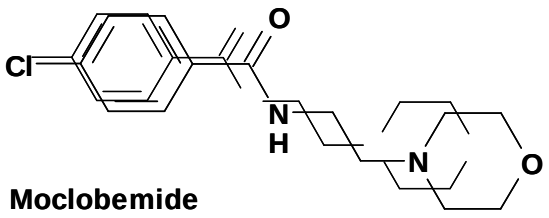

Moclobemide

Figure 2.6 Structure of the reversible MAO-A inhibitor, moclobemide.

This serious side effect led to the search for alternative antidepressant treatment strategies that was not MAO inhibitor related. Due to the role that MAO-A plays in the degradation of 5-HT, it cannot be administered with other 5-HT enhancing drugs such as selective serotonin reuptake inhibitors and tricyclic antidepressants. This combination leads to hyperstimulation of postsynaptic 5-HT receptors and causes the 'serotonin syndrome' a serious adverse reaction which may be possibly life-threatening (Boyer & Shannon, 2005). The 'serotonin syndrome' is characterized by the following symptoms: restlessness, hallucination, rapid heartbeat, sudden blood pressure changes, overactive reflexes, elevated body temperature, nausea, vomiting and diarrhoea (Fernandez & Chen, 2007).

Studies have shown that reversible MAO-A inhibitors are very effective in the treatment of depression in elderly patients (Gareri *et al*., 2000). MAO-A inhibitors have no significant effect on the mood of non-depressed elderly patients and healthy young patients (Bonnet, 2003). Research also indicate that when one isoform of MAO is completely inhibited, the other isoform would metabolize DA adequately, and so the steady-state level of DA will not change with selective inhibition of either MAO-A or MAO-B, but the release of DA will change (Riederer & Youdim, 1986). This could explain why PD patients experience a beneficial anti-symptomatic effect with moclobemide treatment. Furthermore, the antidepressant effect of moclobemide is useful in PD patients because 40-60% of patients show signs of depression (Youdim & Weinstock, 2004).

2.2.3 The therapeutic role of MAO-B

Fowler *et al*. (1980) observed that MAO-B levels in the human brain increases 4-5 fold upon aging and this presents a rationale for the involvement of MAO-B in PD. Increased levels of MAO-B depletes dopamine levels and increases the levels of dopanal and H_2O_2, both products of the catalytic reaction. Dopanal has been implicated in α-synuclein aggregation (Burke *et al*., 2008) and increased levels of H_2O_2 promote apoptotic cell death. Both have been implicated in the pathogenesis of PD.

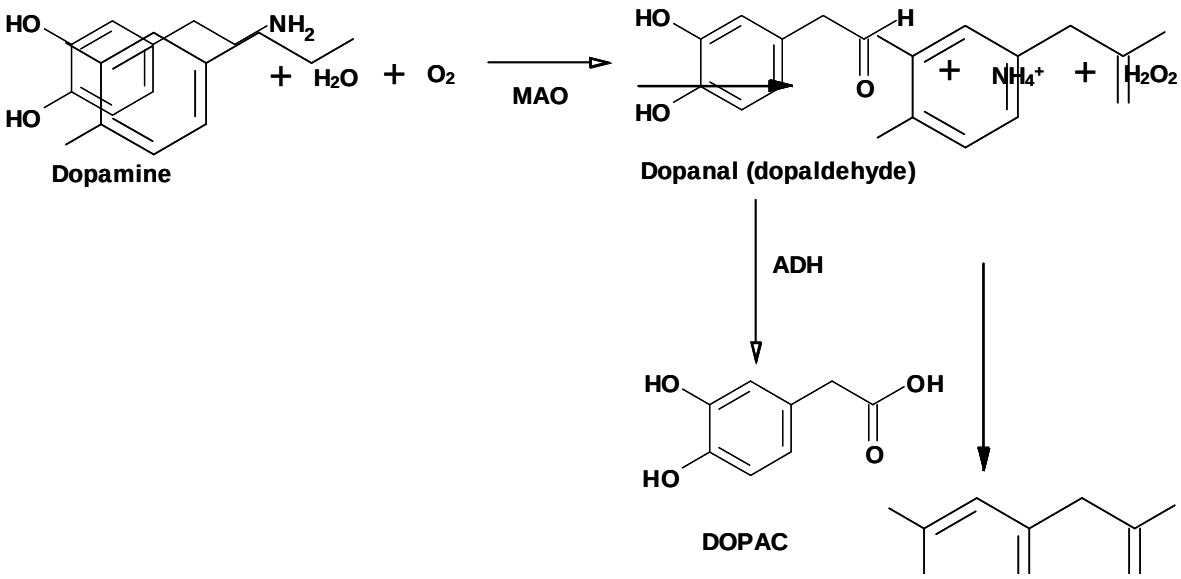

Figure 2.7 Reaction pathway of the degradation of dopamine to dopanal and DOPAC.

MAO oxidatively deaminates amines to the corresponding aldehyde and free imine with the generation H_2O_2 and the reduction of the FAD cofactor. The aldehyde is rapidly metabolized to acidic metabolites by aldehyde dehydrogenase (ADH) (Figure 2.8). Examples of these acidic metabolites are 5-hydroxyindole acetic acid (5-HIAA) from 5-HT and dihydroxyphenylacetic acid (DOPAC) from DA (Youdim & Bakhle, 2006). A deficiency in ADH could allow accumulation of neurotoxic aldehydes derived from DA (Grünblatt *et al*., 2004).

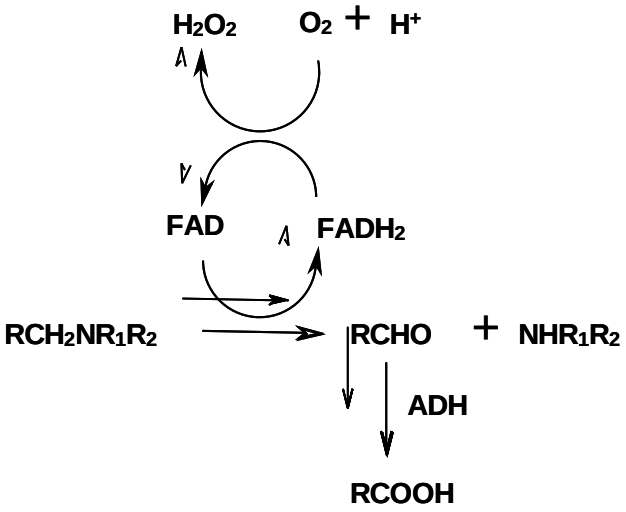

Figure 2.8 Oxidative deamination pathway of amines by MAO. The primary product is the corresponding aldehyde that is rapidly metabolized to a carboxylic acid by aldehyde dehydrogenase (ADH). The FAD-$FADH_2$ cycle generates H_2O_2 which requires inactivation by gluthatione peroxidase (Youdim & Bakhle, 2006).

It is known that MAO activity is influenced by iron levels in the brain (Symes *et al*., 1969). In the brain, gluthatione peroxidase, which uses glutathione (GSH) as cofactor, inactivates the formed H_2O_2. In PD, low GSH levels may lead to oxidative stress, since H_2O_2 accumulate under these conditions and is then available as substrate for the Fenton reaction (Figure 2.9) (Riederer *et al*., 1989). The highly reactive hydroxyl radical, which forms in the Fenton reaction, diminishes cellular anti-oxidants and reacts, and damages, lipids, proteins and DNA (Figure 2.9) (Youdim & Bakhle, 2006). The increase of MAO-B with age, increases the Fenton reaction components (H_2O_2) and subsequently increases hydroxyl radical formation. This increase is also seen in PD patients (Mandel *et al*., 2005).

Inhibition of MAO will reduce the MAO-catalyzed generation of potentially toxic aldehydes and H_2O_2. MAO inhibitors may therefore likely serve as neuroprotectants (Edmondson *et al*., 2009). As already mentioned, (R)-deprenyl is one example of a MAO inhibitor. Studies have shown (R)-deprenyl to slow PD progression. R-Deprenyl is effective both as adjuvant treatment with levodopa or as monotherapy (Pålhagen *et al*., 2006).

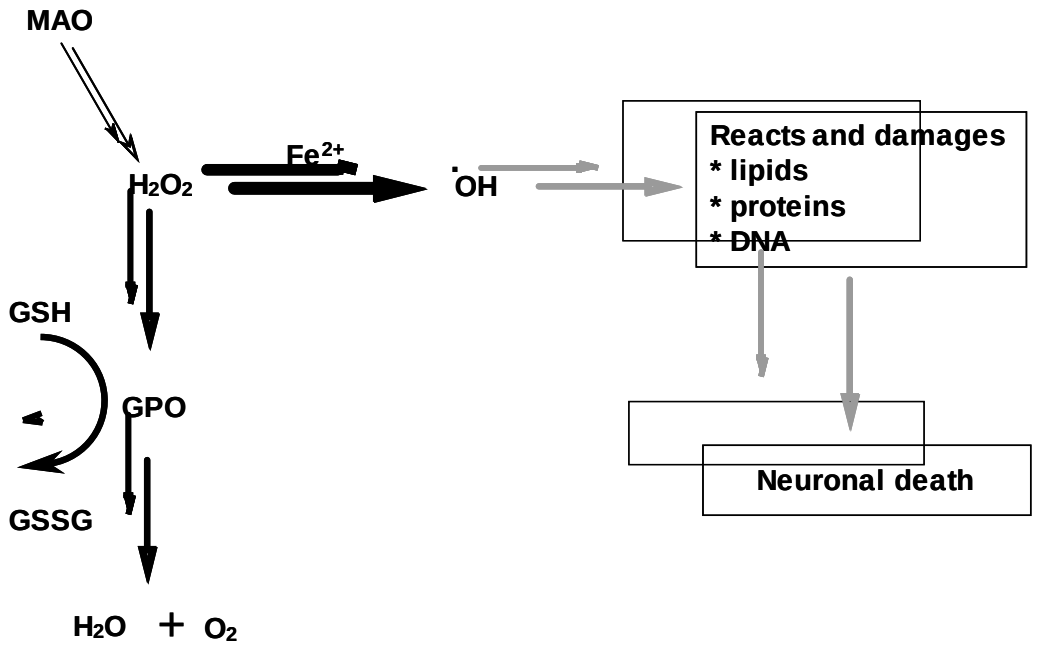

Figure 2.9 The mechanism of neurotoxicity of H_2O_2 induced by the Fenton reaction. Normally H_2O_2 is inactivated by glutathione peroxidase (GPO). In PD, gluthathione levels are low and thus H_2O_2 is converted to the highly reactive hydroxyl radical by Fe^{2+}. This radical has deleterious effects and causes neuronal damage and death (Youdim & Bakhle, 2006).

2.2.4 Inhibitors of MAO

In 1950 MAO inhibitors were clinically used as antidepressants and the first inhibitor to be used was iproniazid. Interestingly, this compound was initially developed for tuberculosis treatment. Iproniazid was found to be ineffective in the treatment of tuberculosis but nonetheless led to the development of other hydrazine derivatives of MAO such as phenelzine. Iproniazid caused severe liver toxicity and hypertensive crises. The liver toxicity was overcome by the development of non-hydrazine derivates such as pargyline and tranylcypromine but the potential of developing hypertensive crises still persisted (Youdim *et al*., 2006). Selective MAO-B inhibitors and reversible MAO-A inhibitors such as moclobemide and lazabemide did not cause this problem (Da Prada *et al*., 1990).

Two classes of MAO-A and MAO-B inhibitors can be distinguished:

- Reversible, inhibitors bind non-covalently to the active site of MAO-A and MAO-B and inhibition can be overcome by an increase of the substrate concentration. Experimental inhibitors include; 1,4-diphenyl-2-butene, a contaminant of polystyrene bridges used in MAO-B crystallization (Binda *et al*., 2003); trans,trans-farnesol a component of tobacco

smoke (Hubálek *et al*., 2005); 8-(3-chlorostyryl)caffeine (CSC) also a A_{2A} adenosine receptor antagonis (Chen *et al*., 2002) and safinamide, a DA modulator which has entered phase III clinical trials (Caccia *et al*., 2006).

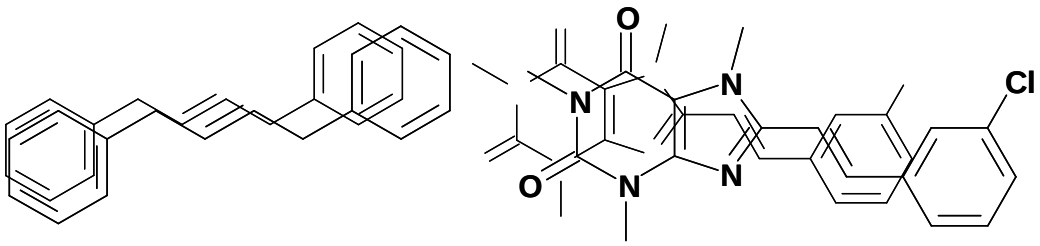

1,4-Diphenyl-2-butene

8-(3-Chlorostyryl)caffeine (CSC)

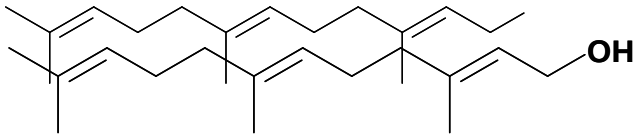

Trans,trans-farnesol

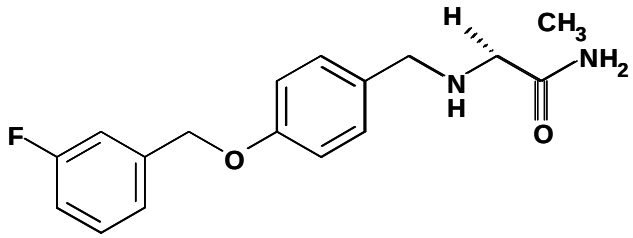

Safinamide

Figure 2.10 Examples of reversible MAO-B inhibitors.

Examples of reversible selective MAO-A inhibitors are brofaromine, toloxatone, cimoxatone and befloxatone, which are clinically used in the treatment of various depression states such as atypical and resistant depression (Bortolato *et al*., 2008).

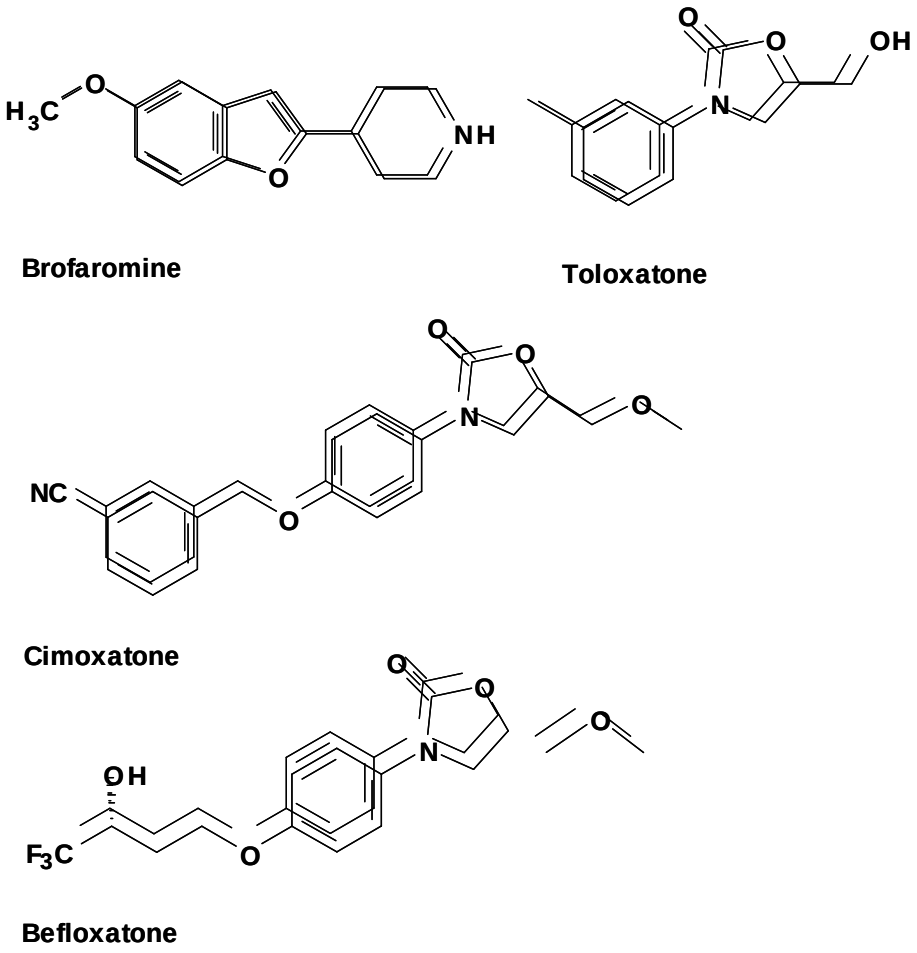

Figure 2.11 Structures of selective reversible MAO-A inhibitors

- Irreversible, suicide inhibitors bind to the enzyme in a irreversible competitive manner. The inhibitor is then oxidized to the active inhibitor which binds covalently to the active site of the enzyme via interaction with the FAD cofactor. No amine metabolism is possible and this inhibition can only be overcome by *de novo* enzyme synthesis (Abeles & Maycock, 1976). Clorgyline is a selective, irreversible inhibitor of MAO-A and isocarbaxazide is a non-selective inhibitor of MAO-A and MAO-B. They prove to be effective in the treatment of depressive disorders but the 'cheese reaction' prevents their clinical use as antidepressants.

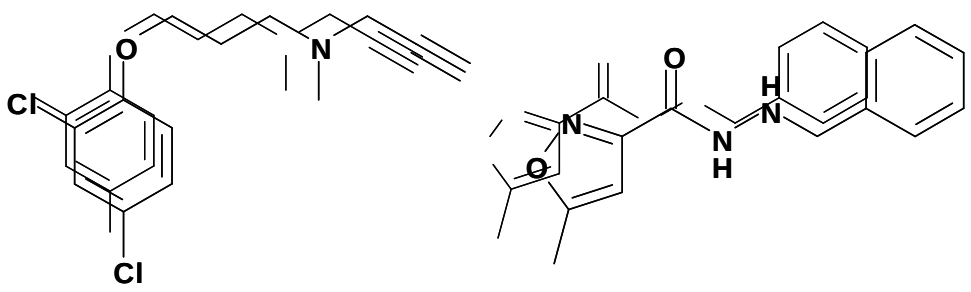

Clorgyline **Isocarboxazide**

Figure 2.12 Structures of the irreversible MAO-A inhibitor, clorgyline and the nonselective irreversible MAO inhibitor, isocarboxazide.

Examples of irreversible MAO-B inhibitors are the propargylamines, R-deprenyl (Knoll & Magyar, 1972), rasagiline (Finberg *et al*., 1981) and the experimental inhibitor PF-9601 N (Perez *et al*., 2003).

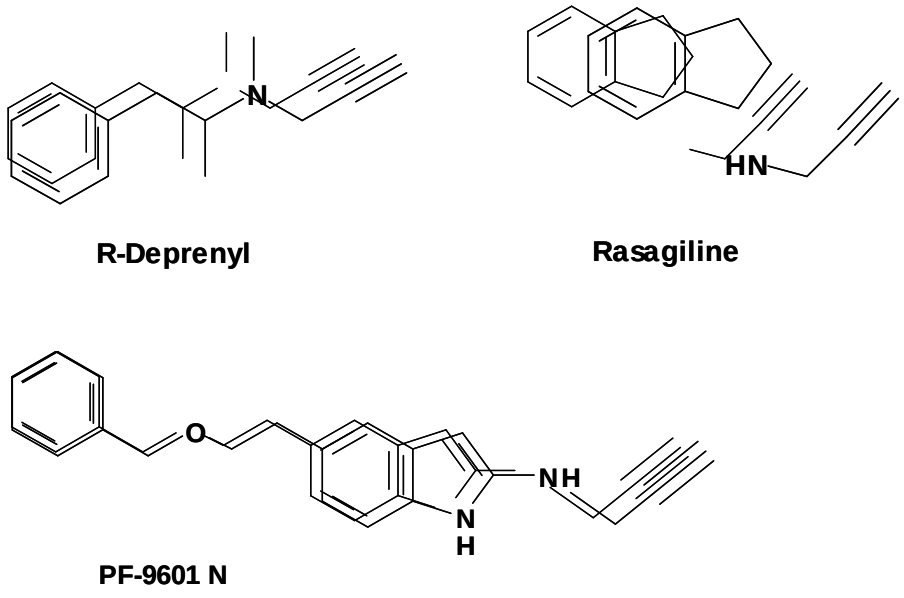

R-Deprenyl **Rasagiline**

PF-9601 N

Figure 2.13 Structures of irreversible MAO-B inhibitors.

R-Deprenyl undergoes first pass hepatic metabolism and forms three metabolites, desmethylselegiline, l-methamphetamine and l-amphetamine. The amphetamine metabolites are potentially neurotoxic and are associated with cardiovascular and psychiatric adverse effects (Churchyard *et al*., 1997).

2.2.5 The three dimensional structure of MAO

Human MAO-A and human MAO-B consist of 527 and 520 amino acids, respectively, and have a subunit molecular weight of 59 700 and 58 000, respectively. Both isoenzymes contain the pentapeptide amino acid sequence, Ser-Gly-Gly-Cys-Tyr, where the FAD cofactor covalently binds through a 8α-thioether linkage to the cysteine (Cys) amino acid (Bach *et al*., 1988).

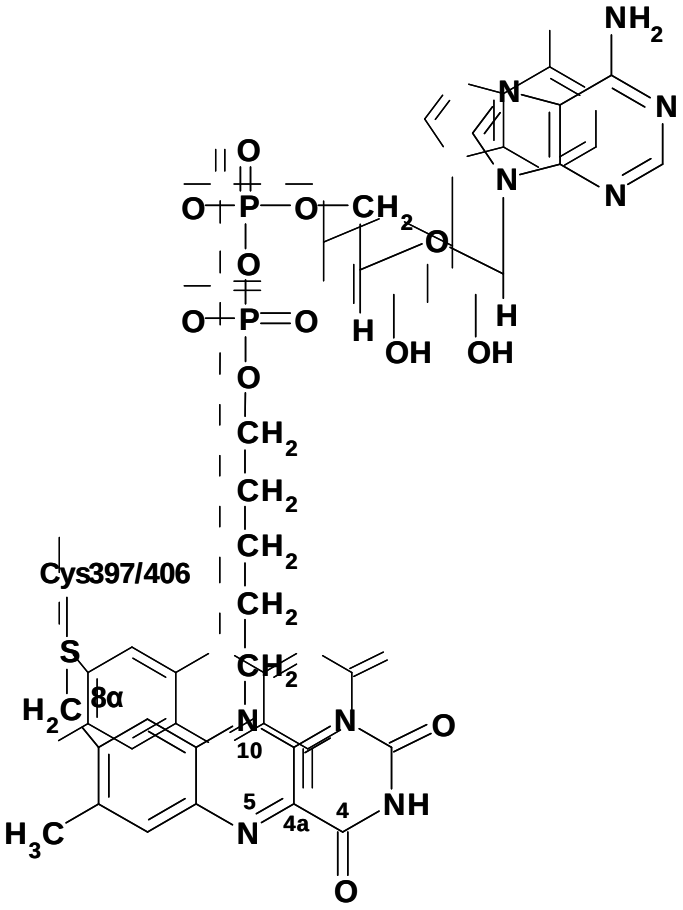

Figure 2.14 The structure of covalent FAD in MAO. FAD binds to MAO via a thioether linkage between the cysteinyl residue, Cys_{397} and Cys_{406} of the enzyme MAO-B and MAO-A, respectively, and the 8α-methylene of the isoalloxazine ring. The reactive sites of the isoalloxazine ring are the N(5) and C(4a) atoms. (Edmondson *et al*., 2004a).

The structure of the flavin ring in free FAD is planar but when bound to MAO-B, is bent 30° from planar. The reactive centers, N(5) and C(4a) atoms, of the flavin ring assumes a sp^3 -like orientation and not the normal sp^2 orientation. This reduced steric effect on the two reactive centers should facilitate the formation of flavin adducts to these positions (Binda *et al*., 2003).

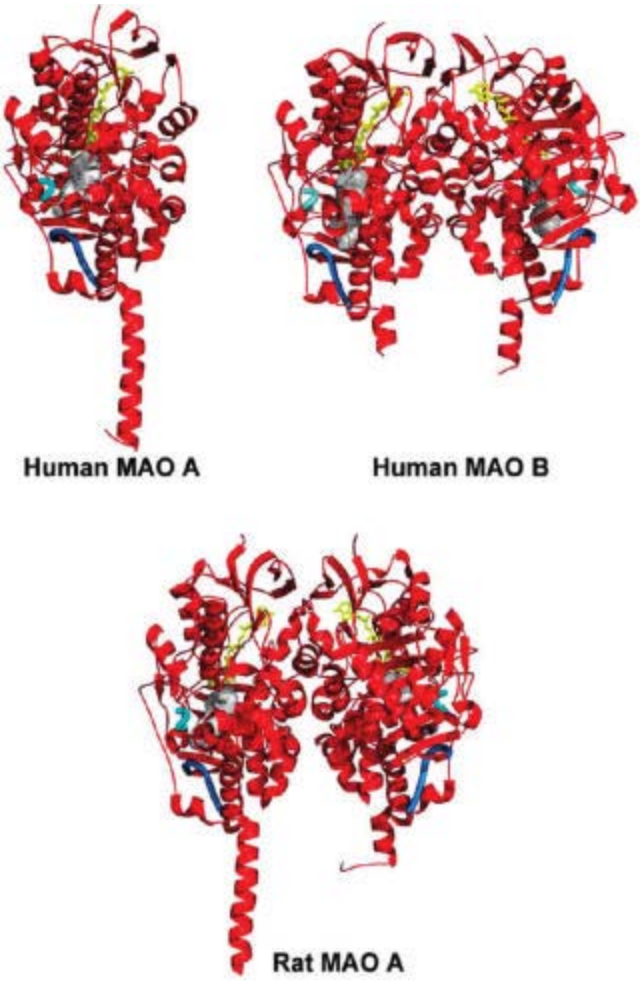

Figure 2.15 Ribbon diagram displaying the structures of human MAO-A, human MAO-B and rat MAO-A. The C-terminal transmembrane helices are pointing down, the FAD cofactor is displayed as yellow balls and sticks and the active site cavity is displayed as a gray surface. The cavity-shaping loop is displayed in cyan. In human and rat MAO-A these residues are 210-216 and in human MAO-B the residues are 201-207. In human MAO-B the entrance cavity loop, residues 99-110 is coloured blue and the corresponding residues in human MAO-A and rat MAO-A has the same conformation (Edmondson *et al*., 2009).

The structures of human MAO-B (Binda *et al*., 2002), human MAO-A (Son *et al*., 2008) and rat MAO-A (Ma *et al*., 2004) have previously been determined. The x-ray structure of MAO-B, MAO-A, and rat MAO-A has been determined at resolutions of 1.65 Å, 2.2 Å and 3.3 Å, respectively. Each monomeric unit contains a membrane binding domain, a flavinbinding

domain and a substrate binding domain. The oligomeric states are the largest difference in these structures where human MAO-B and rat MAO-A are dimers and human MAO-A is a monomer (Figure 2.15).

The MAO-B cavity is bipartite and consists of two separate spaces, termed the entrance cavity and substrate cavity. In order for a substrate to reach the flavin centre, the flexible entrance cavity loop (residue 99-110) must first move away for the substrate to gain entry to either the entrance cavity (volume 290 Å) or substrate cavity (volume 420 Å). Isoleucine (Ile) 199 amino acid side chain acts as a 'gate' to seperate the two cavities. This side chain can either exist in a closed or open conformation depending on the bound substrate. This has been shown to determine inhibitor specificities (Hubálek *et al*., 2005). Depending on the conformation of the gating residue Ile199, the active cavity can host small inhibitors such as isatin and tranylcypromine where the small active site cavity is separate from the entrance cavity and opens up to the exterior like a funnel. The active site cavity can also bind cavity-filling ligands such as safinamide, trans,trans-farnesol and 1,4-diphenyl-2-butene where the cavity is in the shape of a ellipsoid (Figure 2.16). The small inhibitors show lower affinities for the binding to MAO-B whereas the cavity-filling ligands show a higher affinity for MAO-B (Edmondson *et al*., 2009).

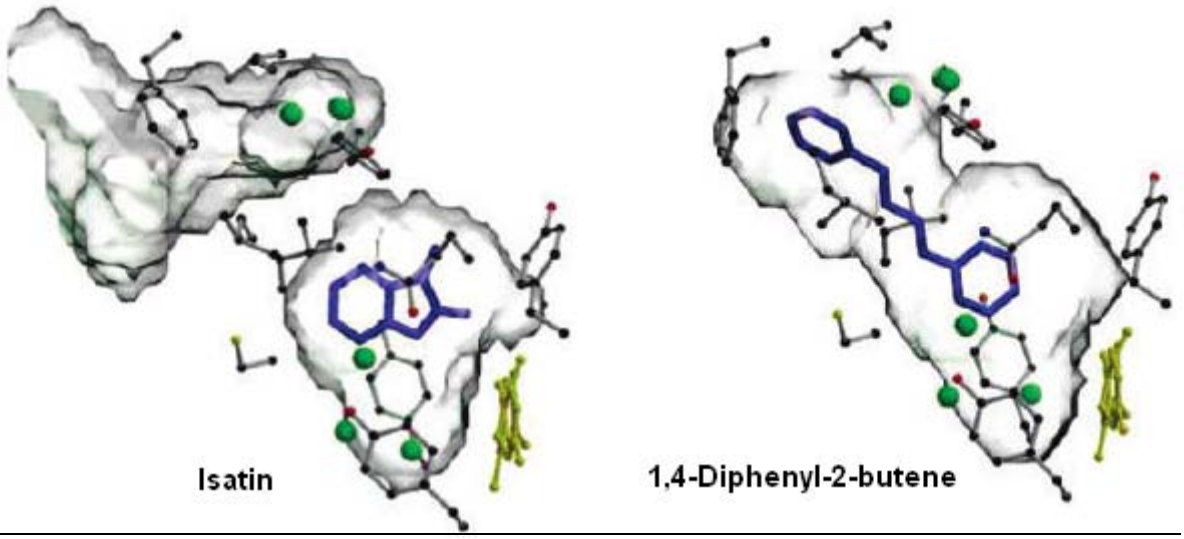

Figure 2.16 The structure of the active site cavity of MAO-B with isatin and 1,4-diphenyl-2-butene bound. The isoleucine 199 side chain is in the closed conformation with isatin (left) and in the open conformation with 1,4-diphenyl-2-butene (right) (Edmondson *et al*., 2009).

In human MAO-B, restriction of the orientation that inhibitors may adopt is caused by the tyrosine side chain (Tyr326). In human MAO-A this restriction is less pronounced because Ile335, a smaller residue occupies that space. Important active site residues that are present in both enzymes include the Tyr pair at the *re* face of the isoalloxazine ring, which is termed the aromatic cage, and the hydrogen bonded Lys residue at the N(5) position (Figure 2.17). These amino acids play an important role in the enzyme specificity towards a substrate or inhibitor (Binda *et al*., 2003).

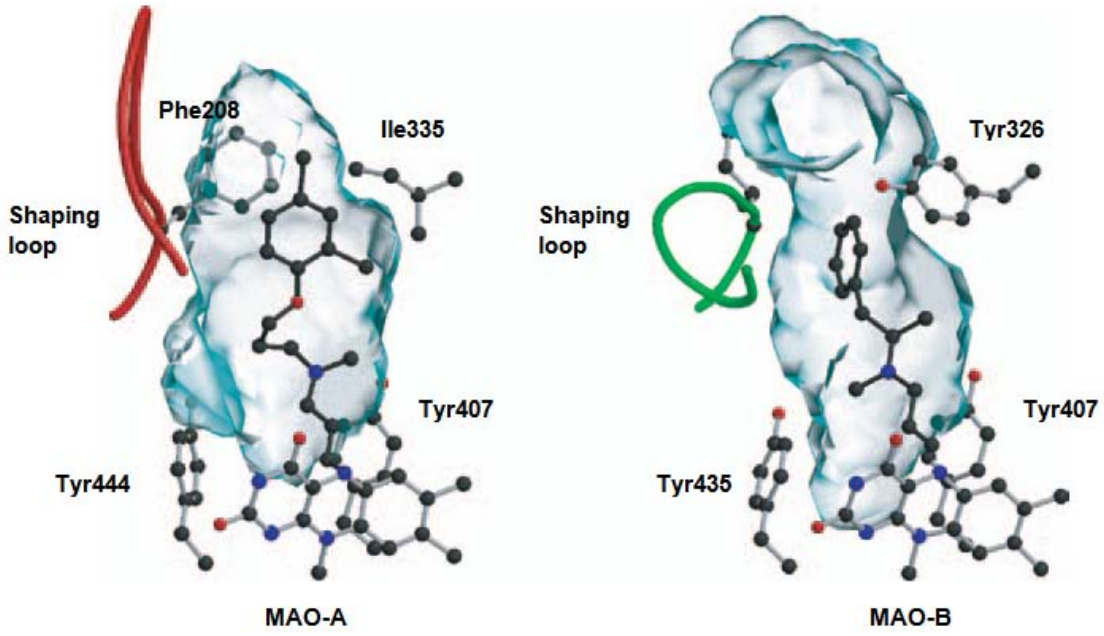

Figure 2.17 An illustration of important amino acids present in human MAO-A and MAO-B. The Tyr side chains (Tyr407 and Tyr444 in MAO-A, Tyr398 and Tyr435 in MAO-B) forms the aromatic cage, respectively. Amino acids Ile335 and Phe208 in MAO-A and Tyr326 and Ile199 in MAO-B play a major role in determining their respective enzyme substrate/inhibitor specificities (Edmondson *et al*., 2007).

Studies have shown that the C-terminal helix of MAO-B, which consists of 29 amino acids, is responsible for anchoring the enzyme to the mitochondrial outer membrane (Mitoma & Ito, 1992). Truncation of these C-terminal residues will lead to a significant decrease in the catalytic activity of MAO-B but will not affect its inhibitor specificity (Rebrin *et al*., 2001).

Andrés *et al*. (2004) proposes that MAO-A crystallizes as a monomer due to a conserved glutamate residue in MAO-B that is mutated to a lysyl residue in human MAO-A. Mutation occurs at a site located near the dimeric interaction and this result in the disruption of the dimer structure. High resolution x-ray structures of MAO-A showed that human MAO-A differs from rat

MAO-A and human MAO-B in loop conformations of residues 108-118 and 210-216. These studies showed that the loop conformations are important components of the active site and that they affect the substrate/inhibitor specificities of human MAO-A (De Colibus *et al*., 2005). Mutations of the Gly110 residue on the 108-118 loop, causes MAO-A to undergo an extensive drop in activity. However, when the enzyme is anchored to the mitochondrial membrane, the drop in activity lessens. This anchoring of the enzyme causes loop 108-118 to be more flexible and proves to be essential in controlling substrate access to the active site (Son *et al*., 2008).

Rat MAO-A share a sequence identity of 87% with human MAO-A over the whole molecule and when the two residue loops, 108-118 and 210-216 are compared, they share a sequence identity of 90%. The backbone structure of rat MAO-A compared to human MAO-A is nearly identical. However, despite the high sequence identity, the difference between the structures of rat MAO-A and human MAO-A is exceptional (Son *et al*., 2008). Subsequently, care should be taken when extrapolating detailed molecular data from rats to humans (Edmondson *et al*., 2009).

2.2.6 Mechanistic proposals for MAO catalysis

Amine substrates undergo oxidative catabolism by MAO and in both MAO-A and –B the FAD cofactor is absolutely crucial for this catalysis. MAO-A and –B uses O_2 as the electron acceptor in the oxidative deamination of neurotransmitters. The deprotonated amine moiety on the substrate firstly binds to the active site of the MAO enzymes and is oxidized to a protonated imine, with the FAD cofactor being reduced to its hydroquinone form. The FAD cofactor reacts with O_2 and generates H_2O_2 and the oxidized flavin. The protonated imine dissociates from the enzyme and undergoes a noncatalyzed hydrolysis to its corresponding aldehyde and ammonia (NH_4^+) (Figure 2.18) (Edmondson *et al*., 1993).

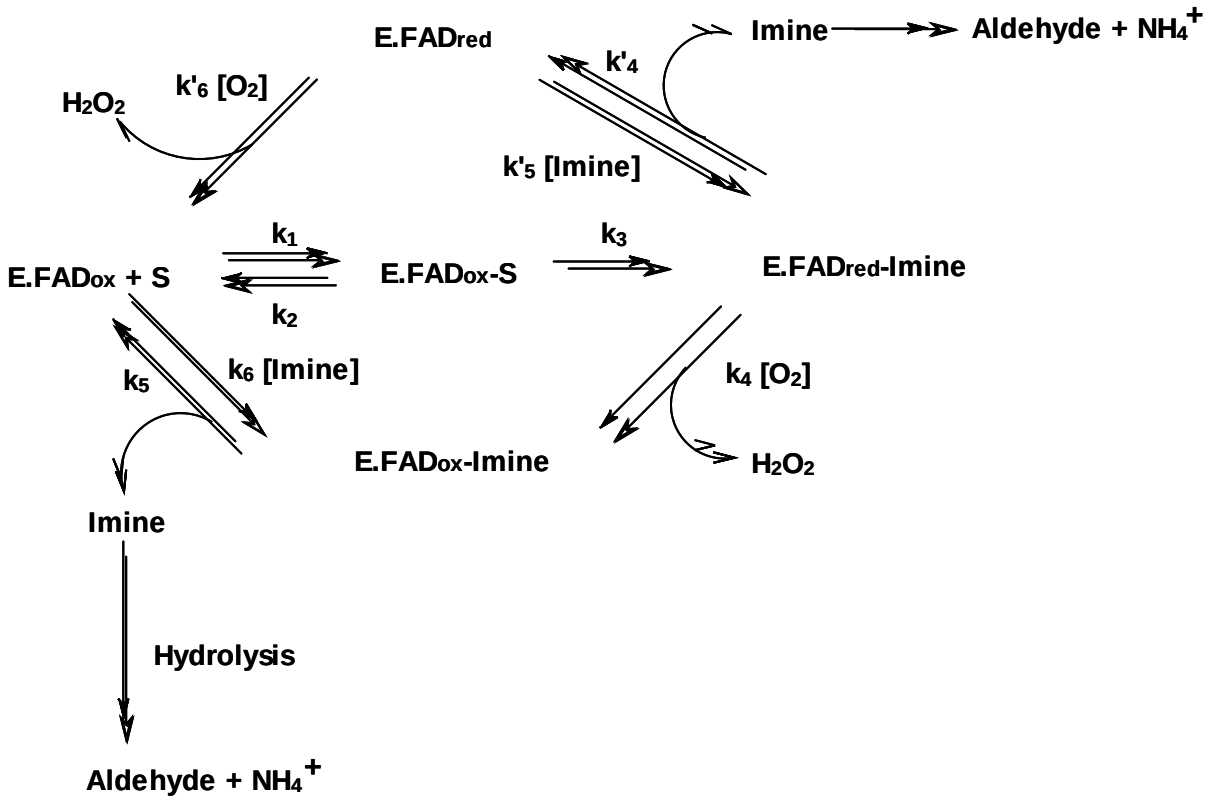

Figure 2.18 The mechanism of MAO catalysis. The catalytic pathway is dependent on the nature of the substrate (S). Benzylamine and its analogs follow the lower branch. Phenethylamine follows the top loop where the imine product dissociates from the reduced enzyme, leaving the enzyme free to react with O_2 and generate H_2O_2. The products of imine hydrolysis are ammonia and aldehyde (Ramsey, 1991).

It is important to note that the deprotonated form of the amine substrate binds to the MAO enzymes for interaction with the flavin. Two mechanisms have been proposed for the electron transfer from the amine to the flavin in MAO catalysis.

- Single electron transfer (SET) mechanism

  This mechanism was proposed by Silverman *et al*. (1980). They proposed that the pKa of α-CH protons of amines requires a very strong base for abstraction and that it is possible by oxidizing the amine to the amine cation radical form, which results in the acidification of the α-CH group. This mechanism takes place through two one-electron transfers from the substrate to the flavin. The first one electron transfer step is a slow process in which the non-bonded electron of the amine nitrogen is transferred to the flavin, resulting in the formation of the amine radical cation and the flavin semiquinone radical. The α-protons of

the amine are now more acidic and a second one electron transfer takes place. The products formed are the iminium ion and the reduced flavin (Figure 2.19).

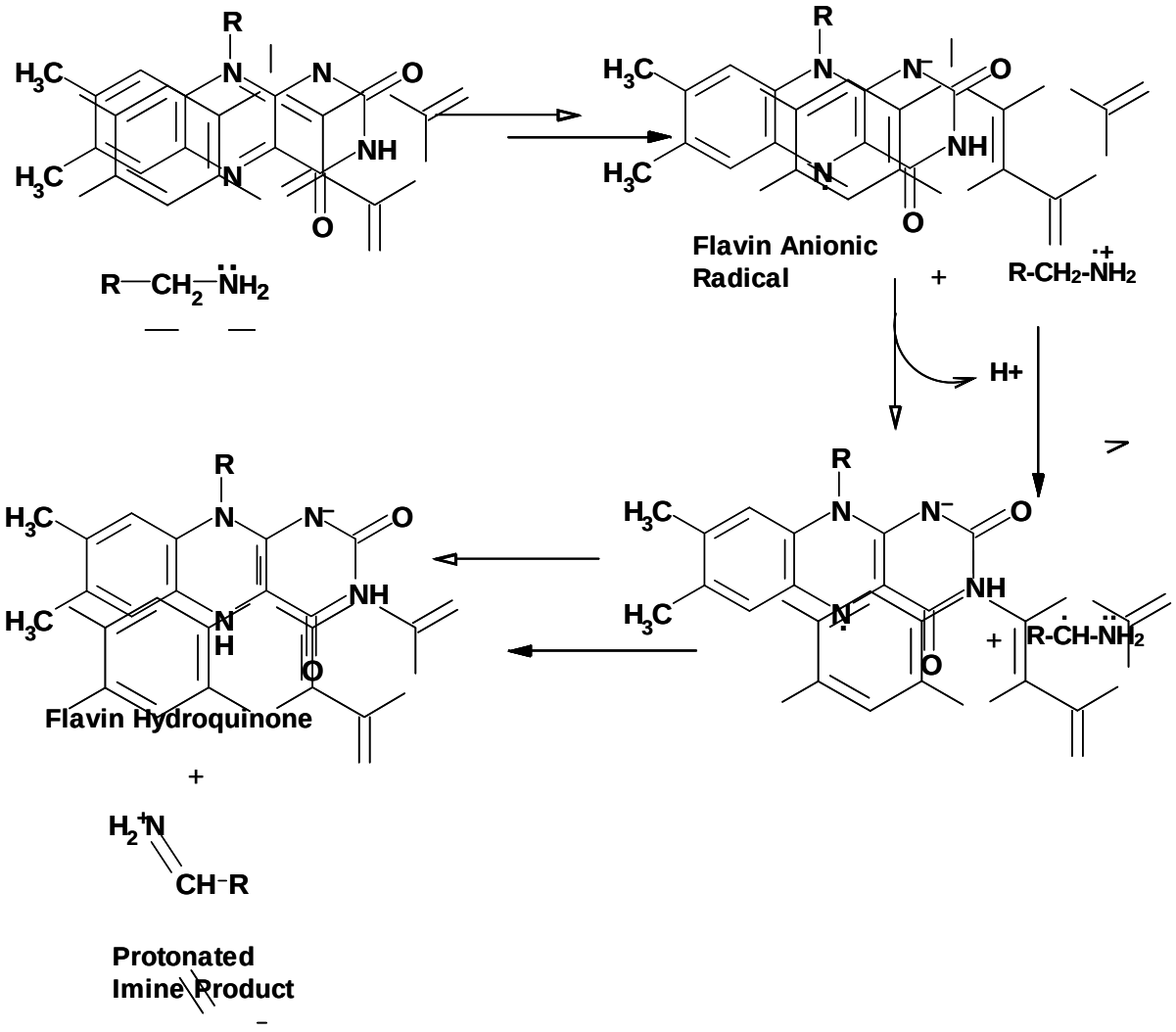

Figure 2.19 The SET mechanism. The first step requires the one electron oxidation of the lone pair on the amine nitrogen substrate to form an aminium cation radical and a flavin radical. H^+ abstraction takes place by an active site base and following a second one electron transfer from the amine to the flavin hydroquinone, the protonated imine is formed as product (Edmondson *et al*., 2004b).

However, there is controversy as to whether this mechanism is possible. With the structural elucidation of MAO-B it was found that there is no basic amino acid residue present in the catalytic site that could act as a base in catalysis. Furthermore, no flavin radical intermediates are detected spectrally in stopped-flow experiments (Walker & Edmondson, 1994). Also magnetic fields have no influence on the rate of enzyme reduction (Miller *et al*.,

1995). Finally, the oxidation-reduction potential of the FAD cofactor is too low (~40 mV) (Newton-Vinson & Edmondson, 1999) for it to be an effective oxidant of the deprotonated amine (E_m = 1.5 V) (Hull *et al*., 1969). This leads to the conclusion that the SET mechanism for amine oxidation is both kinetically and thermodynamically impropable (Edmondson *et al*., 2004b).

- Polar nucleophilic mechanism

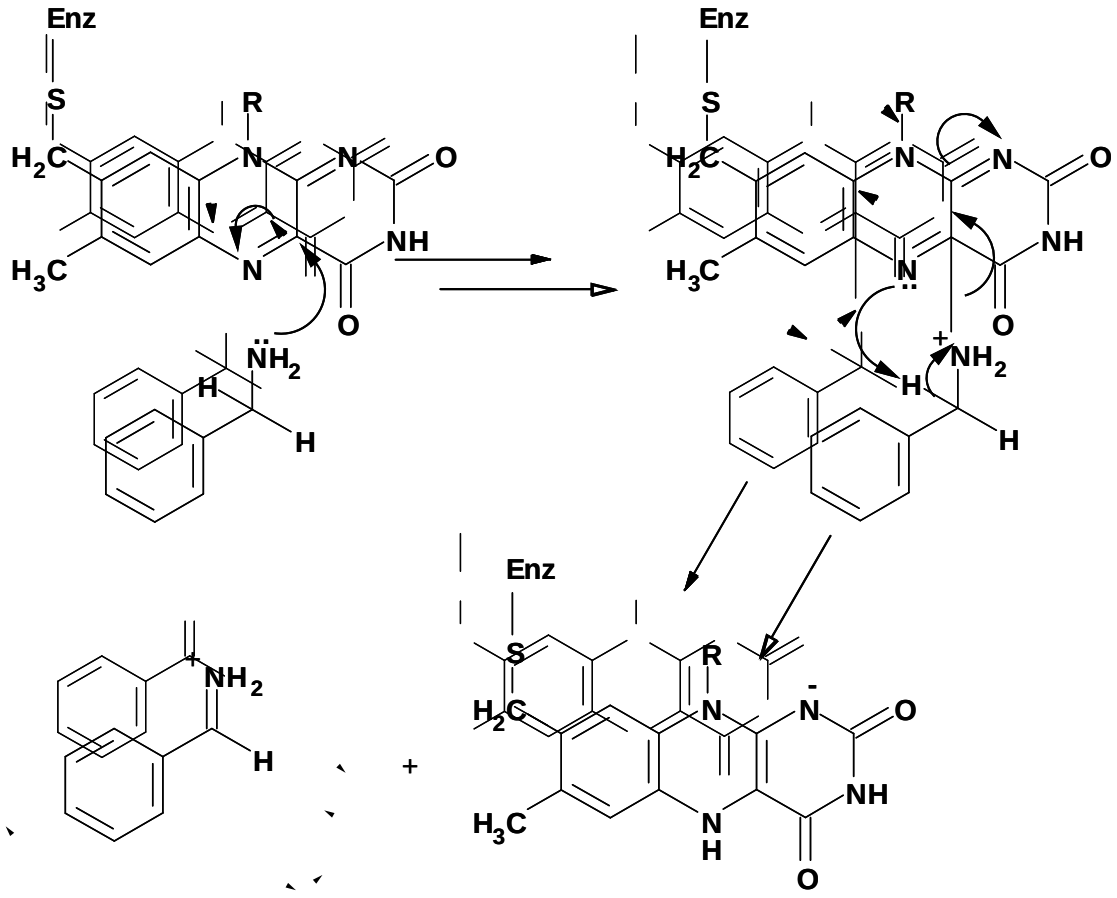

Figure 2.20 The polar nucleophilic mechanism. The deprotonated amine launches a nucleophilic attack on the C(4a) position of the flavin and forms an adduct. This formation causes the N(5) position to become a very strong base which leads to the abstraction of the α-pro-R-H from the substrate. The resulting products are the protonated imine and the flavin hydroquinone (Edmondson *et al*., 2004b).

This mechanism was proposed by Miller & Edmondson (1999). It is based on the observation that Hammett plots of steady-state and rapid reaction kinetic data on a series of para-substituted benzylamine analogues delivers a ρ-value of 2. This was also observed in studies with rat MAO-A and contributes to the proposed mechanism that abstraction of an H^+ from the pro-R α-CH group is the preferred mode of C-H bond cleavage (Wang & Edmondson, 2007). The pKa of the benzyl hydrogen is ~25 and for abstraction to take place the flavin must first be activated to become a strong base, since no basic amino acid residues are present in the catalytic site. The isoalloxazine ring is in a bent conformation and the N(5) atom assumes a sp^3-like conformation. The lone pair of the basic amine substrate facilitates a nucleophilic attack on the C(4a) position, resulting in a flavin-substrate adduct. On formation of this adduct the N(5) position becomes a very strong base, with a pKa of ~25, which would provide sufficient basicity to abstract the α-pro-R-H from the substrate (Figure 2.20) (Edmondson *et al*., 2009).

2.3 Copper containing amine oxidase

Amine oxidases are divided into two main groups, the FAD cofactor containing enzymes and the topaquinone cofactor containing enzymes. The latter is also known as semicarbazide-sensitive amine oxidase (SSAO). SSAOs are copper containing enzymes which, like MAO, catalyses the oxidation of primary amines to the corresponding aldehyde, with the reduction of molecular oxygen to hydrogen peroxide and the simultaneous release of ammonia (Klinman & Mu, 1994). SSAO differs from MAO by their sensitivity of inhibition by carbonyl-group reagents such as semicarbazide. This is due to the presence of a 6-hydroxydopa[2,4,5-trihydroxyphenylalanine quinone (TPQ)] residue, as the redox cofactor.

SSAO enzymes exist in two forms;

- The tissue-bound or cell surface SSAOs.
  They contain a short intracellular domain, a single trans-membrane domain and a long extracellular domain that includes the catalytic site.

- The soluble or plasma forms .
  They are formed through the proteolytic cleavage of the membrane bound SSAO (Tipton *et al*., 2004).

Both these enzymes are present in most mamillian tissue where they utilize benzylamine and methylamine as substrates and are inhibited by semicarbazide and hydroxylamine. Their highest activity is in the smooth muscle cells and the adipose tissue. Their biological functions thus include amine catabolism, glucose uptake and the lipolysis of adipocytes (Jalkanen & Salmi, 2001).

SSAOs are homodimers with an overall mushroom shape and contain subunits ranging in size from 70-95 kDa depending on the species. Each subunit contains a copper ion [Cu(ll)] and a covalently bound TPQ, which is formed through the oxidation of a single tyrosine residue. The structure of E.coli copper containing amine oxidase is representative of all known structures (Figure 2.21). The amino terminal domain D1 is not present in all species and its function is still unknown. D2 and D3 lies in the periphery and D3 plays a role in the substrate entrance/exit channels. D4 contains 440 C-terminal residues and forms the subunit interface which contains the active site (Dawkes & Phillips, 2001).

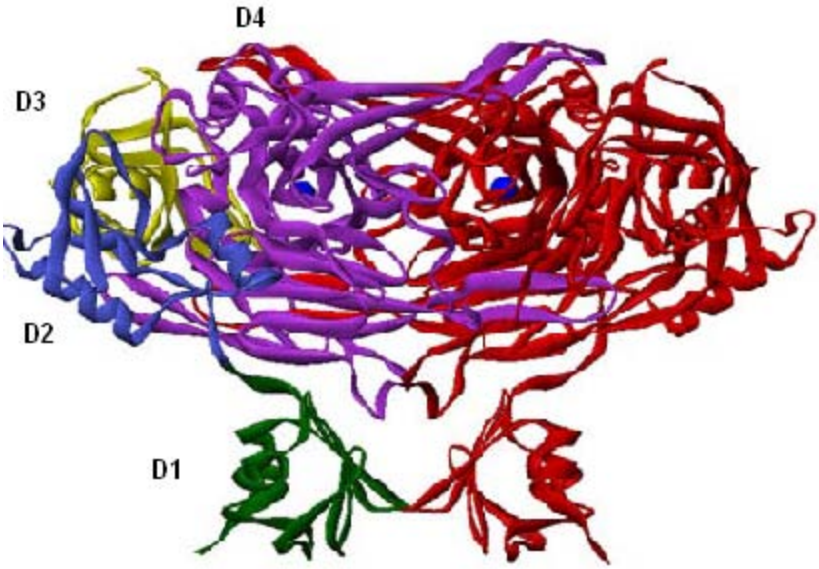

Figure 2.21 A ribbon diagram of the copper containing amine oxidase homodimer found in the *E.coli* species. One monomer is coloured red and the other monomer is divided and coloured in domains; D1 green, D2 blue, D3 yellow and D4 purple. The copper ions are represented as blue spheres (Brazeau *et al*., 2004).

Parsons *et al*. (1995) suggests that there are two conformations in which the TPQ cofactor can exist, “off-copper” or “on-copper”. This implies that the position of TPQ is vital for activity. In the “off-copper” or active state, Cu(II) is coordinated by three histadines (distance ~2.0 Å) and two water molecules, an axial water (distance ~ 2.4 Å) and an equatorial water (distance 2.0 Å), rendering it in a square pyramidal arrangement. In the “on-copper” or inactive state the axial water is displaced by the oxygen on position 4 of the TPQ and the equatorial water is lost, rendering it in a tetrahedral geometry (Figure 2.22) (Murray *et al*., 1999).

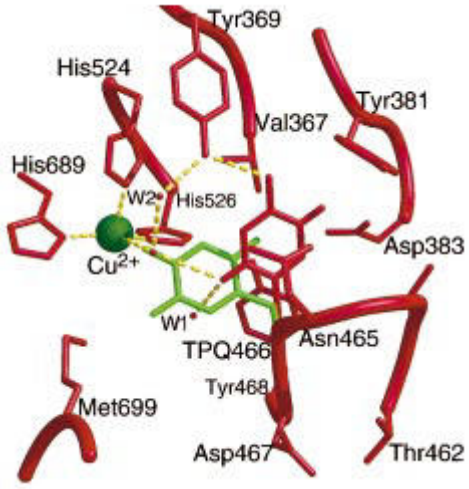

Figure 2.22 A representation of the active site of *E.coli* copper amine oxidase. TPQ (TPQ466) is coloured red and represents the active conformation. The lime coloured TPQ represents the inactive conformation. The copper ion is represented by a green sphere. The axial water molecule is termed W1 and the equatorial water is termed W2 (Murray *et al*., 1999).

The oxidative deamination of amines by SSAO takes place through the formation of Schiff base products as intermediates. This catalytic mechanism involves two half reactions, the reductive and the oxidative half reactions (Figure 2.23).

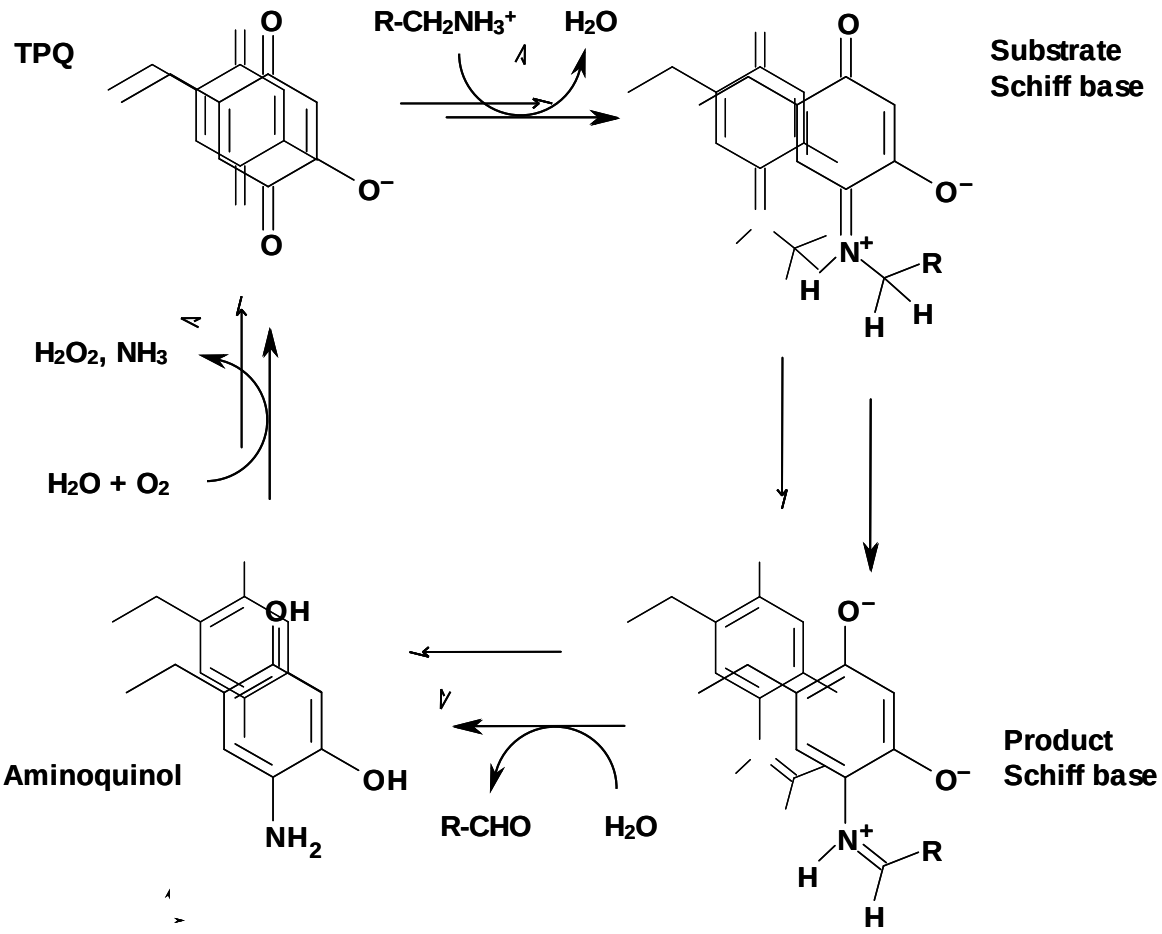

Figure 2.23 The catalytic cycle of amine oxidation through TPQ. Amine oxidation occurs by two half reactions. The first half reaction is the reduction of TPQ to an aminoquinol and the substrate is oxidized to an aldehyde. In the second half reaction, TPQ is re-oxidized by utilizing an oxygen molecule and releasing it as hydrogen peroxide (Sixt & Kaim, 2000).

- Reductive half reaction

  The initial step involves a nucleophilic attack of the primary amine on the C5 position of the oxidized TPQ cofactor. This leads to the formation of the substrate Schiff base. The second step involves an active site base, an aspartic acid residue, to abstract a proton form the α-carbon. This resulting species rearranges to form another Schiff base product. The aldehyde product is formed by hydrolysis and the oxidized TPQ is reduced to an aminoquinol with the amine nitrogen displacing the oxygen on the C5 position of TPQ.

- Oxidative half reaction

  The oxidative half reaction follows directly upon the reductive half reaction. Molecular oxygen binds to the enzyme and two protons and electrons are accepted from aminoquinol. This results in the formation of hydrogen peroxide and an iminoquinone intermediate. The hydrolysis of iminoquinone releases ammonia and re-oxidize TPQ, rendering it available for another catalytic cycle (Brazeau *et al*., 2004).

This generation of harmful byproducts such as hydrogen peroxide, ammonia and aldehydes may contribute to neurodegeneration through the induction of oxidative stress, as discussed with MAO.

2.4 *In vitro* measurements of MAO activity

Determination of MAO activity is important for research, clinical and pharmacological studies. Many of the methods available were developed in the 1960s and were improved on in the following years. They were based on the measuring of reaction products or measuring the disappearance of reagent species (Nicotra & Parvez, 1999) and can be categorized as direct or indirect measurements.

- Direct measurements

  a) The detection of oxygen consumption by using an oxygen-sensitive electrode. The disadvantage of this method is that it requires a well controlled assay environment and is unsuitable for rapid processing of large quantities of samples (Averill-Bates *et al*., 1993).
  b) The detection of the co-products formed during catalysis, such as H_2O_2, by measuring the absorbance of H_2O_2 at a wavelength of 230 nm. The disadvantage of this method is that most biological compounds can interfere with the assay through their absorbance at this wavelength (Stevanato *et al*., 1995).
  c) The detection of absorbance or the detection of fluorescence of the oxidized monoamine product. A disadvantage of this method is that experiments are restricted to one substrate (Zhou *et al*., 1996).

- Indirect measurements

  Indirect measurements are based on horseradish peroxidase coupled reaction systems in which the MAO enzyme generates H_2O_2 through its reaction with a substrate. The H_2O_2 is then detected by using H_2O_2-sensitive probes such as scopletin (Morpurgo *et al*., 1989).

Weissbach *et al*. (1960), proposed a simple and rapid spectrophotometric method for the detection of MAO activity. In this method kynuramine is used as a non-specific substrate for MAO and remains non-fluorescent until it is oxidatively deaminated by MAO to yield 4-hydroxyquinoline (Figure 2.24).

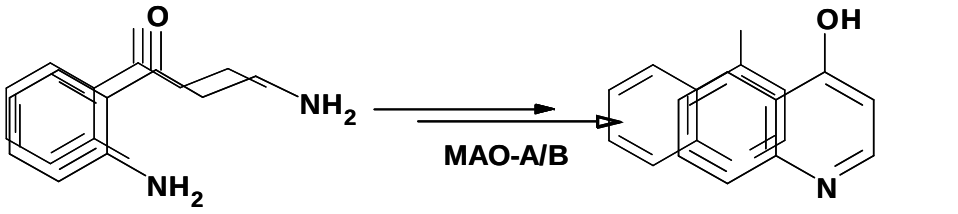

Figure 2.24 The oxidative deamination of kynuramine to yield 4-hydroxyquinoline by MAO-A or MAO-B.

4-Hydroxyquinoline concentrations can be measured with a spectrophotometer at a wavelength of 360 nm. Since 4-hydroxyquinoline also is fluorescent, kynuramine oxidation can be determined fluorometrically by the appearance of 4-hydroxyquinoline at an excitation wavelength of 310 nm and an emission wavelength of 400 nm. The product formation can then be determined by comparing the fluorescence emission with that of standard 4-hydroxyquinoline (Weissbach *et al*., 1960).

Zhou & Panchuk-Voloshina (1997) reported a one-step fluorometric method for the detection of MAO activity. In this method, H_2O_2 in a horseradish peroxidase-coupled reaction is measured by using a highly sensitive and stable H_2O_2 probe, N-acetyl-3,7-dihydroxyphenoxazine (Amplex Red). Amplex Red is unique in that it has an assay sensitivity of 1.2×10^{-5} U/ml compared to the standard assay of benzylamine with a sensitivity of 2.0×10^{-4} U/ml. Amplex Red is oxidized to a fluorescent dye, resorufin, by H_2O_2. The absorption and emission wavelength maximum of resorufin is > 560 nm.

2.5 Enzyme kinetics

Enzyme properties are determined by kinetic studies and play a vital role in determining the potency of inhibitors. These kinetic studies led to the theory that the reaction between an enzyme (E) and its substrate (S) will reach equilibrium with the subsequent formation of an enzyme-substrate (ES) intermediate product (Lineweaver & Burk, 1934). This can be illustrated as:

$$E + S \underset{k_{-1}}{\overset{k_1}{\rightleftarrows}} ES$$

The dissociation of the ES product is represented by the dissociation constant K_d and the affinity of an enzyme for its substrate is the inverse of K_d and can be illustrated as:

$$K_d = \frac{k_{-1}}{k_1}$$

The numeric value of K_d is given at half maximum velocity. Half maximum velocity is represented by the Michaelis constant (K_m) which is defined as the substrate concentration when initial velocity (v_i) is at half maximum velocity (V_{max}). K_m may approximate K_d, provided that the ES complex association and dissociation is more rapid, compared to the rate-limiting step in catalysis. Initial reaction velocity can be illustrated by the Michaelis equation:

$$v_i = \frac{(V_{max} \times S)}{(K_m + S)}$$

Measuring V_{max} directly sometimes requires an extremely high concentration of the substrate and since it may be difficult to achieve saturating conditions, the calculation of V_{max} and K_m may be difficult. Lineweaver & Burk (1934) found that a linear form of the Michealis-Menten equation could resolve this difficulty by extrapolating V_{max} and K_m from v_i, at less than saturating concentrations of the substrate. Manipulating the above equation into the equation of a straight line (y = mx + c) yields the following equation:

$$\frac{1}{v_i} = \left(\frac{K_m}{V_{max}}\right)\frac{1}{[S]} + \frac{1}{V_{max}}$$

Where y = $1/v_i$ and x = 1/[S] with the y-intercept as $1/V_{max}$ and the slope as K_m/V_{max}. A graphical illustration is given in figure 2.25 and this plot is termed a Lineweaver-Burk plot.

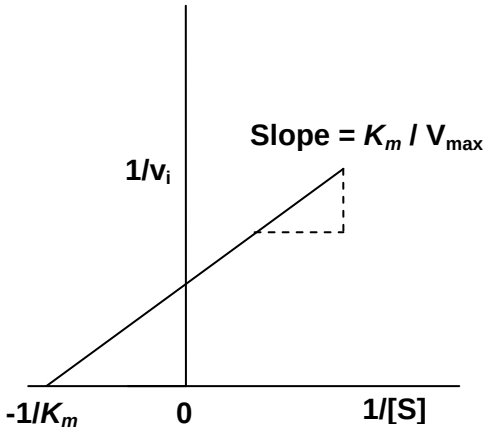

Figure 2.25. An illustration of a Lineweaver-Burk plot. The Y-axis is equal to $1/v_i$, the X-axis is equal to 1/[S] and the x-intercept is equal to $-1/K_m$. This plot may be used to determine V_{max} and K_m.

Setting the y term to zero and solving the x, reveals that the x-intercept is $-1/K_m$ and thus renders it easy to calculate K_m (Murray *et al*., 2003).

Lineweaver-Burk plots are also used to distinguish between competitive and noncompetitive inhibitors and for the evaluation of inhibitor constants K_i. The K_i values allow us to compare the inhibition potencies of inhibitors for the same enzyme. The lower the K_i value, the more potent the inhibitor. In the case of competitive inhibition, the slope is increased and the y-intercept remains constant whereas in the case of noncompetitive inhibition the y-intercept is raised (Lineweaver & Burk, 1934). This means that for competitive inhibition the y-intercept is equal to $1/V_{max}$ and remains the same even if 1/[S] approaches zero. V_{max} is therefore independent of inhibitor presence. However this is not the case with the x-intercept, since it varies with inhibitor concentrations. In the absence of inhibitor, the x-intercept is $-1/K_m$ and in the presence of an inhibitor it is $-1/K_m$'. Since $-1/K_m$' is always larger than $-1/K_m$, the apparent K_m' increases with an increase of inhibitor concentration (Figure 2.26).

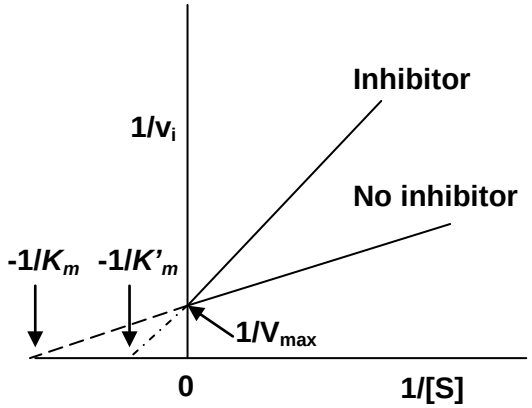

Figure 2.26. A lineweaver-Burk plot of competitive inhibition with y-intercept $1/V_{max}$ and x-intercepts equal to $-1/K_m$ and $-1/K'_m$, for no inhibitor and inhibitor, respectively. A competitive inhibitor has no effect on V_{max} but increases the apparent K_m (K'_m) for the substrate.

The x-intercept can be calculated as follows:

$$x = \frac{-1}{K_m}\left(1 + \frac{[I]}{K_i}\right)$$

This equation can thus be used to determine the K_i value of the inhibitor.

For noncompetitive inhibitors the substrate binding ability is not affected by the binding of the inhibitors but rather the ability of product formation is compromised. In this case, the Lineweaver-Burk plots show a constant apparent K_m value, while V_{max} is decreased in the presence of a noncompetitive inhibitor (Figure 2.27) (Murray *et al*., 2003).

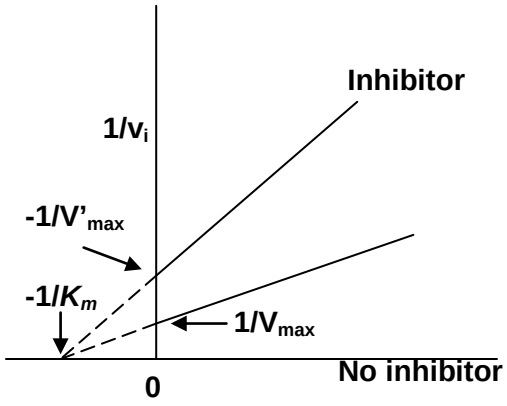

Figure 2.27. A lineweaver-Burk plot of noncompetitive inhibition with the y-intercepts equal to $-1/V'_{max}$ and $1/V_{max}$, for inhibitor and no inhibitor, respectively. The x-intercept is constant and is equal to $-1/K_m$.

Dixon (1953) published an article in which he described a more convenient way to determine the K_i value of an inhibitor. $1/v_i$ is plotted versus the inhibitor concentration [I] while keeping the substrate concentration constant. This gives a straight line. When using two different substrate concentrations two straight lines are obtained which will intersect to the left of the y-axis. The point at the crossing is equal to $-K_i$ and the value can be directly obtained from the graph (Figure 2.28). With competitive inhibitors the lines will cross in the the bottom left quadrant of the y-axis and in the case of noncompetitive inhibitors the lines will meet at a point on the base line.

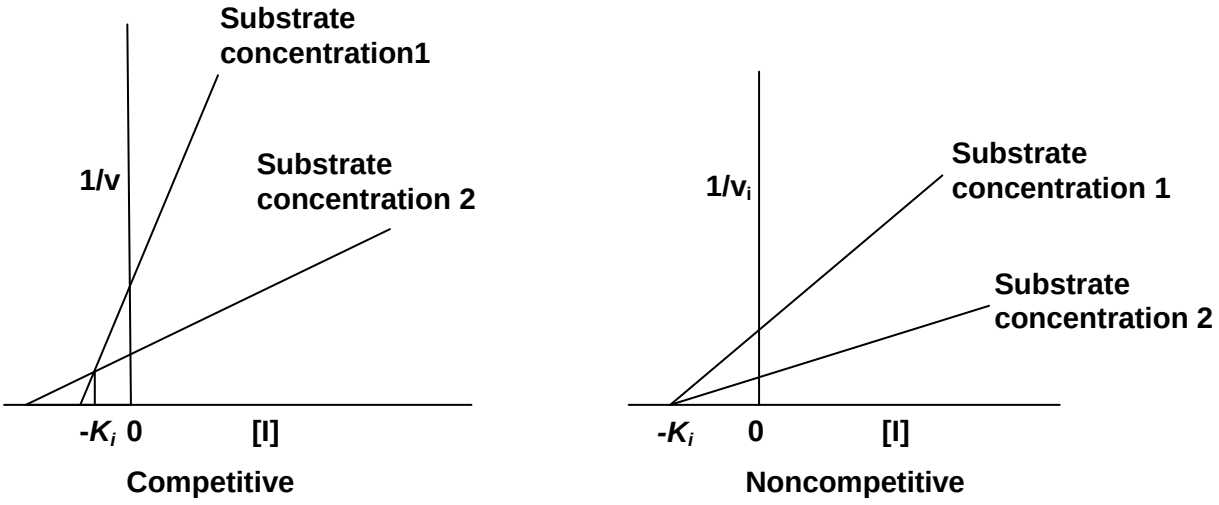

Figure 2.28. Determination of K_i values for competitive inhibition (left) and noncompetitive inhibition (right) according to Dixon's method.

Cheng & Prusoff (1973) described another method for determining the K_i value by using the IC_{50} value. The IC_{50} value is the concentration of an inhibitor that is required for 50% inhibition of the substrate *in vitro*. This relationship can be expressed by the following equation:

$$K_i = \left(\frac{IC_{50}}{1 + \frac{[S]}{K_m}} \right)$$

In the current study the K_i values were determined with the above equation. The respective values for [S] and K_m were as follows:

Enzyme	Substrate	Substrate concentrations (μM)	K_m (μM)
Recombinant human MAO-A	Kynuramine	45	48.297
Recombinant human MAO-B	Kynuramine	30	61.538

These K_m values were determined experimentally as described in section 4.5. The K_i values allow comparison between the inhibition potencies of the selective inhibitors for MAO-A and MAO-B, respectively. This is then ultimately used to obtain the selectivity index for the MAO-B isoform.

2.6 Conclusion

This chapter discussed PD as a neurodegenerative disorder with a largely unknown pathogenesis. Although PD is an incurable disease, symptomatic treatment strategies are available. The use of monoamine oxidase inhibitors is one such approved. The chapter provides background information on monoamine oxidase, such as the therapeutic role of MAO in PD, the three dimensional structure of MAO and the mechanistic proposals for MAO catalysis. Inhibitors of MAO are also discussed, but the focus of this study is to synthesize new, reversible inhibitors with specificity for the MAO-B enzyme. *In vitro* measurements of MAO activity and enzyme kinetics are briefly discussed in an attempt to provide insight into the enzymology section of this study. The MAO-B inhibitors that will be designed in this study may be useful in the future design and development of drugs for the therapy of PD.

Chapter 3

Synthesis

3.1 Introduction

In this study a series of sulfanylcaffeine and sulfinylcaffeine analogues will be synthesized and examined as potential inhibitors of human MAO-A and MAO-B. The analogues that will be prepared in this study are illustrated in table 3.1. As shown in the table, the sulfanylcaffeine analogues differed only in substitution on the *para* position of the phenyl ring. The first homologue, compound **1a**, contains an unsubstituted phenyl ring. The other homologues **1b**–**g** are substituted on the *para* position of the phenyl ring. Compounds **1b**–**d** are substituted with the halogens, chlorine, bromine and fluorine, respectively, while compounds **1e**–**g** are substituted with alkyl and alkyloxy groups: the trifluoromethyl, methyl and methoxy functional groups. Two sulfinylcaffeine analogues are also included in this study, compounds **2a**–**b**. Both these analogues contain substituents on the *para* position of the phenyl ring. For this purpose the halogens, bromine and fluorine are selected.

It should be noted that, while the C8-sulfanyl side chains of compounds **1a**–**g** and the C8-sulfinyl side chains of compounds **2a**–**b** are similar, the oxidation state of the sulfur of compounds **1a**–**g** is -2, while the oxidation state of the sulfur in compounds **2a**–**b** is 0. Considering the structural and electronic features of the compounds that will be synthesized in this study, the following structure–activity relationships may be determined:

- The effect that different substituents on the *para* position of the phenyl ring will have on the MAO–A and MAO–B inhibition potencies of the sulfanylcaffeine analogues **1a**–**g**, will be examined.

- The MAO-A and MAO-B inhibition potencies of the sulfanylcaffeine derivatived inhibitors (**1a**–**g**) will be compared to the inhibition potencies of the sulfinylcaffeine derivatived inhibitors (**2a**–**b**). Form these studies it may be determined which oxidation state of sulfur, 0 or -2, is more suitable for MAO inhibition.

- It will be determined whether the sulfanylcaffeine and sulfinylcaffeine analogues examined in this study exhibit selective inhibition of either MAO-A or MAO-B. Since caffeine derived compounds are reported to be MAO-B selective inhibitors, it may be expected that the

structures that will be synthesized in this study, will also exhibit selectivity for the MAO-B isoform (Booysen *et al*., 2011).

The main goal of this study is, however, to discover new highly potent inhibitors of human MAO-A and MAO-B.

Tabel 3.1 The structures of the 8-[(2-phenylethyl)sulfanyl]caffeine analogues (**1a**–**g**) and 8-[(2-phenylethyl)sulfinyl]caffeine analogues (**2a**–**b**) that will be synthesized.

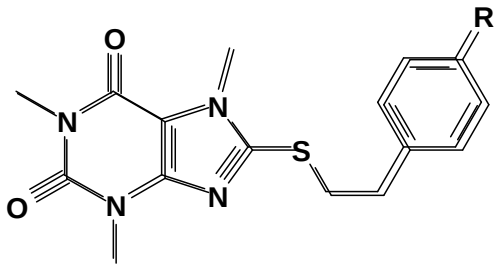

1

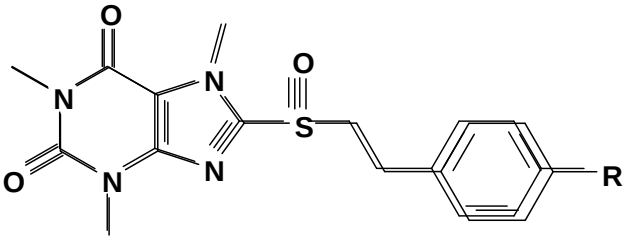

2

	R
1a	H
1b	Cl
1c	Br
1d	F
1e	CF_3
1f	CH_3
1g	OCH_3
2a	Br
2b	F

In this study, the following four synthetic procedures will be followed:

a) The syntheses of 8-sulfanylcaffeine analogues have previously been reported by Long (1947). Employing the reported procedure, 8-chlorocaffeine (**4**) will be reacted with an appropriate mercaptan (**3a**–**g**) (Figure 3.1) in 50% aqueous ethanol as solvent. In this study, it was found that this method is suitable for the preparation of the target 8-[(2-phenylethyl)sulfanyl]caffeine analogues (**1a**–**g**) which are illustrated in table 3.1.

Figure 3.1 A general reaction scheme to illustrate the synthesis of 8-sulfanylcaffeine analogues from 8-chlorocaffeine and a mercaptan.

b) The general synthesis of mercaptans (Figure 3.2) has previously been reported by Manoury *et al*. (1986). Using this procedure, a substituted phenylethylbromide (**5**) will be reacted with thiourea (**6**) under basic conditions. Sodium hydroxide is added to the reaction and causes the mercaptan product to separate since it is largely insoluble in alkaline medium. In the current study, this method was shown to be appropriate for the preparation of mercaptans **3a**–**g**. These mercaptans will be used as starting materials for the synthesis of the 8-thiocaffeine derivates (**1a**–**g**).

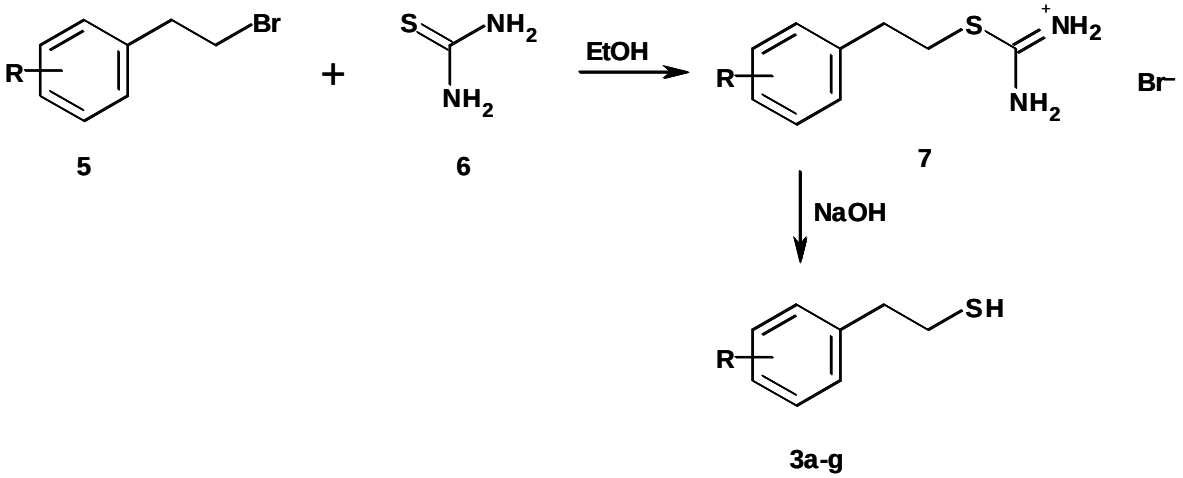

Figure 3.2 The general synthetic route for the preparation of mercaptans from an appropriately substituted phenylethylbromide.

c) The syntheses of the 8-sulfinylcaffeine analogues have previously been reported by Long (1947). Employing this method, a 8-[(2-phenylethyl)sulfanyl]caffeine derivative will be reacted with 30% hydrogen peroxide in the presence of glacial acetic acid and acetic anhydride (Figure 3.3). In this study, this protocol will be followed to synthesize the target 8-[(2-phenylethyl)sulfinyl]caffeine analogues (**2a**–**b**) which are illustrated in table 3.1.

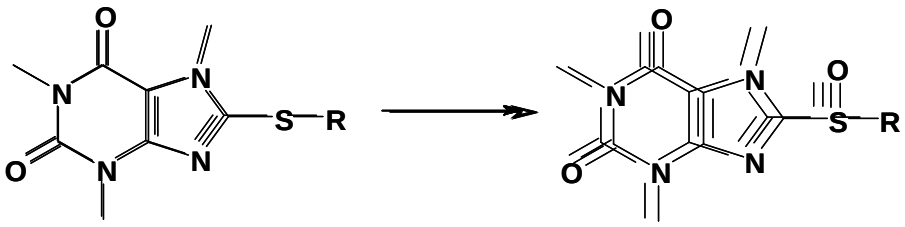

1c-d **2a-b**

Figure 3.3 A general reaction scheme to illustrate the synthesis of 8-sulfinylcaffeine analogues from 8-sulfanylcaffeine analogues.

d) The synthesis of 8-chlorocaffeine was previously reported by Fischer & Reese (1883). Employing this procedure, caffeine will be reacted with chlorine gas in the presence of chloroform as solvent (Figure 3.4). Upon removal of the chloroform, 8-chlorocaffeine should be obtained in good yields. In this study, 8-chlorocaffiene was required as a reagent for the synthesis of the 8-sulfanylcaffeine analogues **1a**–**g**.

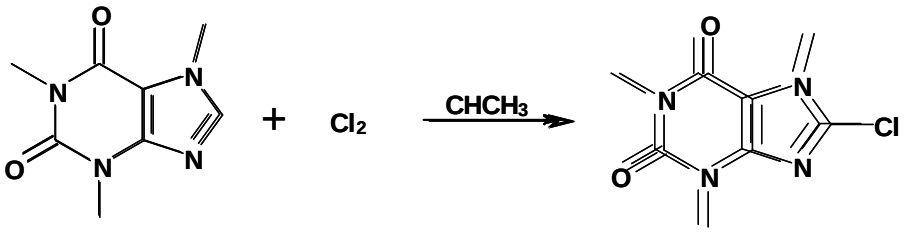

4

Figure 3.4 The synthesis of 8–chlorocaffeine from the reaction between caffeine and chlorine gas.

3.2 Materials and instrumentation

Materials:

All starting materials and solvents were obtained from Sigma-Aldrich and were used without further purification.

Thin layer chromatography (TLC):

TLC was used to determine whether the reactions proceeded to completeness. Silica gel 60 (Merck) TLC sheets with UV_{254} fluorescent indicator were employed with a mobile phase consisting of 60 parts ethyl acetate and 30 parts n-hexane. The developed TLC sheets were observed under an UV-lamp at a wavelength of 354 nm.

Melting points:

The melting points of all the synthesized compounds were determined on a Buchi M-545 melting point apparatus and are uncorrected.

Mass spectra:

High resolution mass spectra (HRMS) were obtained on a DFS high resolution magnetic sector mass spectrometer (Thermo Electron Corporation) in electron impact ionization (EI) mode.

Nuclear magnetic resonance (NMR):

Proton (^{1}H) and carbon (^{13}C) NMR spectra were recorded on a Bruker Avance III 600 spectrometer. ^{1}H NMR spectra were recorded at a frequency of 600 MHz and ^{13}C NMR spectra were recorded at frequency of 150 MHz. All NMR measurements were conducted in $CDCl_3$ and the chemical shifts are reported in parts per million (δ) downfield from the signal of tetramethylsilane added to the deuterated solvent. Spin multiplicities are given as s (singlet), d (doublet), t (triplet) or m (multiplet). The coupling constants (J) are expressed in hertz (Hz).

High pressure liquid chromatography (HPLC):

HPLC was used to estimate the purities of the synthesized compounds. The HPLC analyses were conducted with an Agilent 1100 HPLC system which consisted of a quaternary pump and a diode array detector. HPLC grade acetonitrile (Merck) and Milli–Q water (Millipore) was employed for the chromatography. A Venusil XBP C18 column (4.60 × 150 mm, 5 µm) was used for the separation and the mobile phase consisted at the start of each run of 30%

acetonitrile and 70% Milli–Q water. The flow rate was set to 1 ml/min. At the start of each run a solvent gradient program was initiated. The composition of the acetonitrile in the mobile phase was increased linearly to 85% over a period of 5 min. Each HPLC run lasted 15 min and a time period of 5 min was allowed for equilibration between runs. A volume of 20 µl of solutions of the test compounds (1 mM) was injected into the HPLC system and the eluent was monitored at a wavelength of 254 nm. The test compounds were dissolved in acetonitrile.

3.3 Synthesis of 8-[(2-phenylethyl)sulfanyl]caffeine analogues

The following is an account of the method used for the synthesis of the 8-[(2-phenylethyl)sulfanyl]caffeine analogues **1a**–**g** (figure 3.5 and figure 3.6).

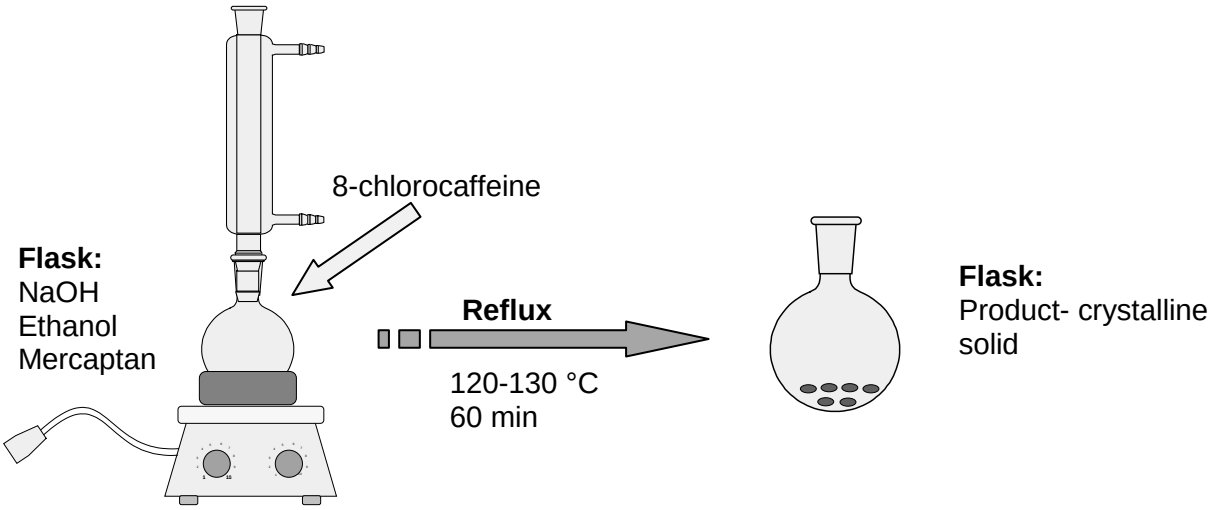

Figure 3.5 Illustration of experimental setup for the synthesis of the 8-[(2-phenylethyl)sulfanyl]caffeine analogues **1a**–**g**.

In a round bottom flask, a solution of 4 mmol sodium hydroxide (NaOH) was prepared by dissolving 0.16 g NaOH in 3.5 ml water. A volume of 3.5 ml ethanol was subsequently added. The flask was cooled on an ice bath for 5 minutes. After the cooling period, the flask was removed from the ice bath and 4 mmol of the appropriate mercaptan (**3**) was added. The solution was stirred while 4 mmol 8-chlorocaffeine (**4**) was added rapidly in a single portion. In an oil bath, set at the reported boiling point temperature of the mercaptan (usually 120–130 °C), the flask was heated under reflux for one hour. The reaction was then allowed to cool to room temperature. TLC was performed to determine the completion of the reaction. Upon cooling to room temperature, the product (**1**) precipitated as a crystalline solid and was washed with 20 mL cold ethanol. The product was subsequently recrystallized from ethanol (Long, 1947).

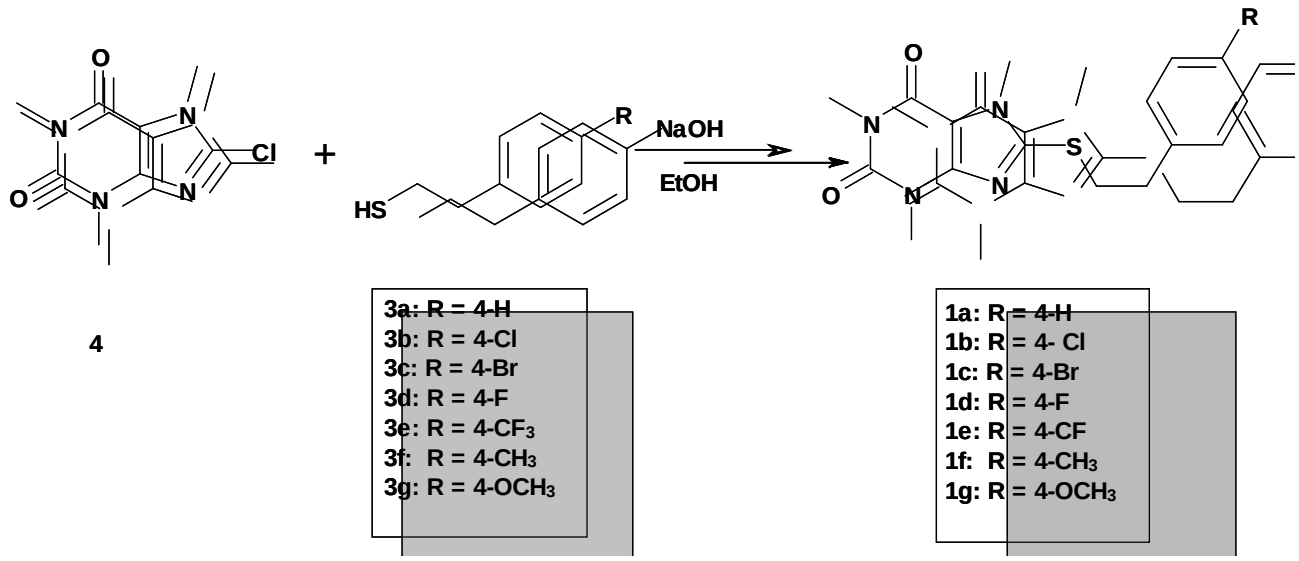

Figure 3.6 Reaction scheme for the synthesis of 8-[(2-phenylethyl)sulfanyl]caffeine analogues **1a**–**g**.

3.4 Synthesis of the appropriate mercaptans

The following is an overview of the method used in the synthesis of the mercaptans (**3b**–**g**) that were required as reactants for the synthesis of the 8-[(2-phenylethyl)sulfanyl]caffeine analogues (figure 3.7 and figure 3.8). Mercaptan **3a** was commercially available, and was thus not synthesized in this study (Table 3.2).

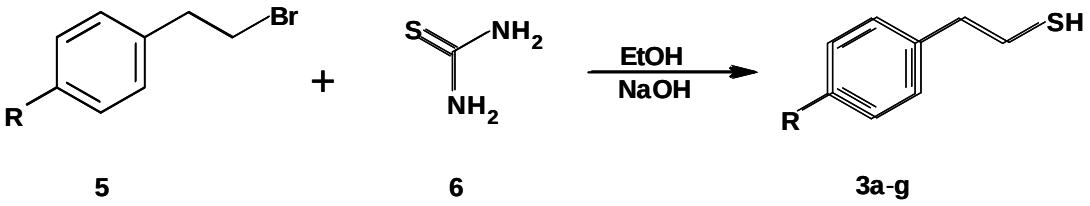

Figure 3.7 Reaction scheme for the synthesis of the required mercaptans **3a**–**g**

Table 3.2 The availability and physical appearance of the appropriate mercaptans (**3a**–**g**) used in this study.

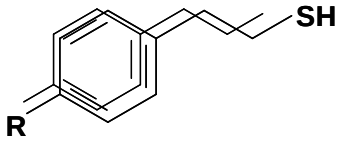

3a-**g**

Mercaptan	R	Availability	Physical appearance
3a	H	Commercial	Colourless oil
3b	Cl	Synthesized	Colourless oil
3c	Br	Synthesized	Light yellow oil
3d	F	Synthesized	Colourless oil
3e	CF_3	Synthesized	Light yellow oil
3f	CH_3	Synthesized	Light yellow oil
3g	OCH_3	Synthesized	Light yellow oil

In a 100 ml round bottom flask, equipped with a magnetic stirrer unit and a reflux condenser, 7 mmol of thiourea (**6**) was dissolved in 13.5 ml ethanol and 7 mmol of the appropriate substituted phenylethylbromide (**5**) was added. The mixture was stirred and heated (85 °C) under reflux for 2 hours. After 30 min the solution became homogenous but the additional heating ensured the completeness of the reaction. The mixture was allowed to cool after which the ethanol was removed via rotary evaporation at high vacuum (-600 mmHg) at a temperature of 40 °C.

A solution containing 10.5 mmol NaOH was prepared by dissolving 0.42 g NaOH in 8.75 ml H_2O. This was added to the residue obtained above, and the reaction was heated again under reflux (120 °C) for 2 hours. The reaction was subsequently cooled to room temperature. An aqueous solution of sulphuric acid (H_2SO_4) was prepared by adding 1 ml concentrated H_2SO_4 to 5 ml H_2O. The reaction was then acidified with the addition of the dilute H_2SO_4 solution. The

mercaptan separated as oil droplets on the bottom of the flask. The mercaptan was subsequently extracted with 30 ml diethylether, and the organic phase was washed twice with water. This extracted mercaptan in the ethereal phase was then dried over anhydrous sodium sulphate and the remaining ether was removed via rotary evaporation. This yielded the appropriate phenylethylmercaptan.

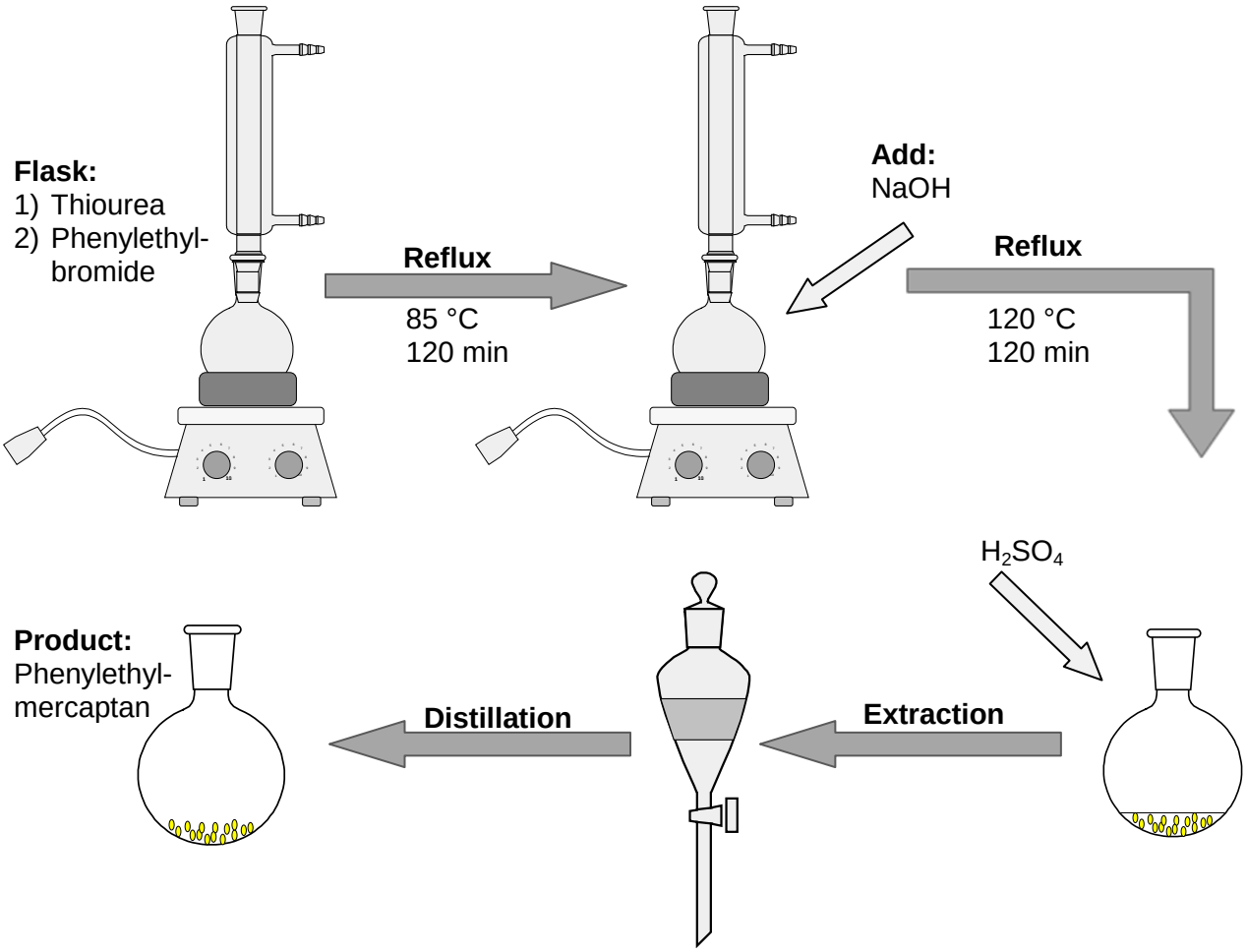

Figure 3.8 Illustration of the experimental setup for synthesis of the required mercaptans **3a**–**g**.

.

3.5 Method for the synthesis of the 8–[(2–phenylethyl)sulfinyl]caffeine analogues

The following is an overview of the method used for the synthesis of the 8-[(2-phenylethyl)sulfinyl]caffeine analogues **2a**–**b** (figure 3.9 and figure 3.10). In a 100 ml round bottom flask, 4 mmol of the appropriate 8-[(2-phenylethyl)sulfanyl]caffeine was placed, followed by 8 ml glacial acetic acid and 2 ml acetic anhydride. The reaction was stirred at room

temperature and 2 ml of a 30% hydrogen peroxide solution was added dropwise. The reaction was stirred for 4 hours after which 25 ml distilled water was added. The water caused the product to precipitate from the reaction solvent. The product was collected by filtration and recrystallized from ethyl acetate (Long, 1947).

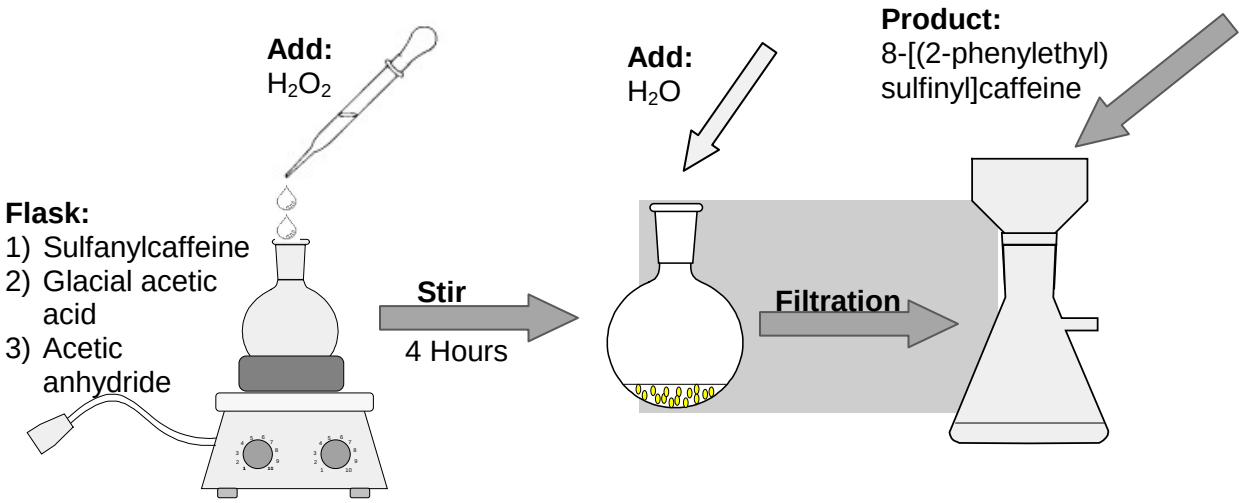

Figure 3.9 Illustration of the experimental setup for synthesis of the 8-[(2-phenylethyl)sulfinyl]caffeine analogues **2a**–**b**.

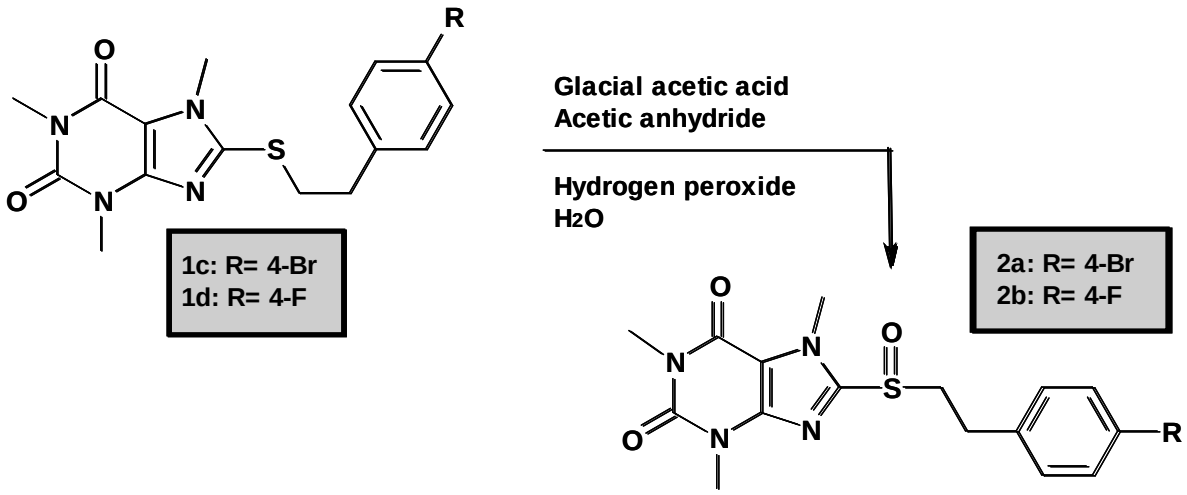

Figure 3.10 The synthetic route for the synthesis of 8-[(2-phenylethyl)sulfinyl]caffeine analogues.

3.6 Synthesis of chlorine gas

Chlorine gas was required for the synthesis of 8-chlorocaffeine. The chlorine gas was conveniently synthesized from the reaction of potassium permanganate ($KMnO_4$) and hydrochloric acid (HCl) (Figure 3.11).

Figure 3.11 The chemical reaction for the synthesis of chlorine gas.

Five two–necked flasks were sequentially connected to each other (Figure 3.12):

- the first flask was filled with 0.367 g $KMnO_4$ and placed on a stirrer plate
- the second flask contained water that removed hydrogen chloride from the chlorine gas
- the third flask was filled with concentrated sulphuric acid to dry the gas
- the fourth flask was left empty and acted as a safety measure
- and the fifth flask contained a chloroform and caffeine mixture

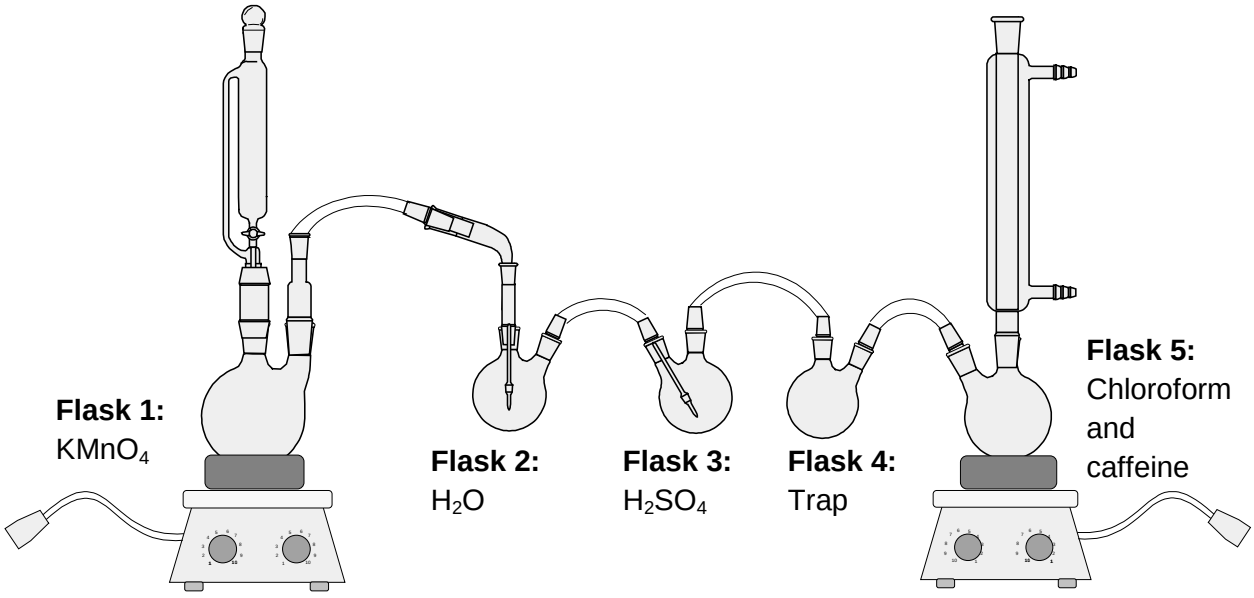

Figure 3.12 An illustration of the apparatus setup for the synthesis of 8-chlorocaffeine.

The first flask containing the $KMnO_4$ was equipped with a pressure equalizing funnel filled with 20.17 ml of concentrated HCl acid (32%) and secured with an elastic band. The acid was set to react dropwise with the $KMnO_4$ while the flask was occasionally shaken. The formation of chlorine gas receded slowly and it was thus necessary to heat the first flask when all of the acid had been added to fully complete the chlorine gas formation (Vogel *et al*., 1989).

3.7 Synthesis of 8-chlorocaffeine

The following is an overview of the literature method for the synthesis of 8-chlorocaffeine (Fischer & Reese, 1883), (figure 3.13):

A mixture of 2.5 g dry caffeine and 20 ml chloroform was prepared in a two-necked flask fitted with an inlet tube and a reflux condenser. The mixture was heated until all the caffeine had dissolved. A rapid stream of dry chlorine gas was passed through the hot solution until the solid that first precipitated subsequently dissolved. No water may be present in the reaction and thus the chlorine gas was first dried by passing it through sulphuric acid. The precipitate that formed at the start of the reaction was the HCl salt of caffeine, which later dissolved with continuation of the reaction. A rotary evaporator was used to remove the chloroform via distillation and white 8-chlorocaffeine crystals were obtained by heating the residue with a small amount of water. The method employed was that of Fischer & Reese (1883).

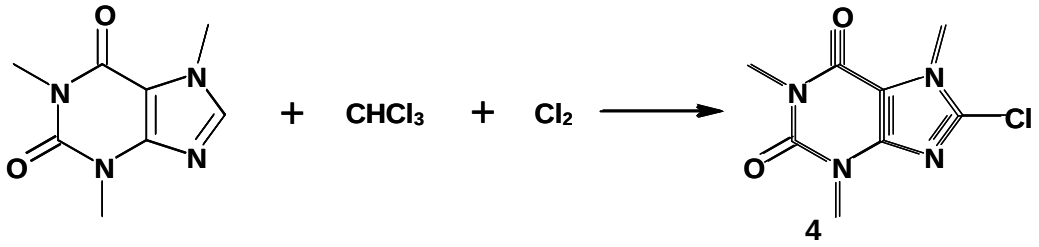

Figure 3.13 Reaction scheme for the synthesis of 8-chlorocaffeine.

3.8 Results- NMR spectra

The NMR spectra of the synthesized compounds are given in appendix A. Below, the structures of the target 8-sulfanylcaffeine analogues are given and correlated with the ^{1}H NMR and ^{13}C NMR data. The appropriate signals were observed for the compounds. These include the 3 singlets for the caffeine methyl groups, the signals (triplets) for the CH_2-CH_2 moiety and the signals for the aromatic protons. The singlets of the methyl and methoxy groups (substituted on

the phenyl ring) of compounds **1f** and **1g** were also observed. The appropriate integration values and chemical shifts were observed for all signals. In addition, the ^{13}C NMR data corresponded to the target structures. The assignment of the ^{13}C NMR signals is based on the DEPT 90 º and DEPT 135 º spectra. An example of these DEPT spectra is given for compound **1a** in the addendum. Interestingly, for certain caffeine analogues (compounds **1a, 1f,**) one ^{13}C signal in the aromatic region is not observed. This is most likely due to an overlap of two ^{13}C signals with similar chemical shifts. Since all the other structural data (^{1}HMR and HRMS) corresponded to the proposed structures, this was not further explored. For structures **2a**–**b**, multiplets were observed for the CH_2-CH_2 signals and not triplets as for the CH_2-CH_2 signals of **1a**–**g**. These multiplicities of the CH_2-CH_2 signals of **2a**–**b** are due to the chirality of the sulfinyl carbon.

A: 8–Chlorocaffeine

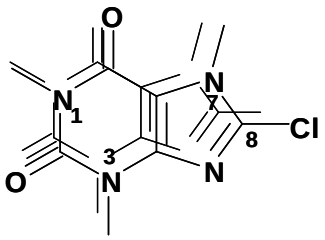

The title compound was prepared from caffeine and chlorine gas in a yield of 93%: mp 188 °C. ^{1}H NMR (Bruker Avance III 600, $CDCl_3$) δ 3.34 (s, 3H), 3.49 (s, 3H), 3.90 (s, 3H); ^{13}C NMR (Bruker Avance III 600, $CDCl_3$) δ 27.9, 29.7, 32.6, 108.5, 138.9, 147.0, 151.2, 154.5.

^{1}H NMR:	**^{13}C NMR:**
• The three methyl groups at N1, N3 and N7 correspond to the singlets at 3.34, 3.49, 3.90 ppm (the signals integrate for 3 protons each).	• Methyl groups at N1, N3 and N7 are represented by the signals at 27.9, 29.7, 32.6 ppm • Aromatic carbons are represented by signals at 108.5, 138.9, 147.0, 151.2 and 154.5 ppm.

1a: 8-{[2-(Phenylethyl)sulfanyl]caffeine

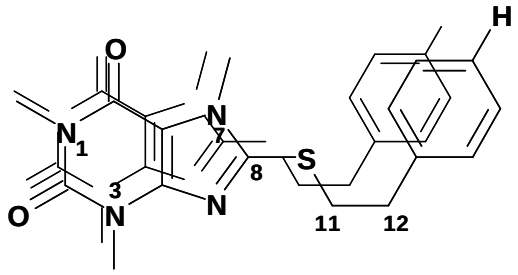

The title compound was prepared from 2–phenylethane-1-thiol in a yield of 83%: mp 95 °C (ethanol). ^{1}H NMR (Bruker Avance III 600, $CDCl_3$) δ 3.04 (t, 2H, J = 7.5 Hz), 3.36 (s, 3H), 3.48 (t, 2H, J = 7.5 Hz); 3.55 (s, 3H), 3.78 (s, 3H), 7.21 (m, 3H), 7.28 (m, 2H); ^{13}C NMR (Bruker Avance III 600, $CDCl_3$) δ 27.8, 29.6, 32.1, 33.8, 36.0, 108.5, 126.7, 128.5, 139.3, 148.4, 150.8, 151.4, 154.5; EI-HRMS *m*/*z*: calcd for $C_{16}H_{18}N_4O_2S$, 330.1150, found 330.1147; Purity (HPLC): 98%.

^{1}H NMR:	**^{13}C NMR:**
• The three methyl groups at N1, N3 and N7 correspond to the singlets at 3.36, 3.55, 3.78 ppm (the signals integrate for 3 protons each) • The methylene groups at C11 and C12 are represented by the triplets at 3.04 and 3.48 ppm (the signals integrate for 2 protons each) • Aromatic protons on the phenyl ring correspond with the multiplets at 7.21 and 7.28 ppm (the signals integrate for 3 protons and 2 protons, respectively).	• Methyl groups at N1, N3 and N7 are represented by the signals at 27.8, 29.6, 32.1 ppm • The methylene groups at C11 and C12 correspond to the signals at 33.8 and 36.0 ppm • Aromatic carbons are represented by signals at 108.5, 126.7, 128.5, 139.3, 148.4, 150.8, 151.4 and 154.5 ppm.
^{13}C DEPT 90 °, ^{13}C DEPT 135 °:	
• Methyl groups at N1, N3 and N7 correspond to the signals at 27.8, 29.6, 32.1 ppm • The methylene groups at C11 and C12 are represented by the signals at 33.8 and 36.0 ppm • Aromatic CH carbons on the phenyl ring correspond to the signals at 126.7 and 128.5 ppm.	

1b: 8-{[2-(4-Chlorophenyl)ethyl]sulfanyl}caffeine

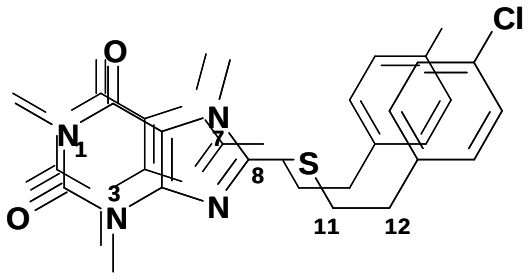

The title compound was prepared from 2–(4–chlorophenyl)ethane-1-thiol in a yield of 69%: mp 164 °C (ethanol). ^{1}H NMR (Bruker Avance III 600, $CDCl_3$) δ 3.01 (t, 2H, J = 7.5 Hz), 3.35 (s, 3H), 3.45 (t, 2H, J = 7.5 Hz); 3.54 (s, 3H), 3.78 (s, 3H), 7.12 (d, 2H, J = 8.3 Hz), 7.23 (d, 2H, J = 8.3 Hz) ; ^{13}C NMR (Bruker Avance III 600, $CDCl_3$) δ 27.8, 29.6, 32.1, 33.6, 35.4, 108.5, 128.6, 129.9, 132.5, 137.7, 148.4, 150.5, 151.4, 154.5; EI-HRMS *m*/*z*: calcd for $C_{16}H_{17}ClN_4O_2S$, 364.0761, found 364.0756; Purity (HPLC): 99%.

^{1}H NMR:	**^{13}C NMR:**
• The three methyl groups at N1, N3 and N7 correspond to the singlets at 3.35, 3.54, 3.78 ppm (the signals integrate for 3 protons each) • The methylene groups at C11 and C12 are represented by the triplets at 3.01 and 3.45 ppm (the signals integrate for 2 protons each) • Aromatic protons on the phenyl ring correspond with the doublets at 7.12 and 7.23 ppm (the signals integrate for 2 protons each).	• Methyl groups at N1, N3 and N7 are represented by the signals at 27.8, 29.6, 32.1 ppm • The methylene groups at C11 and C12 correspond to the signals at 33.6 and 35.4 ppm • Aromatic carbons are represented by signals at 108.5, 128.6, 129.9, 132.5, 137.7, 148.4, 150.5, 151.4 and 154.5 ppm.

1c: 8-{[2-(4-Bromophenyl)ethyl]sulfanyl}caffeine

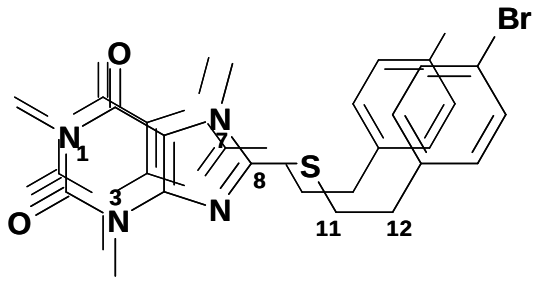

The title compound was prepared from 2-(4-bromophenyl)ethane-1-thiol in a yield of 38%: mp 165 °C (ethanol). ^{1}H NMR (Bruker Avance III 600, $CDCl_3$) δ 3.01 (t, 2H, J = 7.5 Hz), 3.37 (s, 3H), 3.45 (t, 2H, J = 7.5 Hz); 3.54 (s, 3H), 3.79 (s, 3H), 7.07 (d, 2H, J = 8.7 Hz), 7.39 (d, 2H, J = 8.3 Hz); ^{13}C NMR (Bruker Avance III 600, $CDCl_3$) δ 27.8, 29.7, 32.1, 33.6, 35.5, 108.6, 120.6, 130.3, 131.6, 138.2, 148.4, 150.5, 151.5, 154.5; EI-HRMS *m*/*z*: calcd for $C_{16}H_{17}BrN_4O_2S$, 408.0256, found 408.0258; Purity (HPLC): 97%.

^{1}H NMR:	**^{13}C NMR:**
• The three methyl groups at N1, N3 and N7 correspond to the singlets at 3.37, 3.54, 3.79 ppm (the signals integrate for 3 protons each) • The methylene groups at C11 and C12 are represented by the triplets at 3.01 and 3.45 ppm (the signals integrate for 2 protons each) • Aromatic protons on the phenyl ring correspond with the doublets at 7.07 and 7.39 ppm (the signals integrate for 2 protons each).	• Methyl groups at N1, N3 and N7 are represented by the signals at 27.8, 29.7, 32.1 ppm • The methylene groups at C11 and C12 correspond to the signals at 33.6 and 35.5 ppm • Aromatic carbons are represented by signals at 108.6, 120.6, 130.3, 131.6, 138.2, 148.4, 150.5, 151.1 and 154.5 ppm.

1d: 8-{[2-(4-Fluorophenyl)ethyl]sulfanyl}caffeine

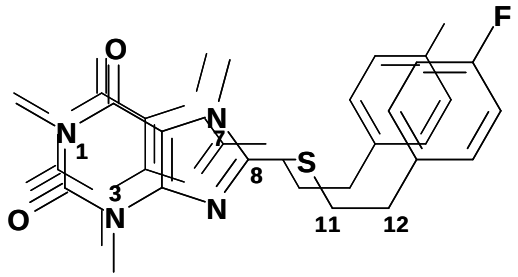

The title compound was prepared from 2-(4-fluorophenyl)ethane-1-thiol in a yield of 53%: mp 145 °C (ethanol). ^{1}H NMR (Bruker Avance III 600, $CDCl_3$) δ 3.01 (t, 2H, J = 7.5 Hz), 3.36 (s, 3H), 3.45 (t, 2H, J = 7.5 Hz); 3.55 (s, 3H), 3.78 (s, 3H), 6.97 (t, 2H, J = 8.7 Hz), 7.16 (m, 2H); ^{13}C NMR (Bruker Avance III 600, $CDCl_3$) δ 27.8, 29.7, 32.1, 33.8, 35.2, 108.6, 115.4, 130.0, 135.0, 135.1, 148.4, 150.7, 151.4, 154.5, 160.9, 162.5; EI-HRMS *m*/*z*: calcd for $C_{16}H_{17}FN_4O_2S$, 348.1056, found 348.1045; Purity (HPLC): 99%.

^{1}H NMR:	**^{13}C NMR:**
• The three methyl groups at N1, N3 and N7 correspond to the singlets at 3.36, 3.55, 3.78 ppm (the signals integrate for 3 protons each) • The methylene groups at C11 and C12 are represented by the triplets at 3.01 and 3.45 ppm (the signals integrate for 2 protons each) • Aromatic protons on the phenyl ring correspond with the signals at 6.97 and 7.16 ppm (the signals integrate for 2 protons each).	• Methyl groups at N1, N3 and N7 are represented by the signals at 27.8, 29.7, 32.1 ppm • The methylene groups at C11 and C12 correspond to the signals at 33.8 and 35.2 ppm • Aromatic carbons are represented by signals at 108.6 115.4, 130.0, 135.0, 135.1, 148.4, 150.7, 151.4, 154.5, 160.9 and 162.5 ppm. The two additional signals are due to the coupling between fluorine and adjacent carbon atoms.

1e: 8-{[2-(4-(Trifluoromethyl)phenyl)ethyl]sulfanyl}caffeine

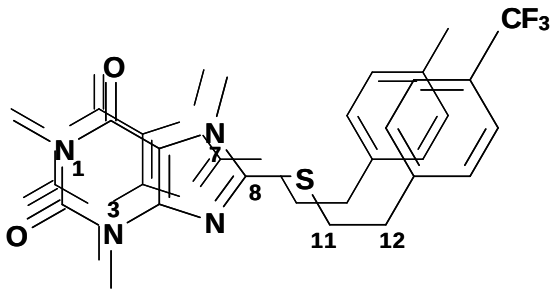

The title compound was prepared from 2-[4-(trifluoromethyl)phenyl]ethane-1-thiol in a yield of 37%: mp 178 °C (ethanol). ^{1}H NMR (Bruker Avance III 600, $CDCl_3$) δ 3.12 (t, 2H, J = 7.5 Hz), 3.36 (s, 3H), 3.49 (t, 2H, J = 7.5 Hz); 3.54 (s, 3H), 3.79 (s, 3H), 7.33 (d, 2H, J = 7.9 Hz), 7.54 (d, 2H, J = 8.2 Hz); ^{13}C NMR (Bruker Avance III 600, $CDCl_3$) δ 27.8, 29.6, 32.1, 33.3, 35.8, 108.6, 121.4, 123.2, 125.0, 125.5 (q), 126.8, 128.7, 128.9, 129.2, 129.4, 143.3, 148.4, 150.4, 151.4, 154.5; EI-HRMS *m*/*z*: calcd for $C_{17}H_{17}F_3N_4O_2S$, 398.1024, found 398.1007; Purity (HPLC): 99%.

^{1}H NMR:	**^{13}C NMR:**
• The three methyl groups at N1, N3 and N7 correspond to the singlets at 3.36, 3.54, 3.79 ppm (the signals integrate for 3 protons each) • The methylene groups at C11 and C12 are represented by the triplets at 3.12 and 3.49 ppm (the signals integrate for 2 protons each) • Aromatic protons on the phenyl ring correspond with the doublets at 7.33 and 7.54 ppm (the signals integrate for 2 protons each).	• Methyl groups at N1, N3 and N7 are represented by the signals at 27.8, 29.6, 32.1 ppm • The methylene groups at C11 and C12 correspond to the signals at 33.3 and 35.8 ppm • Aromatic carbons are represented by signals at 108.6, 121.4, 123.2, 125.0, 125.5, 126.8, 128.7, 128.9, 129.2, 129.4, 143.3, 148.4, 150.4, 151.4 and 154.5 ppm.

1f: 8-{[2-(4-Methylphenyl)ethyl]sulfanyl}caffeine

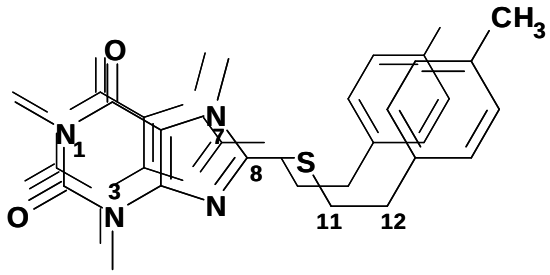

The title compound was prepared from 2-(4-methylphenyl)ethane-1-thiol in a yield of 36%: mp 122 °C (ethanol). ^{1}H NMR (Bruker Avance III 600, $CDCl_3$) δ 2.29 (s, 3H), 2.99 (t, 2H, J = 7.5 Hz), 3.36 (s, 3H), 3.46 (t, 2H, J = 7.5 Hz), 3.55 (s, 3H), 3.78 (s, 3H), 7.09 (m, 4H); ^{13}C NMR (Bruker Avance III 600, $CDCl_3$) δ 21.0, 27.8, 29.6, 32.1, 34.0, 35.6, 108.4, 128.4, 129.2, 136.3, 148.4, 150.9, 151.5, 154.5; EI-HRMS *m*/*z*: calcd for $C_{17}H_{20}N_4O_2S$, 344.1307, found 344.1307; Purity (HPLC): 97%.

^{1}H NMR:	**^{13}C NMR:**
• The three methyl groups at N1, N3 and N7 may correspond to the singlets at 3.36, 3.55 and 3.78 ppm (the signals integrate for 3 protons each) • Methylene groups at C11 and C12 are represented by the triplets at 2.99 and 3.46 ppm (the signals integrate for 2 protons each) • The methyl on the phenyl ring may correspond with a singlet at 2.29 (integrate for 3 protons) • Aromatic protons on the phenyl ring correspond with the multiplet at 7.09 ppm (the signal integrates for 4 protons).	• Methyl groups at N1, N3, N7 and on the phenyl ring are represented by the signals at 21.0, 27.8, 29.6 and 32.1 ppm • The methylene groups at C11 and C12 correspond to the signals at 34.0 and 35.6 ppm • Aromatic carbons are represented by signals at 108.4, 128.4, 129.2, 136.3, 148.4, 150.9, 151.1 and 154.5 ppm.

1g: 8-{[2-(4-Methoxyphenyl)ethyl]sulfanyl}caffeine

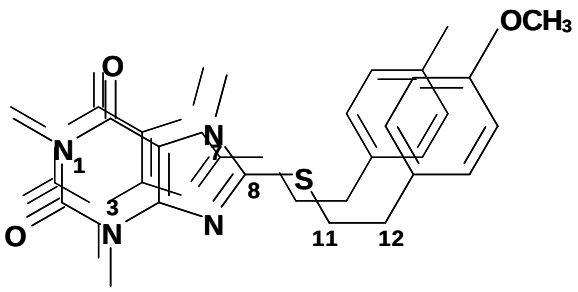

The title compound was prepared from 2-(4-methoxyphenyl)ethane-1-thiol in a yield of 45%: mp 125 °C (ethanol). ^{1}H NMR (Bruker Avance III 600, $CDCl_3$) δ 2.98 (t, 2H, J = 7.5 Hz), 3.36 (s, 3H), 3.44 (t, 2H, J = 7.5 Hz); 3.55 (s, 3H), 3.76 (s, 3H), 3.79(s, 3H), 6.82 (d, 2H, J = 8.7 Hz), 7.11 (d, 2H, J = 8.7 Hz); ^{13}C NMR (Bruker Avance III 600, $CDCl_3$) δ 27.8, 29.7, 32.1, 34.1, 35.2, 55.2, 108.5, 113.9, 129.5, 131.4, 148.5, 151.0, 151.5, 154.5, 158.4; EI-HRMS *m*/*z*: calcd for $C_{17}H_{20}N_4O_3S$, 360.1256, found 360.1248; Purity (HPLC): 99%.

^{1}H NMR:	**^{13}C NMR:**
• The three methyl groups at N1, N3 and N7 and the methyl group on the phenyl ring may correspond to the singlets at 3.36 and 3.55 and 3.76 ppm (the singlets integrate for 3 protons each) • Methylene groups at C11 and C12 are represented by the triplets at 2.98 and 3.44 ppm (the signals integrate for 2 protons each) • Aromatic protons on the phenyl ring correspond with the doublets at 6.82 and 7.11 ppm (the signal integrates for 2 protons) • The methoxy group on the phenyl ring	• Methyl groups at N1, N3, N7 are represented by the signals at 27.8, 29.7 and 32.1 ppm • The methylene groups at C11 and C12 correspond to the signals at 34.1 and 35.2 ppm • The methoxy group on the phenyl ring corresponds to the signal at 55.2 ppm • Aromatic carbons are represented by signals at 108.5, 113.9, 129.5, 131.4, 148.5, 151.0, 151.5, 154.5 and 158.4 ppm.

may correspond to the singlet at 3.79 ppm which integrates for 3 protons.	

2a: 8-{[2-(4-Bromophenyl)ethyl]sulfinyl}caffeine

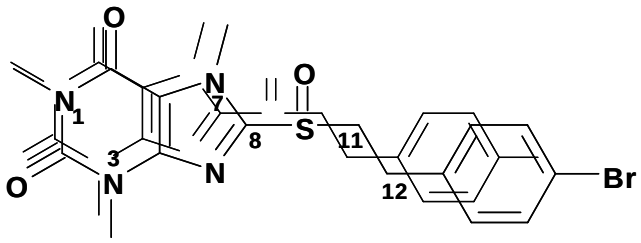

The title compound was prepared from 8-{[2-(4-bromophenyl)ethyl]sulfanyl}caffeine in a yield of 45%: mp 166 °C (ethanol). ^{1}H NMR (Bruker Avance III 600, $CDCl_3$) δ 3.11 (t, 2H, J = 7.5 Hz), 3.37 (s, 3H), 3.50 (m, 1H), 3.51 (s, 3H); 3.74 (m, 1H), 4.20 (s, 3H), 7.09 (d, 2H, J = 7.9 Hz); 7.38 (d, 2H, J = 7.5 Hz); ^{13}C NMR (Bruker Avance III 600, $CDCl_3$) δ 27.5, 28.1, 29.8, 33.3, 53.6, 110.0, 120.8, 130.3, 131.8, 136.7, 147.1, 149.1, 151.2, 155.0; EI-HRMS *m*/*z*: calcd for $C_{16}H_{17}BrN_4O_3S$ 424.0205, found 424.02004; Purity (HPLC): 96%.

^{1}H NMR:	**^{13}C NMR:**
• The three methyl groups at N1, N3 and N7 correspond to the singlets at 3.37, 3.51 and 4.20 ppm (the signals integrate for 3 protons each) • Methylene groups at C11 and C12 are represented by the triplet at 3.11, and multiplets at 3.50 and 3.74 ppm. These signals integrate for the 4 protons of the methylene groups. The multiplicity and observation that there are 3 signals may be explained by the chirality of the sulfinyl carbon atom • Aromatic protons on the phenyl ring correspond with the doublets at 7.09 and	• Methyl groups at N1, N3, N7 are represented by the signals at 27.5, 28.1 and 29.8 ppm • The methylene groups at C11 and C12 correspond to the signals at 53.6 and 33.3 ppm • Aromatic carbons are represented by signals at 110.0, 120.8, 130.3, 131.8, 136.7, 147.1, 149.1, 151.1 and 155.0 ppm.

7.38 ppm (the signal integrates for 2 protons each).	

2b: 8-{[2-(4-Fluorophenyl)ethyl]sulfinyl}caffeine

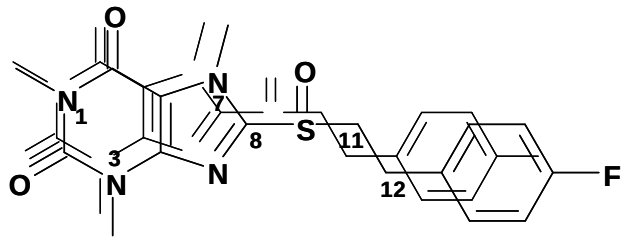

The title compound was prepared from 8-{[2-(4-fluorophenyl)ethyl]sulfanyl}caffeine in a yield of 38.8%: mp 126 °C (ethanol). ^{1}H NMR (Bruker Avance III 600, $CDCl_3$) δ 3.13 (m, 2H), 3.37 (s, 3H), 3.50 (m, 1H), 3.53 (m, 3H), 3.74 (m, 1H), 4.21 (s, 3H), 6.98 (t, 2H, J = 6.4 Hz); 7.18 (m, 2H); ^{13}C NMR (Bruker Avance III 600, $CDCl_3$) δ 27.4, 28.1, 29.8, 33.3, 54.0, 110.1, 115.6, 130.1, 133.5, 147.2, 149.3, 151.2, 155.0, 161.0, 162.6; EI-HRMS *m*/*z*: calcd for $C_{16}H_{17}FN_4O_3S$ 364.1006, found 364.0995; Purity (HPLC): 96%.

^{1}H NMR:	**^{13}C NMR:**
• The three methyl groups at N1, N3 and N7 correspond to the singlets at 3.37, 3.53 and 4.21 ppm (the signals integrate for 3 each) • Methylene groups at C11 and C12 are represented by the multiplets at 3.13, 3.50 and 3.74 ppm (collectively, these signals integrate for 4 protons as expected for the two methylene groups) • Aromatic protons on the phenyl ring correspond with the triplets at 6.98 and 7.18 ppm (the signal integrates for 2 protons each).	• Methyl groups at N1, N3, N7 are represented by the signals at 27.4, 28.1 and 29.8 ppm • The methylene groups at C11 and C12 correspond to the signals at 54.0 and 33.3 ppm • Aromatic carbons are represented by signals at 110.1, 115.6, 130.1, 133.5, 147.2, 149.3, 151.2, 155.0, 161.1 and 162.6 ppm. The additional signal is due to the coupling between fluorine and the carbon atom to which it is attached.

3.9 Interpretation of the mass spectra

All the synthesized compounds were characterized by mass spectrometry. In table 3.2 the calculated and experimentally determined high resolution masses are noted. The small differences between the calculated and experimentally determined masses are indicative that the structures of the compounds correspond to those given in table 3.1.

Tabel 3.2 The calculated and experimentally determined high resolution masses of the synthesized compounds. All masses are given as M^+.

Compound	Mass Spectrometry			
	Calculated	Found	Formula	Ppm
1a	330.11505	330.11465	$C_{16}H_{18}N_4O_2S$	-1.2
1b	364.07608	364.07559	$C_{16}H_{17}ClN_4O_2S$	-1.3
1c	408.02556	408.02583	$C_{16}H_{17}BrN_4O_2S$	0.7
1d	348.10563	348.10446	$C_{16}H_{17}FN_4O_2S$	-3.4
1e	398.10243	398.10070	$C_{17}H_{17}F_3N_4O_2S$	-4.3
1f	344.13070	344.13074	$C_{17}H_{20}N_4O_2S$	0.1
1g	360.12561	360.12480	$C_{17}H_{20}N_4O_3S$	-2.2
2a	424.02047	424.02004	$C_{16}H_{17}BrN_4O_3S$	-1.0
2b	364.10054	364.09951	$C_{16}H_{17}FN_4O_3S$	-2.8

ppm = [(found - calcd.)/calcd]. x 1000000. In general a ppm difference smaller than 5 is considered to be good agreement.

3.10 Interpretation of the HPLC analysis

All the synthesized compounds were analysed for purity by HPLC analysis. Strong eluting conditions were selected (up to 85% acetonitrile). Under these conditions most compounds present in the samples are expected to elute. Furthermore, at the low wavelength selected, 210 nm, most organic compounds are expected to absorb and therefore should be detectable. The

chromatograms obtained for the test compounds are given in the addendum. As shown by the chromatograms, a single peak for each compound analysed indicates that the compounds are of a high degree of purity. Where additional peaks occurred, the percentage purities were calculated. These calculations were based on the integrated areas of the analyte and impurity peaks. As cited in section 3.8, the purities of the synthesized compounds were estimated to be 96–99%, which may be deemed acceptable.

3.11 Conclusion

Seven 8-[(2-phenylethyl)sulfanyl]caffeine analogues were successfully synthesized from 8-chlorocaffeine and the appropriate substituted phenylethylmercaptan. Two 8-[(2-phenylethyl)sulfinyl]caffeine analogues were also successfully synthesized by reacting the required 8-[(2-phenylethyl)sulfanyl]caffeine derivative with hydrogen peroxide in, the presence of glacial acetic acid and acetic acid anhydride. All of the synthesized compounds structures were characterized and confirmed by MS and NMR analyses. The ^{1}H NMR and ^{13}C NMR spectra correspond to the suggested structures of the compounds and their experimentally determined masses correspond with the calculated masses. The purities of the compounds were estimated by HPLC analysis and a single peak was noted for each compound analyzed. It can therefore be concluded that the synthesized compounds correspond with the proposed structures of the 8-[(2-phenylethyl)sulfanyl]caffeine and 8-[(2-phenylethyl)sulfinyl]caffeine analogues, and that the compounds are of an acceptable degree of purity.

Chapter 4

Enzymology

4.1 Introduction

In this chapter the 8-[(2-phenylethyl)sulfanyl]caffeine (**1a**–**g**) and 8-[(2-phenylethyl) sulfinyl]caffeine (**2a**–**b**) analogues that were synthesized in the previous chapter, will be investigated as inhibitors of human MAO-A and MAO-B. As previously discussed in Chapter 2, there are several methods available to measure MAO activity *in vitro*. In this study a fluorometric assay was used to determine the IC_{50} values of the inhibitors. For this purpose kynuramine was used as substrate. This assay is based on the measurement of the extent by which an inhibitor reduces the MAO-catalyzed oxidation of kynuramine to the fluorescent product, 4-hydroxyquinoline. The concentrations of 4-hydroxyquinoline were measured fluorometrically at an excitation wavelength of 310 nm and an emission wavelength of 400 nm.

4.2 Chemicals and instrumentation

A Varian Cary Eclipse fluorescence spectrophotometer was employed for the fluorometric measurements. Insect cell microsomes containing recombinant human MAO-A and MAO-B (5 mg/ml) and kynuramine.2HBr were obtained from Sigma-Aldrich. The Graphpad Prism 5 software package was used to construct sigmoidal dose-response curves and to determine the IC_{50} values.

4.3 Determining the IC_{50} values

In this study, IC_{50} values were determined for the 8-[(2-phenylethyl)sulfanyl]caffeine (**1a**–**g**) and 8-[(2-phenylethyl)sulfinyl]caffeine (**2a**–**c**) analogues. This was done to determine the potency by which each compound inhibits MAO-A and MAO-B. From these results the most potent MAO-A and MAO-B inhibitors may be identified, and the SAR for the inhibition of the MAO enzymes may be examined (see 4.4 and 4.5).

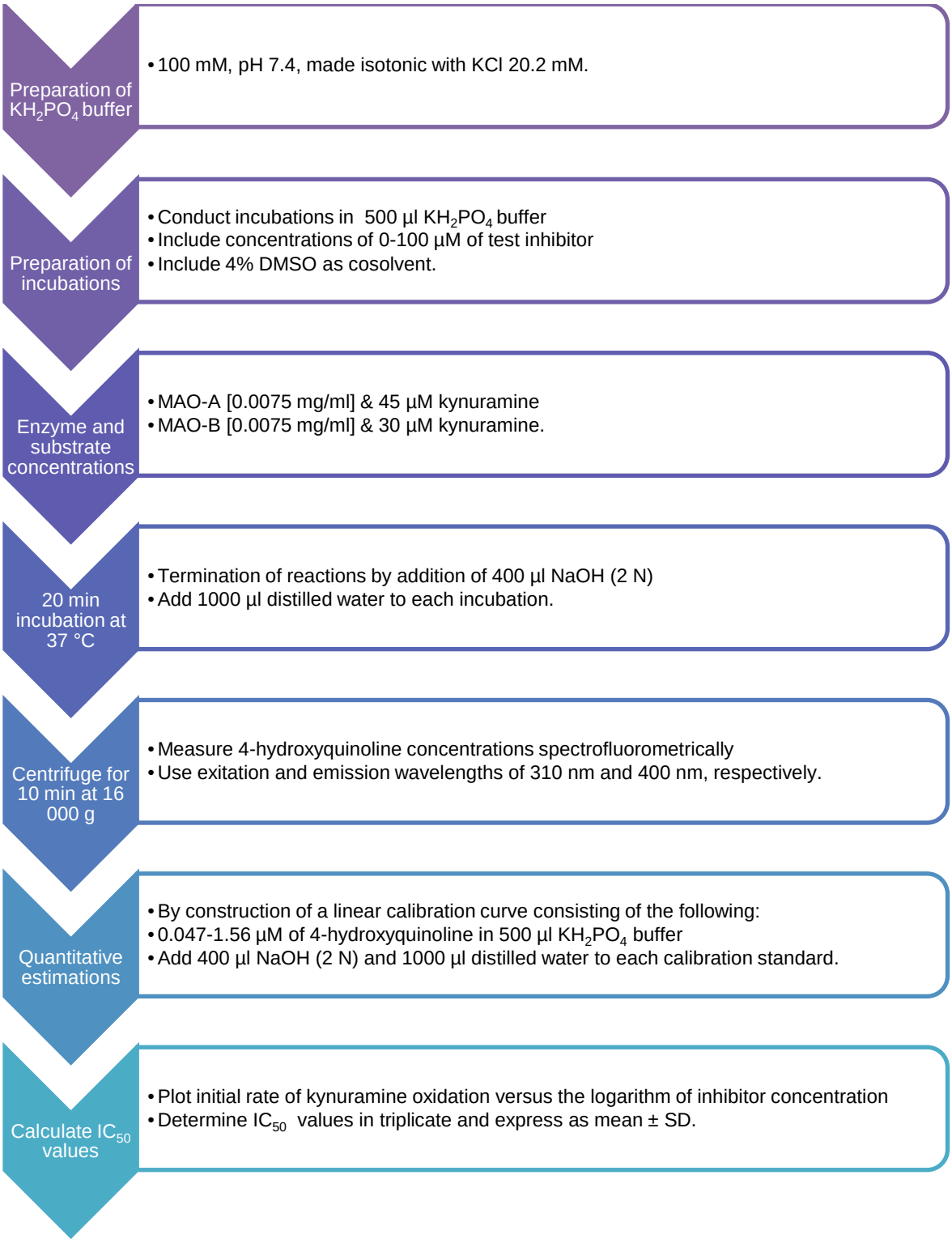

Figure 4.1 Diagrammatic representation of the method for determining IC_{50} values for the inhibition of MAO-A and MAO-B.

4.3.1 Method (see figure 4.1. for a diagrammatic overview):

Recombinant human MAO-A (5 mg/ml) and human MAO-B (5 mg/ml) were obtained from Sigma-Aldrich and were pre-aliquoted and stored at -70 °C. For the purpose of the IC_{50} determinations the incubations contained:

- 500 µl potassium phosphate buffer (100 mM, pH 7.4, made isotonic with KCl),
- MAO-A (0.0075 mg/ml) or MAO-B (0.0075 mg/ml),
- various concentrations of the test inhibitor (0–100 µM),
- 4% DMSO as cosolvent and
- kynuramine as substrate. The final concentrations of the kynuramine substrate were 30 µM and 45 µM for MAO-B and MAO-A, respectively.

These reactions were incubated for 20 min at 37 °C and were subsequently terminated by the addition of 400 µl NaOH. Distilled water (1000 µl) was added to each reaction to make up the final volume. Centrifugation followed for 10 min at 16 000 g.

Concentration measurements of 4-hydroxyquinoline in each incubation were carried out spectrofluorometrically by measuring the fluorescence of the supernatant at an excitation wavelength of 310 nm and an emission wavelength of 400 nm. The PMT voltage of the spectrofluorometer was set to medium with an excitation and emission slit width of 5 mm each.

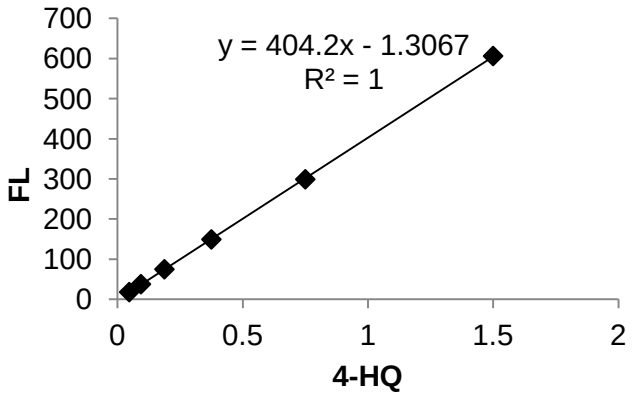

Figure 4.2 An example of the calibration curves routinely constructed in this study. The graph is that of the fluorescence intensity (FL) of 4-hydroxyquinoline versus the concentration of authentic 4-hydroxyquinoline (4-HQ), expressed in micromolar.

Quantitative estimations were made with a linear calibration curve. This linear calibration curve was constructed with known amounts (0.047–1.56 μM) of 4-hydroxyquinoline dissolved in 500 μL potassium phosphate buffer (100 mM, pH 7.4, made isotonic with KCl 20.2 mM). To each calibration standard, volumes of 400 μl NaOH (2 N) and 1000 μl water were added. Control samples were included to confirm that the test inhibitors do not fluoresce or quench the fluorescence of 4-hydroxyquinoline under these assay conditions. The calibration curve values that are obtained should bracket the obtained fluorescence values for the inhibition studies and it should also display linearity.

In order to determine an IC_{50} value, the initial rate of oxidation was graphically plotted against the logarithm of the inhibitor concentration and a sigmoidal dose-response curve was obtained. For each sigmoidal curve, 6 different inhibitor concentrations spanning at least 3 orders of magnitude were used. Graphpad prism 5 was used to fit the inhibition data to the one site competition model. The IC_{50} values were determined in triplicate and expressed as mean ± standard deviation (SD).

4.3.2 Results

Table 4.1 The IC_{50} values for the inhibition of human MAO-A and MAO-B by 8-[(2-phenylethyl) sulfanyl]caffeine analogues (**1a**–**g**).

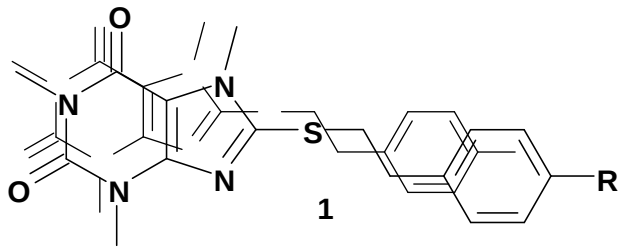

1

		IC_{50} (μM)[a]	
	R	**MAO-A**	**MAO-B**
1a	**-H**	18.7 ± 0.31	0.271 ± 0.006
1b	**-Cl**	8.46 ± 0.98	0.020 ± 0.005

1c	**-Br**	108 ± 18	0.019 ± 0.003
1d	**-F**	14.7 ± 0.94	0.071 ± 0.012
1e	**-CF_3**	No inhibition[b]	0.019 ± 0.003
1f	**-CH_3**	125 ± 9.1	0.072 ± 0.012
1g	**-OCH_3**	168 ± 9.1	0.023 ± 0.003

[a] All values are expressed as the mean ± SD of triplicate determinations
[b] No inhibition observed at a maximal tested concentration of 100 µM.

The IC_{50} values obtained for the inhibition of MAO-A and MAO-B by the 8-[(2-phenylethyl) sulfanyl]caffeine (**1a**–**g**) and 8-[(2-phenylethyl)sulfinyl]caffeine analogues (**2a**–**b**) are listed in tables 4.1 and 4.2. The IC_{50} values are expressed as the mean ± SD and the units are given as µM. Inhibition potencies can be classified according to the IC_{50} value, the more potent a compound is, the lower the IC_{50} value. The most potent compounds are highlighted in blue.

Table 4.2 The IC_{50} values for the inhibition of human MAO-A and MAO-B 8-[(2-phenylethyl) sulfinyl]caffeine analogues (**2a**–**b**).

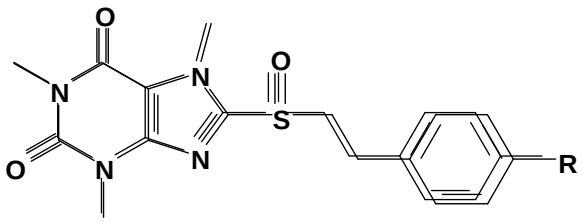

2

		IC_{50} (µM)[a]	
	R	**MAO-A**	**MAO-B**
2a	**-Br**	57.3 ± 12.8	0.471 ± 0.057
2b	**-F**	451 ± 380	3.504 ± 0.083

[a] All values are expressed as the mean ± SD of triplicate determinations

Figure 4.3 and 4.4 depicts typical sigmoidal graphs that were constructed in this study for the measurement of IC_{50} values. The rate of the MAO catalyzed oxidation of kynuramine is plotted

against the logarithm of the inhibitor concentration. The IC_{50} value is then determined by calculating the inhibitor concentration that produces 50% inhibition of the enzyme catalytic rate. The sigmoidal graph constructed for 8-{[2-(4-bromophenyl)ethyl]sulfanyl}caffeine (**1c**) is depicted in this graph since it was found to be one of the most potent inhibitors of human MAO-B with an IC_{50} value of 0.019 µM.

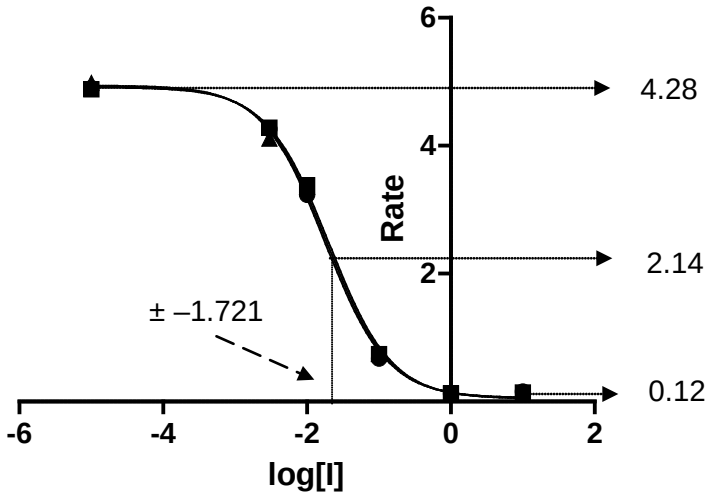

Figure 4.3 A sigmoidal graph used to determine the IC_{50} value of 8-{[2-(4-bromophenyl)ethyl]sulfanyl}caffeine towards MAO-B. At 50% inhibition, log [I] = -1.721, which is equal to [I] = 0.019 µM. The rate is expressed as nmol product formed/min/mg protein.

8-{[2-(4-Chlorophenyl)ethyl]sulfanyl}caffeine (**1b**) was found to be the most potent inhibitor for MAO-A with an IC_{50} value of 8.458 µM. The sigmoidal graph constructed for **1c** is given below.

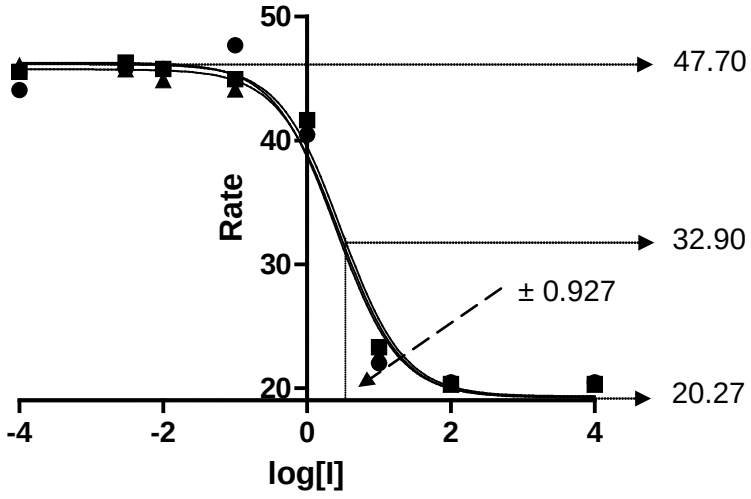

Figure 4.4 A sigmoidal graph used to determine the IC_{50} value of 8-{[2-(4-chlorophenyl)ethyl]sulfanyl}caffeine towards MAO-A. At 50% inhibition, log [I] = 0.927, which is equal to [I] = 8.458 µM. The rate is expressed as nmol product formed/min/mg protein.

The 8-[(2-phenylethyl)sulfanyl]caffeine analogues (**1a**–**g**) show exceptionally high inhibition potencies towards MAO–B since the inhibition potencies are well within the nM range. The most potent inhibitors were the 8-{[2-(4-phenyl)ethyl]sulfanyl}caffeine analogues substituted with chlorine, bromine and the trifluoromethyl group at the C-4 position of the phenyl ring. The IC_{50} values of these compounds were found to be 0.019–0.020 µM. The 8-[(2-phenylethyl)sulfinyl] caffeine analogues (**2a**–**b**) were also found to be inhibitors of MAO-B. The sulfinyl analogues are however, weaker MAO-B inhibitors than the corresponding sulfanyl derivatives. All the compounds were found to be weak inhibitors of MAO-A with 8-{[2-(4-trifluorophenyl) ethyl]sulfanyl}caffeine exhibiting no inhibition. Thus the synthesized compounds are selective inhibitors of MAO-B.

Considering the results of the MAO inhibition studies the following comparisons and conclusions may be made:

a) Firstly, the MAO-B inhibition potencies of the 8-[(2-phenylethyl)sulfanyl]caffeine analogues, that are substituted with halogens on the phenyl ring were compared to the IC_{50} value of the unsubstituted homologue, 8-[(2-phenylethyl) sulfanyl]caffeine analogue (**1a**) (Table 4.3).

Table 4.3 A comparison of the IC_{50} values for the inhibition of MAO-B by the halogen substituted 8-[(2-phenylethyl)sulfanyl]caffeine analogues with the unsubstituted homologue, 8-[(2-phenylethyl)sulfanyl]caffeine analogue (**1a)**

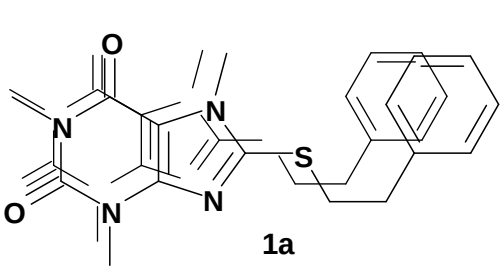

1a

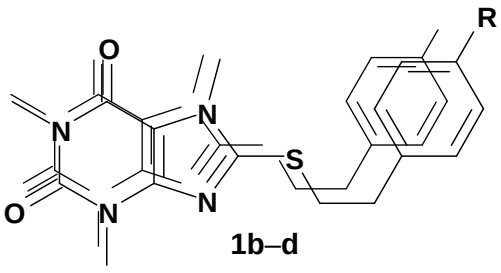

1b–**d**

Compound	R	MAO–B IC_{50} (µM)	Ratio 1a/ 1b–d [a]
1a	-H	0.271	——

1b	-Cl	0.020	13.55
1c	-Br	0.019	14.26
1d	-F	0.071	3.82

[a] The ratio of IC_{50}(**1a**)/IC_{50}(**1b**–**d**)

The results given in table 4.3 show that the inhibition potencies of 8-[(2-phenylethyl)sulfanyl]caffeine (**1a**) may be enhanced by substitution on the C-4 position of the phenyl ring with halogens. The inhibition potencies increase from 3.82–14.26 fold with halogen substitution. The best halogen substituted 8-[(2-phenylethyl)sulfanyl]caffeine analogue is the bromine substituted homologue, compound **1c**, which is 14.26 times more potent than the unsubstituted 8-[(2-phenylethyl)sulfanyl]caffeine analogue (**1a**).

b) Secondly, the MAO-B inhibition potencies of the 8-[(2-phenylethyl)sulfanyl]caffeine analogues which are substituted with methyl and methoxy functional groups were compared to the inhibition potency of the unsubstituted 8-[(2-phenylethyl)sulfanyl]caffeine analogue (**1a**). The results are given in table 4.4.

Table 4.4 A comparison of the IC_{50} values for the inhibition of MAO-B by the methyl (**1f**) and methoxy (**1g**) substituted 8-[(2-phenylethyl)sulfanyl]caffeine analogues with the unsubstituted 8-[(2-phenylethyl)sulfanyl]caffeine analogue (**1a**)

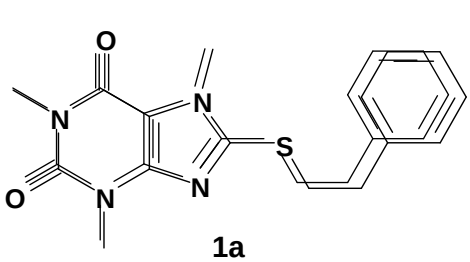

1a

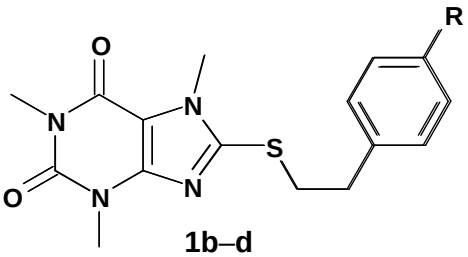

1b–**d**

Compound	R	MAO-B IC_{50} (μM)	Ratio 1a/1f-1g [a]
1a	-H	0.271	——
1f	$-CH_3$	0.072	3.76

1g	-OCH_3	0.023	11.78

[a] The ratio of IC_{50}(**1a**)/IC_{50}(**1f** or **1g**)

Table 4.4 shows that, similar to halogen substitution, substitution with methyl and methoxy functional groups also increases the inhibition potencies of the 8-[(2-phenylethyl) sulfanyl]caffeine analogues. Interestingly, substitution with the methoxy group enhances the inhibition potency of **1a** by 11.78-fold, whereas the methyl functional group enhances the potency of **1a** by 3.76-fold. This indicates that the methoxy functional group is more suitable for enhancing the inhibition potency of **1a** than the methyl group.

c) Substitution on C-4 with a halogen containing substituent, the trifluoromethyl group, enhances the MAO-B inhibition potency of 8-[(2-phenylethyl)sulfanyl]caffeine to the same degree as bromine. The trifluoromethyl substituted homologue, compound **1e**, inhibits human MAO-B with an IC_{50} value of 0.019 µM, which is equal to the bromine substituted homologue, compound **1c**.

d) Table 4.5 compares the potencies of the halogen substituted 8-[(2-phenylethyl)sulfanyl] caffeine analogues may also be compared to that of the halogen substituted 8-[(2-phenylethyl) sulfinyl]caffeine analogues.

Table 4.5 A comparison of the IC_{50} values for the inhibition of MAO-B by substituted 8-[(2-phenylethyl)sulfanyl]caffeine with the corresponding 8-[(2-phenylethyl)sulfinyl]caffeine analogues.

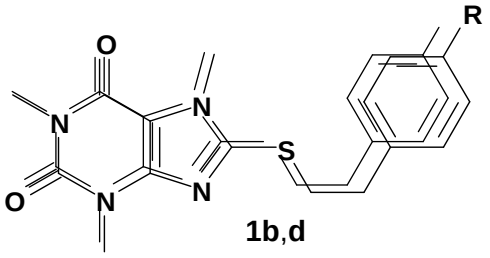

1b,**d**

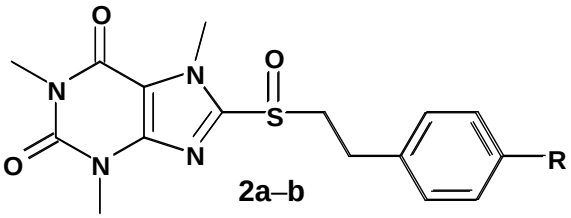

2a–**b**

Compound	R	MAO-B IC_{50} (µM)	Ratio
1c	-Br	0.019	24.79[a]
2a	-Br	0.471	
1d	-F	0.071	11.00[b]

2b	-F	0.781	

[a] The ratio of IC_{50}(**2a**)/ IC_{50}(**1c**), respectively.
[b] The ratio of IC_{50}(**2b**)/ IC_{50}(**1d**), respectively.

Table 4.5 shows that the 8-[(2-phenylethyl)sulfanyl]caffeine analogues exhibit a 11.0 to 24.79-fold higher MAO-B inhibition potency than the 8-[(2-phenylethyl)sulfinyl]caffeine analogues.

e) The results of the MAO-A inhibition studies document that both the 8-[(2-phenylethyl)sulfanyl]caffeine and the 8-[(2-phenylethyl)sulfinyl]caffeine analogues are relatively weak human MAO-A inhibitors with IC_{50} values in the µM range. While no clear SAR are observed, it may be concluded that **1e** is a particularly promising inhibitor when potent and selective MAO-B inhibition are desired. Compound **1e** is a highly potent MAO-B inhibitor while exhibiting no MAO-A inhibition. Compound **1b** was found to be the most potent MAO-A inhibitor of the series with an IC_{50} value of 8.454 µM. Considering that its IC_{50} value for the inhibition of MAO-B is 0.020 µM, **1b** may, however, also be considered a selective MAO-B inhibitor.

4.4 Time-dependent studies

Time-dependent studies were carried out on a selected inhibitor in order to determine whether it acts as a reversible inhibitor or as a time-dependent inactivator of human MAO-A and MAO-B.

4.4.1 Method (see figure 4.5. for a diagrammatic overview):

For this study, kynuramine was used as substrate and compound **1b** was selected as inhibitor. The human recombinant enzymes were pre-incubated with the selected inhibitor for periods of 0, 15, 30 and 60 minutes at 37 °C. The concentration of the enzymes in the reactions were 0.03 mg/ml for MAO-A and MAO-B, and the inhibitor concentrations were equal to 2-fold the measured IC_{50} values for the inhibition of MAO–A or MAO–B, respectively. These incubations were conducted in a potassium phosphate buffer (100 mM, pH 7.4, made isotonic with KCl 20.2 mM) to a final volume of 500 µl. Following the addition of kynuramine (45 µM for MAO-A and 30 µM for MAO-B), the reactions were incubated at 37 °C for a further 20 minutes. After the

incubation period, the reactions were terminated by the addition of 400 µl NaOH and 1000 µl distilled water to each incubation. Centrifugation followed for 10 minutes at 16 000 g.

The concentrations of the MAO generated 4-hydroxyquinoline were measured spectrofluorometrically as described in paragraph 4.3.1. The experiments were carried out in triplicate and a calibration curve was prepared for each data set. This calibration curve was constructed with known amounts (0.047–1.56 µM) of 4-hydroxyquinoline dissolved in 500 µl potassium phosphate buffer (100 mM, pH 7.4, made isotonic with KCl 20.2 mM). To each calibration standard, volumes of 400 µl NaOH (2 N) and 1000 µl water were added.

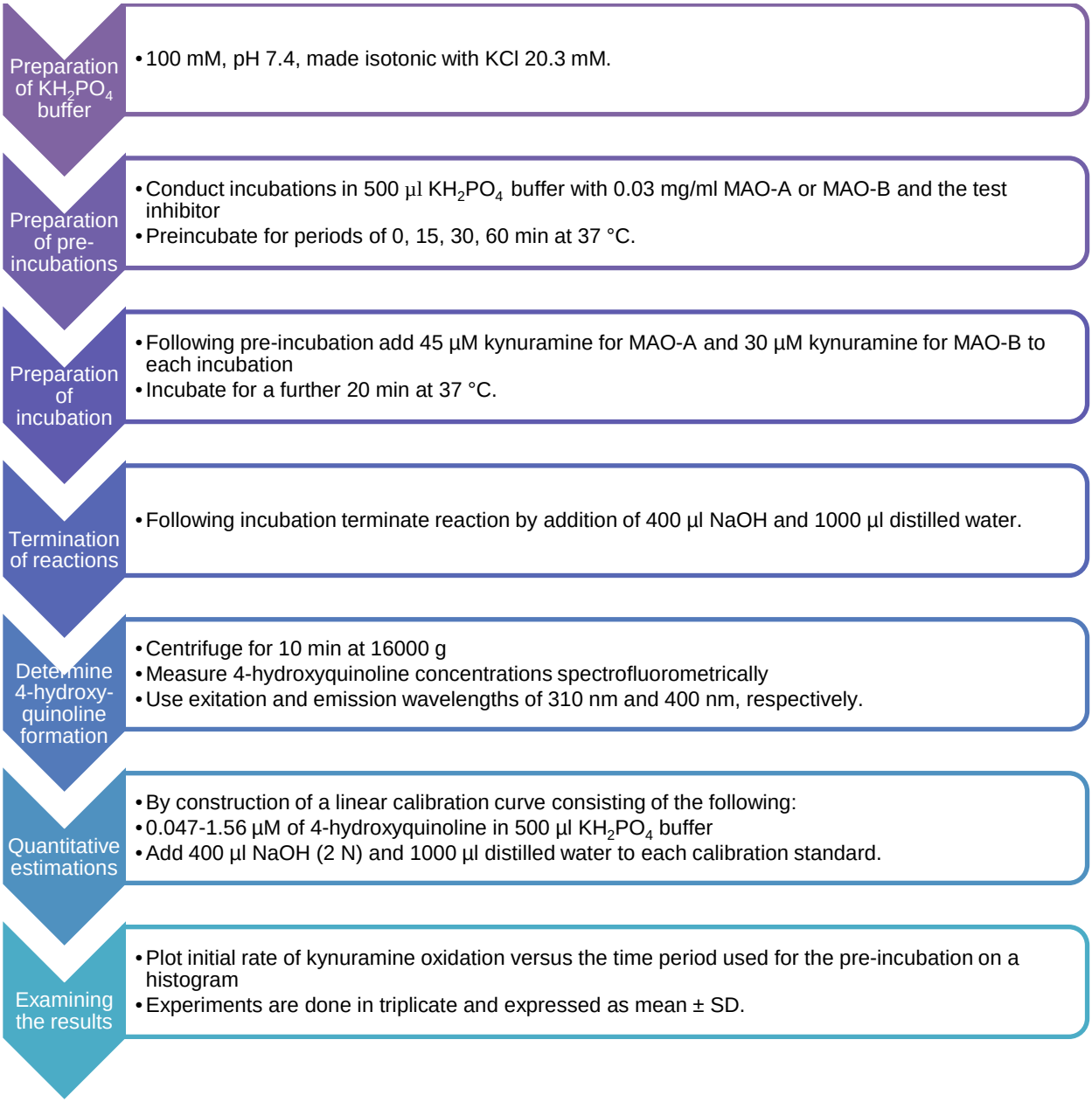

Figure 4.5 Diagrammatic representation of the method followed for the time–dependent studies.

4.4.2 Results

8-{[2-(4-Chlorophenyl)ethyl]sulfanyl}caffeine (**1b**) was selected as representative inhibitor for the reversibility studies with both human MAO-A and MAO-B. Figures 4.6 and 4.7 depict histograms where the rate of substrate oxidation was plotted versus the time periods used for the pre-incubations.

In the case of reversible inhibition, the rate of MAO catalysis will be constant for all the incubation times. In contrast, for irreversible inhibition the rate of MAO catalysis will decrease in a time-dependent manner.

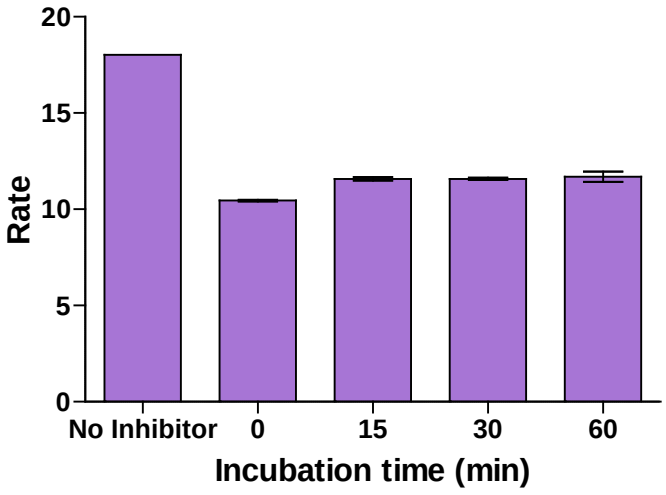

Figure 4.6 A histogram depicting the rate of kynuramine oxidation by MAO-A after pre-incubation of the enzyme with inhibitor **1b** for various periods of time (0–60 min). The rate (V) is expressed as nmol product formed/min/mg protein.

Reversible inhibition for 8-{[2-(4-chlorophenyl)ethyl]sulfanyl}caffeine (**1b**) was observed for both MAO-A and MAO-B. The graphs show no time–dependent decrease of the MAO-A and MAO-B

catalyzed oxidation rates of kynuramine as a function of pre–incubation time. It can therefore be concluded that (**1b**), and most likely the other 8-[(2-phenylethyl)sulfanyl]caffeine analogues examined in this study, are reversible inhibitors of human MAO-A and MAO-B.

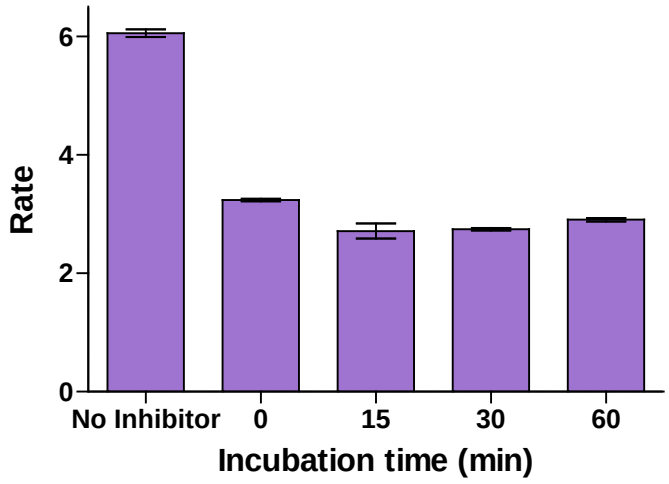

Figure 4.7 A histogram depicting the rate of kynuramine oxidation by MAO-B after pre-incubation of the enzyme with inhibitor **1b** for various periods of time (0–60 min). The rate (V) is expressed as nmol product formed/min/mg protein.

4.5 Lineweaver–Burk plots

Lineweaver-Burk plots are used to determine whether an inhibitor exhibits a competitive or noncompetitive mode of inhibition. Since the 8-[(2-phenylethyl)sulfanyl]caffeine analogues were found to be potent inhibitors of MAO-B, in this study a set of Lineweaver-Burk plots for the inhibition of MAO-B were constructed for a selected inhibitor, 8-{[2-(4-chlorophenyl)ethyl] sulfanyl}caffeine (**1b**).

4.5.1 Method (see figure 4.8. for a diagrammatic overview):

Recombinant human MAO-B (5 mg/ml) obtained from Sigma-Aldrich was pre-aliquoted and stored at -70 °C. The incubations were conducted in 500 μl potassium phosphate buffer (100 mM, pH 7.4, made isotonic with KCl), and contained the substrate, kynuramine, MAO-B (0.015 mg/ml) and three selected concentrations of the test inhibitor (0.005 μM, 0.010 μM and 0.020

μM). A Lineweaver-Burk plot was also constructed in the absence of inhibitor. Kynuramine was included in the incubations at four different concentrations (15–90 μM). These reactions were subsequently incubated for 20 min at 37 °C and terminated by the addition of 400 μl NaOH and 1000 μl distilled water. The reactions were centrifuged for 10 min at 16 000 g.

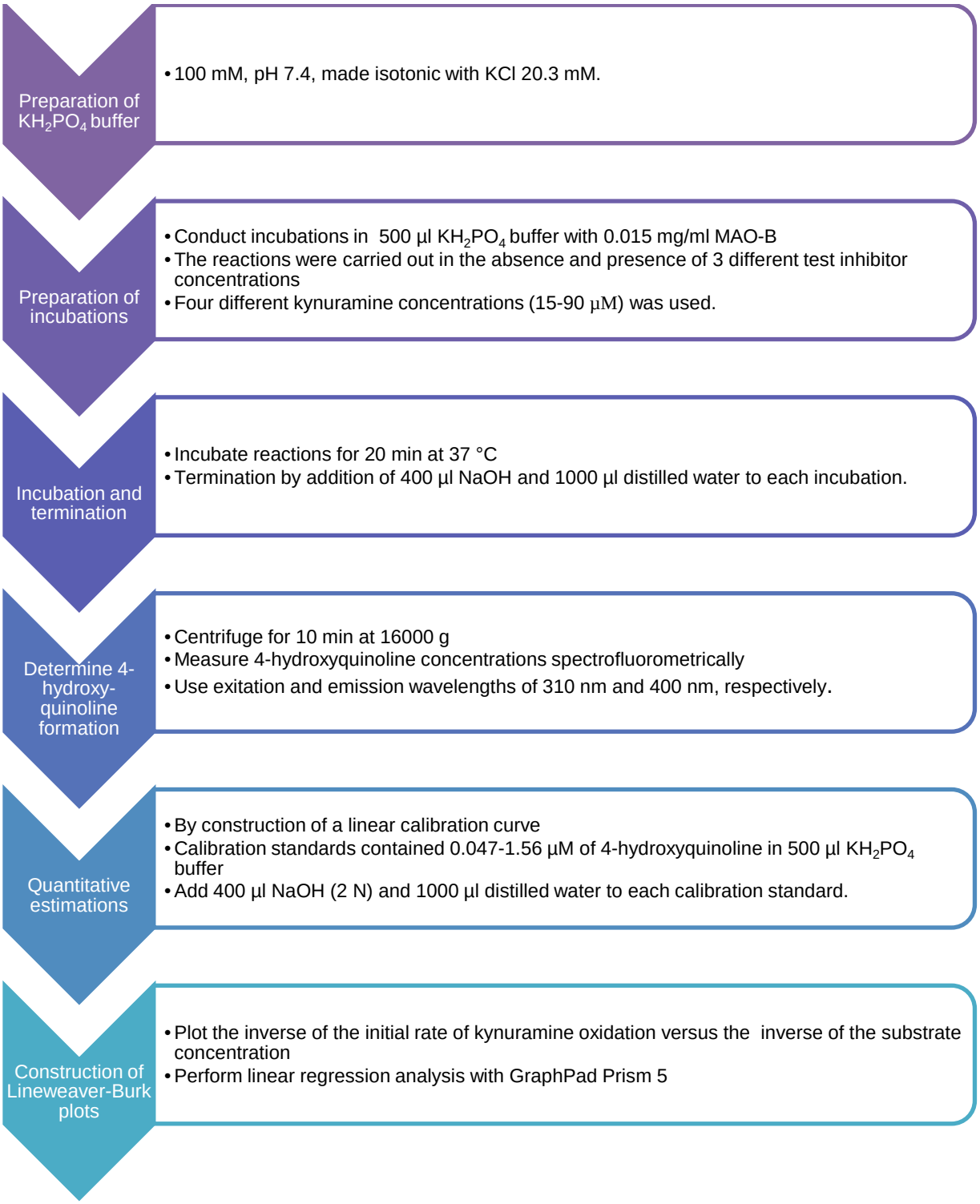

Figure 4.8 Diagrammatic presentation of the method used for the construction of Lineweaver-Burk plots.

The initial rates by which MAO catalyzes the oxidation of kynuramine were subsequently determined spectrofluorometrically. The concentration of 4-hydroxyquinoline in each incubation was determined by measuring the fluorescence of the supernatant at an excitation wavelength of 310 nm and an emission wavelength of 400 nm. The PMT voltage of the spectrofluorometer was set to medium with an excitation and emission slit width of 5 mm each. A calibration curve was constructed with known amounts (0.047-1.56 μM) of 4-hydroxyquinoline dissolved in 500 μl potassium phosphate buffer (100 mM, pH 7.4, made isotonic with KCl 20.2 mM). To each calibration standard, volumes of 400 μl NaOH (2 N) and 1000 μl water were added. Lineweaver-Burk plots were constructed from these data sets and linear regression analysis was performed using the GraphPad Prism 5 software package.

4.5.2 Results

8-{2-4-Chlorophenyl)ethyl]sulfanyl}caffeine (**1b**) was selected as representative inhibitor for the construction of the Lineweaver-Burk plots in this study (figure 4.9). The inverse of the measured rates were plotted versus the inverse of the substrate concentrations used. The plots were constructed in the absence of inhibitor and presence of 3 different inhibitor concentrations.

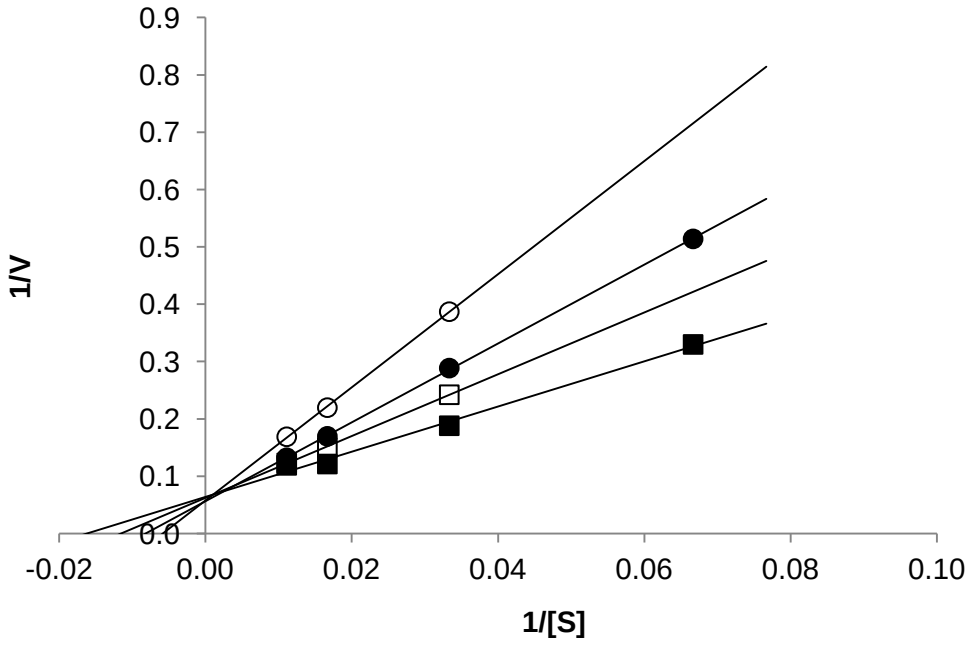

Figure 4.9 Lineweaver-Burk plots for the oxidation of kynuramine by MAO-B in the absence (filled squares) and presence of various concentrations of 8–{2–4–chlorophenyl)ethyl]sulfanyl} caffeine (open squares, 5 nM; filled circles, 10 nM; open circles, 20 nM). The rate (V) is expressed as nmol product/min/mg protein.

As shown in figure 4.9, this set of Lineweaver-Burk plots is typical of competitive inhibition. Competitive inhibition is evident from the intersecting set of Lineweaver-Burk plots at the Y-axis. It may therefore be concluded that 8-{[2-(4-chlorophenyl)ethyl]sulfanyl}caffeine (**1b**) is a competitive inhibitor of MAO-B.

As discussed in 2.5, Lineweaver-Burk plots are used not only to distinguish between competitive and noncompetitive inhibitors, but can also be used for the evaluation of the inhibitor constant, K_i. K_i values allow us to compare the inhibition potencies between inhibitors for the same enzyme as well as to compare the potencies of inhibition for different enzymes. As with the IC_{50} values, the lower the K_i value the more potent the inhibitor. The K_i value can be determined by replotting the slopes of the Lineweaver-Burk plots against the inhibitor concentrations (figure 4.10). The negative of the x-axis intercept is equal to K_i.

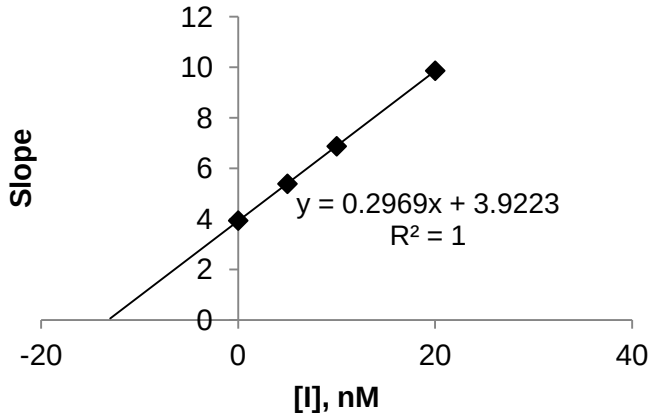

Figure 4.10 Graph of the slopes of the Lineweaver-Burk plots versus the concentration of inhibitor **1b**.

The equation of the linear line, y = 0.2969x + 3.9223, can thus be used to calculate K_i. Since the x-axis intercept is -13.21 nM, it can be concluded that the K_i value 8-{[2-(4-chlorophenyl)ethyl] sulfanyl}caffeine (**1b**) for the inhibition of human MAO-B is 13.21 nM

The K_i value can also be determined from the experimentally determined IC_{50} value by the equation suggested by Cheng & Prusoff (1973):

$$K_i = \frac{IC_{50}}{\left(1 + \frac{[S]}{K_m}\right)}$$

As described in figure 2.25 the K_m value for the oxidation of kynuramine by MAO-B may be obtained from the x-axis intercept of the Lineweaver-Burk plot constructed in the absence of inhibitor. The x-axis intercept is equal to $-1/K_m$ (figure 4.11). Thus, by solving the linear equation, the value of the x-axis intercept is -0.016 μM^{-1} and the apparent K_m value is therefore 61.5 µM.

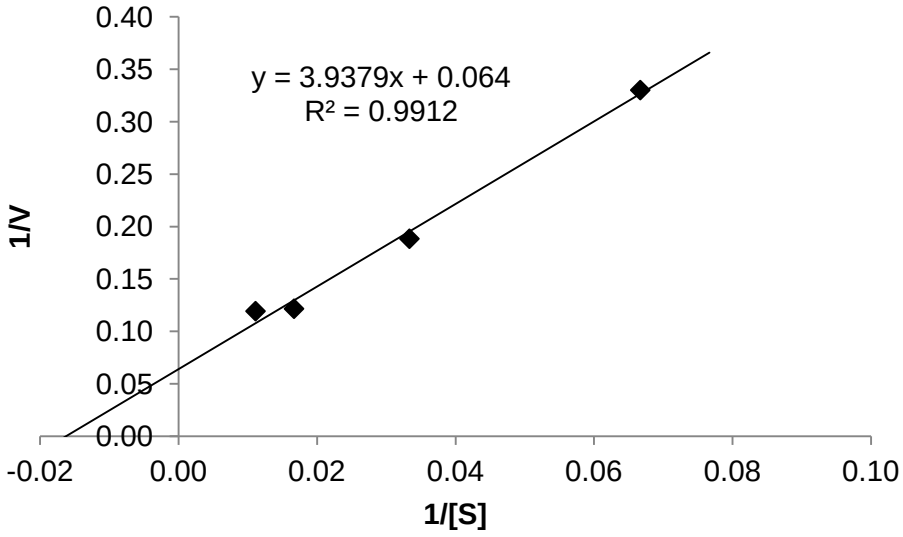

Figure 4.11 Experimental determination of the K_m value for the oxidation of kynuramine by MAO-B. For this purpose the Lineweaver–Burk plot constructed in the absence of inhibitor is employed.

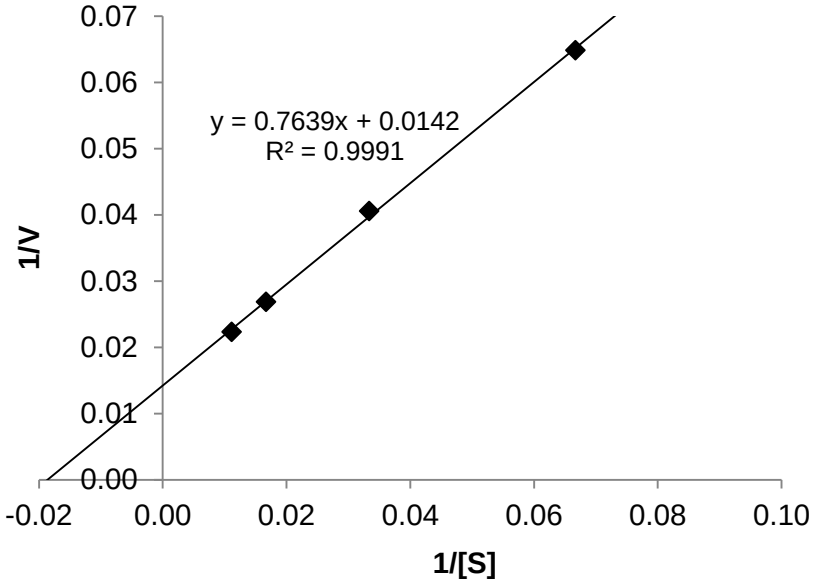

Figure 4.12 Experimental determination of the K_m value for the oxidation of kynuramine by MAO-A. For this purpose the Lineweaver–Burk plot constructed in the absence of inhibitor is employed.

Using a K_m value of 61.5 µM and a substrate concentration of 30 µM, the K_i values for the inhibition of MAO-B by the synthesized inhibitors were calculated according to the Cheng-Prusoff equation and are illustrated in table 4.6.

A Lineweaver-Burk plot was also constructed for the oxidation of kynuramine by MAO-A. This was done in the absence of inhibitor. As shown in figure 4.12, the x-axis intercept of this plot is equal to -0.018 μM^{-1}. Considering the x-axis intercept is equal to $-1/K_m$, a K_m value for the oxidation of kynuramine by MAO-A may be calculated as 53.8 µM. The substrate concentration used for the inhibition studies with human MAO-A was 45 µM. Using a K_m value of 53.8 µM and a substrate concentration of 45 µM, the K_i values for the inhibition of MAO-A by the synthesized inhibitors were calculated according to the Cheng-Prusoff equation and are also illustrated in table 4.6.

Tabel 4.6 K_i values for the inhibition of human MAO-A and MAO-B by the 8-[(2-phenylethyl) sulfanyl]caffeine and 8-[(2-phenylethyl)sulfinyl]caffeine analogues calculated by the Cheng-Prusoff equation.

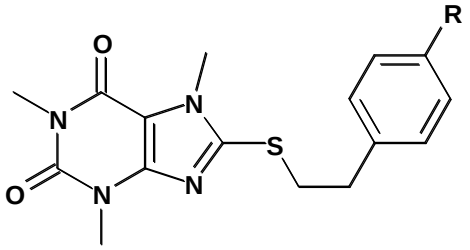

1

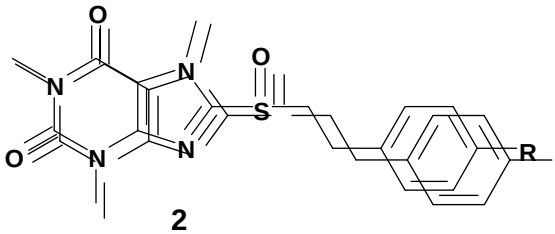

2

Compounds		Human MAO-A	Human MAO-B	Selectivity[a]
	R	K_i (µM)	K_i (µM)	
1a	-H	10.17	0.182	56
1b	-Cl	4.61	0.013	655
1c	-Br	58.77	0.012	4897
1d	-F	8.00	0.011	727

1e	$-CF_3$	No inhibition	0.012	——
1f	$-CH_3$	68.16	0.048	1420
1g	$-OCH_3$	91.16	0.011	8287
2a	-Cl	161.76	2.356	69
2b	-Br	31.20	0.317	98

[a] The selectivity index is the selectivity for the MAO-B isoform and is given as the ratio of K_i(MAO-A)/ K_i(MAO-B).

Considering the data, it can be concluded that the synthesized compounds are highly selective towards human MOA-B, with the least selective compound, compound **1a** being 56-fold more selective for MAO-B than the MAO-A isoform. The most selective compound is **1g**, with a selectivity index of 8287. It should be noted that the K_i value calculated for compound **2b** from the slopes of the Lineweaver-Burk plots (Fig. 4.10) is 13.21 nM, while that calculated via the Cheng-Prusoff equation is 13 nM. Since these values are nearly identical, it may be concluded that the Cheng-Prusoff equation is an accurate method of calculating K_i values from the corresponding IC_{50} values.

4.6 Hansch-type quantitative structure-activity relationships (QSAR) studies

In this study, a Hansch-type QSAR study was carried out to describe the relationship between MAO inhibition and the physicochemical properties of the substituents at the C-4 position of the phenyl ring of inhibitors **1a**–**g**. The physicochemical parameters that were selected to describe the substituents were selected on the basis that they are experimentally determined values and not calculated values. In this study, the bulkiness of a substituent is described by the Van der Waals volume (V_w) and Taft steric parameter (E_s). The lipophilicity is described by the Hansch constant (π) of the substituents. The electronic properties of the substituents are described by the Swain–Lupton constant (F) and the Hammett constant (σ). The values of these physicochemical parameters were obtained from literature sources as indicated in table 4.7 (Hansch & Leo, 1995). For the purpose of the QSAR study, inhibitors **1a**–**g** were selected.

Table 4.7 The physicochemical parameter values used for the Hansch-type QSAR study.

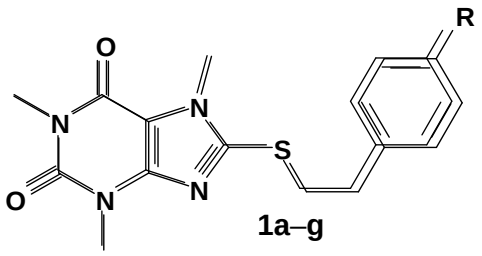

1a–g

R	V_w	E_s	Π	σ_p	F
-H	0.08	0.00	0.00	0.00	0.00
-Cl	1.07	-0.97	0.71	0.23	0.42
-Br	1.32	-1.16	0.86	0.23	0.45
-F	0.36	-0.46	0.14	0.06	0.45
-CF_3	1.11	-2.40	0.88	0.54	0.38
-CH_3	1.01	-1.24	0.56	-0.17	0.01
-OCH_3	1.49	-0.55	-0.02	-0.27	0.29

When carrying out a Hansch-type QSAR study, the logarithm of the measured inhibitor potencies ($\log IC_{50}$) of a series of inhibitors are correlated with the physicochemical parameter values by means of linear equations. For this purpose, the logarithm of the measured IC_{50} values of a series inhibitors are correlated with the substituent descriptor values using linear ($y = ax + c$) or multivariate linear ($y = ax_1 + bx_2 + c$) equations. In these equations, y is equal to the $\log IC_{50}$ and x_1, x_2 equals the parameter values of V_w, E_s, π, σ, F. A good correlation (R^2) indicates that the particular substituent parameter is a determinant of inhibition activity. These equations may be used to predict the effect of different substituents on an inhibitor's potency

(Gnerre *et al*., 2000). The equations may also be used to predict the inhibition potencies of yet to be evaluated compounds.

The statistical significance of the QSAR equations is evaluated with the aid of the R^2 and statistical *F* values. R^2 values close to 1 indicate a high degree of correlation between the logarithm of the inhibition potency (y) and the physicochemical parameters (x_1, x_2). The higher the *F* of the equation, the better the fit. When the *F* value of the correlation is higher than the F_{max}, then the correlation is deemed significant. For models constructed from seven $logIC_{50}$ values and which contain two out of a possible five parameters, the critical F_{max} value of 95% significance was calculated to be 30.18. When only one parameter was used for the construction of the model, the F_{max} value is 25.32 (Livingstone & Salt, 2005).

The Hansch–type QSAR studies were carried out with the seven 8-[(2-phenylethyl) sulfanyl]caffeine analogues (**1a–g**) containing substituents on C-4 of the phenyl ring. The Statistica software (version 10; StatSoft Inc.) was used to carry out this statistical analysis.

4.6.1 Results

Statistical analyses were carried out with the IC_{50} values obtained from the inhibition studies with MAO-A and MAO-B, and the results are shown in tables 4.8 and 4.9, respectively.

Table 4.8 Correlations of the MAO-A inhibition potencies ($logIC_{50}$) of the 8-[(2-phenylethyl) sulfanyl]caffeine analogues with steric, electronic and hydrophobic parameters of the substituents on C-4 of the phenyl ring[a].

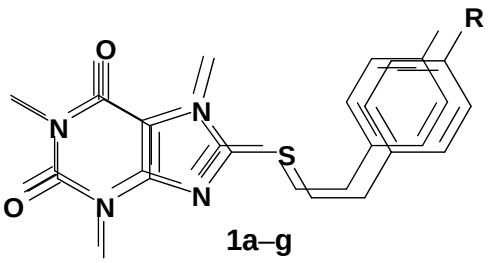

1a–g

Parameter	Slope	y–intercept	R^2	*F*	Significance[b]
σ_p	-1.608 ± 1.106	1.643 ± 0.208	0.346	2.112	0.220
F	-0.564 ± 1.281	1.774 ± 0.427	0.215	0.194	0.682
V_w	0.653 ± 1.682	1.042 ± 0.396	0.414	2.829	0.168

Π	0.072 ± 0.731	1.595 ± 0.375	0.002	0.010	0.927
E_s	-0.458 ± 0.540	1.287 ± 0.460	0.152	0.719	0.444
$\sigma_p + \pi$	-2.843 ± 1.218 1.039 ± 0.652	1.270 ± 0.293	0.649	2.735	0.102 0.209
$\sigma_p + V_w$	-1.402 ± 0.911 0.585 ± 0.338	1.121 ± 0.346	0.673	3.084	0.221 0.182
$\sigma_p + E_s$	-1.904 ± 0.360 -0.625 ± 0.428	1.191 ± 0.360	0.617	2.418	0.152 0.241
***F* + π**	-0.690 ± 1.561 0.204 ± 0.871	1.732 ± 0.521	0.063	0.101	0.689 0.830
***F* + V_w**	-1.326 ± 0.975 0.834 ± 0.377	1.239 ± 0.388	0.638	2.641	0.267 0.114
***F* + E_s**	-0.870 ± 1.349 -0.554 ± 0.603	1.452 ± 0.559	0.256	0.515	0.565 0.426

[a] The logarithm of the IC_{50} values (expressed in μM) was used in the linear regression analysis.
[b] The significance is the fractional probability that the coefficient of parameter is zero.

As seen in table 4.8 there is no significant correlation between any physicochemical parameters and the inhibition potencies for MAO-A. Thus only the results for MAO-B will be discussed further.

Table 4.9 Correlations of the MAO-B inhibition potencies ($logIC_{50}$) of the 8-[(2-phenylethyl)sulfanyl]caffeine analogues with steric, electronic and hydrophobic descriptors of the substituents on C-4 of the phenyl ring[a].

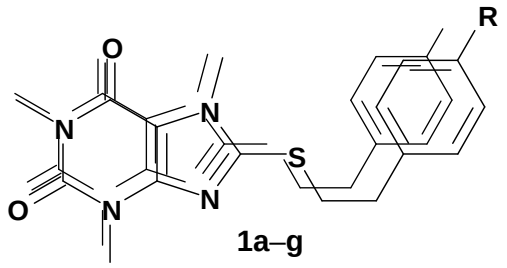

1a–g

Parameter	Slope	y-intercept	R^2	*F*	Significance[b]
σ_p	-0.617 ± 0.683	-1.411 ± 0.183	0.140	0.820	0.408
F	-2.069 ± 0.403	-0.874 ± 0.137	0.840	26.325	0.004

V_w	-0.533 ± 0.313	-0.975 ± 0.324	0.367	2.899	0.149
π	-0.489 ± 0.456	-1.247 ± 0.264	0.187	1.152	0.332
E_s	0.273 ± 0.232	-1.201 ± 0.279	0.217	1.383	0.292
$\sigma_p + \pi$	-0.205 ± 1.084 -0.386 ± 0.744	-1.275 ± 0.329	0.194	0.483	0.859 0.631
$\sigma_p + V_w$	-0.586 ± 0.587 -0.523 ± 0.313	-0.932 ± 0.327	0.494	1.949	0.374 0.170
$\sigma_p + E_s$	-0.178 ± 0.989 0.230 ± 0.352	-1.227 ± 0.342	0.223	0.574	0.866 0.549
F + π	-1.994 ± 0.160 -0.095 ± 0.241	-0.853 ± 0.160	0.846	11.015	0.014 0.714
$F + V_w$	-1.811 ± 0.343 -0.268 ± 0.134	-0.701 ± 0.138	0.920	23.141	0.006 0.115
$F + E_s$	-1.929 ± 0.416 0.118 ± 0.108	-0.799 ± 0.152	0.877	14.296	0.010 0.334

[a] The logarithm of the IC_{50} values (expressed in μM) was used in the linear regression analysis.
[b] The significance is the fractional probability that the coefficient of the parameter is zero.

The results of the QSAR study for the inhibition of MAO-B by the 8-[(2-phenylethyl)sulfanyl]caffeine analogues (**1a–g**) are presented in table 4.9. The results show that a good correlation exists between the logIC_{50} values and the Swain–Lupton constant (F), with an R^2 value of 0.82 and an *F* value of 26.3 (F_{max} = 25.32). Since the *F* value is higher than the F_{max}, the correlation is deemed significant. The mathematical description for this correlation is thus:

$$\mathbf{LogIC_{50} = -2.069(\pm 0.403)F - 0.874(\pm 0.137)} \quad \mathbf{(1)}$$

$$\mathbf{R^2 = 0.84 \text{ and } \mathit{F} = 26.3}$$

An even better correlation may be obtained when the model is constructed from two parameters, the Swain-Lupton constant F and V_w. For this correlation, the R^2 value of 0.92. However, the *F* value is 23.14 which is lower than the F_{max} value (30.18). This correlation is thus not statistically significant and the probability that F and V_w are zero for this correlation is 0.6% and 11.5%, respectively. The best mathematical description for the binding of C-4 substituted,

8-[(2-phenylethyl)sulfanyl]caffeine analogues to MAO-B is therefore equation 1 and is graphically represented in figure 4.13.

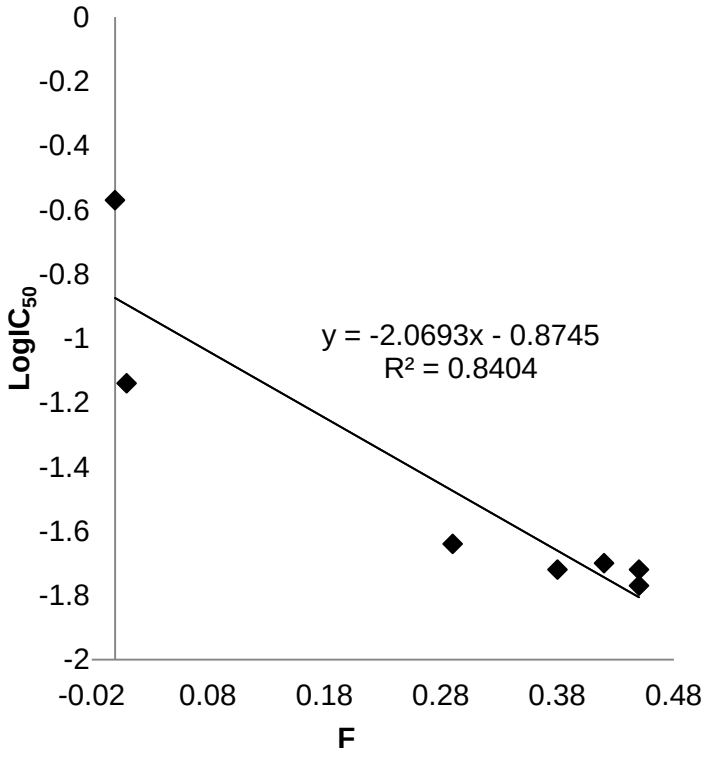

Figure 4.13 Graph depicting the correlation between the inhibition potencies ($logIC_{50}$ values) of MAO-B by C-4 substituted 8-[(2-phenylethyl)sulfanyl]caffeine analogues and the Swain-Lupton constant (F). The linear regression line is a representation of equation 1.

The negative sign of the F parameter coefficient indicates that the MAO-B inhibition potencies of the 8-[(2-phenylethyl)sulfanyl]caffeine analogues may be enhanced by substituting on the C-4 position of the phenyl ring with electron withdrawing groups. The higher the F value, the higher the degree of electron withdrawing potential of the functional group, and hence the more potent the MAO-B inhibition would be.

It can be concluded that the 8-[(2-phenylethyl)sulfanyl]caffeine analogues are potent reversible and competitive inhibitors of MAO-B. The QSAR study shows that, for the compounds to act as potent MAO-B inhibitors, the C-4 position of the phenyl ring should contain electron withdrawing functional groups. In this study the best linear equation correlates the $logIC_{50}$ values to the F parameter coefficient ($LogIC_{50}$ = -2.069F - 0.874). This QSAR equation was derived from 7 compounds. The correlation may be judged as significant (as judged by the statistical *F* value) and may be used to calculate the theoretical IC_{50} values for the inhibition of MAO-B by C-4

substituted 8-[(2-phenylethyl)sulfanyl]caffeine analogues. Given in Table 4.10 are the calculated IC_{50} values of three 8-[(2-phenylethyl)sulfanyl]caffeine analogues according to the equation cited above. These compounds may be synthesized in future studies and evaluated as human MAO-B inhibitors in order to confirm the validity of the equation.

Table 4.10 The calculated IC_{50} values of three 8-[(2-phenylethyl)sulfanyl]caffeine analogues according to the equation 1 cited above.

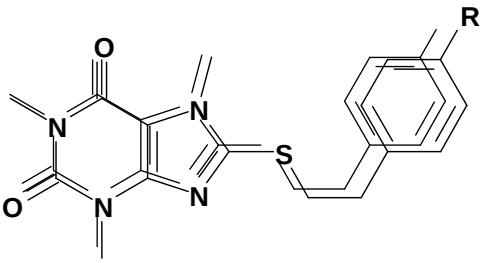

R	F	Calculated IC_{50} (μM)
I	0.42	0.018
NO_2	0.65	0.006
CN	0.08	0.012

Although not judged as significant, the model constructed from two parameters (F and V_w) may provide additional insight in the SAR of MAO-B inhibition by 8-[(2-phenylethyl)sulfanyl]caffeine analogues. The mathematical equation describing this correlation is:

$$\mathbf{Log IC_{50} = -1.811(\pm 0.343)F - 0.268(\pm 0.134)V_w - 0.701(\pm 0.138)} \qquad \mathbf{(2)}$$

$$\mathbf{R^2 = 0.92} \qquad \mathbf{\mathit{F} = 23.14}$$

As previously noted: the negative sign of the F parameter coefficient indicates that the inhibition potencies of the 8-[(2-phenylethyl)sulfanyl]caffeine analogues for MAO-B may be enhanced by the substitution on the C-4 position on the phenyl ring with electron withdrawing groups The negative sign of the V_w parameter coefficient indicates that the inhibition potencies of the 8-[(2-phenylethyl)sulfanyl]caffeine analogues for MAO–B may be enhanced by substituting the C-4 position of the phenyl ring with functional groups that possess a high degree of bulkiness with regards to shape and volume. The two parameter model for the binding of C4 substituted 8-[(2-

phenylethyl)sulfanyl]caffeine analogues to MAO-B (as given by equation 2) may be graphically represented in figure 4.14.

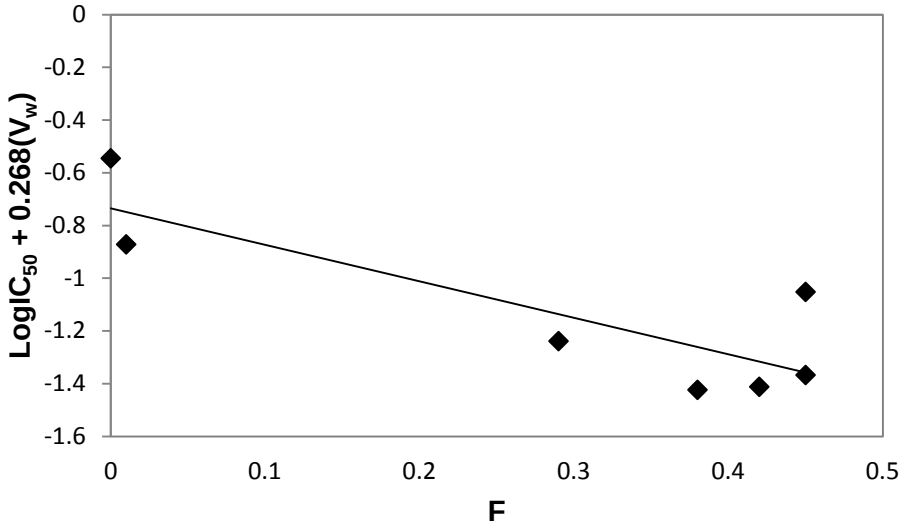

Figure 4.14 Graph depicting the correlation between the MAO–B inhibition potencies ($logIC_{50}$ values) of the C-4 substituted 8-[(2-phenylethyl)sulfanyl]caffeine analogues and the Swain-Lupton constant (F) and the Van der Waals volume (V_w) parameters. The $logIC_{50}$ values were adjusted according to the contribution of the V_w values as indicated on the y-axis title. The linear regression line is a representation of equation 2.

The correlation may also be used to calculate the theoretical IC_{50} values for the inhibition of MAO-B by C-4 substituted 8-[(2-phenylethyl)sulfanyl]caffeine analogues, Given in Table 4.11 are the calculated IC_{50} values of three 8-[(2-phenylethyl)sulfanyl]caffeine analogues according to equation 2 cited above.

Table 4.11 The calculated IC_{50} values of three 8-[(2-phenylethyl)sulfanyl]caffeine analogues according to the equation 2 cited above.

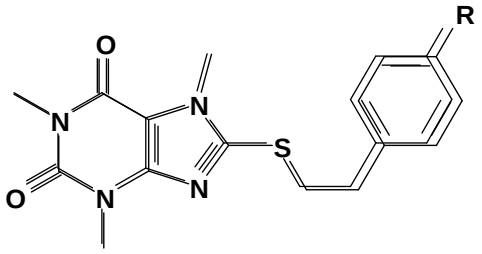

R	F	V_w	Calculated IC_{50} (μM)
I	0.42	1.90	0.0085

NO_2	0.65	1.20	0.005
CN	0.51	1.14	0.012

As expected, the IC_{50} values calculated with the two equations yield similar results. For example, according to equation 1, the iodo substituted 8-[(2-phenylethyl)sulfanyl]caffeine analogue has a calculated IC_{50} value of 0.018 µM, while its IC_{50} value calculated with equation 2 is 0.0085 µM. Similarly, the nitro substituted homologue has IC_{50} values of 0.006 µM and 0.005 µM according to equations 1 and 2, respectively.

To conclude, the 8-[(2-phenylethyl)sulfanyl]caffeine analogues are potent reversible and competitive inhibitors of MAO-B. The QSAR study indicates that, for the compounds to be potent MAO-B inhibitors, the C-4 position of the phenyl ring should contain electron withdrawing functional groups. The QSAR study also indicates that, in addition to the electron withdrawing functional group, sterically bulky substituents on the C-4 position of the phenyl ring may further enhance the inhibition potencies of the 8-[(2-phenylethyl)sulfanyl]caffeine analogues towards MAO-B.

4.7 Molecular docking studies

Molecular docking is a computational process in which a ligand can be fitted into a receptor or enzyme. This allows for the examination of the interaction between the binding site of the protein and the docked inhibitor. When used in combination with QSAR studies, it can be used to identify critical structural features of inhibitors that are required for optimal activity towards a specific enzyme or receptor. Molecular docking studies are ideally used to design new ligands for a specific receptor. These ligands can be used for the design and development of drugs for future therapeutic use.

4.7.1 Method:

The Windows based Discovery Studio 3.1 modelling software (Accelrys) was used to carry out the molecular docking studies.

- *Selection of protein models*: The crystallographic structure of MAO-A co-crystallized with harmine (PDB code: 2Z5X) (Son *et al*., 2008) was retrieved from the Brookhaven Protein Data Bank, along with the crystallographic structure of MAO-B co-crystallized with safinamide (PDB code: 2V5Z) (Binda *et al*., 2007).

- *Protein preparation*: All calculations were carried out at a pH of 7.4. The valences of the FAD cofactors and the co–crystallized ligands were corrected. Hydrogen atoms were added to the receptor models according to the appropriate protonation states of the ionisable amino acids, FAD cofactors and co–crystallized ligands. The protein structure was then typed with the Momany and Rone CHARMm forcefield.

- *Minimization*: The protein backbone was fixed while the structure was energy minimized. For these minimization protocols the implicit generalized Born solvation model with simple switching (GBSW) was used with the dielectric constant set to 4. For the purpose of the minimization of the protein structure, steepest descent minimization was carried out first, followed by conjugate gradient minimization. The parameter values used for both protocols were identical, with the termination criteria set to 2500 steps and a minimum value of 0.1 for the root mean square of the energy gradient. Thirdly, an adopted basis Newton-Rapheson minimization was carried out with the termination criteria set to 5000 steps or a minimum value of 0.01 for the root mean square of the energy gradient.

- *Removal of waters and ligands*: The water molecules and the co-crystillazed ligands in both MAO-A and MAO-B were deleted. The backbone constraint was subsequently removed from the models. In both MAO-A and –B only three active site water molecules were retained. In MAO-A these are waters 710, 739 and 718. In the A-chain of MAO-B, these are 1351, 1155 and 1170. These waters are considered to be conserved and non-diplacable (Binda *et al*., 2007).

- *Binding site identification*: The binding sites were identified by a flood-filling algorithm.

- *Construction of ligands to be docked*: The structures of the selected representative 8-[(2-phenylethyl)sulfanyl]caffeine analogues (**1a–b**) and the 8-[(2-phenylethyl)sulfinyl]caffeine analogue **2a** were constructed within Discovery Studio. Hydrogen atoms were added to the ligands according to the protonation states of the analogues at pH 7.4. Their geometries were optimized in Discovery Studio using a fast Dreiding-like forcefield (1000 iterations) and they were subsequently typed with the Momany and Rone CHARMm forcefield.

- *Docking and refinement*: The Ligandfit application of Discovery studio was used to dock the ligands. The Monte Carlo conformation search method set to a variable number of trial runs was used to determine the final ligand conformations. Docking solutions were further refined using the Smart Minimizer algorithm. The parameters used in the docking runs were

set to default values and ten possible solutions were computed for each docked ligand. The DockScore values were used to determine the best-ranked binding conformation of each ligand.

4.7.2 Results

MAO-B

The 8-[(2-phenylethyl)sulfanyl]caffeines **1a**–**b** and the 8-[(2-phenylethyl)sulfinyl]caffeine **2a** were successfully docked within the active site of MAO–B. Figure 4.15 illustrates how 8-[(2-phenylethyl)sulfanyl]caffeine (**1a**) orientates itself in order to bind in the active site cavity. The caffeine ring is orientated towards the FAD cofactor and binds in the substrate cavity. The phenylethyl side chain of **1a** protrudes into the entrance cavity.

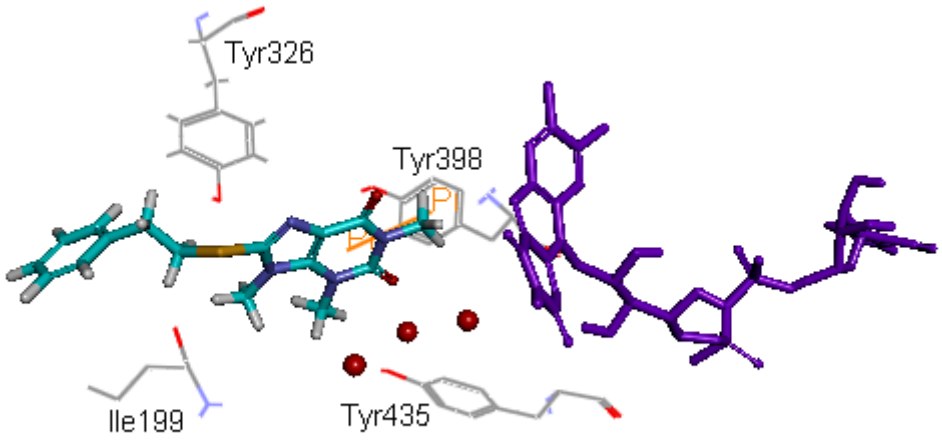

Figure 4.15 An illustration of 8-[(2-phenylethyl)sulfanyl]caffeine (**1a**) docked within the active site of MAO–B. The inhibitor is displayed in cyan, the FAD cofactor in purple and the π–π interaction is shown in orange. The red spheres represent water molecules.

The representative inhibitor that was selected for the time-dependant and reversibility studies, 8-{[2-(4-chlorophenyl)ethyl]sulfanyl}caffeine (**1b**) was also docked into the active site of MAO-B (figure 4.16). 8-{[2-(4-Chlorophenyl)ethyl]sulfanyl}caffeine (**1b**) is 13.55 fold more potent than 8-[(2-phenylethyl)sulfanyl]caffeine as an inhibitor of human MAO-B. As expected, **1b** adopts a similar binding orientation in MAO-B to that observed for **1a**. An important interaction between these inhibitors and the MAO-B active site is a π-π interaction between their caffeine ring and the aromatic moiety of Tyr398. Also, a possible hydrogen bond interaction may occur between the carbonyl oxygen at C-3 of the caffeine ring, and Tyr435. It is interesting to note that the C-8 phenylethyl side chain protrudes into the entrance cavity of MAO–B. The entrance cavity is a

highly hydrophobic environment, which may stabilize the C-8 side chain through Van der Waals interactions.

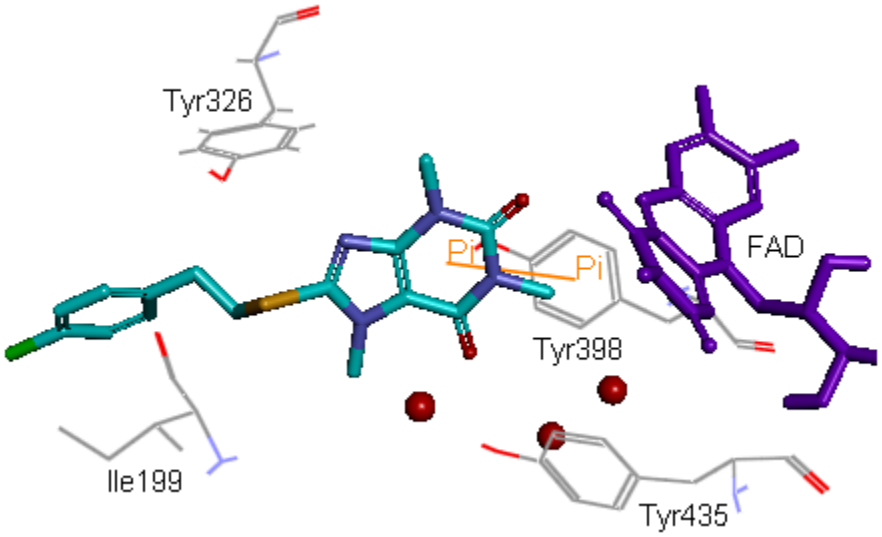

Figure 4.16 An illustration of 8-{[2-(4-chlorophenyl)ethyl]sulfanyl}caffeine (**1b**) docked within the active site of MAO-B. The inhibitor is displayed in cyan, the FAD cofactor in purple, and the π-π interaction in orange. The red spheres represent water molecules.

To further explore the orientation of the inhibitors within the MAO-B binding site, a selected 8-[(2-phenylethyl)sulfinyl]caffeine, compound **2a**, was also docked. Figure 4.17 illustrates the binding of 8-{[2-(4-bromophenyl)ethyl]sulfinyl}caffeine (**2a**) within the active site of MAO-B. As observed for 8-[(2-phenylethyl)sulfanyl] caffeine, the caffeine moiety is orientated towards the FAD cofactor with the phenylethyl side chain protruding into the entrance cavity. Hydrogen bonding occurs between the carbonyl oxygen at C-3 and active site water molecules. Also, π-π interactions are present between the caffeine ring and the aromatic moiety of Tyr398. The entrance cavity, which is a hydrophobic environment, may stabilize the C-8 side chain via Van der Waals interactions.

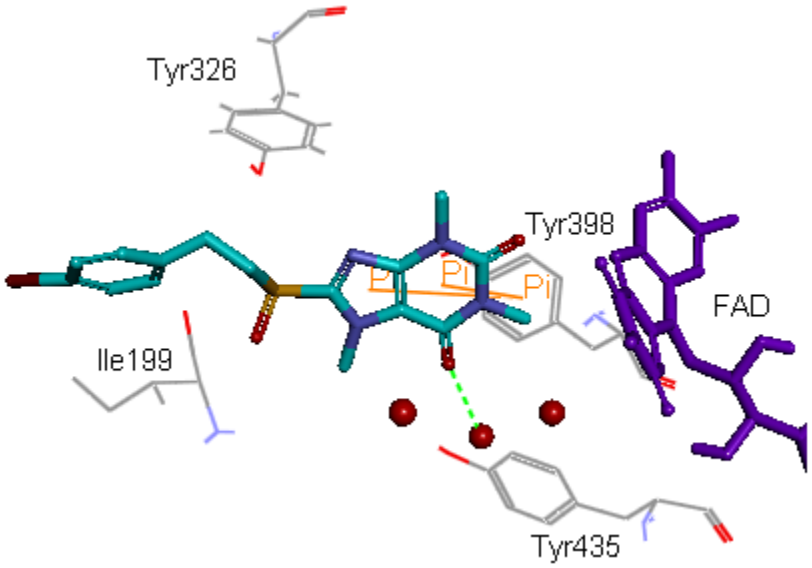

Figure 4.17 An illustration of 8-{[2-(4-bromophenyl)ethyl]sulfinyl}caffeine (**2a**) docked within the active site of MAO-B. The inhibitor is displayed in cyan, the FAD cofactor in purple, hydrogen bonds in green and the π-π interaction in orange. The red spheres represent water molecules.

MAO-A

8-{[2-(4-Chlorophenyl)ethyl]sulfanyl}caffeine (**1b**) was docked into the active site of human MAO-A in order to investigate why the synthesized analogues show weak inhibition towards MAO-A. Figure 4.18 illustrates the binding modes of harmine (a potent MAO-A inhibitor) and 8-{[2-(4-chlorophenyl)ethyl]sulfanyl}caffeine (**1b**) to MAO-A. Harmine is a small molecule and fits well in the active site cavity of MAO–A. However, 8-{[2-(4-chlorophenyl)ethyl]sulfanyl} caffeine (**1b**) is a large molecule compared to harmine. The size of the inhibitor may restrict the orientation that the inhibitor may adopt in the MAO-A active site and thus prevent favourable interactions with the amino acid residues. The restriction imposed by, particularly Phe208, on the binding of larger inhibitors may explain the observation that relatively large inhibitors act as selective MAO-B inhibitors, and do not bind to MAO-A (Hubalek *et al.,* 2005). This may explain why 8-{[2-(4-chlorophenyl)ethyl]sulfanyl}caffeine (**1b**) exhibits weak MAO-A inhibition activity.

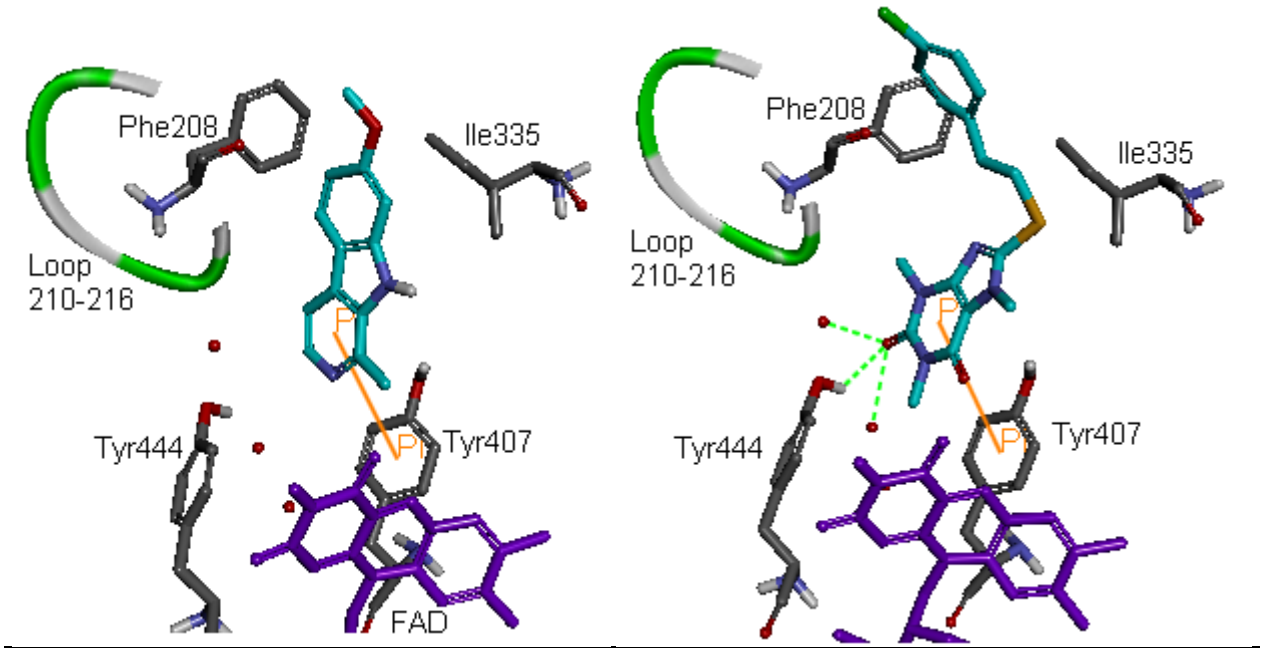

Figure 4.18 An illustration of the co–crystallized ligand, harmine in the human active site (left) and, 8-{[2-(4-chlorophenyl)ethyl]sulfanyl}caffeine (**1b**, right) docked into the active site of MAO-A. The inhibitors are displayed in cyan, the FAD cofactor in purple and π-π interactions in orange. The red spheres represent water molecules.

Docking studies revealed how the synthesized inhibitors bind within the active site cavities of MAO-A and MAO-B. The results support the finding that 8-[(2-phenylethyl)sulfanyl]caffeine analogues and 8-[(2-phenylethyl)sulfinyl]caffeine analogues are selective towards MAO-B. It is, however, unclear why the 8-[(2-phenylethyl)sulfanyl]caffeine analogues are much more potent inhibitors compared to the corresponding sulfinylcaffeine analogues. The docking studies indicated that sulfinylcaffeine **2a** fits into the active site cavity of MAO-B with a similar binding orientation compared to the sulfanylcaffeine **1b**. In fact **2a** undergoes numerous hydrogen bond interactions with MAO–B which suggests that it should act as a potent inhibitor. It is however noteworthy that the sulfanyl carbon is chiral, and **2a** is represented by a racemic mixture of two enantiomers. It may be possible that only one enantiomer may be inactive as a MAO-B inhibitor, which would reduce the potency of a racemic mixture. Another possible explanation for the weak MAO–B inhibition potency of the sulfinylcaffeine analogues may be that the strain energy of the bound inhibitor is relatively higher than that that of the bound sulfanylcaffeine analogues. Although, the sulfinylcaffeine exhibits favourable binding modes in MAO-B, the high degree of strain reduces the binding energy, and subsequently the inhibition potency.

4.8 Conclusion

The 8-[(2-phenylethyl)sulfanyl]caffeine analogues are potent inhibitors of human MAO-B. Lineweaver-Burk plots and time-dependant studies are indicative that the analogues are competitive reversible inhibitors. The results indicate that substitution on the C-4 position of the phenyl ring enhances the inhibition activities of the sulfanylcaffeine analogues. Inhibition activities may further be increased by employing functional groups that have electron withdrawing properties. Docking the inhibitors within the active sites of human MAO-A and MAO-B revealed that Phe208 may restrict the binding of the inhibitors to MAO-A, which may explain their weak inhibition potencies towards MAO-A. While both the sulfanylcaffeine and sulfinylcaffeine analogues adopt favourable binding orientations in MAO-B, the internal strain energy of the bound sulfinylcaffeine analogues may reduce their overall binding energies and inhibition potencies. Furthermore, the sulfinylcaffeine analogues are racemic mixtures of two enantiomers. Considering the possibility that one enantiomer may be inactive as a MAO-B inhibitor, the racemic mixture is expected to possess lower activity than the active enantiomer.

Chapter 5

Summary

The clinical syndrome termed Parkinsonism is characterized by motor complications such as bradikinesia, resting tremors and muscle rigidity. Parkinson's disease onset is slow and progressively worsens in severity over time. This progressive worsening leads to severe disability such as falling and immobility if left untreated. Levodopa is the main treatment for PD symptoms, but with disease progression the sensitivity towards levodopa is reduced. Moreover, with an increase in levodopa dosage, levodopa induced dyskinesias may develop. However, a conjunctive treatment regime such as levodopa with MAO inhibitors may help delay these induced dyskinesias. Despite extensive research done over the years the main cause of PD remains unclear and thus treatment is only symptomatic. The main pathology by which PD is characterized is the progressive death of nigrostriatal dopaminergic neurons. This results in a decrease in the DA content of the SN and striatum. One strategy employed to replenish this lost DA is by inhibiting the enzymes responsible for the degradation of DA. MAO-B is the main enzyme responsible for the degradation of DA. Also, PD is an age related disease and the MAO-B levels in the PD brain increase 4-5 fold with aging. Thus MAO-B inhibitors present an attractive strategy that may help conserve the depleted DA in the PD brain by inhibiting the excess MAO-B. The other isoenzyme of MAO is MAO-A. MAO-A is mostly present in the intestinal tract but is also found in the brain. MAO-A also is responsible for the degradation of neurotransmitters in the brain, but to a lesser extent than MAO-B. Inhibition of MAO-A in the brain is employed in treatment strategies of depression but because it resides mainly in the intestinal tract irreversible inhibition of MAO-A may lead to serious side-effects.

The present study aimed to discover new reversible inhibitors of the MAO enzymes, particularly the MAO-B isoform. This study is a continuation of an investigation of the MAO inhibitory properties of caffeine derived compounds. We have recently reported that a series of 8-sulfanylcaffeine analogues act as selective inhibitors of human MAO-B. Among the compounds examined, 8-[(phenylethyl)sulfanyl]caffeine (**1a**) was found to be a particularly potent inhibitor of MAO-B with an IC_{50} value of 0.223 μM. In an attempt to further enhance the MAO-B inhibition potency of 8-[(phenylethyl)sulfanyl]caffeine, and possibly to discover highly potent MAO-B inhibitors, a series of 8-[(phenylethyl)sulfanyl]caffeine analogues (**1a**–**g**) were synthesized and evaluated as inhibitors of human MAO-A and –B. The current study also aimed to examine the SAR of MAO inhibition by 8-[(phenylethyl)sulfanyl]caffeine analogues. For this purpose those 8-

[(phenylethyl)sulfanyl]caffeine homologues containing C-4 alkyl (CF_3, CH_3, OCH_3) and halogen (Cl, Br, F) substituents on the phenyl ring were employed (compounds **1a**–**g**). Furthermore, a series of 8-sulfinylcaffeine analogues (**2a**–**d**) were synthesized and their MAO inhibitory potencies were measured (table 1). The purpose with these compounds was to compare the MAO inhibitory properties of the 8-sulfinylcaffeine analogues (**2**) with those of the 8-sulfanylcaffeine analogues (**1**).

Table 5.1 The IC_{50} values for the inhibition of human MAO-A and MAO-B by 8-[(2-phenylethyl) sulfanyl]caffeine analogues (**1a**–**g**) and 8-[(2-phenylethyl)sulfinyl]caffeine analogues (**2a**–**b**).

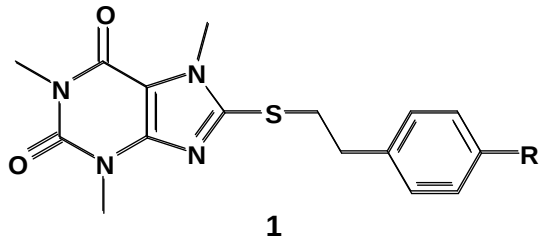

1

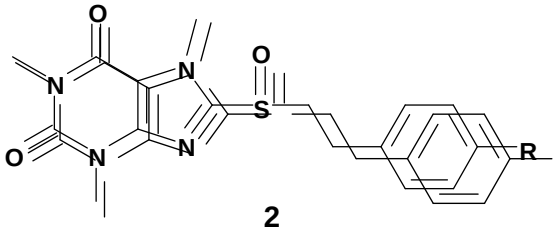

2

	IC_{50} (μM)		
	R	**MAO-A**	**MAO-B**
1a	**-H**	18.7	0.271
1b	**-Cl**	8.46	0.020
1c	**-Br**	108	0.019
1d	**-F**	14.7	0.071
1e	**-CF_3**	No inhibition	0.019
1f	**-CH_3**	125	0.072
1g	**-OCH_3**	168	0.023
2a	**-Br**	57.3	0.471
2b	**-F**	451	3.50

Furthermore, to demonstrate the inhibition potencies of the 8-sulfanylcaffeine analogues, the IC_{50} values can be compared to that of lazabemide. Lazabemide is a well known reversible MAO-B inhibitor with an IC_{50} value of 0.091 µM. Compared to lazabemide compounds 1b, 1c and 1e are 4.8-fold more potent.

The 8-[(2-phenylethyl)sulfanyl]caffeine analogues (**1a**–**g**) were successfully synthesized by reacting an appropriate substituted mercaptan with 8-chlorocaffeine in a basic medium. The 8-[(2-phenylethyl)sulfinyl]caffeine analogues (**2a**–**d**), in turn, were synthesized by treating the synthesized sulfanylcaffeines with 30% hydrogen peroxide in the presence of glacial acetic acid and acetic acid anhydride. The structures and purities of the synthesized compounds were verified by MS, NMR and HPLC. It was found that the synthesized structures correspond with the proposed structures and that the sulfanylcaffeines and sulfinylcaffeines are of an acceptable degree of purity.

The 8-[(2-phenylethyl)sulfanyl]caffeine (**1a**–**g**) and 8-[(2-phenylethyl)sulfinyl]caffeine analogues (**2a**–**d**) were subsequently evaluated as inhibitors of human MAO-A and MAO-B. The MAO activity measurements were based on measuring the rate by which kynuramine undergoes oxidative deamination towards the fluorescent product, 4-hydroxyquinoline (4-HQ). The results showed that the 8-[(2-phenylethyl)sulfanyl]caffeines (**1a**–**g**) are highly potent and selective inhibitors of the MAO-B enzyme, with IC_{50} values ranging from 0.019–0.072 µM. The most potent inhibitors were compounds **1c** and **1e**, with IC_{50} values of 0.019 µM. It was observed that the homologues substituted with halogens (Cl, Br and F) on C-4 of the phenyl ring were the most potent MAO-B inhibitors. In contrast to MAO-B, the 8-[(2-phenylethyl)sulfanyl]caffeine analogues (**1a**–**g**) were relatively weak MAO-A inhibitors, with IC_{50} values ranging from 8.458 µM to no inhibition.

The 8-[(2-phenylethyl)sulfinyl]caffeine analogues (**2a**–**d**) were found to be weak inhibitors of both MAO-A and -B with IC_{50} values of 0.471–3.50 µM for MAO-B and 57.3–451 µM for MAO-A. Compared to the sulfanylcaffeines, the sulfinylcaffeine analogues are therefore weak MAO inhibitors. It may thus be concluded that the oxidation state of the sulfur plays a role in the inhibition potencies. An oxidation state of -2, as for the sulfanylcaffeine analogues, is more suitable for MAO inhibition.

Time-dependent studies were carried out with one selected inhibitor, compound **1b**. The purpose of this study was to determine whether the compound acts as a reversible inhibitor or as a time-dependent inactivator of human MAO-A and MAO-B. The results showed that when

the inhibitor was incubated with the MAO enzymes for various periods of time, no decrease in the oxidation rate of kynuramine occurred. This indicates that the inhibitor binds reversibly to MAO-A and MAO-B enzymes. This is of significance since irreversible inhibitors may lead to side-effects. A set of Lineweaver-Burk plots were also constructed for the inhibition of MAO-B by one selected inhibitor, compound **1b**. The Lineweaver-Burk plots were found to be linear and plots for various inhibitor concentrations intersected on the y-axis. This is indicative that the mode of inhibition is competitive. Thus, it may be assumed that 8-[(2-phenylethyl)sulfanyl]caffeine analogues act as competitive reversible inhibitors of MAO-A and MAO-B.

A QSAR study was also carried out to gain more insight into the effect that the C-4 substituents on the phenyl ring of compounds **1a**–**g** have on the MAO inhibition potencies. This study attempted to mathematically describe the relationship between MAO inhibition and the physiochemical properties of the substituents on the C-4 position of the phenyl ring of the inhibitors. The parameters that were used for this study were the Van der Waals volume (V_w) and Taft steric parameter (E_s), as descriptors of bulkiness, the Hansch constant (π) as a descriptor of lipophilicity, and the electronic parameters, the Swain-Lupton constant (F) and the Hammett constant (σ). The QSAR study revealed two possible mathematical equations for the correlation between the physiochemical parameters and the MAO-B inhibition potencies. The first equation suggested that the Swain-Lupton constant (F) of the C-4 substituent is significant for the inhibition activities:

$$\mathbf{Log IC_{50} = -2.069(\pm 0.403)F - 0.874(\pm 0.137)} \quad \mathbf{(1)}$$

$$\mathbf{R^2 = 0.84 \text{ and } F = 26.3}$$

The higher the F value, the more electron-withdrawing the functional group. Thus the substitution of the C-4 position of the phenyl ring with more electron-withdrawing functional groups may enhance the MAO-B inhibition activities of the 8-[(2-phenylethyl)sulfanyl]caffeine analogues for MAO-B.

Although not significant, the second equation also provided some insight. This equation correlates the Van der Waals volume (V_w) and Swain-Lupton constant (F) of the C-4 substituents with the inhibition activities of the 8-[(2-phenylethyl)sulfanyl]caffeine analogues for MAO-B.

$$\mathbf{LogIC_{50} = -1.811(\pm 0.343)F - 0.268(\pm 0.134)V_w - 0.799(\pm 0.138)} \quad \mathbf{(2)}$$

$$\mathbf{R^2 = 0.92 \qquad F = 23.14}$$

Equation 2 suggests that the inhibition potencies may be further enhanced if the value of the Van der Waals volume (V_w) parameter is enhanced. V_w describes the bulkiness of the functional groups. The higher the V_w value, the higher the degree of bulkiness.

Results of the QSAR study may be used in the development of future 8-[(2-phenylethyl)sulfanyl]caffeine analogues and possibly to predict the MAO-B inhibition potencies of 8-[(2-phenylethyl)sulfanyl]caffeine analogues. For example, the 8-[(2-phenylethyl)sulfanyl] caffeine analogues containing I, NO_2 and CN on C-4 of the phenyl ring have the following calculated IC_{50} values according to equation 2 (table 5.2):

Table 5.2 The calculated IC_{50} values of selected 8-[(2-phenylethyl)sulfanyl]caffeine analogues according to the equation 2 cited above.

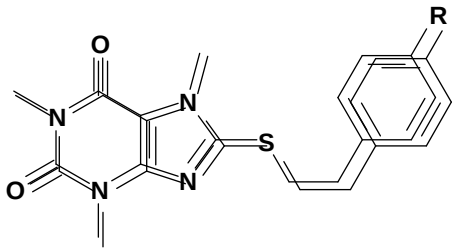

R	F	V_w	Calculated IC_{50} (μM)
I	0.42	1.90	0.0085
NO_2	0.65	1.20	0.005
CN	0.51	1.14	0.012

Representative inhibitors, compounds **1a** and **1b** were docked within the active sites of MAO-A and MAO-B. The results showed that the inhibitors are orientated in the active site of MAO-B with the caffeine ring directed towards the FAD cofactor. The phenylethyl side chain of **1a** protrudes into the entrance cavity. An important interaction between these inhibitors and the MAO-B active site is a π–π interaction between the caffeine ring and the aromatic moiety of Tyr398. The entrance cavity is a highly hydrophobic environment and this may help stabilize the

C-8 side chain through Van der Waals interactions. The docking studies also showed that that the sulfinylcaffeine **2a** fits into the active site cavity of MAO-B with a similar binding orientation compared to the sulfanylcaffeine **1b**. In fact **2a** undergoes numerous hydrogen bond interactions with MAO-B which suggests that it should act as a potent inhibitor. While it is unclear why the sulfanylcaffeine analogues are weak MAO-B inhibitors, a relatively higher strain energy of the bound inhibitor, compared to the sulfanylcaffeine analogues may explain the lower potencies of the sulfinylcaffeine analogues. Furthermore, the sulfinylcaffeine analogues are racemic mixtures of two enantiomers. Considering the possibility that one enantiomer may be inactive as a MAO-B inhibitor, the racemic mixture is expected to possess lower activity than the active enantiomer.

Docking of **1b** into the MAO-A active site reveals that, because of the relatively large size of **1b**, it is not well accommodated within the MAO-A active site and may undergo steric interactions with Phe 208. The restriction imposed by Phe208 on the binding of larger inhibitors may explain the observation that the sulfanylcaffeines examined here act as selective MAO-B inhibitors, and do not bind well to MAO-A.

Considering the role that MAO-B plays in PD novel MAO-B inhibitors which act reversibly are required for the treatment of PD. This highlights the need for the design and development of new novel reversible MAO-B inhibitors. This study identifies several new promising caffeine derived inhibitors of MAO-B. The sulfanylcaffeine analogues are highly potent, reversible and competitive inhibitors of MAO-B with little or no affinity for MAO-A. This is of great importance since the MAO-B enzyme is the main enzyme responsible for the metabolism of DA in the SN. The progressive deterioration of the dopaminergic neurons in the SN is the main pathology of PD. Thus inhibitors of MAO-B may conserve the depleted DA in the PD brain and may potentially be beneficial in the symptomatic treatment of PD. It can thus be concluded the 8-[(2-phenylethyl)sulfanyl]caffeine analogues are promising drug candidates in the future symptomatic treatment of PD.

Bibliography

Abeles, R.H. & Maycock, A.L. 1976. Suicide enzyme inactivators. *Accounts of chemical research,* 9:313-319.

Andrés, A.M., Soldevila, M., Navarro, A., Kidd, K.K., Oliva, B. & Bertranpetit, J. 2004. Positive selection in MAO-A gene is human exclusive: Determination of the putative amino acid change selected in the human lineage. *Human genetics,* 115:377-386.

Averill-Bates, D.A., Agostinelli, E., Przybytkowski, E., Mateescu, M.A. & Mondovi, B. 1993. Cytotoxicity and kinetic analysis of purified bovine serum amine oxidase in the presence of spermine in chinese hamster ovary cells. *Archives of biochemistry and biophysics,* 300:75-79.

Bach, A.W., Lan, N.C., Johnson, D.L., Abell, C.W., Bembenek, M.E., Kwan, S.W., Seeburg, P.H. & Shih, J.C. 1988. cDNA cloning of human liver monoamine oxidase A and B: Molecular basis of differences in enzymatic properties. *Proceedings of the national academy of sciences of the United States of America,* 85:4934-4938.

Bara-Jimenez, W., Sherzai, A., Dimitrova, T., Favit, A., Bibbiani, F., Gillespie, M., Morris, M.J., Mouradian, M.M. & Chase, T.N. 2003. Adenosine A_{2A} receptor antagonist treatment of Parkinson's disease. *Neurology,* 61:293-296.

Bartels, A.L. & Leenders, K.L. 2009. Parkinson's disease: The syndrome, the pathogenesis and pathophysiology. *Cortex,* 45:915-921.

Betarbet, R., Sherer, T.B. & Greenamyre, J.T. 2005. Ubiquitin-proteasome system and Parkinson's diseases. *Experimental neurology,* 191(Suppl. 1):S17-S27.

Binda, C., Li, M., Hubálek, F., Restelli, N., Edmondson, D.E. & Mattevi, A. 2003. Insights into the mode of inhibition of human mitochondrial monoamine oxidase B from high-resolution crystal structures. *Proceedings of the national academy of sciences of the United States of America,* 100:9750-9755.

Binda, C., Newton-Vinson, P., Hubálek, F., Edmondson, D.E. & Mattevi, A. 2002. Structure of human monoamine oxidase B, a drug target for the treatment of neurological disorders. *Nature structural biology,* 9:22-26.

Bonnet, U. 2003. Moclobemide: Therapeutic use and clinical studies. *CNS drug reviews,* 9:97-140.

Booysen, H.P., Moraal, C., Terre'Blanche, G., Petzer, A., Bergh, J.J., Petzer, J.P. 2011. Thio- and aminocaffeine analogues as inhibitors of human monoamine oxidase. *Bioorganic & medicinal chemistry,* 19:7507-7518.

Bortolato, M., Chen, K. & Shih, J.C. 2008. Monoamine oxidase inactivation: From pathophysiology to therapeutics. *Advanced drug delivery reviews,* 60:1527-1533.

Boyer, E.W. & Shannon, M. 2005. Current concepts: The serotonin syndrome. *New England journal of medicine,* 352:1112-1120.

Brazeau, B.J., Johnson, B.J. & Wilmot, C.M. 2004. Copper-containing amine oxidases. biogenesis and catalysis; a structural perspective. *Archives of biochemistry and biophysics,* 428:22-31.

Burke, W.J., Kumar, V.B., Pandey, N., Panneton, W.M., Gan, Q., Franko, M.W., O'Dell, M., Li, S.W., Pan, Y., Chung, H.D. & Galvin, J.E. 2008. Aggregation of α-synuclein by DOPAL, the monoamine oxidase metabolite of dopamine. *Acta neuropathologica,* 115:193-203.

Caccia, C., Maj, R., Calabresi, M., Maestroni, S., Faravelli, L., Curatolo, L., Salvati, P. & Fariello, R.G. 2006. Safinamide: From molecular targets to a new anti-parkinson drug. *Neurology,* 67(Suppl. 2):S18-S23.

Carlsson, A. 1959. The occurrence, distribution and physiological role of catecholamines in the nervous system. *Pharmacological reviews,* 11(Part 2):490-493.

Chen, J.-F., Steyn, S., Staal, R., Petzer, J.P., Xu, K., Van Der Schyf, C.J., Castagnoli, K., Sonsalla, P.K., Castagnoli Jr., N. & Schwarzschild, M.A. 2002. 8-(3-Chlorostyryl)caffeine may attenuate MPTP neurotoxicity through dual actions of monoamine oxidase inhibition and A_{2A} receptor antagonism. *Journal of biological chemistry,* 277:36040-36044.

Chen, J.J. & Swope, D.M. 2005. Clinical pharmacology of rasagiline: A novel, second-generation propargylamine for the treatment of Parkinson disease. *Journal of clinical pharmacology,* 45:878-894.

Cheng, Y.C. & Prusoff, W.H. 1973. Relationship between the inhibition constant (K_i) and the concentration of inhibitor which causes 50 per cent inhibition (I_{50}) of an enzymatic reaction. *Biochemical pharmacology,* 22:3099-3108.

Choi, J., Levey, A.I., Weintraub, S.T., Rees, H.D., Gearing, M., Chin, L.-S. & Li, L. 2004. Oxidative modifications and down-regulation of ubiquitin carboxyl-terminal hydrolase L1 associated with Idiopathic Parkinson's and Alzheimer's diseases. *Journal of biological chemistry,* 279:13256-13264.

Choonara, Y.E., Pillay, V., Du Toit, L.C., Modi, G., Naidoo, D., Ndesendo, V.M.K. & Sibambo, S.R. 2009. Trends in the molecular pathogenesis and clinical therapeutics of common neurodegenerative disorders. *International journal of molecular sciences,* 10:2510-2557.

Churchyard, A., Mathias, C.J., Boonkongchuen, P. & Lees, A.J. 1997. Autonomic effects of selegiline: Possible cardiovascular toxicity in Parkinson's disease. *Journal of neurology neurosurgery and psychiatry,* 63:228-234.

Clarke, C.E. 2004. Neuroprotection and pharmacotherapy for motor symptoms in Parkinson's disease. *The lancet neurology,* 3:466-474.

Conley, S.C. & Kirchner, J.T. 1999. Parkinson's disease - the shaking palsy. Underlying factors, diagnostic considerations, and clinical course. *Postgraduate medicine,* 106:39-52.

Conway, K.A., Lee, S.-J., Rochet, J.-C., Ding, T.T., Williamson, R.E. & Lansbury Jr., P.T. 2000. Acceleration of oligomerization, not fibrillization, is a shared property of both α-synuclein mutations linked to early-onset Parkinson's disease: Implications for pathogenesis and therapy. *Proceedings of the national academy of sciences of the United States of America,* 97:571-576.

Cookson, M.R. & Van der Brug, M. 2008. Cell systems and the toxic mechanisms of α-synuclein. *Experimental neurology,* 209:5-11.

Da Prada, M., Kettler, R., Keller, H.H., Cesura, A.M., Richards, J.G., Saura Marti, J., Muggli-Maniglio, D., Wyss, P.C., Kyburz, E. & Imhof, R. 1990. From moclobemide to ro 19-6327 and ro 41-1049: The development of a new class of reversible, selective MAO-A and MAO-B inhibitors. *Journal of neural transmission, 29(Suppl.*):S279-S292.

Dauer, W. & Przedborski, S. 2003. Parkinson's disease: Mechanisms and models. *Neuron,* 39:889-909.

Dawkes, H.C. & Phillips, S.E.V. 2001. Copper amine oxidase: Cunning cofactor and controversial copper. *Current opinion in structural biology,* 11:666-673.

De Colibus, L., Li, M., Binda, C., Lustig, A., Edmondson, D.E. & Mattevi, A. 2005. Three-dimensional structure of human monoamine oxidase A (MAO-A): Relation to the structures of rat MAO-A and human MAO-B. *Proceedings of the national academy of sciences of the United States of America,* 102:12684-12689.

Dexter, D.T., Wells, F.R., Agid, F., Agid, Y., Lees, A.J., Jenner, P. & Marsden, C.D. 1987. Increased nigral iron content in postmortem parkinsonian brain. *Lancet,* 2:1219-1220.

Dixon, M. 1953. The determination of enzyme inhibitor constants. *The biochemical journal,* 55:170-171.

Dorsey, E.R., Constantinescu, R., Thompson, J.P., Biglan, K.M., Holloway, R.G., Kieburtz, K., Marshall, F.J., Ravina, B.M., Schifitto, G., Siderowf, A. & Tanner, C.M. 2007. Projected number of people with Parkinson disease in the most populous nations, 2005 through 2030. *Neurology,* 68:384-386.

Double, K.L., Ben-Shachar, D., Youdim, M.B.H., Zecca, L., Riederer, P. & Gerlach, M. 2002. Influence of neuromelanin on oxidative pathways within the human substantia nigra. *Neurotoxicology and teratology,* 24:621-628.

Edmondson, D.E., Bhattacharyya, A.K. & Walker, M.C. 1993. Spectral and kinetic studies of imine product formation in the oxidation of p-(N,N-dimethylamino)-benzylamine analogues by monoamine oxidase B. *Biochemistry,* 32:5196-5202.

Edmondson, D.E., Binda, C. & Mattevi, A. 2004a. The FAD binding sites of human monoamine oxidases A and B. *Neurotoxicology,* 25:63-72.

Edmondson, D.E., Binda, C., Wang, J., Upadhyay, A.K. & Mattevi, A. 2009. Molecular and mechanistic properties of the membrane-bound mitochondrial monoamine oxidases. *Biochemistry,* 48:4220-4230.

Edmondson, D.E., DeColibus, L., Binda, C., Li, M., Mattevi, A. 2007. New insights into the structures and functions of human monoamine oxidase A and B. *Journal of neural transmission,* 114:703-705.

Edmondson, D.E., Mattevi, A., Binda, C., Li, M. & Hubálek, F. 2004b. Structure and mechanism of monoamine oxidase. *Current medicinal chemistry,* 11:1983-1993.

El-Agnaf, O.M.A., Walsh, D.M. & Allsop, D. 2003. Soluble oligomers for the diagnosis of neurodegenerative diseases. *Lancet neurology,* 2:461-462.

Fernandez, H.H. & Chen, J.J. 2007. Monoamine oxidase B inhibition in the treatment of Parkinson's disease. *Pharmacotherapy,* 27(Part 2):174S-185S.

Finberg, J.P.M., Tenne, M. & Youdim, M.B.H. 1981. Tyramine antagonistic properties of AGN 1135, an irreversible inhibitor of monoamine oxidase type B. *British journal of pharmacology,* 73:65-74.

Fischer, E. & Reese, L. 1883. Ueber Caffein, Xanthin und Guanin. *Liebigs annalen der chemie,* 221:336-344.

Forno, L.S. 1996. Neuropathology of parkinson's disease. *Journal of neuropathology and experimental neurology,* 55:259-272.

Fowler, C.J., Wiberg, A. & Oreland, L. 1980. The effect of age on the activity and molecular properties of human brain monoamine oxidase. *Journal of neural transmission - general section,* 49:1-20.

Fowler, J.S., Volkow, N.D., Wang, G.-J., Logan, J., Pappas, N., Shea, C. & MacGregor, R. 1997. Age-related increases in brain monoamine oxidase B in living healthy human subjects. *Neurobiology of aging,* 18:431-435.

Gareri, P., Falconi, U., De Fazio, P. & De Sarro, G. 2000. Conventional and new antidepressant drugs in the elderly. *Progress in neurobiology,* 61:353-396.

Gasser, T. 1998. Genetics of Parkinson's disease. *Clinical genetics,* 54:259-265.

Giasson, B.I., Duda, J.E., Murray, I.V.J., Chen, Q., Souza, J.M., Hurtig, H.I., Ischiropoulos, H., Trojanowski, J.Q. & Lee, V.M.-Y. 2000. Oxidative damage linked to neurodegeneration by selective α-synuclein nitration in synucleinopathy lesions. *Science,* 290:985-989.

Glover, V., Sandler, M., Owen, F. & Riley, G.J. 1977. Dopamine is a monoamine oxidase B substrate in man. *Nature,* 265:80-81.

Gnerre, C., Catto, M., Leonetti, F., Weber, P., Carrupt, P.-A., Altomare, C., Carotti, A. & Testa, B. 2000. Inhibition of monoamine oxidases by functionalized coumarin derivatives: Biological activities, QSARs, and 3D-QSARs. *Journal of medicinal chemistry,* 43:4747-4758.

Gomes, B., Naguwa, G., Kloepfer, H.G. & Yasunobu, K.T. 1969. Amine oxidase. XV. The sulfhydryl groups of beef liver mitochondrial amine oxidase. *Archives of biochemistry and biophysics,* 132:28-33.

Grimsby, J., Lan, N.C., Neve, R., Chen, K. & Shih, J.C. 1990. Tissue distribution of human monoamine oxidase A and B mRNA. *Journal of neurochemistry,* 55:1166-1169.

Grünblatt, E., Mandel, S., Jacob-Hirsch, J., Zeligson, S., Amariglo, N., Rechavi, G., Li, J., Ravid, R., Roggendorf, W., Riederer, P. & Youdim, M.B.H. 2004. Gene expression profiling of parkinsonian substantia nigra pars compacta; alterations in ubiquitin-proteasome, heat shock protein, iron and oxidative stress regulated proteins, cell adhesion/cellular matrix and vesicle trafficking genes. *Journal of neural transmission,* 111:1543-1573.

Haefely, W., Bukard, W.P., Cesura, A.M., Kettler, R., Lorez, H.P., Martin, J.R., Richards, J.G., Scherschlicht, R. & Da Prada, M. 1992. Biochemistry and pharmacology of moclobemide, a prototype RIMA. *Psychopharmacology,* 106(Suppl.):S6-S14.

Hallett, P.J. & Standaert, D.G. 2004. Rationale for and use of NMDA receptor antagonists in Parkinson's disease. *Pharmacology and therapeutics,* 102:155-174.

Hansch, C. & Leo, A. 1995. Exploring QSAR. *Fundamentals and applications in chemistry and biology*. Washington DC: American chemical society. 1-124.

Harada, M., Mizutani, K. & Nagatsu, T. 1971. Purification and properties of mitochondrial monoamine oxidase in beef brain. *Journal of neurochemistry,* 18:559-569.

Hastings, T.G., Lewis, D.A. & Zigmond, M.J. 1996. Reactive dopamine metabolites and neurotoxicity: Implications for Parkinson's disease. *Advances in experimental medicine and biology*, 387:97-106.

Hernán, M.A., Zhang, S.M., Rueda-DeCastro, A.M., Colditz, G.A., Speizer, F.E. & Ascherio, A. 2001. Cigarette smoking and the incidence of Parkinson's disease in two prospective studies. *Annals of neurology,* 50:780-786.

Hubálek, F., Binda, C., Khalil, A., Li, M., Mattevi, A., Castagnoli, N. & Edmondson, D.E. 2005. Demonstration of isoleucine 199 as a structural determinant for the selective inhibition of human monoamine oxidase B by specific reversible inhibitors. *Journal of biological chemistry,* 280:15761-15766.

Hull, L.A., Davis, G.T., Rosenblatt, D.H. & Mann, C.K. 1969. Oxidations of amines. VII. Chemical and electrochemical correlations. *Journal of physical chemistry,* 73:2142-2146.

Irizarry, M.C., Growdon, W., Gomez-Isla, T., Newell, K., George, J.M., Clayton, D.F. & Hyman, B.T. 1998. Nigral and cortical lewy bodies and dystrophic nigral neurites in Parkinson's disease and cortical lewy body disease contain α-synuclein immunoreactivity. *Journal of neuropathology and experimental neurology,* 57:334-337.

Jalkanen, S. & Salmi, M. 2001. Cell surface monoamine oxidases: Enzymes in search of a function. *EMBO journal,* 20:3893-3901.

Jenner, P., Dexter, D.T., Sian, J., Schapira, A.H.V. & Marsden, C.D. 1992. Oxidative stress as a cause of nigral cell death in Parkinson's disease and incidental lewy body disease. *Annals of neurology,* 32(Suppl.):S82-S87.

Klinman, J.P. & Mu, D. 1994. Quinoenzymes in biology. *Annual review of biochemistry,* 63:299-344.

Knoll, J. 1978. The possible mechanisms of action of (-)deprenyl in Parkinson's disease. *Journal of neural transmission,* 43:177-198.

Knoll, J. & Magyar, K. 1972. Some puzzling pharmacological effects of monoamine oxidase inhibitors. *Advances in biochemical psychopharmacology,* 5:393-408.

Korrell, M. & Tanner, C.M. 2005. Epidemiology of Parkinson's disease: An overview. (*In* Ebadi, M. & Pfeiffer, R., eds. Parkinson's disease. Florida: CRC Press. 39-50).

Lees, A.J., Hardy, J. & Revesz, T. 2009. Parkinson's disease. *The lancet,* 373:2055-2066.

Leroy, E., Boyer, R., Auburger, G., Leube, B., Ulm, G., Mezey, E., Harta, G., Brownstein, M.J., Jonnalagada, S., Chernova, T., Dehejia, A., Lavedan, C., Gasser, T., Steinbach, P.J., Wilkinson, K.D. & Polymeropoulos, M.H. 1998. The ubiquitin pathway in Parkinson's disease. *Nature,* 395:451-452.

Lewy, F.H. 1912. Paralysis agitans.I. Pathologische Anatomie. (In Lewandowski, M., ed. Handbuch der neurologie. 3rd ed. Berlin: Springer. 920-933).

Lineweaver, H. & Burk, D. 1934. The determination of enzyme dissociation constants. *Journal of the American chemical society,* 56:658-666.

Livingstone, D.J. & Salt, D.W. 2005. Judging the significance of multiple linear regression models. *Journal of medicinal chemistry,* 48:661-663.

Löhle, M. & Reichmann, H. 2010. Clinical neuroprotection in Parkinson's disease - still waiting for the breakthrough. *Journal of the neurological sciences,* 289:104-114.

Long, L.M. 1947. 8-R-Thio- and 8-R-sulfonylcaffeine derivatives. *Journal of the American chemical society,* 69:2939-2941.

Lücking, C.B., Dürr, A., Bonifati, V., Vaughan, J., De Michele, G., Gasser, T., Harhangi, B.S., Meco, G., Denèfle, P., Wood, N.W., Agid, Y., Brice, A., Nicholl, D., Breteler, M.M.B., Oostra, B.A., De Mari, M., Marconi, R., Filla, A., Bonnet, A.-M., Broussolle, E., Pollak, P., Rascol, O., Rosier, M. & Arnould, I. 2000. Association between early-onset Parkinson's disease and mutations in the parkin gene. *New England journal of medicine,* 342:1560-1567.

Ma, J., Yoshimura, M., Yamashita, E., Nakagawa, A., Ito, A. & Tsukihara, T. 2004. Structure of rat monoamine oxidase A and its specific recognitions for substrates and inhibitors. *Journal of molecular biology,* 338:103-114.

Mandel, S., Weinreb, O., Amit, T. & Youdim, M.B.H. 2005. Mechanism of neuroprotective action of the anti-parkinson drug rasagiline and its derivatives. *Brain research reviews,* 48:379-387.

Manoury, P.M., Binet, J.L., Rousseau, J., Lefèvre-Borg, F.M., Cavero. I.G. 1986. Synthesis of a series of compounds related to betaxolol, a new β-adrenoceptor antagonist with a pharmacological and pharmacokinetic profile optimized for the treatment of chronic cardiovascular diseases. *Journal of medicinal chemistry*, 30:1003-1011.

Markey, S.P., Johannessen, J.N. & Chiueh, C.C. 1984. Intraneuronal generation of a pyridinium metabolite may cause drug-induced parkinsonism. *Nature,* 311:464-466.

Masliah, E., Rockenstein, E., Veinbergs, I., Mallory, M., Hashimoto, M., Takeda, A., Sagara, Y., Sisk, A. & Mucke, L. 2000. Dopaminergic loss and inclusion body formation in α-synuclein mice: Implications for neurodegenerative disorders. *Science,* 287:1265-1269.

McNaught, K.S.P. & Olanow, C.W., 2003. Proteolytic stress: A unifying concept for the etiopathogenesis of Parkinson's disease. *Annals of neurology,* 53(Suppl. 3):S73-S86.

Miller, J.R. & Edmondson, D.E. 1999. Structure-activity relationships in the oxidation of para-substituted benzylamine analogues by recombinant human liver monoamine oxidase A. *Biochemistry,* 38:13670-13683.

Miller, J.R., Edmondson, D.E. & Grissom, C.B. 1995. Mechanistic probes of monoamine oxidase B catalysis: Rapid-scan stopped flow and magnetic field independence of the reductive half-reaction. *Journal of the American chemical society,* 117:7830-7831.

Mitoma, J.-Y., & Ito, A. 1992. Mitochondrial targeting signal of rat liver monoamine oxidase B is located at its carboxy terminus. *Journal of biochemistry,* 111:20-24.

Morpurgo, L., Agostinelli, E., Muccigrosso, J., Martini, F., Mondovi, B. & Avigliano, L. 1989. Benzylhydrazine as a pseudo-substrate of bovine serum amine oxidase. *Biochemical journal,* 260:19-25.

Murray, J.M., Saysell, C.G., Wilmot, C.M., Tambyrajah, W.S., Jaeger, J., Knowles, P.F., Phillips, S.E.V. & McPherson, M.J. 1999. The active site base controls cofactor reactivity in Escherichia coli amine oxidase: X-ray crystallographic studies with mutational variants. *Biochemistry,* 38:8217-8227.

Murray, R.K., Granner, D.K., Mayes, P.A. & Rodwell, V.W. 2003. Enzymes: Kinetics. *Harper's illustrated biochemistry*. 26th ed. s.l.:McGraw-Hill. 60-71.

Nagatsu, T. 2004. Progress in monoamine oxidase (MAO) research in relation to genetic engineering. *Neurotoxicology,* 25:11-20.

Newton-Vinson, P. & Edmondson, D.E. 1999. High-level expression, structural, kinetic, and redox characterization of recombinant human liver monoamine oxidase B. (*In* Ghisla, S., Kroneck, P., Macheroux, P. & Sund, H., eds. Flavins and flavoproteins. Berlin: Agency for Scientific Publications. 431-438).

Nicotra, A. & Parvez, S.H. 1999. Methods for assaying monoamine oxidase A and B activities: Recent developments. *Biogenic amines,* 15:307-320.

Pålhagen, S., Heinonen, E., Hägglund, J., Kaugesaar, T., Mäki-Ikola, O. & Palm, R. 2006. Selegiline slows the progression of the symptoms of Parkinson disease. *Neurology,* 66:1200-1206.

Parkinson, J. An essay on the shaking palsy. 2002. (Republished) *Journal of neuropsychiatry and clinical neuroscience,* 14:223-236.

Parsons, M.R., Convery, M.A., Wilmot, C.M., Yadav, K.D.S., Blakeley, V., Corner, A.S., Phillips, S.E.V., McPherson, M.J. & Knowles, P.F. 1995. Crystal structure of a quinoenzyme: Copper amine oxidase of Escherichia coli at 2 Å resolution. *Structure,* 3:1171-1184.

Perez, V., Romera, M., Lizcano, J.M., Marco, J.L. & Unzeta, M. 2003. Protective effect of N-(2-propynyl)-2-(5-benzyloxy-indolyl) methylamine (PF 9601N), a novel MAO-B inhibitor, on dopamine-lesioned PC12 cultured cells. *Journal of pharmacy and pharmacology,* 55:713-716.

Petzer, J.P., Steyn, S., Castagnoli, K.P., Chen, J.-F., Schwarzschild, M.A., Van der Schyf, C.J. & Castagnoli, N. 2003. Inhibition of monoamine oxidase B by selective adenosine A_{2A} receptor antagonists. *Bioorganic & medicinal chemistry,* 11:1299-1310.

Pletscher, A. 1991. The discovery of antidepressants: A winding path. *Experientia,* 47:4-8.

Ramsay, R.R. 1991. Kinetic mechanism of monoamine oxidase A. *Biochemistry,* 30:4624-4629.

Rascol, O., Goetz, C., Koller, W., Poewe, W. & Sampaio, C. 2002. Treatment interventions for Parkinson's disease: An evidence based assessment. *Lancet,* 359:1589-1598.

Rebrin, I., Geha, R.M., Chen, K. & Shih, J.C. 2001. Effects of carboxyl-terminal truncations on the activity and solubility of human monoamine oxidase B. *Journal of biological chemistry,* 276:29499-29506.

Riederer, P., Sofic, E., Rausch, W.-D., Schmidt, B., Reynolds, G.P., Jellinger, K. & Youdim, M.B.H. 1989. Transition metals, ferritin, glutathione, and ascorbic acid in parkinsonian brains. *Journal of neurochemistry,* 52:515-520.

Riederer, P. & Youdim, M.B.H. 1986. Monoamine oxidase activity and monoamine metabolism in brains of parkinsonian patients treated with l-deprenyl. *Journal of neurochemistry,* 46:1359-1365.

Saura, M. J., Kettler, R., Da Prada, M. & Richards, J.G. 1990. Molecular neuroanatomy of MAO-A and MAO-B. *Journal of neural transmission,* 32(Suppl.):S49-S53.

Schnaitman, C., Erwin, V.G. & Greenawalt, J.W. 1967. The submitochondrial localization of monoamine oxidase. An enzymatic marker for the outer membrane of rat liver mitochondria. *Journal of cell biology,* 32:719-735.

Schwarzschild, M.A., Agnati, L., Fuxe, K., Chen, J. & Morelli, M. 2006. Targeting adenosine A_{2A} receptors in Parkinson's disease. *Trends in neurosciences,* 29:647-654.

Shih, J.C., Chen, K. & Ridd, M.J. 1999. Monoamine oxidase: From genes to behavior. *Annual review of neuroscience,* 22:197-217.

Sian, J., Dexter, D.T., Lees, A.J., Daniel, S., Agid, Y., Javoy-Agid, F., Jenner, P. & Marsden, C.D. 1994. Alterations in glutathione levels in Parkinson's disease and other neurodegenerative disorders affecting basal ganglia. *Annals of neurology,* 36:348-355.

Silverman, R.B., Hoffman, S.J. & Catus, W.B. 1980. A mechanism for mitochondrial monoamine oxidase catalyzed amine oxidation. *Journal of the American chemical society,* 102:7126-7128.

Sixt, T. & Kaim, W. 2000. Copper(I) complexes with N,O-donor schiff base ligands related to intermediate forms of the TPQ cofactor in amine oxidases. *Inorganica chimica acta,* 300-302:762-768.

Son, S.-Y., Ma, J., Kondou, Y., Yoshimura, M., Yamashita, E. & Tsukihara, T. 2008. Structure of human monoamine oxidase A at 2.2-Å resolution: The control of opening the entry for substrates/inhibitors. *Proceedings of the national academy of sciences of the United States of America,* 105:5739-5744.

Souza, J.M., Giasson, B.I., Chen, Q., Lee, V.M.-Y. & Ischiropoulos, H. 2000. Dityrosine cross-linking promotes formation of stable α-synuclein polymers: Implication of nitrative and oxidative stress in the pathogenesis of neurodegenerative synucleinopathies. *Journal of biological chemistry,* 275:18344-18349.

Stevanato, R., Vianello, F. & Rigo, A. 1995. Thermodynamic analysis of the oxidative deamination of polyamines by bovine serum amine oxidase. *Archives of biochemistry and biophysics,* 324:374-378.

Symes, A.L., Sourkes, T.L., Youdim, M.B., Gregoriadis, G. & Birnbaum, H. 1969. Decreased monoamine oxidase activity in liver of iron-deficient rats. *Canadian journal of biochemistry,* 47:999-1002.

Tipton, K.F., Boyce, S., O'Sullivan, J., Davey, G.P. & Healy, J. 2004. Monoamine oxidases: Certainties and uncertainties. *Current medicinal chemistry,* 11:1965-1982.

Vogel, A.I., Furniss, B.S., Hannaford, A.J., Smith, P.W.G. & Tatchell, A.R. 1989. Aliphatic sulphur compounds. (*In* Vogel, A.I., Furniss, B.S., Hannaford, A.J., Smith, P.W.G & Tatchell, A.R., eds. Vogel's textbook of practical organic chemistry. 5 ed. London: Prentice Hall. 786-789).

Walker, M.C. & Edmondson, D.E. 1994. Structure-activity relationships in the oxidation of benzylamine analogues by bovine liver mitochondrial monoamine oxidase B. *Biochemistry,* 33:7088-7098.

Walker, W.H., Kearney, E.B., Seng, R. & Singer, T.P. 1971. Sequence and structure of a cysteinyl flavin peptide from monoamine oxidase. *Biochemical and biophysical research communications,* 44:287-292.

Wang, J. & Edmondson, D.E. 2007. Do monomeric vs dimeric forms of MAO-A make a difference? Comparison of the catalytic properties of rat and human MAO-A's. *Journal of neural transmission,* 114:721-724.

Weissbach, H., Smith, T.E., Daly, J.W., Witkop, B. & Udenfriend, S. 1960. A rapid spectrophotometric assay of monoamine oxidase based on the rate of disappearance of kynuramine. *The journal of biological chemistry,* 235:1160-1163.

Yacoubian, T.A. & Standaert, D.G. 2009. Targets for neuroprotection in Parkinson's disease. *Biochimica et biophysica acta,* 1792:676-687.

Youdim, M.B.H. & Bakhle, Y.S. 2006. Monoamine oxidase: Isoforms and inhibitors in Parkinson's disease and depressive illness. *British journal of pharmacology,* 147(Suppl. 1):S287-S296.

Youdim, M.B.H., Edmondson, D. & Tipton, K.F. 2006. The therapeutic potential of monoamine oxidase inhibitors. *Nature reviews neuroscience,* 7:295-309.

Youdim, M.B.H., Finberg, J.P.M. & Tipton, K.F. 1988. Monoamine oxidase. *In* Trendelenburg, U. & Weiner, N., eds. Catecholamine II. Handbook of experimental pharmacology. Berlin: Springer. 119-192.

Youdim, M.B.H. & Weinstock, M. 2004. Therapeutic applications of selective and non-selective inhibitors of monoamine oxidase A and B that do not cause significant tyramine potentiation. *Neurotoxicology,* 25:243-250.

Zecca, L., Youdim, M.B.H., Riederer, P., Connor, J.R. & Crichton, R.R. 2004. Iron, brain ageing and neurodegenerative disorders. *Nature reviews neuroscience,* 5:863-873.

Zhou, J.J.P., Zhong, B. & Silverman, R.B. 1996. Direct continuous fluorometric assay for monoamine oxidase B. *Analytical biochemistry,* 234:9-12.

Zhou, M. & Panchuk-Voloshina, N. 1997. A one-step fluorometric method for the continuous measurement of monoamine oxidase activity. *Analytical biochemistry,* 253:169-174.

Appendix

Section 1: List of ^{1}H and ^{13}C NMR spectra of the following compounds

- 8-Chlorocaffeine (**A**)
- 8-[(Phenylethyl)sulfanyl]caffeine (**1a**)
- 8-[(Phenylethyl)sulfanyl]caffeine (**1a**) - ^{13}C NMR DEPT 90 °, ^{13}C NMR DEPT 135 °
- 8-{[2-(4-Chlorophenyl)ethyl]sulfanyl}caffeine (**1b**)
- 8-{[2-(4-Bromophenyl)ethyl]sulfanyl}caffeine (**1c**)
- 8-{[2-(4-Fluorophenyl)ethyl]sulfanyl}caffeine (**1d**)
- 8-{[2-(4-(Trifluoromethyl)phenyl)ethyl]sulfanyl}caffeine (**1e**)
- 8-{[2-(4-Methylphenyl)ethyl]sulfanyl}caffeine (**1f**)
- 8-{[2-(4-Methoxyphenyl)ethyl]sulfanyl}caffeine (**1g**)
- 8-{[2-(4-Bromophenyl)ethyl]sulfinyl}caffeine (**2a**)
- 8-{[2-(4-Fluorophenyl)ethyl]sulfinyl}caffeine (**2b**)

Section 2: List of HPLC traces of the following new compounds

- 8-[(Phenylethyl)sulfanyl]caffeine (**1a**)
- 8-{[2-(4-Chlorophenyl)ethyl]sulfanyl}caffeine (**1b**)
- 8-{[2-(4-Bromophenyl)ethyl]sulfanyl}caffeine (**1c**)
- 8-{[2-(4-Fluorophenyl)ethyl]sulfanyl}caffeine (**1d**)
- 8-{[2-(4-(Trifluoromethyl)phenyl)ethyl]sulfanyl}caffeine (**1e**)
- 8-{[2-(4-Methylphenyl)ethyl]sulfanyl}caffeine (**1f)**
- 8-{[2-(4-Methoxyphenyl)ethyl]sulfanyl}caffeine (**1g**)
- 8-{[2-(4-Bromophenyl)ethyl]sulfinyl}caffeine (**2a**)
- 8-{[2-(4-Fluorophenyl)ethyl]sulfinyl}caffeine (**2b**)

Section 3: List of Mass spectra of the following compounds

- 8-[(Phenylethyl)sulfanyl]caffeine (**1a**)
- 8-{[2-(4-Chlorophenyl)ethyl]sulfanyl}caffeine (**1b**)
- 8-{[2-(4-Bromophenyl)ethyl]sulfanyl}caffeine (**1c**)
- 8-{[2-(4-Fluorophenyl)ethyl]sulfanyl}caffeine (**1d**)

- 8-{[2-(4-(Trifluoromethyl)phenyl)ethyl]sulfanyl}caffeine (**1e**)
- 8-{[2-(4-Methylphenyl)ethyl]sulfanyl}caffeine (**1f**)
- 8-{[2-(4-Methoxyphenyl)ethyl]sulfanyl}caffeine (**1g**)
- 8-{[2-(4-Bromophenyl)ethyl]sulfinyl}caffeine (**2a**)
- 8-{[2-(4-Fluorophenyl)ethyl]sulfinyl}caffeine (**2b**)

Section 1 -^{1}H and ^{13}C NMR spectra

8-Chlorocaffeine

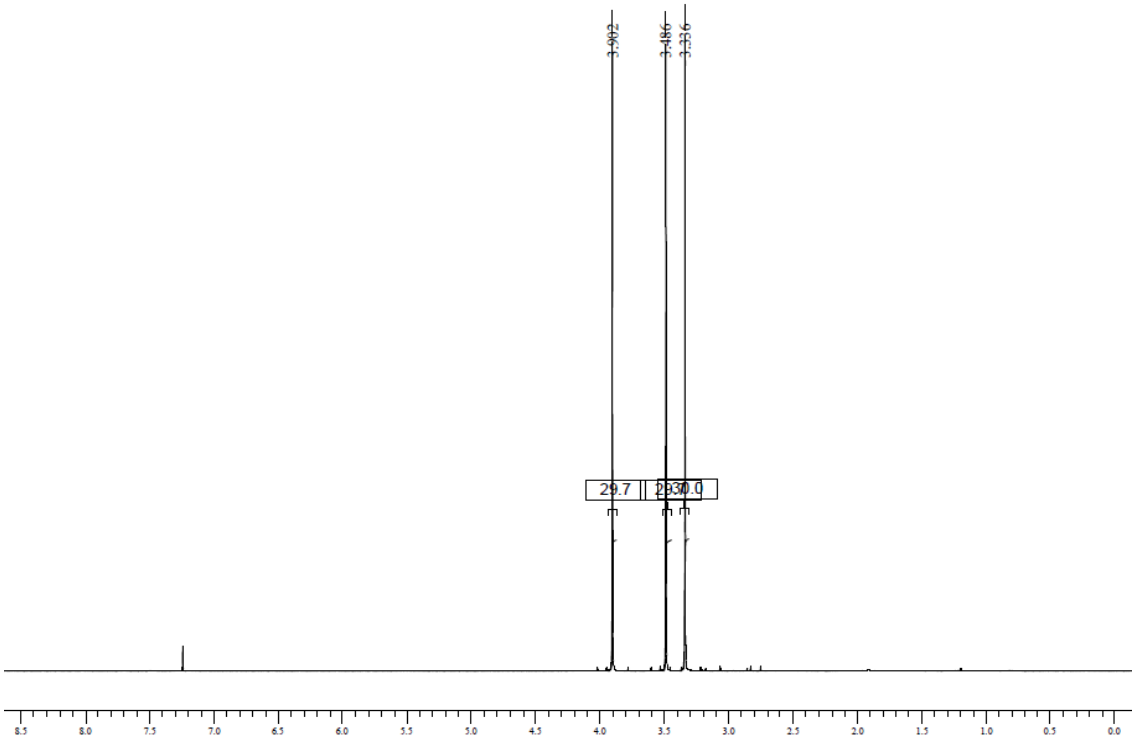

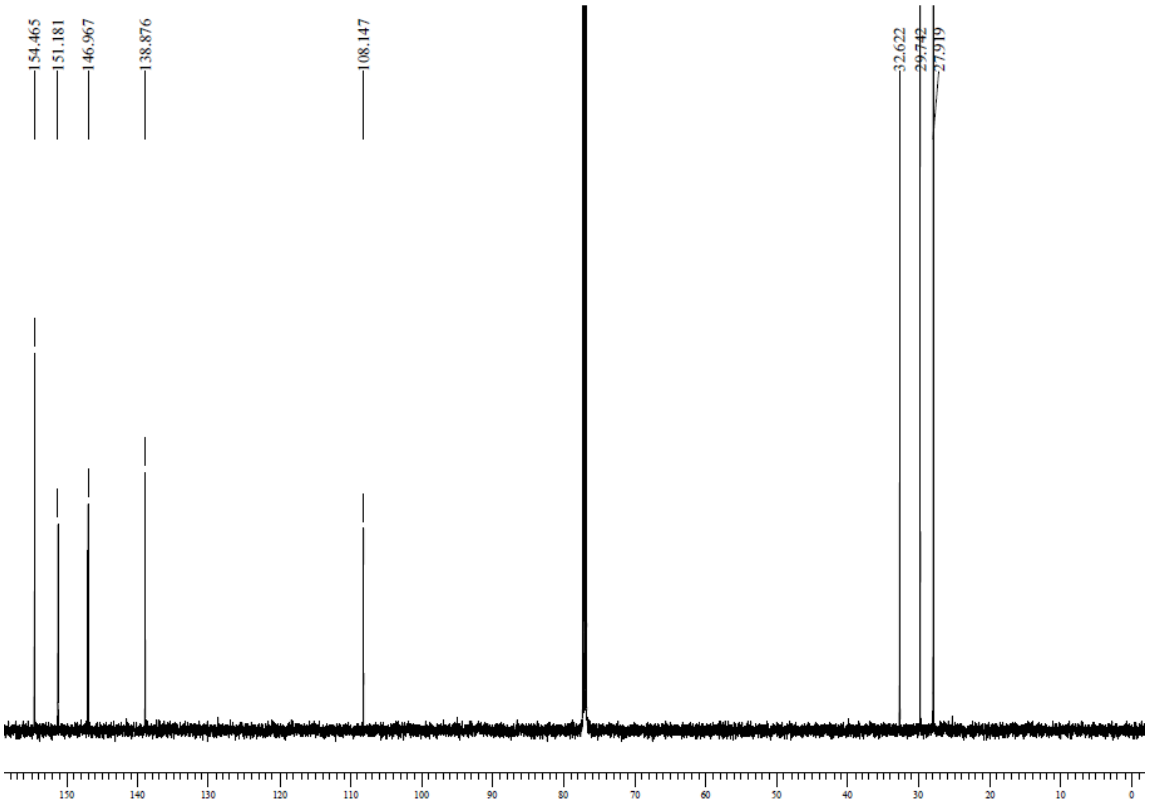
154.465
151.181
146.967
138.876
108.147
32.622
29.742
27.919
150
140
130
120
110
100
90
80
70
60
50
40
30
20
10
0

8-[(Phenylethyl)sulfanyl]caffeine (1a)

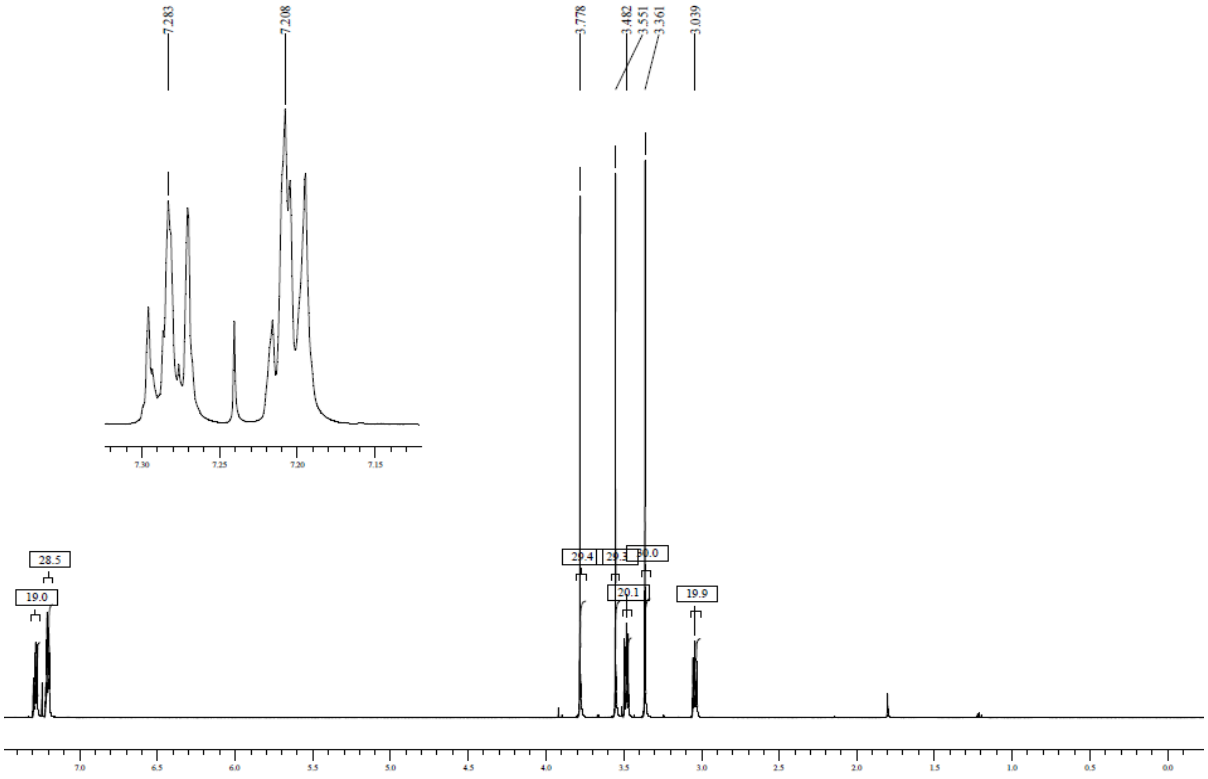

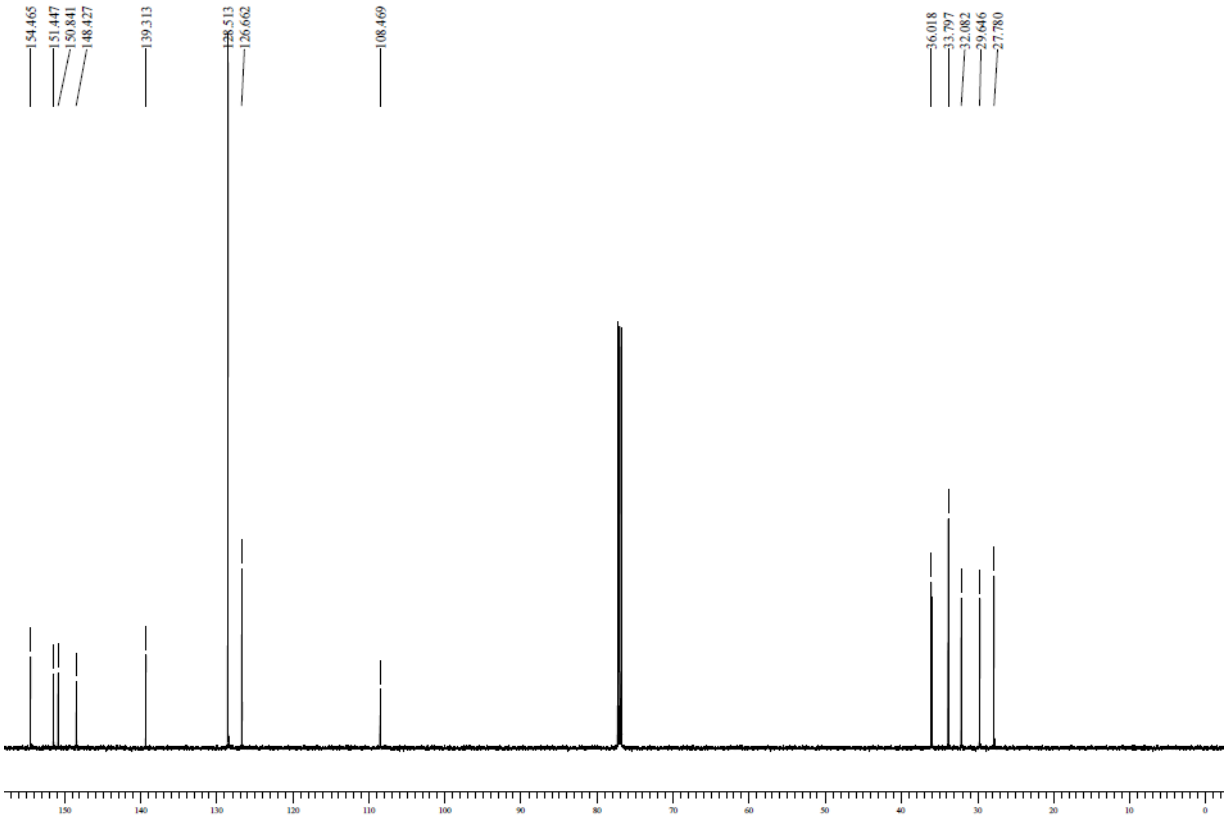

8-[(Phenylethyl)sulfanyl]caffeine (1a) -^{13}C NMR DEPT 90 °

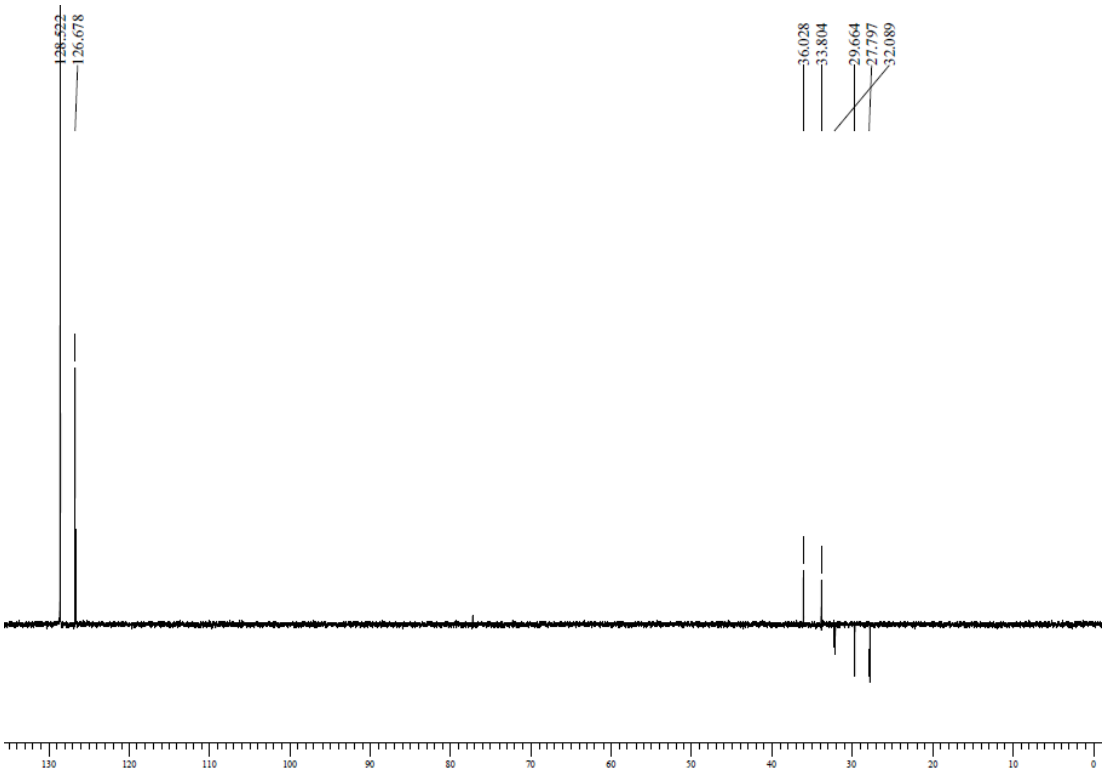

^{13}C NMR DEPT 135 °

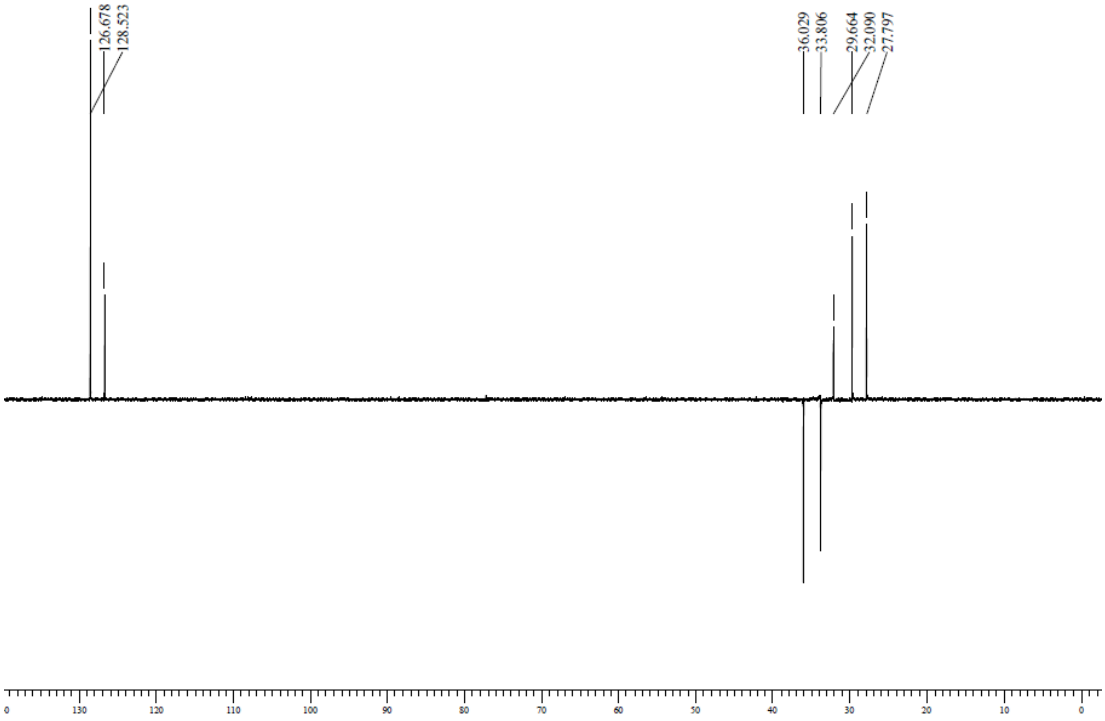

8-{[2-(4-Chlorophenyl)ethyl]sulfanyl}caffeine (1b)

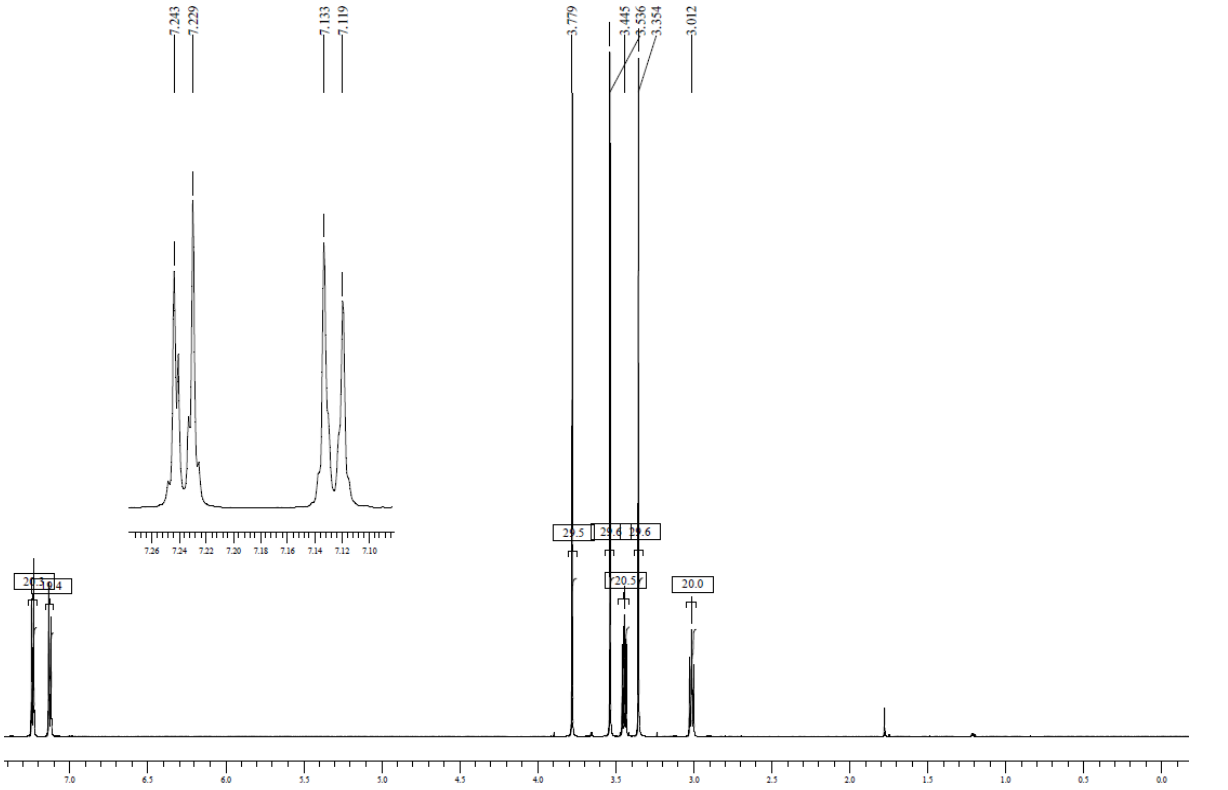

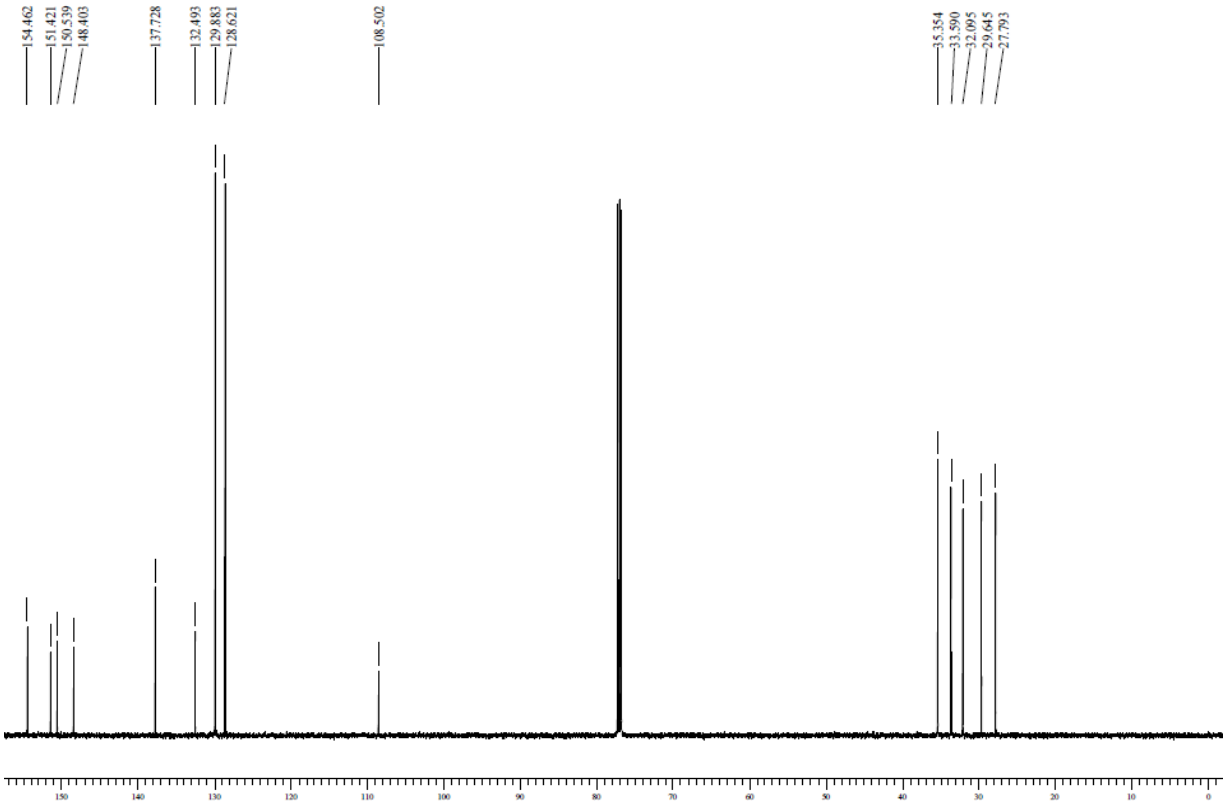

8-{[2-(4-Bromophenyl)ethyl]sulfanyl}caffeine (1c)

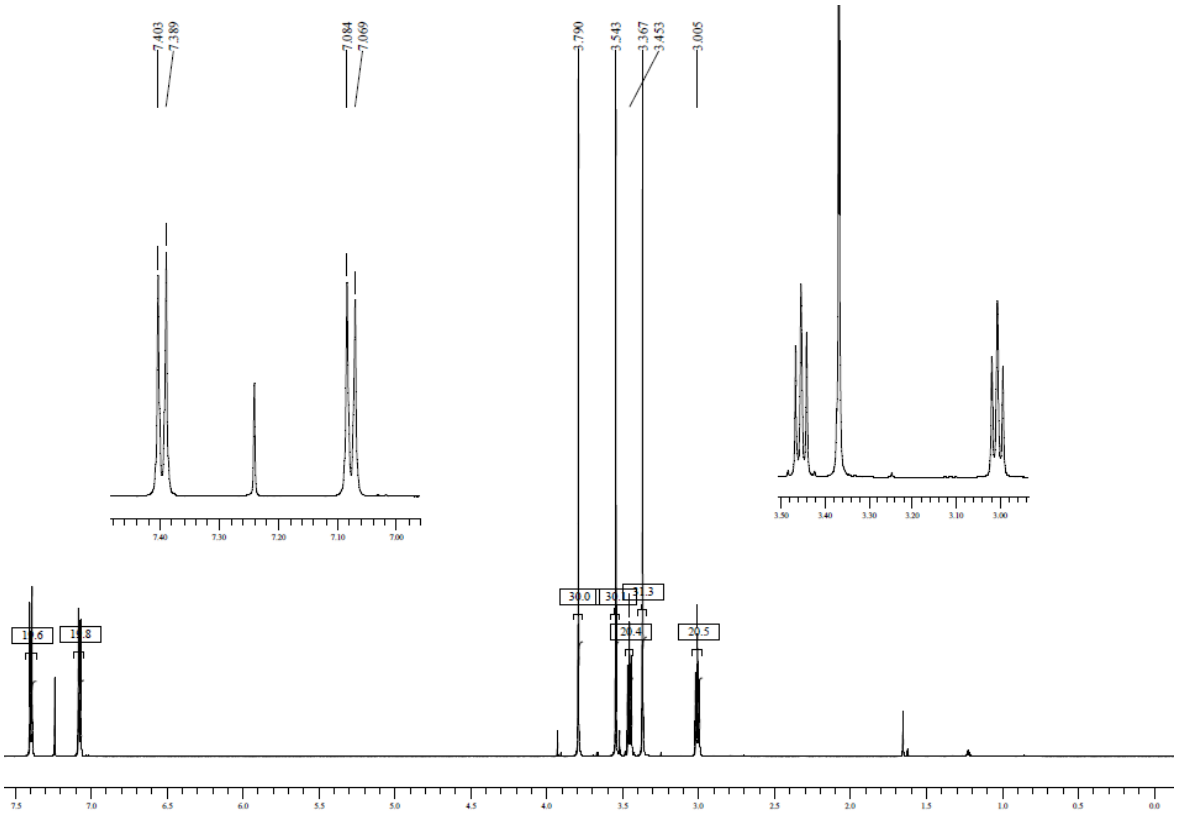

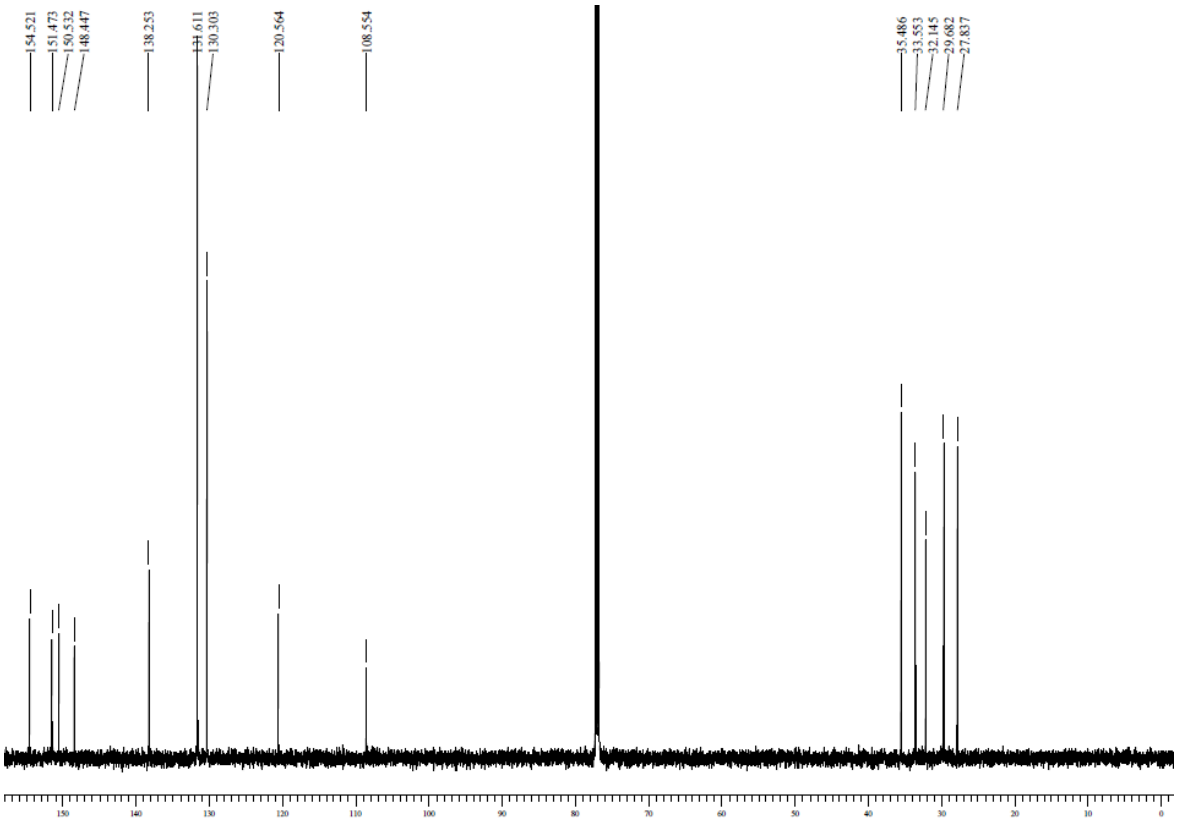

8-{[2-(4-Fluorophenyl)ethyl]sulfanyl}caffeine (1d)

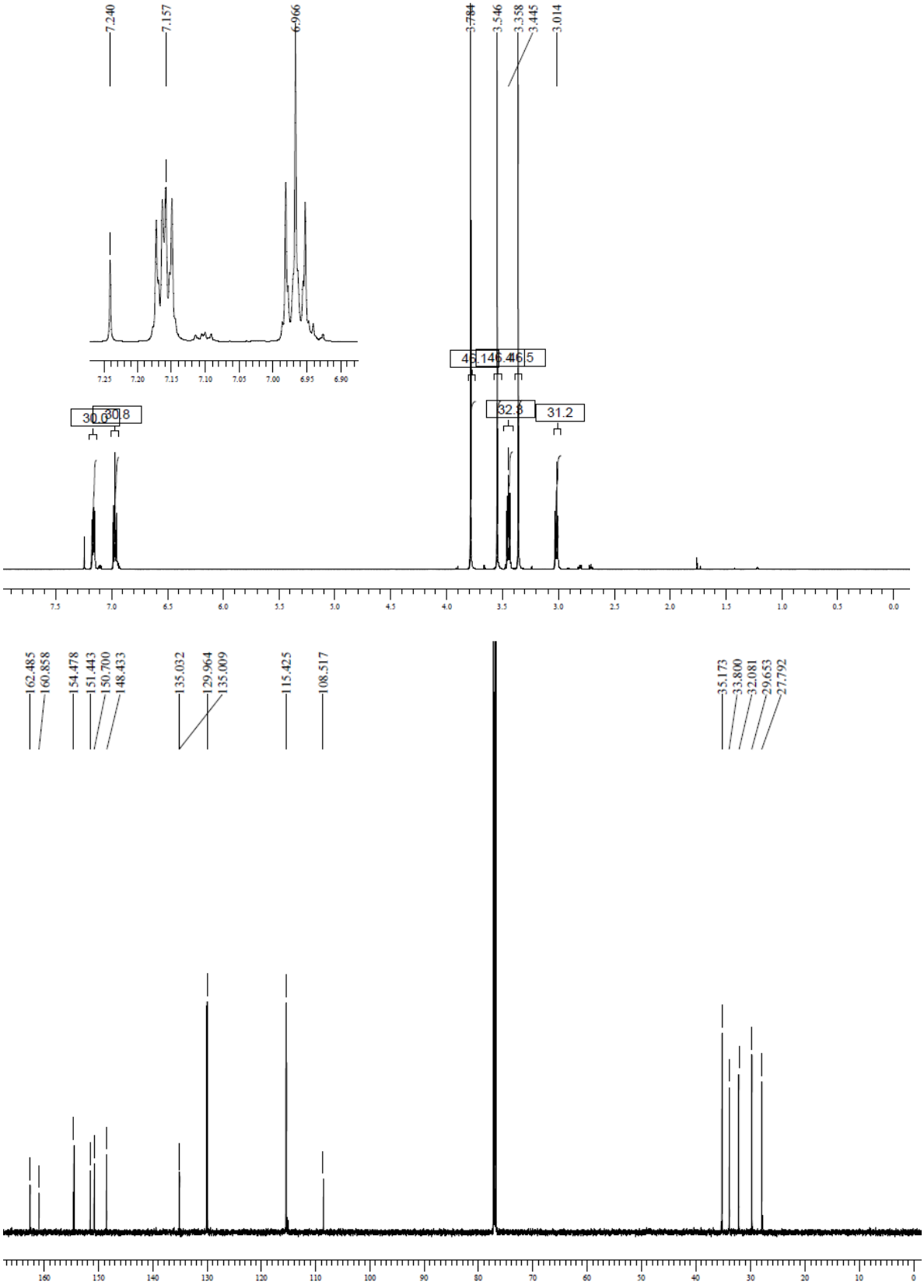

8-{[2-(4-(Trifluoromethyl)phenyl)ethyl]sulfanyl}caffeine (1e)

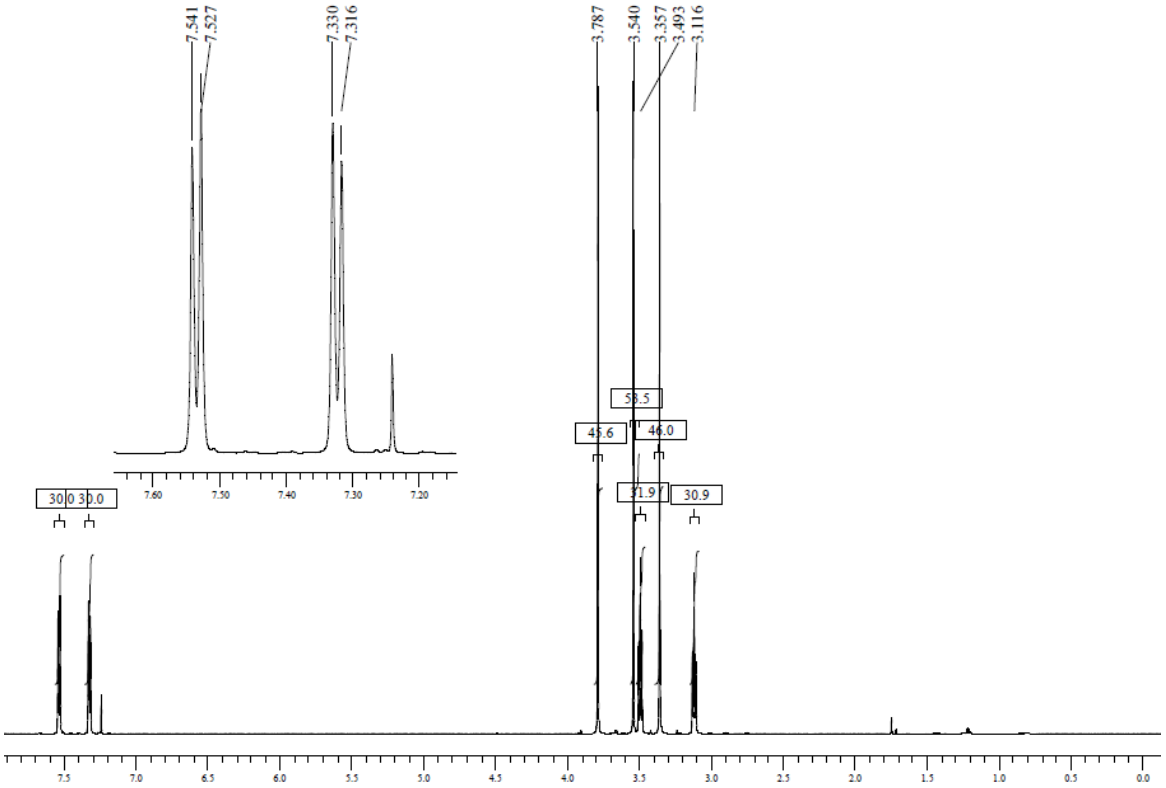

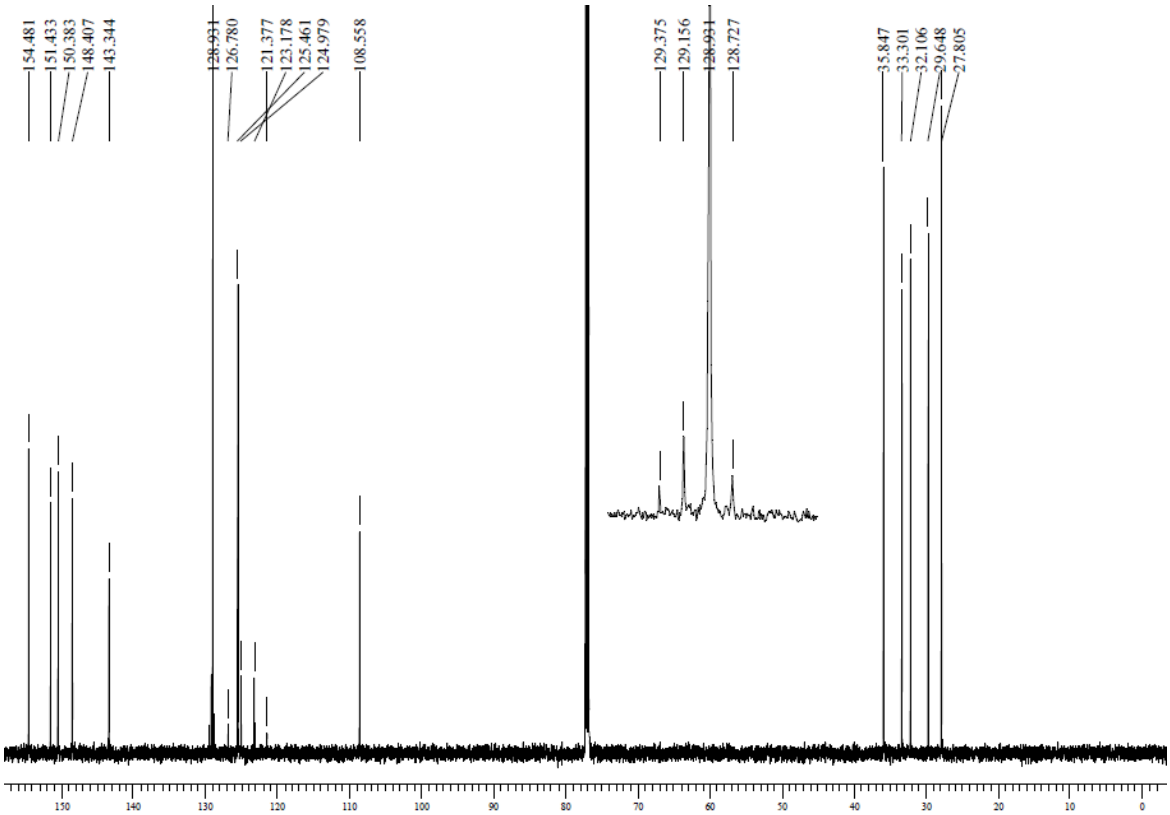

8-{[2-(4-Methylphenyl)ethyl]sulfanyl}caffeine (1f)

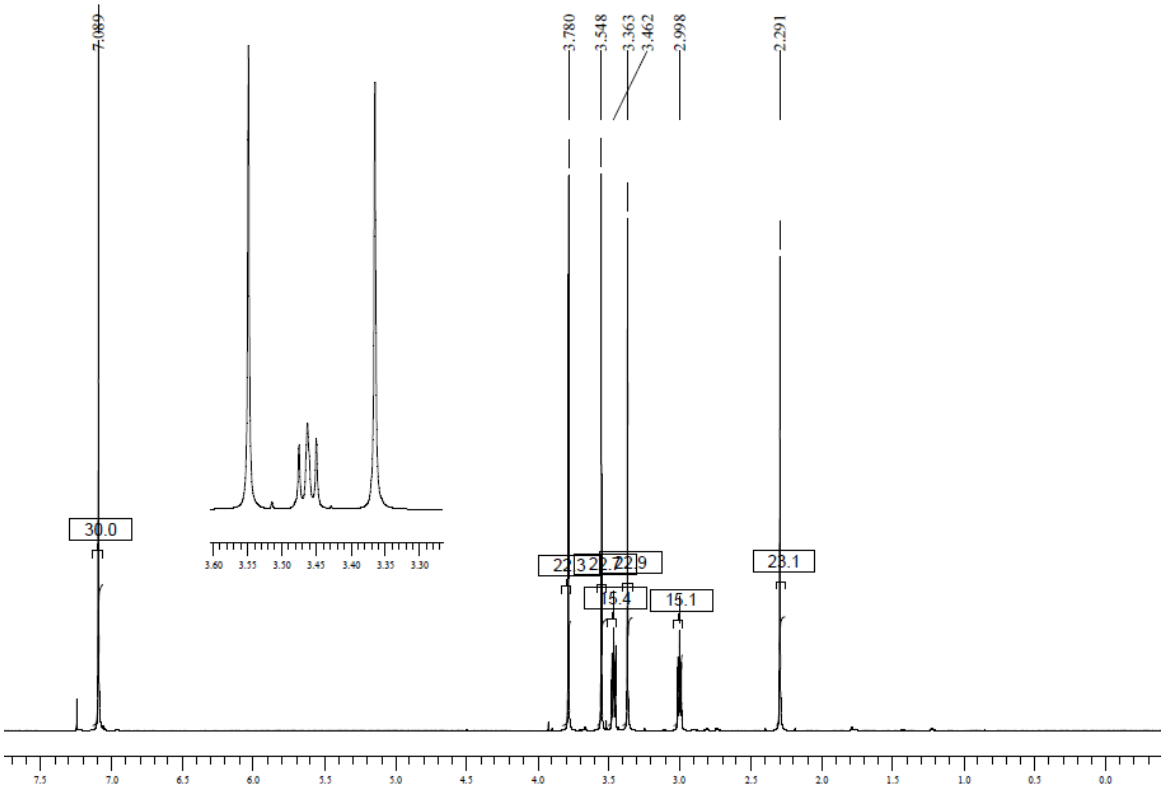

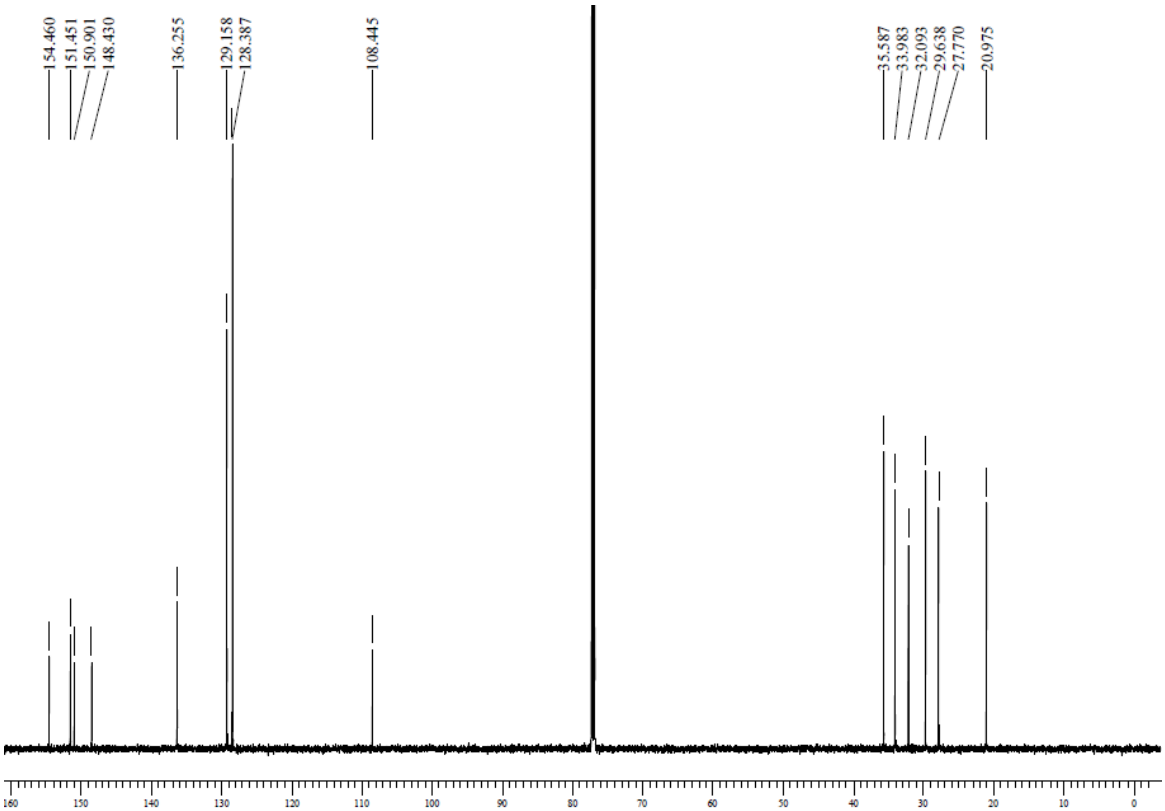

8-{[2-(4-Methoxyphenyl)ethyl]sulfanyl}caffeine (1g)

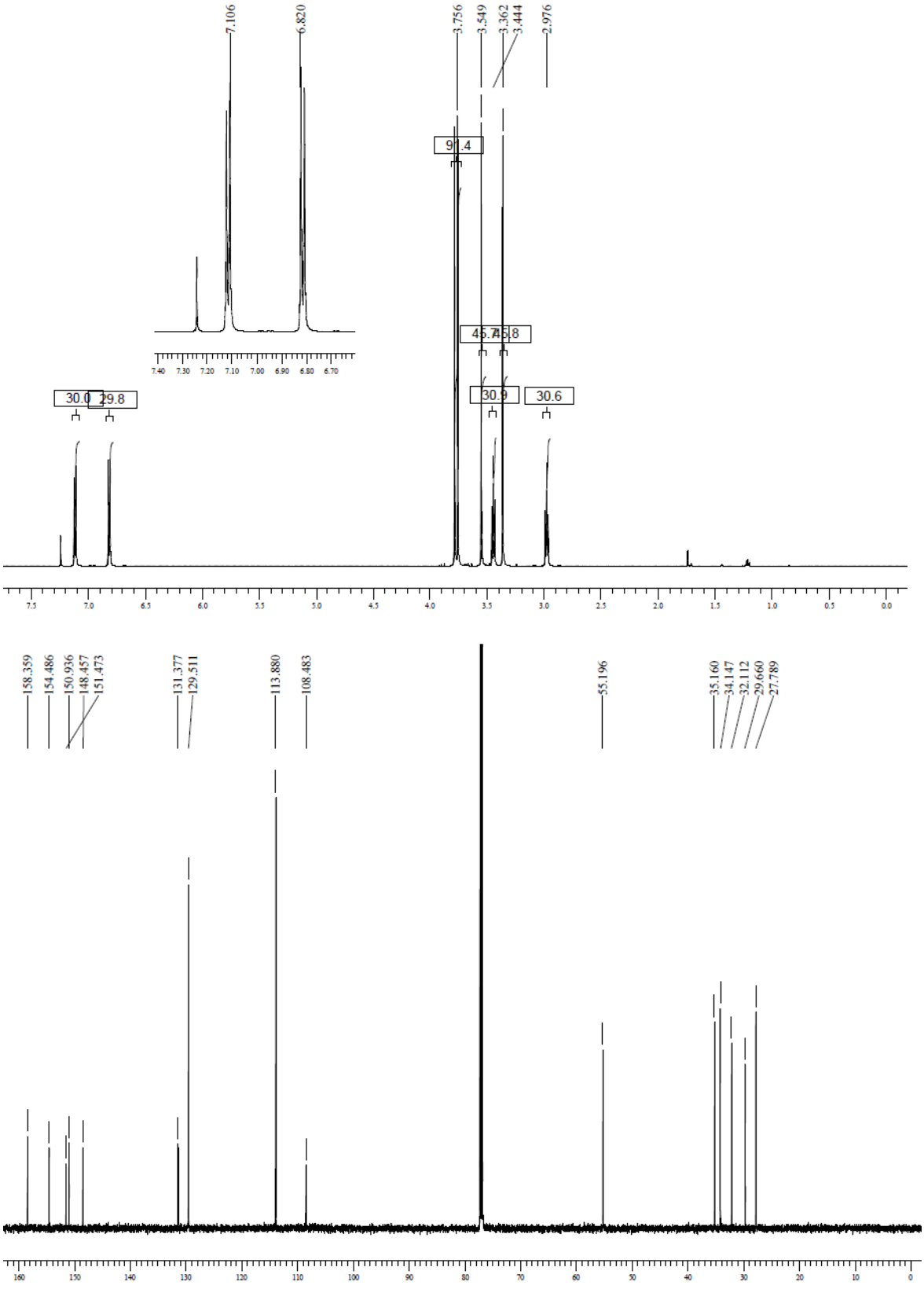

8-{[2-(4-Bromophenyl)ethyl]sulfinyl}caffeine (2a)

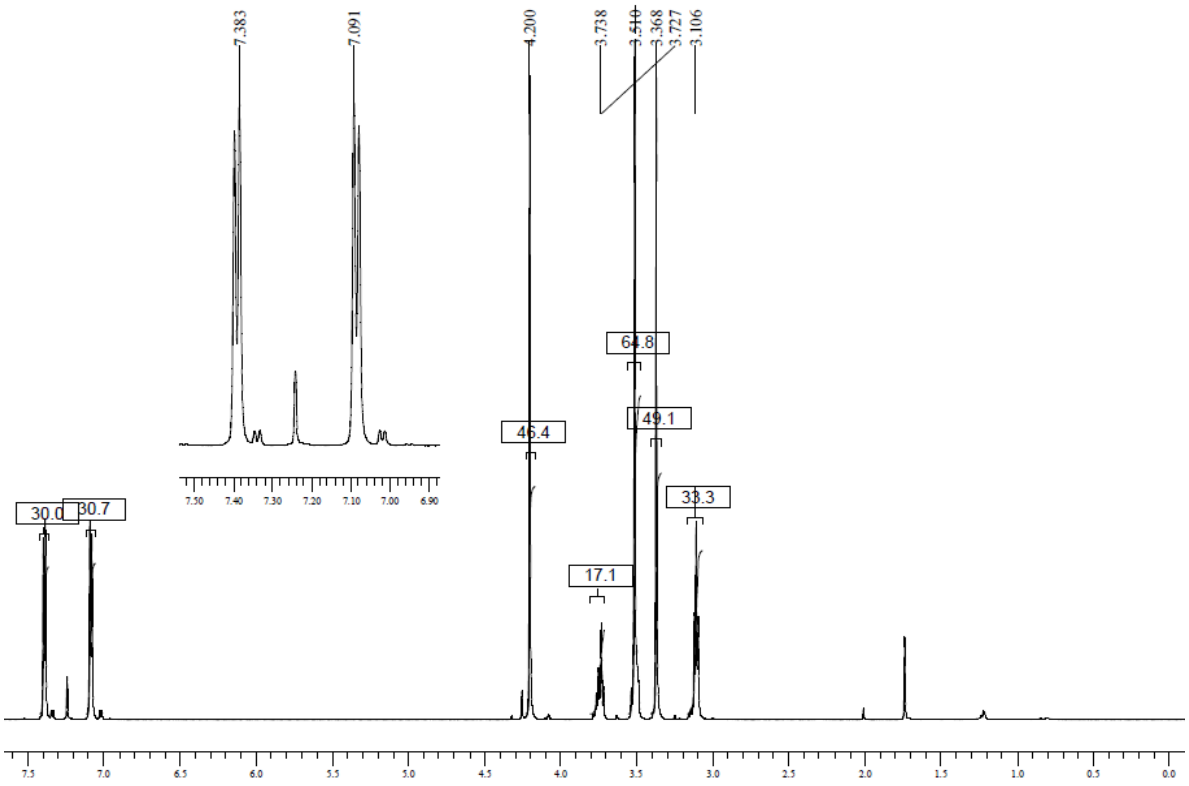

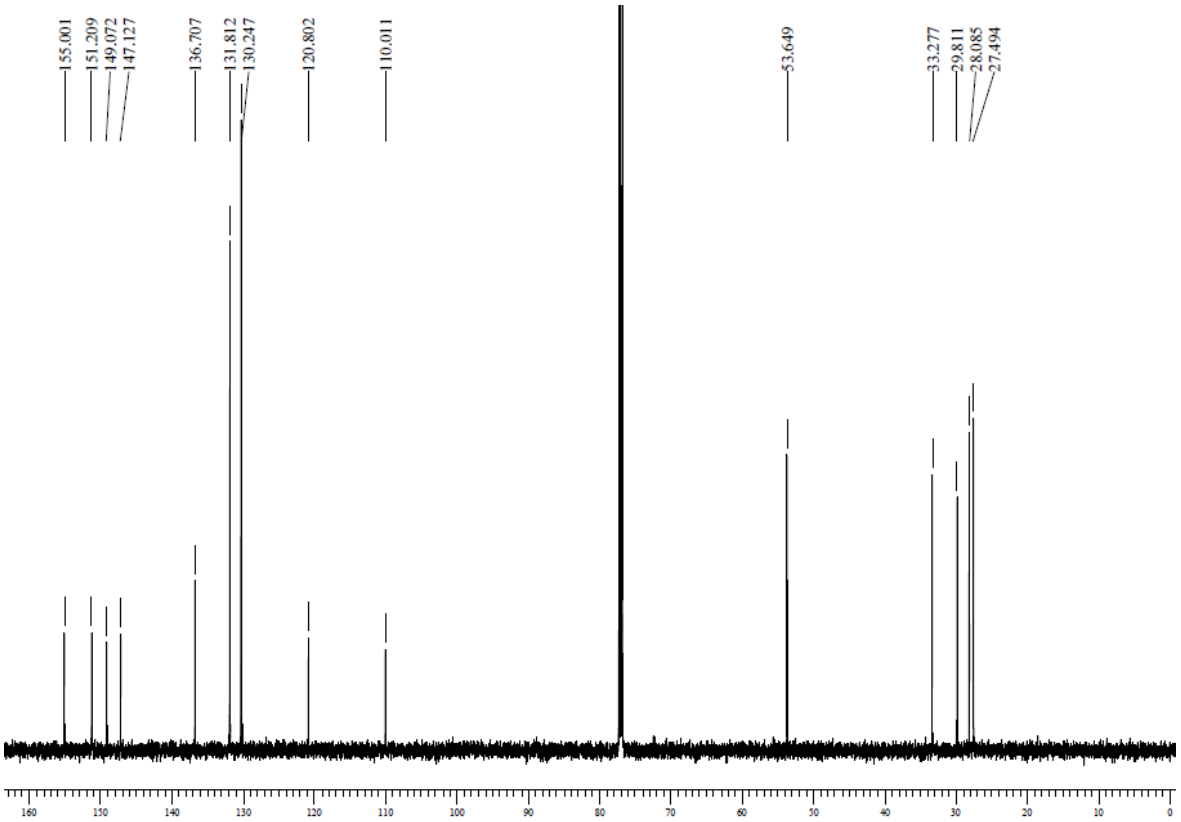

8-{[2-(4-Fluorophenyl)ethyl]sulfinyl}caffeine (2b)

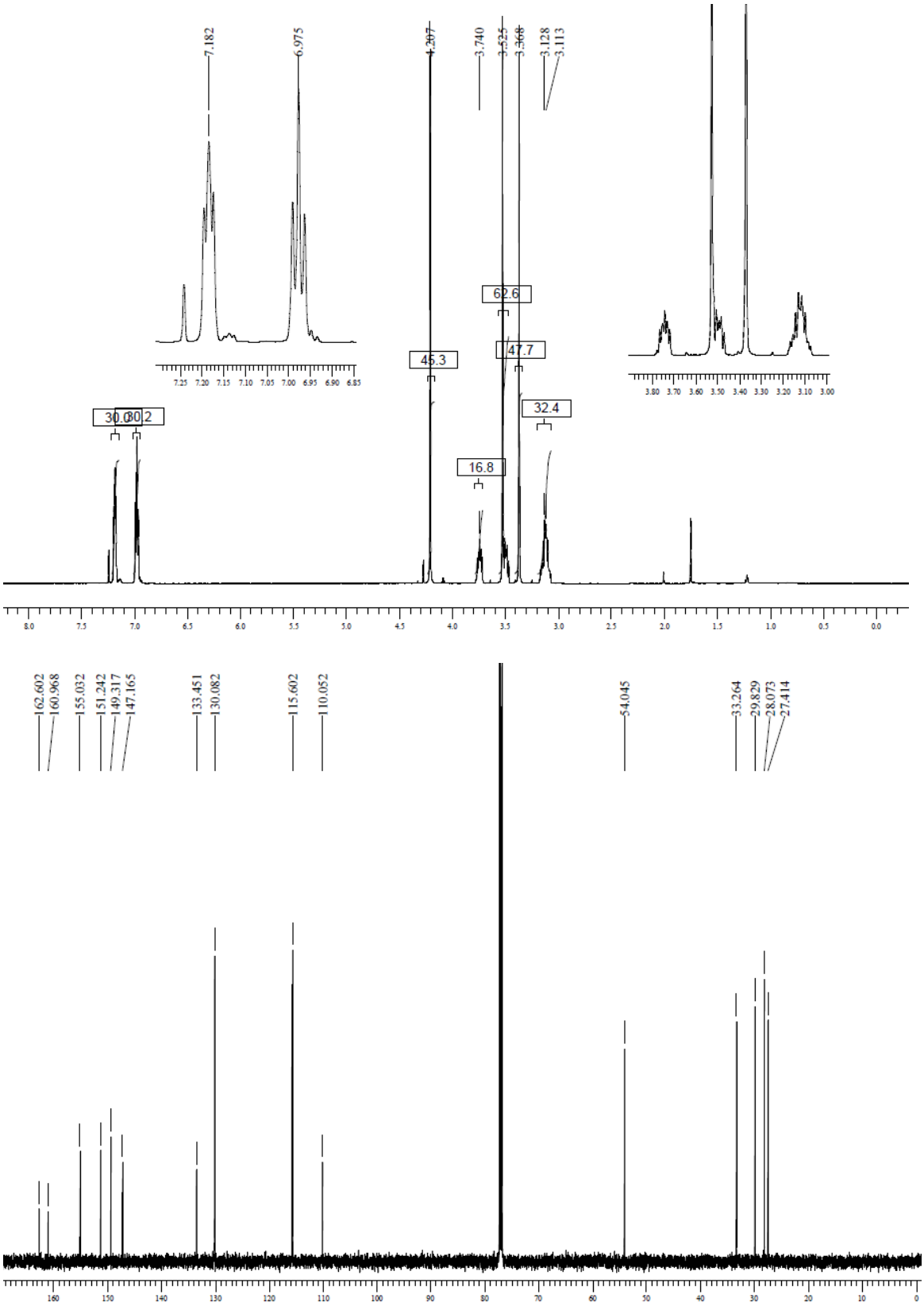

Section 2 - HPLC traces

8-[(Phenylethyl)sulfanyl]caffeine (1a)

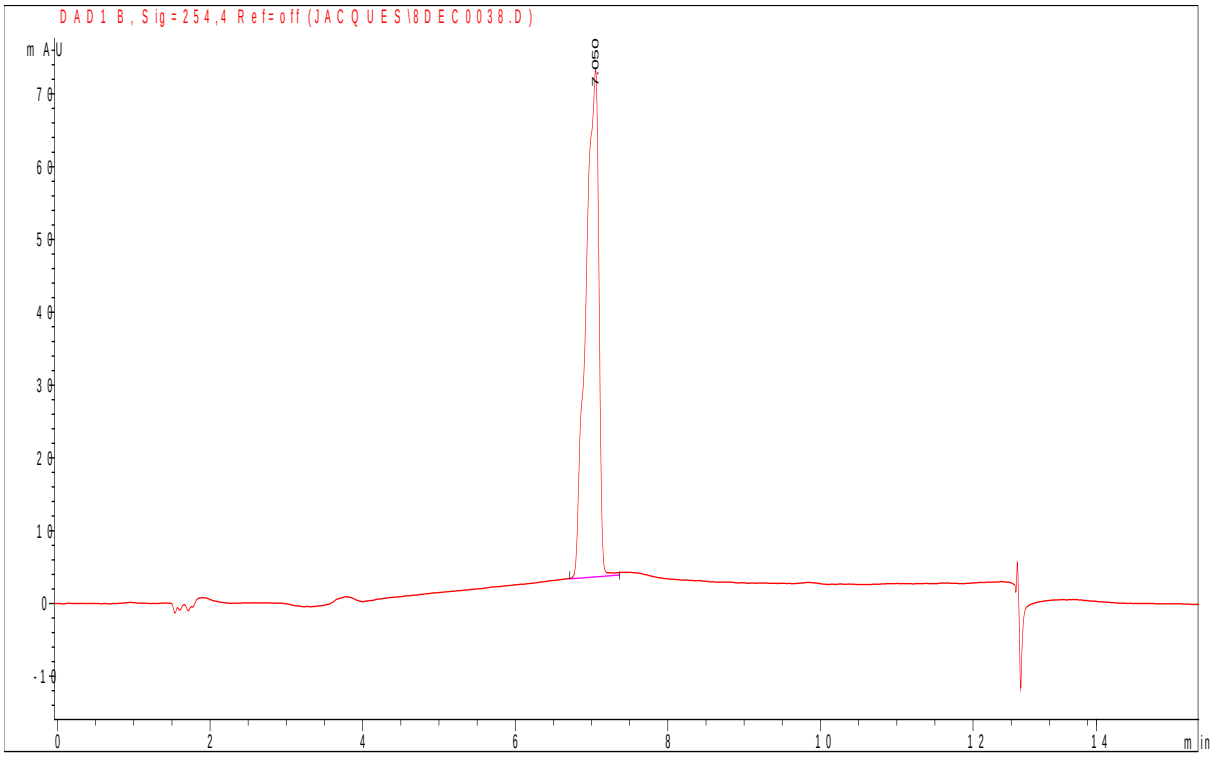

8-{[2-(4-Chlorophenyl)ethyl]sulfanyl}caffeine (1b)

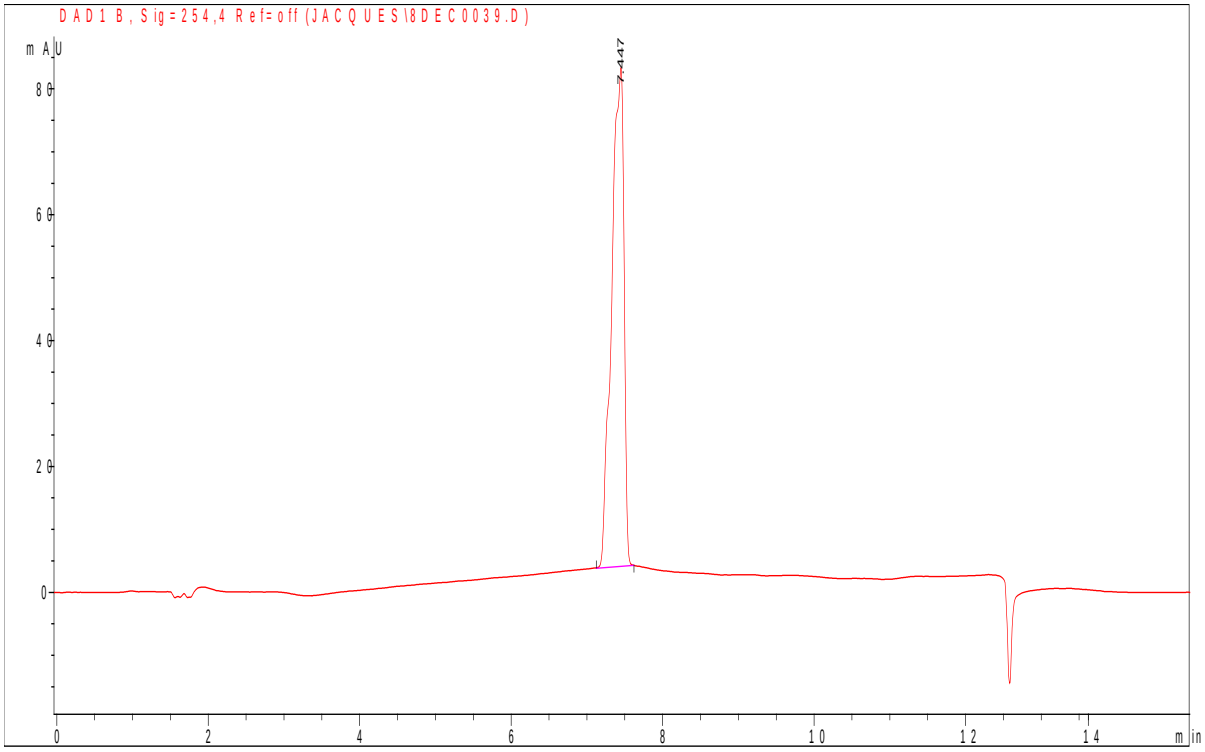

8-{[2-(4-Bromophenyl)ethyl]sulfanyl}caffeine (1c)

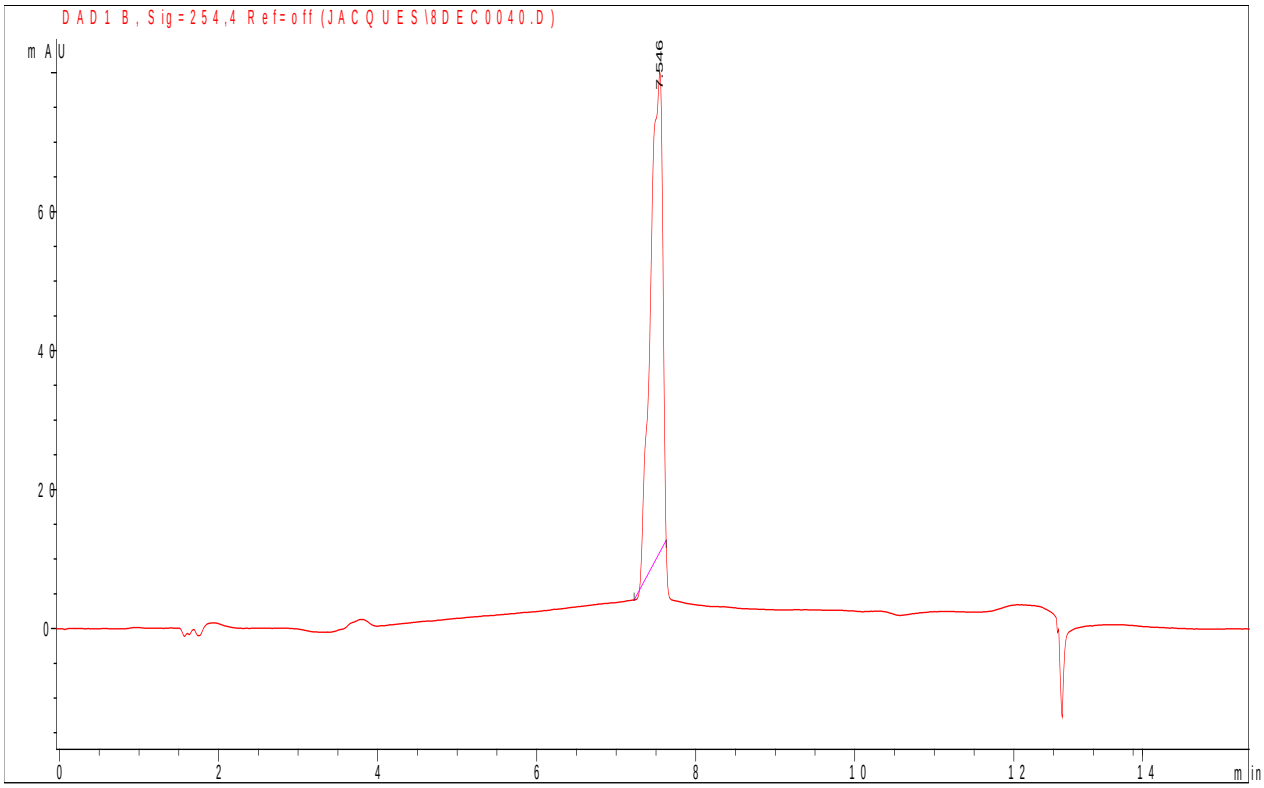

8-{[2-(4-Fluorophenyl)ethyl]sulfanyl}caffeine (1d)

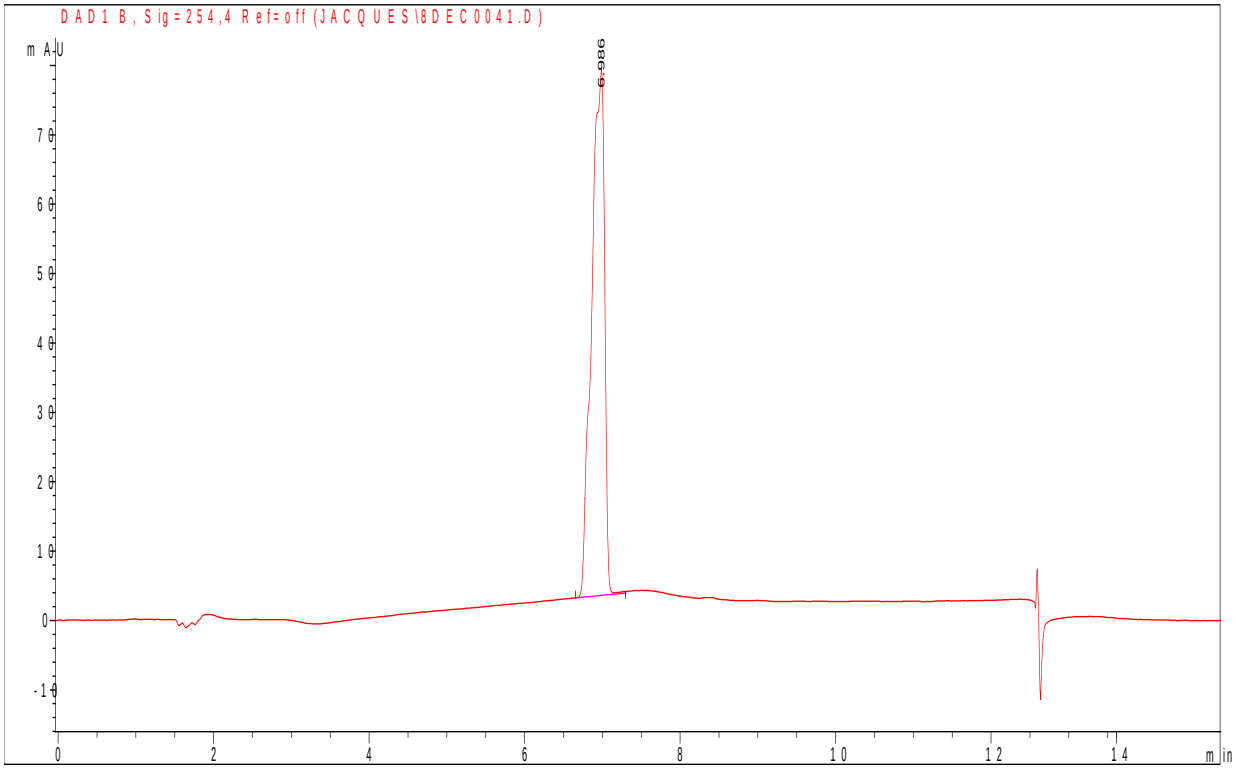

8-{[2-(4-(Trifluoromethyl)phenyl)ethyl]sulfanyl}caffeine (1e)

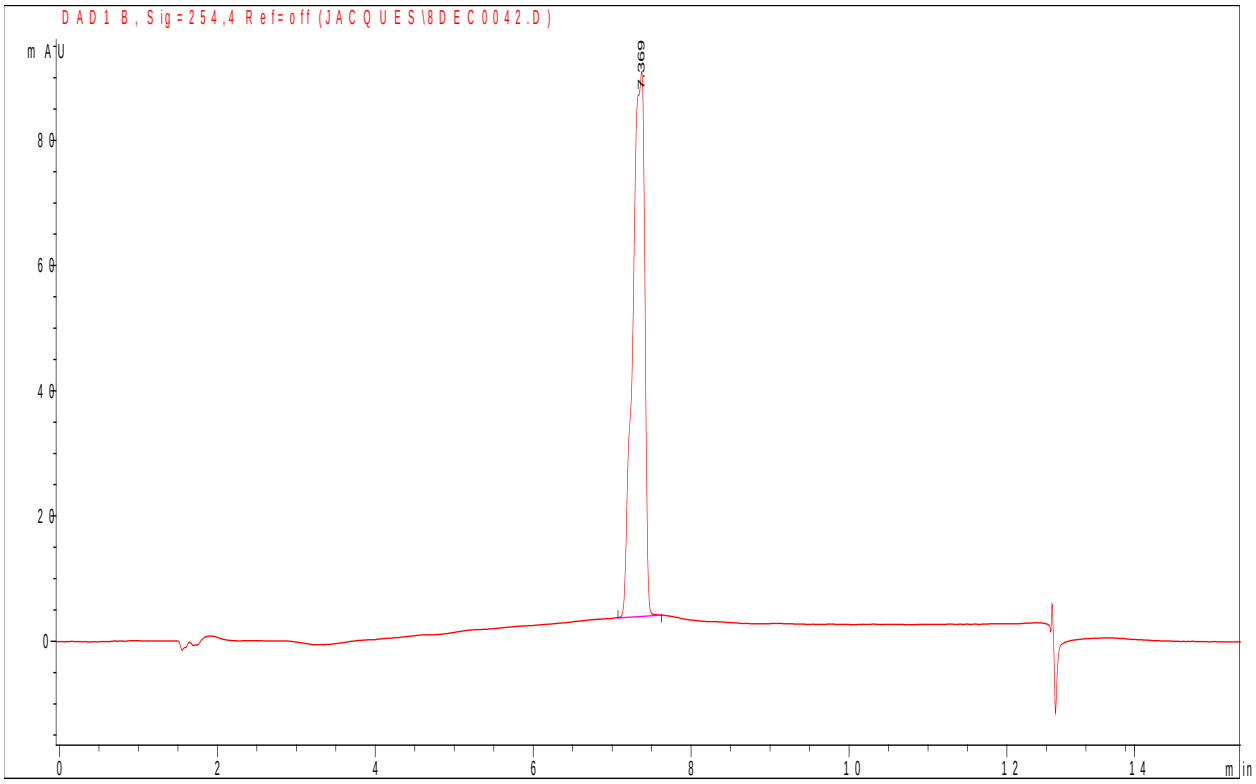

8-{[2-(4-Methylphenyl)ethyl]sulfanyl}caffeine (1f)

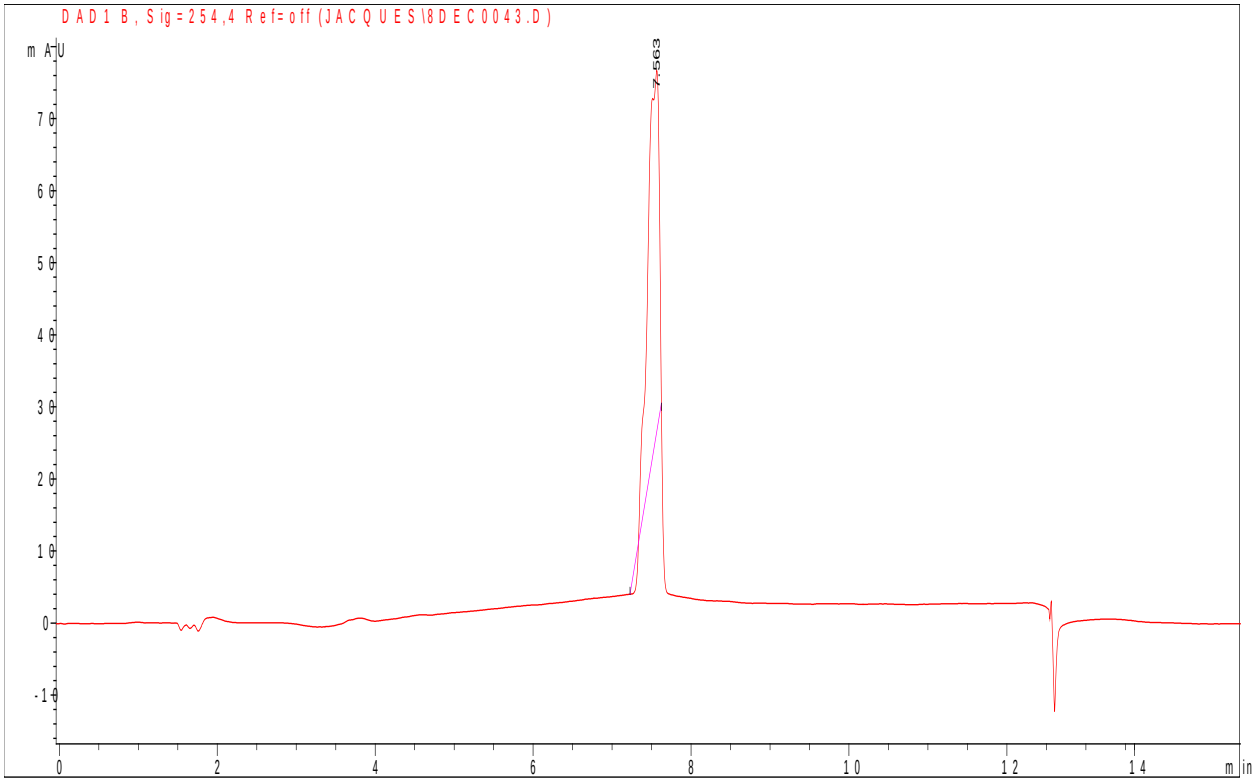

8-{[2-(4-Methoxyphenyl)ethyl]sulfanyl}caffeine (1g)

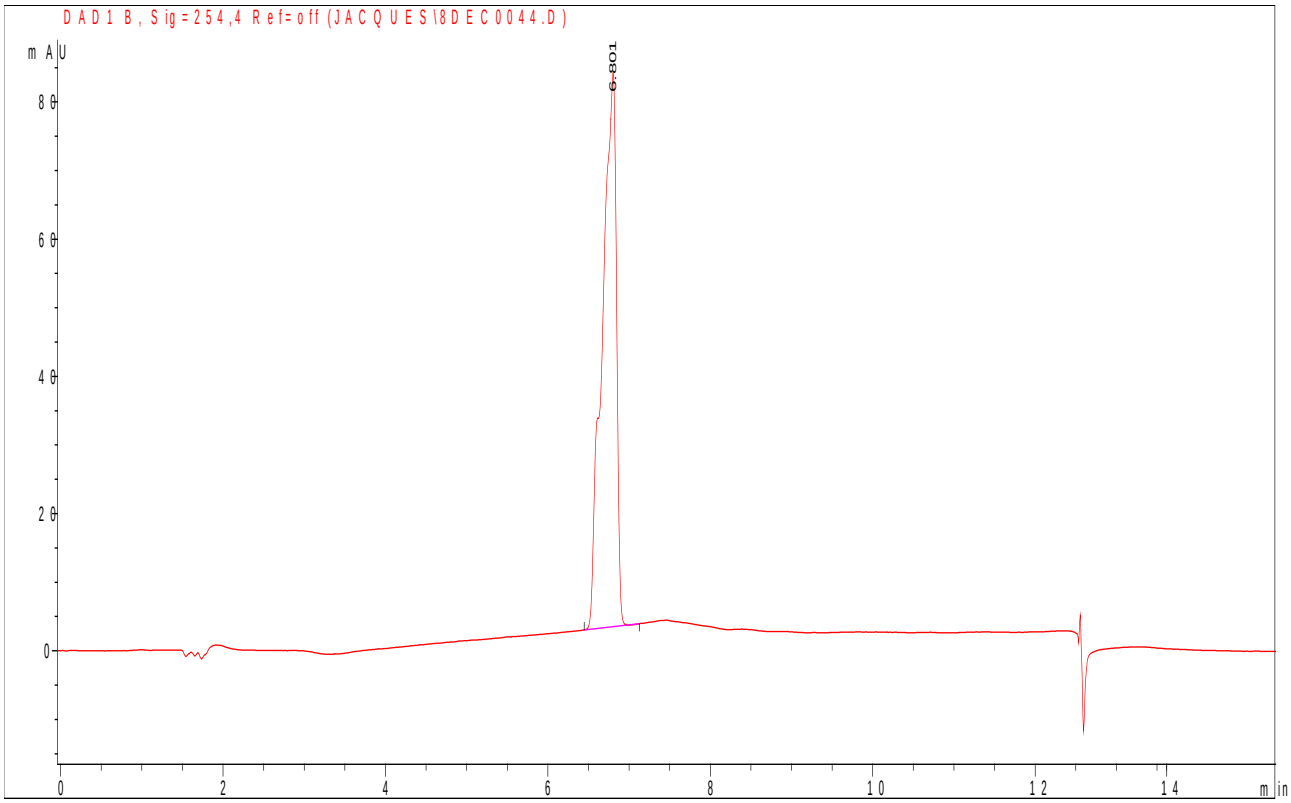

8-{[2-(4-Bromophenyl)ethyl]sulfinyl}caffeine (2a)

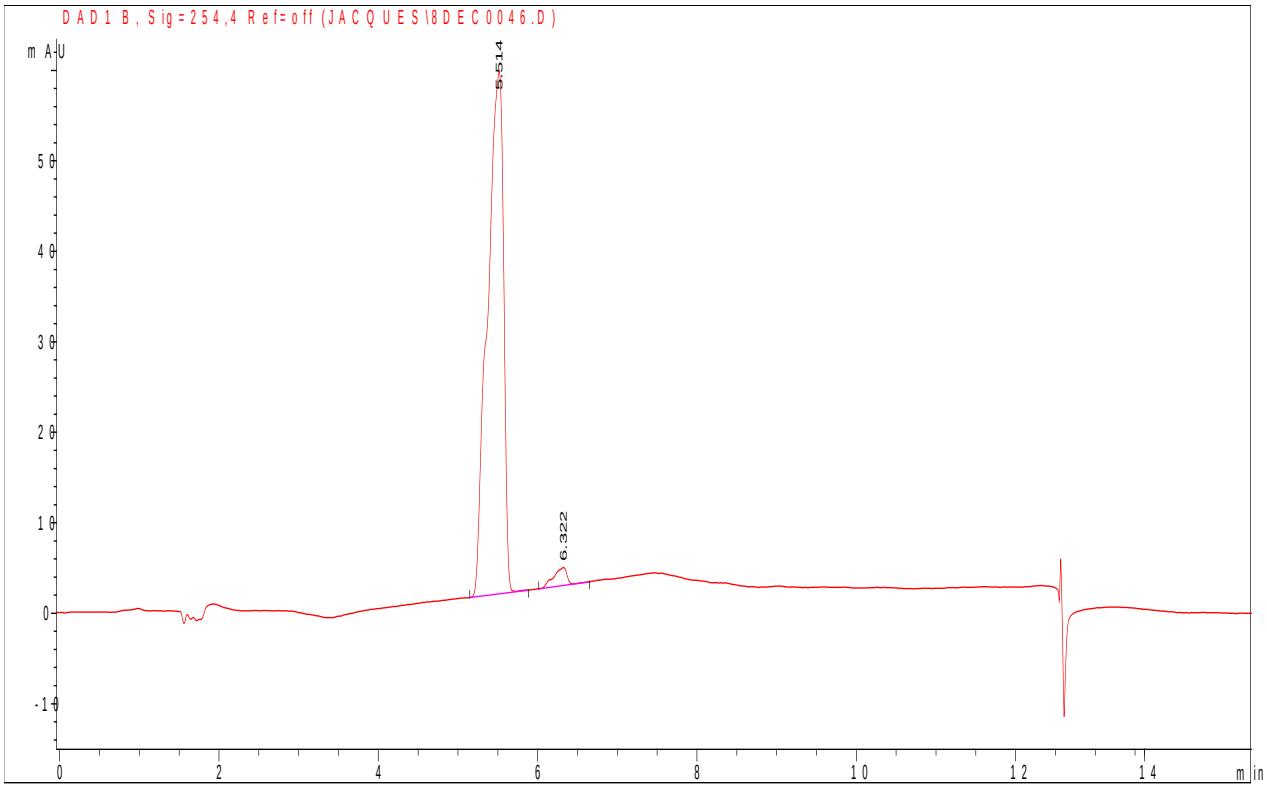

8-{[2-(4-Fluorophenyl)ethyl]sulfinyl}caffeine (2b)

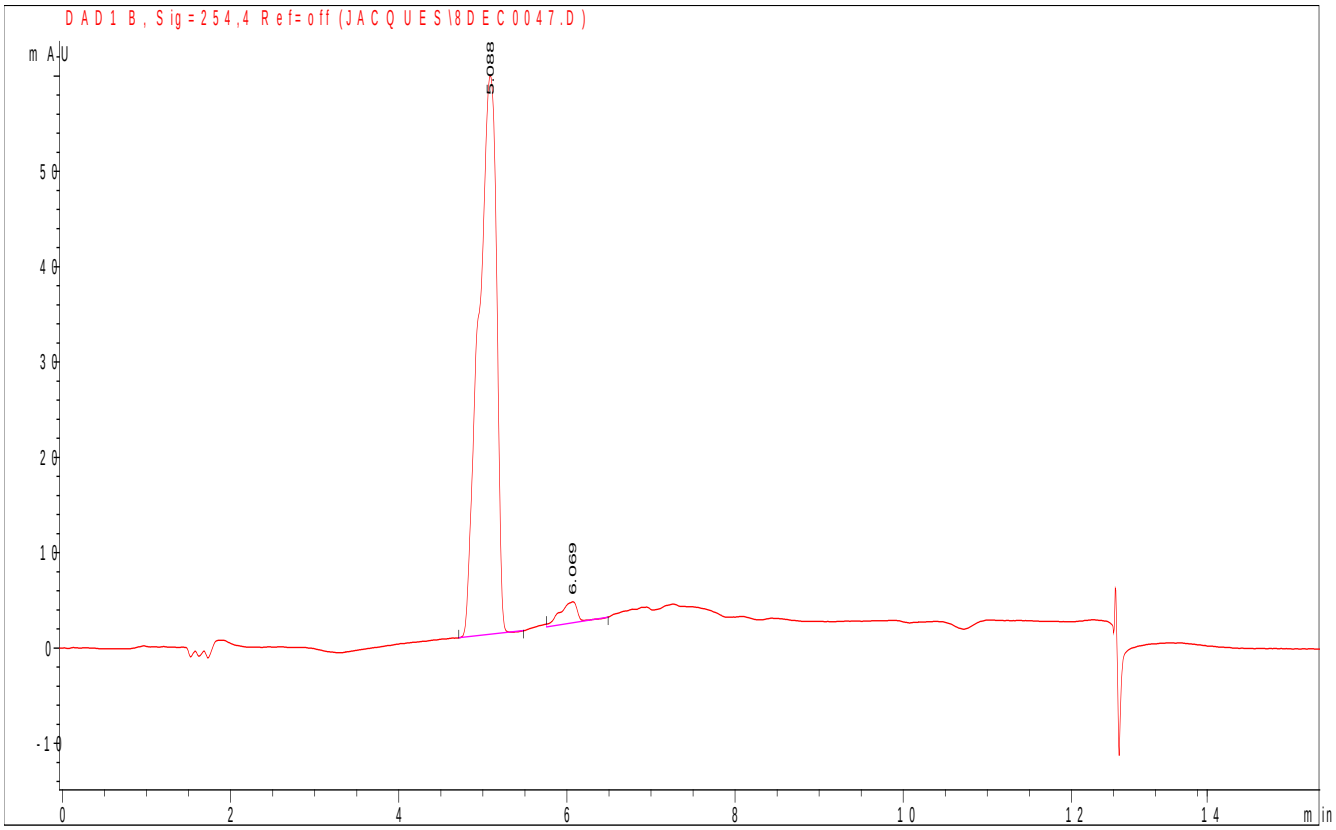

Section 3 - Mass spectra

8-[(Phenylethyl)sulfanyl]caffeine (1a)

SM01_HR-c1 #54 RT: 1.12 AV: 1 NL: 9.89E5
T: + c EI Full ms [317.50-345.50]

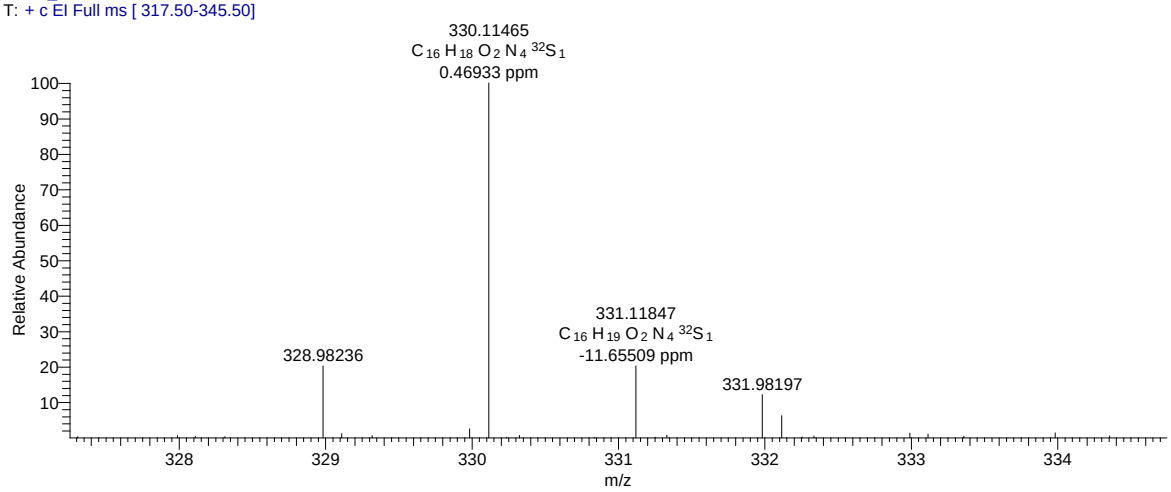

8-{[2-(4-Chlorophenyl)ethyl]sulfanyl}caffeine (1b)

SM02_HR-c1 #57 RT: 0.81 AV: 1 NL: 1.04E6
T: + c EI Full ms [353.50-372.50]

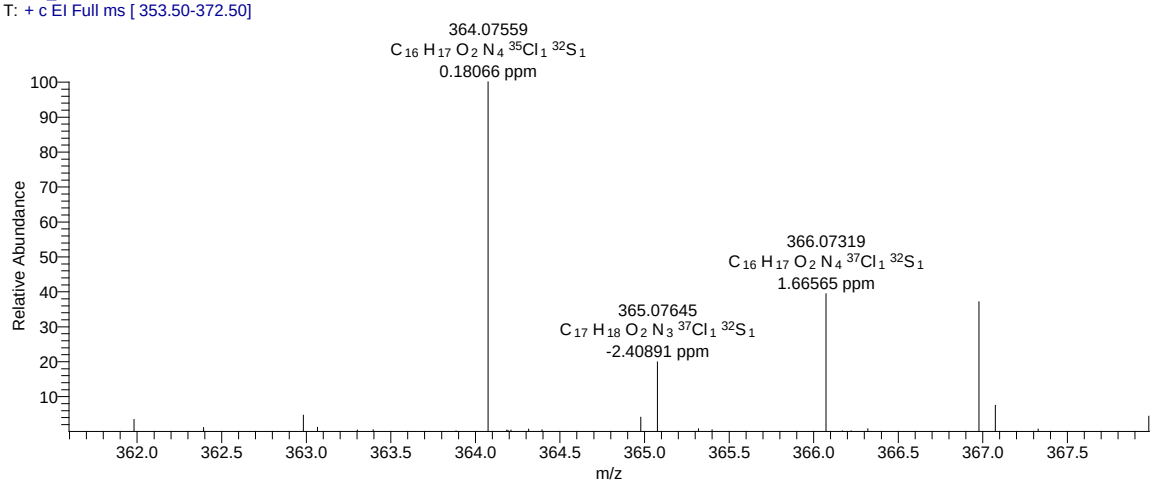

8-{[2-(4-Bromophenyl)ethyl]sulfanyl}caffeine (1c)

SM03_HR-c1 #88 RT: 1.03 AV: 1 NL: 5.23E6
T: + c EI Full ms [403.50-420.50]

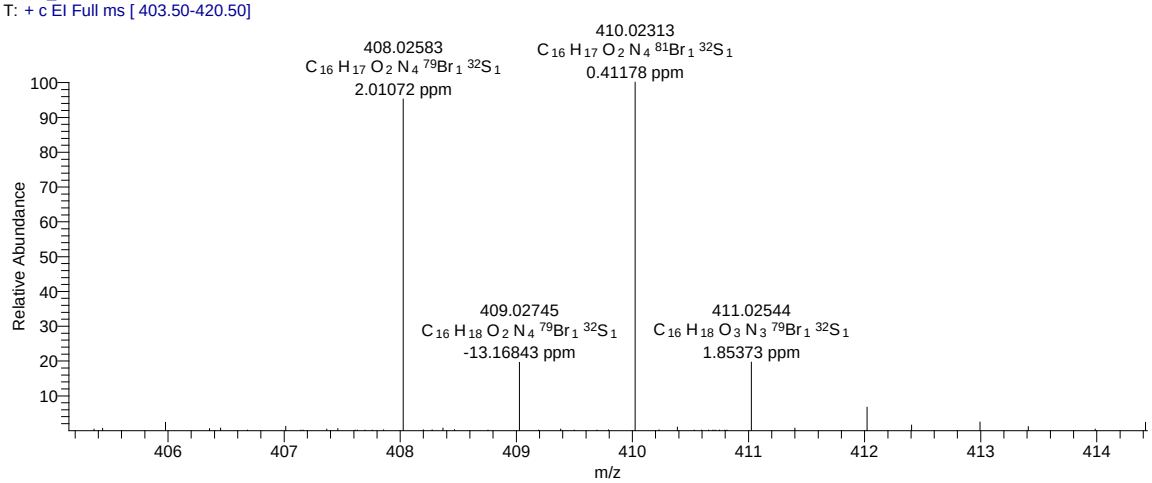

8-{[2-(4-Fluorophenyl)ethyl]sulfanyl}caffeine (1d)

SM04_HR-c1 #126 RT: 1.59 AV: 1 NL: 1.22E6
T: + c EI Full ms [341.50-357.50]

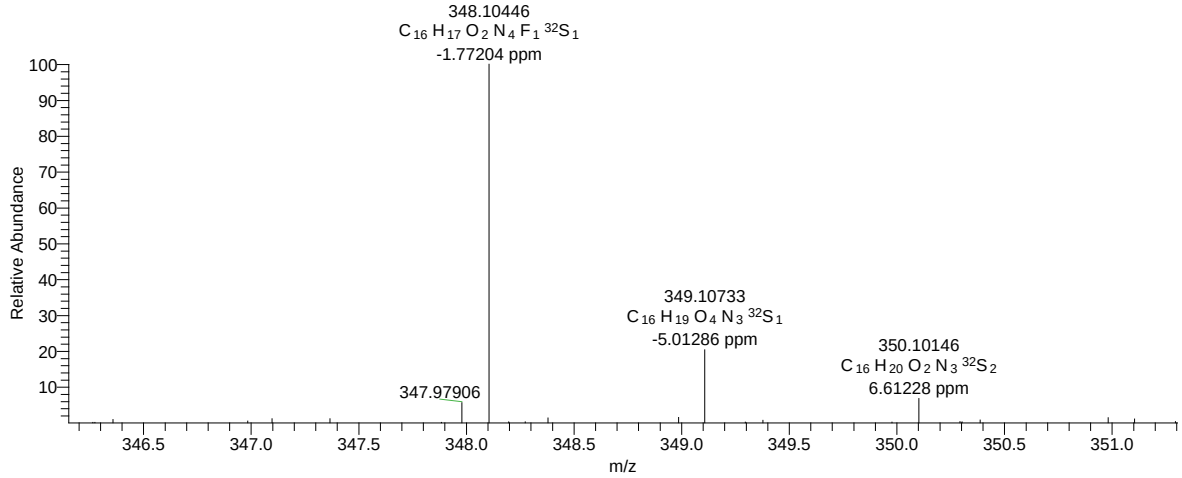

8-{[2-(4-(Trifluoromethyl)phenyl)ethyl]sulfanyl}caffeine (1e)

SM05_HR-c1 #80-92 RT: 0.96-1.10 AV: 13 NL: 2.56E6
T: + c EI Full ms [391.50-408.50]

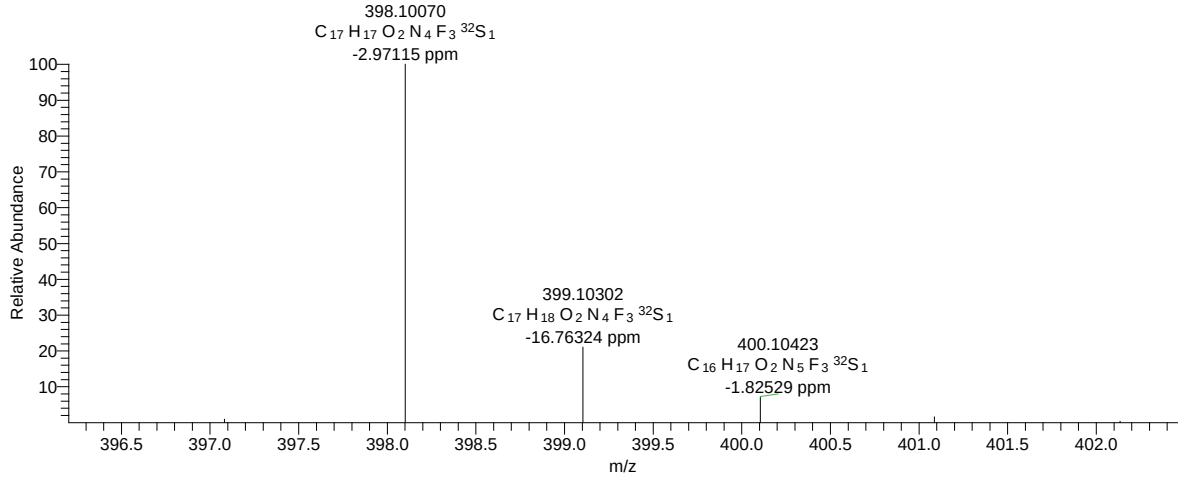

8-{[2-(4-Methylphenyl)ethyl]sulfanyl}caffeine (1f)

SM06_HR-c1 #65 RT: 0.83 AV: 1 NL: 7.44E5
T: + c EI Full ms [341.50-357.50]

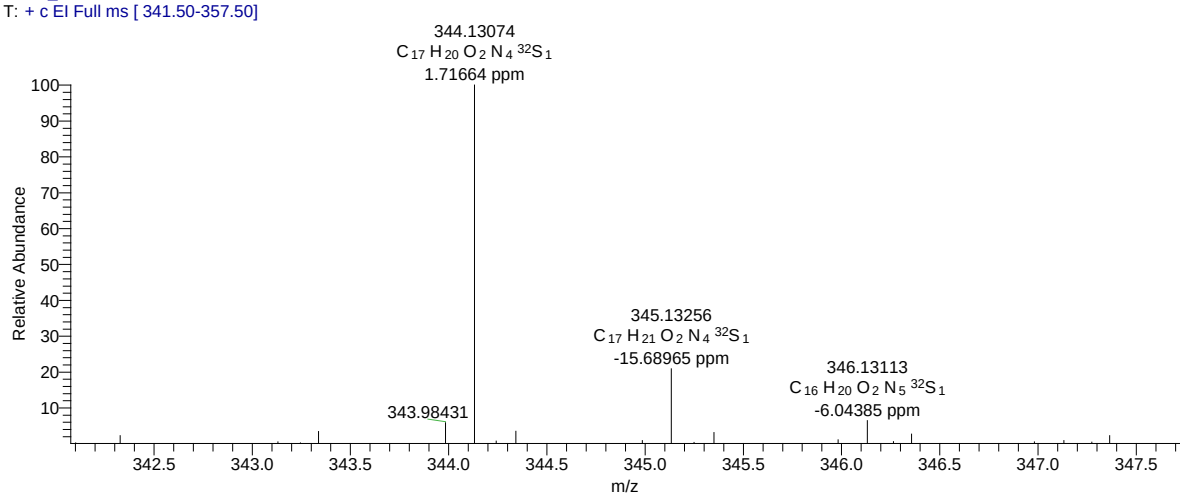

8-{[2-(4-Methoxyphenyl)ethyl]sulfanyl}caffeine (1g)

SM07_HR-c1 #25 RT: 0.94 AV: 1 NL: 2.65E6
T: + c EI Full ms [353.50-371.50]

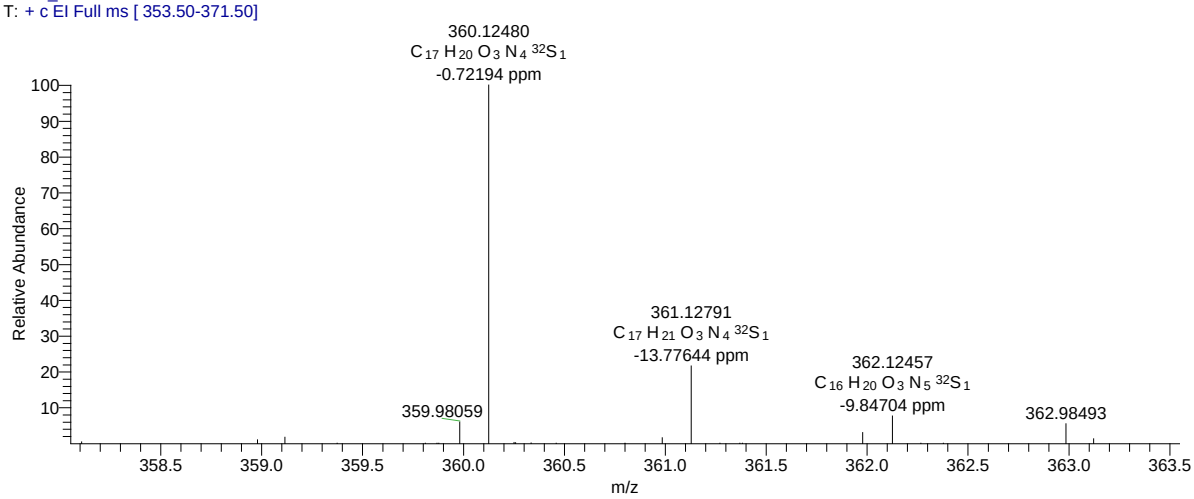

8-{[2-(4-Bromophenyl)ethyl]sulfinyl}caffeine (2a)

SM09_HR-c1 #59 RT: 0.73 AV: 1 NL: 3.54E5
T: + c EI Full ms [415.50-434.50]

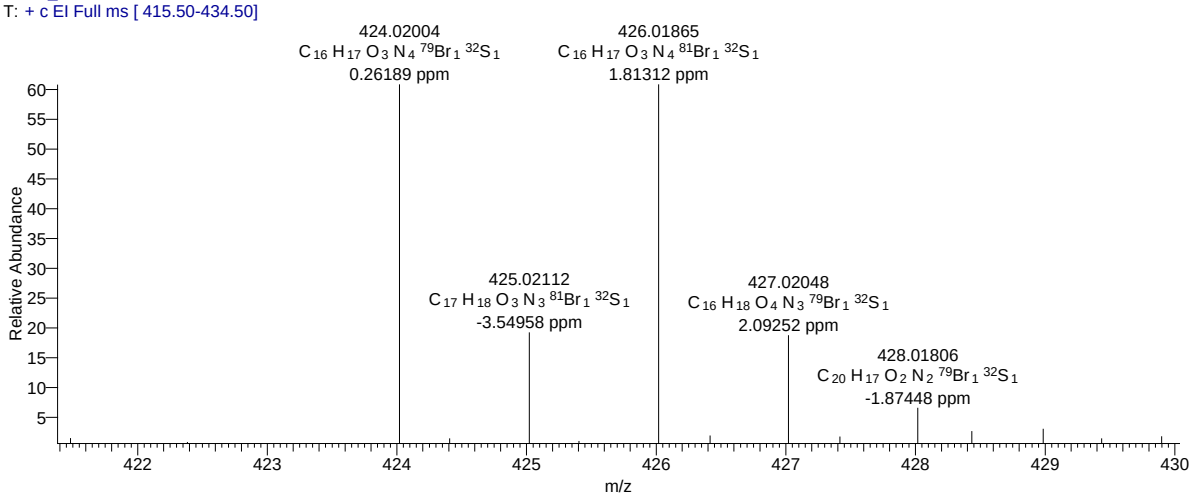

8-{[2-(4-Fluorophenyl)ethyl]sulfinyl}caffeine (2b)
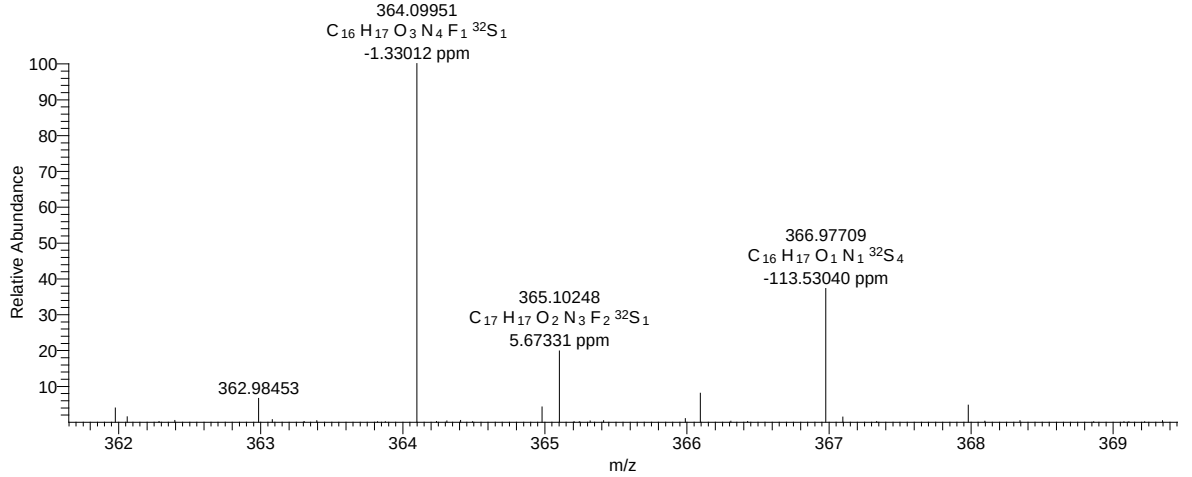
SM10_HR-c1 #41 RT: 0.57 AV: 1 NL: 2.09E6
T: + c EI Full ms [353.50-372.50]